AD-A097 123 ARIZONA UNIV TUCSON ENGINEERING EXPERIMENT STATION F/G 17/2
DIGITAL COMMUNICATIONS SYSTEMS: TEST AND EVALUATION STUDIES. VO--ETC(U)
AUG 79 L C SCHOOLEY, G R DAVIS DAEA18-74-A-0271

UNCLASSIFIED NL

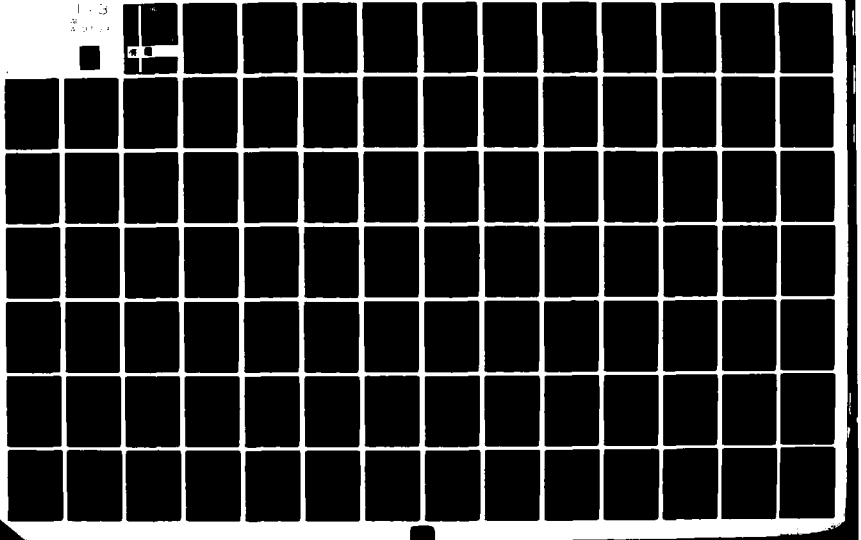

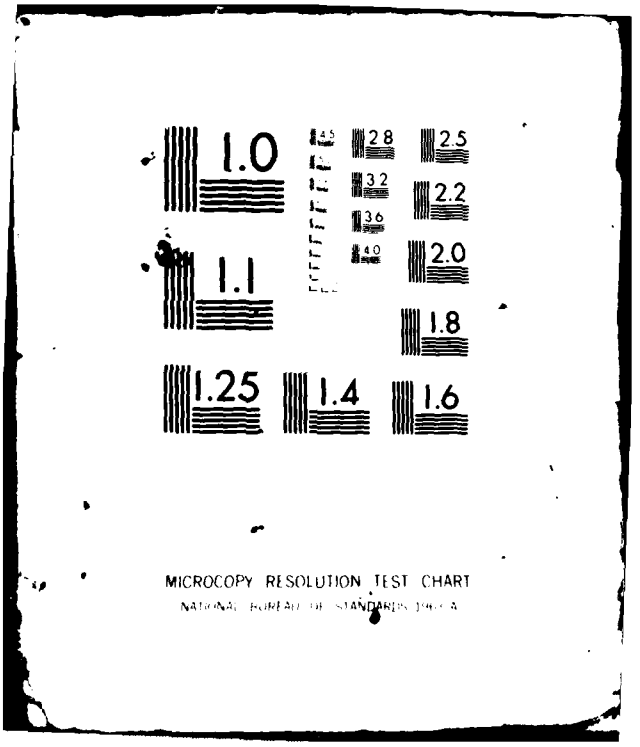
1.0
1.1
1.25
1.4
1.6
2.8
3.2
3.6
4.0
2.5
2.2
2.0
1.8
MICROCOPY RESOLUTION TEST CHART

LEVEL III

(1)

Final Report.

Contract No. DAEA18-74-A0271/0005

DIGITAL COMMUNICATIONS SYSTEMS: TEST AND EVALUATION STUDIES. VOLUME II: EXTRAPOLATION TECHNIQUES FOR THE EVALUATION OF DIGITAL COMMUNICATIONS EQUIPMENT.

Prepared for

U. S. Army Electronic Proving Ground
Fort Huachuca, Arizona

Prepared by

L. C. Schooley
G. R. Davis

31 AUGUST 1979

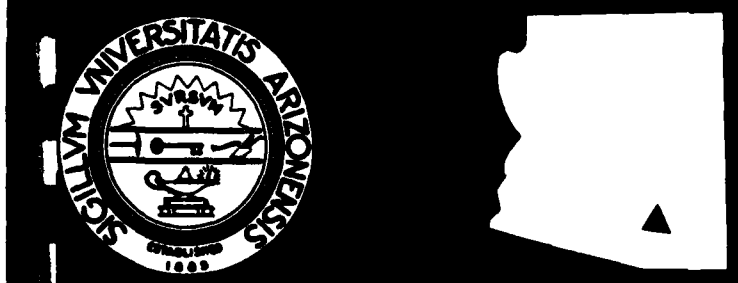

ENGINEERING EXPERIMENT STATION
COLLEGE OF ENGINEERING
THE UNIVERSITY OF ARIZONA
TUCSON, ARIZONA

Final Report

DIGITAL COMMUNICATIONS SYSTEMS: TEST AND EVALUATION STUDIES VOLUME II: EXTRAPOLATION TECHNIQUES FOR THE EVALUATION OF DIGITAL COMMUNICATIONS EQUIPMENT

Contract No. DAEA18-74-A0271/0005 ✓

A097122

Prepared for

U. S. Army Electronic Proving Ground
Fort Huachuca, Arizona

Prepared by

L. C. Schooley, Ph.D., P.E.
Associate Professor

and

G. R. Davis, Ph.D.
Research Associate

Approved by

L. C. Schooley

Department of Electrical Engineering
University of Arizona
Tucson, Arizona 85721

31 AUGUST 1979

ACKNOWLEDGEMENT

The experimental work for this dissertation was for the most part conducted at the Digital Transmission Evaluation Program (DTEP) test facility at Fort Huachuca, Arizona, with some additional work at Bell Aerospace in Tucson. The cooperation and assistance provided by the personnel at these facilities was truly outstanding and greatly appreciated. Without this valuable assistance the task would have been considerably more difficult and prolonged, indeed, impossible to accomplish within the time frame.

TABLE OF CONTENTS

TABLE OF CONTENTS, Continued.

TABLE OF CONTENTS, Continued.

LIST OF ILLUSTRATIONS

LIST OF ILLUSTRATIONS, Continued.

LIST OF ILLUSTRATIONS, Continued.

LIST OF ILLUSTRATIONS, Continued.

LIST OF ILLUSTRATIONS, Continued.

LIST OF ILLUSTRATIONS, Continued.

LIST OF TABLES

ABSTRACT

An accepted method for determining the expected performance of digital communications equipment is to obtain data experimentally from which to plot a curve of long term bit error rate versus received signal-to-noise ratio. Present procedures for obtaining complete data are very time consuming. A technique has been devised to extrapolate the desired information accurately from more readily obtainable data. The validity of the technique is established both analytically and experimentally.

In order to validate the extrapolation method for obtaining the desired curves of long term bit error rate, it is necessary to prove the basic hypothesis that small variations of the internal anomalies (in digital receivers) that contribute to errors in the detection process cause lateral shifts of the curves, but the curves retain their characteristic shape depending upon the modulation scheme. This hypothesis is proved first by calculating the anomaly effects on the curves based upon theoretical analysis. Experimental verification is then obtained by examining the effects upon the curves by anomalies induced into representative items of digital communications equipment.

In the process of experimentally verifying the extrapolation technique a new procedure was discovered for the alignment of digital communications equipment that has potentially greater significance

than the reduction of test time. The method is to perform final adjustments on the equipment while monitoring the bit error rate at a very low signal-to-noise ratio. Although analog alignment techniques are well established and necessary to obtain proper operation, these methods may not produce the best possible operational performance. The experimental results show that final alignment while monitoring BER can produce the desired optimum performance.

CHAPTER 1

INTRODUCTION

The primary objective of this dissertation is to establish the validity of a new technique for evaluating digital communications equipment. The technique, which has broad applications, is of major significance in that it permits reduction of testing time by as much as three or four orders of magnitude.

In the process of experimentally verifying the technique, which is based upon the extrapolation of long term bit error rates, a new procedure for equipment alignment was discovered which has potentially even more significance. This procedure is described in detail and its validity established.

The chapter devoted to theoretical derivations is structured so that it may stand alone as a basic reference for the effects of internal equipment anomalies on the probability of bit error in the presence of noise.

A disparity discovered between the experimental results and calculations based upon the theoretical derivations led to a new and revealing insight into the operation of digital communications equipment not previously discussed in the literature.

The dissertation has been structured so that a complete overview of the material can be obtained from Chapters 1 and 6 which are

relatively short. For someone desiring more particulars without complete details, Chapter 5 compares the more significant aspects of the theoretical and experimental results.

Background

During the past decade there has been a rapid movement toward the use of all digital communications systems and equipment. This movement has been spurred primarily by the revolutionary development of inexpensive, microminiaturized, integrated digital circuitry. The military has been leading this trend due to the requirement for total system security which has not been met successfully with the use of analog equipment.

The ability to test and evaluate digital communications systems and equipment has not kept pace with the development. In most cases, analog techniques have been applied and modified where possible in attempts to determine operating characteristics. Although these methods have some value, the only true measure of the effectiveness of digital systems or equipment lies in the digital performance. The only digital evaluation technique in general use is the determination of long term bit error rate (BER) as a function of the signal level at the input to the receiver or as a function of the signal-to-Gaussian noise ratio when a noise figure for the receiver is available.

Investigations of test methods and performance criteria for digital communications systems have shown that long term bit error rate, by itself, provides an incomplete picture of the characteristics of a

real channel (Schooley and Davis, 1977a). An adequate description of real channel operation requires statistics, such as error burst distributions, which are obtained from analysis of the error patterns. It has been shown, however, in the evaluation of modulators/demodulators exclusive of the transmission media, that relative performance in the presence of Gaussian noise is a sufficient criterion (Lucky, Saltz, and Weldon, 1968). Curves of long term bit error rate versus signal-to-Gaussian noise ratio or received signal level are, therefore, useful results of bench testing of digital modulation hardware.

At low to moderate data rates, considerable test time can be expended in obtaining reasonably accurate data points for the plotting of such error curves. For example, at 32 Kbps it would require approximately one hour to count sufficient errors to obtain a single data point at an error rate in the neighborhood of 10^{-7} with reasonable confidence in the result. When it is necessary to reconstruct complete error curves under a variety of conditions, the test time required can quickly become excessive. For this reason, methods other than simple counting of errors were sought for estimating very low bit error rates (Schooley and Davis, 1977b).

The technique of extrapolation was shown to have considerable promise as an accurate and relatively fast method for obtaining curves of long term bit error rate versus signal-to-noise ratio. The procedure is to obtain a single point of the curve at a high error rate (possibly 10^{-4}) with a high degree of confidence, and then to fit a

theoretical error curve (error function or exponential based upon the modulation scheme) through this point.

In an effort to establish some validity for the use of this method, a large number of examples were gathered from a variety of sources where BER curves had been plotted versus received signal level or signal-to-noise ratio in the process of testing digital communications equipment. In each case, a theoretically shaped curve based upon the type of modulation was drawn to the scale of the experimental results and intersecting the experimental curve at the 10^{-4} BER point. In most cases, the curves fit very closely for BER less than 10^{-4}, and even in the worst case, the deviation was less than 1.5 db at the extreme tail.

Although the above results were in no way conclusive, no counter examples could be found to indicate that the technique was not valid. Since use of the extrapolation method could reduce required test time by as much as 3 to 4 orders of magnitude, it was decided to attempt to prove its validity. To do so would require showing that small changes in the internal anomalies that affect the detection process and contribute to digital errors cause lateral shifts of the BER curve but do not affect its shape. From the preliminary investigation this appeared to be a logical hypothesis, but no evidence was found that it had ever been stated as such, much less proven. The objective of this dissertation is then to either verify the hypothesis or to establish bounds on its validity.

Statement of the Problem

The basic hypothesis to be proved is that small variations in the internal anomalies which contribute to errors in digital demodulators cause a lateral displacement of the characteristic curve of bit error rate versus received signal-to-noise ratio while the curve retains its theoretical shape at the higher levels of signal-to-noise ratio. The objective is to verify the hypothesis both mathematically and experimentally to the extent possible for a variety of modulation schemes.

Approach

In Chapter 2 expressions are derived for the probability of error for ideal detection of signals in additive white Gaussian noise for the most common methods of modulation. These ideal theoretical expressions are then modified to determine the effects of carrier phase reference error and symbol synchronization error. Since closed form expressions cannot be determined for the effects of intersymbol interference and receiver nonlinearities, the theoretical aspects of these anomalies are discussed in Chapter 3 as calculated results.

It must be pointed out that only a few of the derivations presented are original. However, only the most common expressions can be found in text books, with many of the derivations spread widely throughout the literature. Unfortunately, there are almost as many variations in notation as there are articles. In some cases, common derivations are extended to obtain expressions for probability

of error for modulation schemes or anomaly effects not found in the literature.

In addition to being necessary to verify the basic hypothesis, Chapter 2 provides a convenient stand alone reference which relates comparable expressions in a common notation for the various modulation systems. In many cases, the derivations as well as the resulting expressions are quite complex and sometimes abstract. Efforts were made to relate the mathematics to the physical situation to provide insight into the effects of the anomalies on the probability of error.

In the next chapter the derived expressions are used to calculate and plot BER curves to examine the effects of the various factors on their position and shape. In those cases where closed form expressions were not attainable, the anomalies are studied directly in terms of how they affect the BER curves.

Chapter 4 contains descriptions and analyses of the results of the experiments that were conducted in an effort to verify the basic hypothesis. These experiments were conducted on four available digital communications systems which encompassed three different methods of modulation. Where feasible, perturbations of error causes were introduced into the systems to determine their effect upon the BER curves.

Baud timing jitter effects were investigated for a three level partial response modulation system, a frequency shift keyed modulation system, and a quadrature phase shift keyed modulation system. The effects of carrier phase jitter were examined in two quadrature phase

shift keyed systems of different design. Receiver nonlinearities were investigated in the three level partial response system.

Due to limited resources (primarily availability of equipment), it was not possible to study all types of digital modulation systems. Also, due to individual design details, it was not feasible to introduce each type of perturbation into each system studied. Nevertheless, the experiments performed appear to be sufficiently representative to form an adequate experimental base for the completion of the task.

Although, as previously mentioned, BER curves have been used widely to analyze the performance of digital communications systems, no evidence was found of anyone attempting to induce error causing anomalies in order to study their effect upon the curves. Indeed, prior to this undertaking it was not completely understood that it would be at all feasible to accomplish the desired results. These experiments, therefore, served not only to support the conclusions regarding the basic hypothesis, but also to provide original results that have not appeared previously in the literature.

During the course of the experimental work the patterns of the error curves suggested a new procedure for the alignment of digital communications equipment that could have a far greater significance than the reduction of test time. This procedure, which is based upon the validity of the extrapolation technique, is described in some detail.

The first section of Chapter 5 is devoted to correcting an apparent disparity between the calculated effects of jitter and the experimentally obtained BER curves. The theoretical predictions of Chapter 3, as corrected, are then compared with the experimental results in terms of the shapes of the curves, and where measurements were possible, in terms of the amount of shift obtained.

A summary and conclusions are contained in Chapter 6.

CHAPTER 2

THEORETICAL ANALYSIS

As was mentioned in the introduction, only a few of the derivations contained in this chapter are original. However, the gathering of the information under a single cover, with common notation and in such a manner that comparisons of modulation techniques and anomaly effects can be made, is felt to be useful. In some cases derivations have been extended to fill apparent gaps in the literature. Some of the derivations have been modified to provide insight into the physical aspects and to gain understanding of the close relationships among many of the detection methods and the error causes.

Often the derivations as well as the resulting expressions will be quite complex. In some cases closed form expressions are not obtainable. In others approximations will be necessary to reduce the formulae to usable forms. In each case the mathematics and the necessary approximations will be related to the physical situation for greater understanding.

The specific modulation techniques that are presented here have been selected either because they are widely used or because they are basic systems from which expressions for most variations can be obtained readily. For each modulation scheme the expression of probability of error is first derived for optimum detection in the presence of additive white Gaussian noise. These expressions are then modified to reflect

the effects of carrier phase reference error where applicable and symbol synchronization error.

Discussions of intersymbol interference and receiver nonlinearities have been deferred until Chapter 3 since closed form expressions for their effects cannot be derived. These anomalies will be more readily described directly in terms of their effects upon the characteristic curves of BER versus signal-to-noise ratio.

Throughout this chapter only additive white Gaussian noise will be considered. The justification for this is that the primary interest is in internal receiver anomalies and not outside channel effects. Linear filtering does cause band limiting of the noise. Where this affects the results it is so noted; however, the noise distribution is still Gaussian. The effect of square law devices upon Gaussian noise is described in the discussion of non-coherent detection of ASK and FSK.

The chapter has been organized so that, where possible, previous derivations and expressions can be cited to preclude duplications. Toward this end it is appropriate to begin with a discussion of the coherent correlation receiver.

Performance of the Ideal Coherent Communication Receiver

In order to establish the desired common notation it will be necessary in each case that follows to begin with the derivation of the probability of error for optimum detection. Figure 2.1 is a block diagram of the well known correlation receiver which, for most cases, is optimum for the detection of binary signals. For a straightforward derivation of the correlation receiver, see Whalen (1971). The received

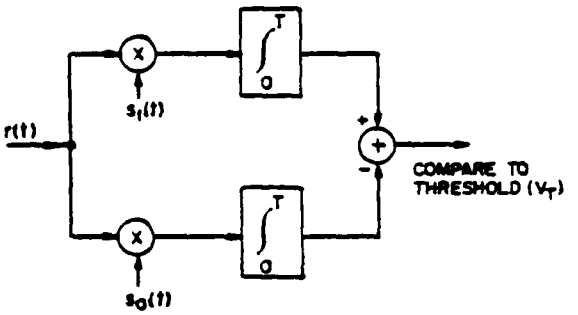

Fig. 2.1. Correlation Receiver for Binary Signals.

signal r(t) is assumed to be the sum of the transmitted signal and white Gaussian noise, $r(t) = s_i(t) + n(t)$. The transmitter output is a known signal $s_0(t)$ for T seconds if the bit to be transmitted is a zero, and a second known signal $s_1(t)$ if the bit is a one. The noise n(t) is assumed to have zero mean and spectral density $N_o/2$.

Note that the spectral density $N_o/2$ is a two-sided spectral density; i.e., the frequency response is uniform from $-\infty$ to ∞. Many authors define a one-sided spectral density that is uniform with frequency from 0 to ∞ with amplitude N_o. Although possibly confusing, the results are identical when considered over a finite bandwidth, -B to B on the one hand and 0 to B on the other, the total noise power being N_oB in both cases.

With the assumption that the transmitted signals are equally probable, the decision rule may be expressed: decode $r(t)$ as $s_1(t)$ (call this decision D_1) if:

$$G \equiv \int_0^T r(t)s_1(t)dt - \int_0^T r(t)s_0(t) + \frac{1}{2}\int_0^T [s_0^2(t) - s_1^2(t)]dt \geq 0 \tag{2.1}$$

otherwise decode $r(t)$ as $s_0(t)$ (decision D_0). The third integral represents half the difference of the energy per bit of the two signals. If the two signals were of equal power then the value of the third integral would be zero and the decision rule would be simply: choose D_1 if the output of the upper correlator (first integral) is the greater.

The sum of the three integral terms of Eq. (2.1) have been denoted G for convenience. The first two terms of G are integrals of Gaussian random processes and the third is a constant; therefore, G is a Gaussian random variable and only its mean and variance will be required to determine its probability density function. The error probability for the decision rule will be:

$$P_e = P\{D_1|s_0\}P\{s_0\} + P\{D_0|s_1\}\ P\{s_1\} \tag{2.2}$$

or, in terms of the density function of G conditioned upon $s_0(t)$ and $s_1(t)$:

$$P_e = \frac{1}{2}\int_0^\infty p(G|s_0)dG + \frac{1}{2}\int_{-\infty}^0 p(G|s_1)dG \quad . \tag{2.3}$$

This is illustrated in Fig. 2.2.

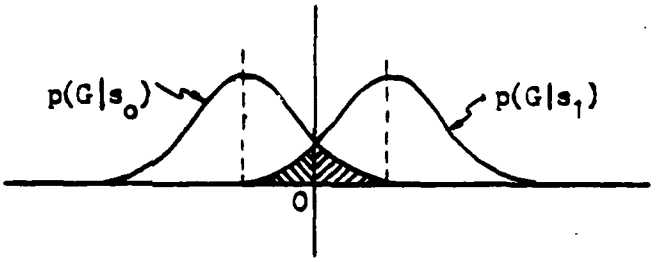

Fig. 2.2. Conditional Probability Density Functions of G, and Error Regions.

The expected value of G conditioned on $s_0(t)$, denoted by η_{G_0} is:

$$\eta_{G_0} = E\{G|s_o\} = E\left\{\int_0^T [s_0(t) + n(t)]s_1(t)dt - \int_0^T [s_0(t) + n(t)]\, s_0(t)dt + \frac{1}{2}\int_0^T [s_0^2(t) - s_1^2(t)]dt\right\} \tag{2.4}$$

Since the mean of n(t) is assumed to be zero, this becomes:

$$\eta_{G_0} = E\left\{\int_0^T s_0(t)s_1(t)dt - \int_0^T s_0^2(t)dt + \frac{1}{2}\int_0^T [s_0^2(t) - s_1^2(t)]dt\right\}$$

$$= -\frac{1}{2}\int_0^T [s_0(t) - s_1(t)]^2 dt\ . \tag{2.5}$$

Assuming that $s_0(t)$ was sent, Eq. (2.1) may be rearranged to show that:

$$G - \eta_{G_0} = \int_0^T n(t)[s_1(t) - s_0(t)]dt$$

so that the variance of G conditioned on s_0 denoted by $\sigma^2_{G_0}$ is then:

$$\sigma^2_{G_0} = E\left\{[G - \eta_{G_0}]^2\right\} = E\left\{\int_0^T n(t)[s_1(t) - s_0(t)]dt \int_0^T n(\tau)[s_1(\tau) - s_0(\tau)]d\tau\right\} = \int_0^T\int_0^T E\left\{n(t)\, n(\tau)\right\}[s_1(t) - s_0(t)][s_1(\tau) - s_0(\tau)]dtd\tau \quad . \tag{2.6}$$

Since the noise is assumed to be stationary white Gaussian with spectral density $N_o/2$;

$$E\{n(t)n(\tau)\} = (N_o/2)\delta(t - \tau)$$

the variance is therefore:

$$\sigma^2_{G_0} = \frac{1}{2} N_o \int_0^T [s_1(t) - s_0(t)]^2 dt \quad . \tag{2.7}$$

It can be similarly shown that the expected value of G conditioned on $s_1(t)$ being sent is:

$$\eta_{G_1} = \frac{1}{2} \int_0^T [s_0(t) - s_1(t)]^2 dt \tag{2.8}$$

and the variance is

$$\sigma^2_{G_1} = \frac{1}{2} N_o \int_0^T [s_0(t) - s_1(t)]^2 dt \quad . \tag{2.9}$$

Now define the average energy of the two signals:

$$E = \frac{1}{2} \int_0^T [s_0^2(t) + s_1^2(t)]dt \tag{2.10}$$

and a time cross correlation coefficient:

$$\rho = \frac{1}{E} \int_0^T s_0(t)s_1(t)\, dt \; . \tag{2.11}$$

The means and variance can then be expressed:

$$\eta_{G_1} = -\eta_{G_0} = E(1-\rho)$$

$$\sigma^2_{G_0} = \sigma^2_{G_1} = N_o E(1-\rho) \; . \tag{2.12}$$

The conditional probability density functions are then:

$$p(G|s_0) = \frac{1}{[2\pi N_o E(1-\rho)]^{1/2}} \exp\left\{ - \frac{[G + E(1-\rho)]^2}{2N_o E(1-\rho)} \right\}$$

$$p(G|s_1) = \frac{1}{[2\pi N_o E(1-\rho)]^{1/2}} \exp\left\{ - \frac{[G - E(1-\rho)]^2}{2N_o E(1-\rho)} \right\} \; . \tag{2.13}$$

As is illustrated in Fig. 2.2 the error probabilities will be equal; i.e., $P\{D_1|s_0\} = P\{D_0|s_1\}$, so that the overall bit error probability will be:

$$P_b = \int_0^\infty p(G|s_0)dG$$

which, with a change of variable becomes:

$$P_b = \frac{1}{(2\pi)^{1/2}} \int_{[E/N_o(1-\rho)]^{1/2}}^\infty e^{-z^2/2}\, dz$$

where

$$z^2 = \frac{[G - E(1-\rho)]^2}{N_o E(1-\rho)} \quad . \tag{2.14}$$

This form is convenient for evaluation if the complimentary error function is defined:

$$\text{erfc}(x) = \frac{1}{(2\pi)^{1/2}} \int_x^\infty e^{-z^2/2} dz \quad . \tag{2.15}$$

The probability of bit error can then be expressed:

$$P_b = \text{erfc}\left[\frac{E}{N_o}(1-\rho)\right]^{1/2} \quad . \tag{2.16}$$

The above analysis has primarily been summarized from Whalen (1971). A particular note of caution is required here. Many authors utilize a definition of the error function which is similar and very often found in tables of functions; i.e.,

$$\text{erfc}(x) = \frac{2}{(\pi)^{1/2}} \int_x^\infty e^{-u^2} du \quad . \tag{2.17}$$

With this definition, the probability of bit error becomes:

$$P_b = \frac{1}{2} \text{erfc}\left[\frac{E}{2N_o}(1-\rho)\right]^{1/2} \quad . \tag{2.18}$$

In some publications this conflict of definitions is avoided by referring to Eq. (2.15) as Q(x), the normal probability integral, yet defining erfc(x) as in Eq. (2.17). Throughout this work the definition and probability of error of Eqs. (2.15) and (2.16) will be used.

Coherent Phase Shift Keying (CPSK)

In a binary CPSK system it will be assumed that the signals are sine waves 180° out of phase and designated by:

$$s_0(t) = A \sin \omega t \qquad s_1(t) = A \sin(\omega t + \pi) = - A \sin \omega t \ .$$

With these signals it is readily seen that:

$$E = \frac{A^2 T}{2} \qquad \rho = \frac{1}{E} \int_0^T - A^2 \sin^2 \omega t \, dt = - 1 \ .$$

Since it can be shown (Whalen, 1971) that $|\rho| \leq 1$ for any two possible signals, it is apparent that binary CPSK is the optimum binary communication system. The probability of bit error from Eq. (2.16) is then:

$$P_b = \operatorname{erfc}\left[\frac{2E}{N_o}\right]^{1/2} \ . \tag{2.19}$$

The exact probability of error for a quadrature phase shift keying system can be obtained in closed form, however the derivation is quite complex (Bennett and Davey, 1965) and generally serves only the purpose of justifying approximations to simplify the form. The precise expression for probability of symbol error for QPSK in terms of symbol signal-to-noise ratio is:

$$P_s = 2 \operatorname{erfc}\left[\frac{E_s}{N_o}\right]^{1/2} - \frac{1}{2} \operatorname{erfc}^2\left[\frac{E_s}{N_o}\right]^{1/2} \ . \tag{2.20}$$

For any E_s/N_o in the area of particular interest (i.e., $E_s/N_o > 5$) P_s is well approximated by dropping the second term. Also, whenever the symbol error rate is small (say less than 10^{-3}) the bit error rate will be approximately 1/2 the symbol error rate. Therefore the bit error probability for QPSK is generally approximated by the expression:

$$P_b = \operatorname{erfc}\left[\frac{E_s}{N_o}\right]^{1/2} \ . \tag{2.21}$$

Another note of caution is required at this point. Since there are two bits per symbol, the energy per bit $E_b = 1/2\ E_s$, and therefore many authors write the probability of bit error as:

$$P_b = \text{erfc}\left[\frac{2E_b}{N_o}\right]^{1/2} \tag{2.22}$$

and claim the performance to be essentially the same as binary CPSK. The primary advantage of QPSK is to obtain twice the bit rate in approximately the same bandwidth as binary CPSK. When this is done, approximately 3 db additional signal-to-noise ratio is required for the same error rate. The detection schemes are different and it is rather pointless to dwell on how one should be compared with the other.

The probability of error for multi-phase systems beyond four phases cannot be derived precisely in closed form. However an approximate form for N phases, N > 2, has been shown (Cahn, 1959) to produce accurate results. The symbol error probability is given by:

$$P_s = 2\ \text{erfc}\left[\frac{2E_s}{N_o}\sin^2\frac{\pi}{N}\right]^{1/2} . \tag{2.23}$$

If a Grey code is used in assigning symbols (adjacent symbols differ by only one bit) then the probability of bit error can be estimated by:

$$P_b = \frac{P_s}{\log_2 N} \tag{2.24}$$

CPSK with Carrier Phase Reference Error

In any practical communications system the synchronization signals needed to perform coherent detection are not known exactly since

they are derived at the receiver in the presence of noise. When the synchronization signal is used to provide a carrier phase reference for coherent detection of phase shift keying the resulting carrier phase reference error is a random variable and is commonly called phase jitter. A discussion of synchronizing signals and the probability distribution of the phase error (jitter) is contained in Chapter 3.

The immediate effect of carrier phase reference error is degradation in system performance from the optimum or ideal. More specifically, phase jitter increases the probability of error relative to the ideal for a given signal-to-noise ratio. The objective of this section is then to derive an analytical expression from which the increase in the probability of error can be determined.

Rather than initially assuming a probability density function for the phase jitter and attempting to obtain an expression for the probability of error directly, the approach will be to determine the error function conditioned on the jitter so that the average probability of error can be obtained by integrating the expression over the density of the jitter. To determine this conditional probability for CPSK it will be convenient and will lose no generality to assume that $s_0(t)$ and $s_1(t)$ are of equal magnitude but opposite polarity. Then the test statistic G of Eq. (2.1), assuming $s_0(t)$ is sent and introducing 1/T as a normalizing factor, becomes:

$$G(\theta) = \frac{1}{T}\int_0^T [A\sin\omega t + n(t)][A\sin(\omega t + \theta)]dt$$

$$- \frac{1}{T}\int_0^T [A\sin\omega t + n(t)][- A\sin(\omega t + \theta)]dt$$

$$= \frac{2}{T}\int_0^T [A\sin\omega t + n(t)][A\sin(\omega t + \theta)]dt \qquad (2.25)$$

where θ is the assumed phase error. The mean is then (remembering that $n(t)$ has zero mean):

$$E\{G(\theta)\} = E\left\{\frac{2A^2}{T}\int_0^T \sin\omega t \sin(\omega t + \theta)dt\right\}$$

$$= E\left\{\frac{A^2}{T}\int_0^T [\cos(2\omega t + \theta) - \cos\theta]dt\right\} . \qquad (2.26)$$

Now assuming that $\omega = \frac{n\pi}{T}$ for n either an integer or else large compared to unity, the integral of the first term is zero, and

$$E\{G(\theta)\} = -\frac{A^2}{T}\int_0^T \cos\theta\, dt . \qquad (2.27)$$

It can similarly be shown for $s_1(t)$ sent:

$$E\{G(\theta)\} = \frac{A^2}{T}\int_0^T \cos\theta\, dt . \qquad (2.28)$$

The variance of G conditioned on θ for either signal sent will be:

$$\sigma_G^2 = E\{G^2(\theta)\} - E^2\{G(\theta)\} = E\left\{\frac{4}{T}\int_0^T A^2\sin\omega t \sin(\omega t + \theta)\right.$$

$$\left. + n(t)A\sin(\omega t + \theta)]^2 dt - \left[\frac{A^2}{T}\int_0^T \cos\theta\, dt\right]^2\right\} . \qquad (2.29)$$

After some straightforward but messy manipulation this becomes:

$$\sigma_G^2 = \left[\frac{A^2}{T}\int_0^T \cos\theta\, dt\right]^2 + A^2N_o - \left[\frac{A^2}{T}\int_0^T \cos\theta\, dt\right]^2 = A^2N_o \,. \tag{2.30}$$

The variance is independent of the phase error and the overall effect is to reduce the average signal power by:

$$\frac{1}{T}\int_0^T \cos\theta\, dt \,.$$

Note that at this point in the derivation, we have allowed θ to be a function of t; i.e., the phase error may change during the symbol interval.

Now with $E = A^2/2$ (a normalizing factor 1/T was introduced) and letting

$Y = \frac{1}{T}\int_0^T \cos\theta\, dt$ the conditional density becomes

$$p(G|\theta) = \frac{1}{[4\pi EN_o]^{1/2}} \exp\left\{\frac{-[G - 2EY]^2}{4EN_o}\right\} \tag{2.31}$$

substituting:

$$z = \frac{G - 2EY}{\sqrt{2EN_o}}$$

and recalling that the conditional probability of bit error is

$$P_{b|\theta} = \int_0^\infty p(G|\theta)dG \,.$$

We see that

$$P_{b|\theta} = \frac{1}{(2\pi)^{1/2}} \int_{(2E/N_o)^{1/2}\gamma}^{\infty} \frac{z^2 dz}{2} = \operatorname{erfc}\left[\left(\frac{2E}{N_o}\right)^{1/2} \frac{1}{T} \int_0^T \cos\theta \, dt\right] \tag{2.32}$$

This derivation of Eq. (3.32) is straightforward and the results agree with those found in the literature. However, the method used here which is consistent with the previous derivations is thought to be unique.

Although Eq. (2.32) appears simple, it would still be a formidible task to evaluate the expression in general to determine an average probability of error. To further simplify the process, two special cases will be examined. The first will assume that the phase error varies slowly with respect to the data rate so that θ may be considered constant during a symbol interval. The second case of interest is where the error is assumed to vary rapidly over the duration of a single symbol. The transition point between these two cases is a matter of engineering judgment based upon the ratio of the system data rate T^{-1} and the bandwidth of the tracking loop. For most communications problems, the first assumption provides a close approximation to actual system performance. Indeed, most authors do not treat any other case. However, the second case could be applicable for relatively slow data rates such as used in some telemetry systems. For a treatment of the intermediate case, see Lindsey and Simon (1973).

Under the assumption of constant phase error in the symbol interval the conditional error probability becomes:

$$P_{b|\theta} = \operatorname{erfc}\left[\left(\frac{2E}{N_o}\right)^{1/2} \cos\theta\right] \tag{2.33}$$

and the average probability of bit error may be determined by integrating this expression over the probability density function of the phase error $P(\theta)$:

$$P_b = \int_{-\pi}^{\pi} p(\theta)\,\mathrm{erfc}\left[\left(\frac{2E}{N_o}\right)^{1/2}\cos\theta\right]d\theta \ . \tag{2.34}$$

The results of this integration will be discussed in Chapter 3.

In the second case the assumption is made that the phase error varies rapidly over the symbol time interval T. If this is true, then the quantity:

$$Y = \frac{1}{T}\int_0^T \cos\theta(t)\,dt$$

is a good measure of the true time average of the function $\cos\theta\,(t)$, and if this process is ergodic (which is a reasonable assumption) then the time average may be replaced by the statistical mean, i.e.,

$$Y = \overline{\cos\theta}$$

and the average probability of error becomes:

$$P_b = \mathrm{erfc}\left[\left(\frac{2E}{N_o}\right)^{1/2}\overline{\cos\theta}\right] . \tag{2.35}$$

It is interesting to note that, if the random variable θ has zero mean and if its density is symmetrical about zero (which will be shown to be true in many cases), then $\overline{\cos\theta} = 1$ and the jitter has no effect upon this estimate of the average probability of error, at least to the extent that the time averaging is valid. If the mean of θ is not zero then the mean of $\cos\theta$ must be determined by integrating $\cos\theta$ over the probability density of θ.

Similar arguments can now be used to extend these results to QPSK. The conditional probability of bit error in terms of symbol signal-to-noise ratio for Case 1 above is:

$$P_{b|\theta} = \text{erfc}\left[\left(\frac{E_s}{N_o}\right)^{1/2} \cos\theta\right] \tag{2.36}$$

and for Case 2:

$$P_b = \text{erfc}\left[\left(\frac{E_s}{N_o}\right)^{1/2} \overline{\cos\theta}\right] . \tag{2.37}$$

Note that Eq. (2.37) is not a conditional probability since $\overline{\cos\theta}$ is a real number and not a random variable.

CPSK with Symbol Synchronization Error

As with carrier phase reference error, if the synchronization signal used to time the symbol interval is in error, the result is to degrade the system performance from the optimum for coherent detection as previously determined. Again this symbol synchronization error is a random variable and is commonly referred to as baud timing jitter.

The approach to determining the effects of baud timing jitter will also be to obtain an expression for the probability of bit error conditioned on the timing error. The average error probability is then evaluated by integrating the conditional probability over the density of the jitter. The results of this integration will be discussed in Chapter 3.

If baud timing is derived from the same synchronization signal as the carrier phase reference, Stiffler (1971) has shown that in a CPSK system the degredation due to the combined symbol and carrier

phase errors is well approximated by that due to the carrier phase error alone.

In order to better understand the effects of baud timing jitter, in this section it will first be assumed that all symbol timing is obtained from a separate source resulting in independent timing error. It will also be assumed that the error is constant over the duration of a symbol. That this latter is a reasonable assumption will become evident from the discussion of phase-locked-loops in Chapter 3.

It will be instructive to first examine the timing of the integrators in the coherent correlators of the ideal CPSK receiver. With a baud timing error of τ seconds the integration will take place over the interval $(\tau, T + \tau)$. It is evident that the effect of this error will be dependent upon the presence or absence of a symbol transition. If the successive symbols are identical, the timing error will have no effect on the correlator output and thus not affect the probability of error. On the other hand, if transitions occur at every symbol, the period of integration will be reduced by 2τ (since $\rho = -1$). The expected value of the correlator output will then be reduced by the factor $(1 - \frac{2|\tau|}{T})$. If the successive symbols are independent and equally likely to be either of the binary signals, then for binary CPSK the probability of error conditioned on the symbol synchronization error will be:

$$P_{b|\tau} = \frac{1}{2}\,\mathrm{erfc}\left[\frac{2E}{N_o}\right]^{1/2} + \frac{1}{2}\,\mathrm{erfc}\left[\left(\frac{2E}{N_o}\right)^{1/2}\left(1 - \frac{2|\tau|}{T}\right)\right]. \qquad (2.38)$$

This expression has been derived for the symbol interval timing of the correlator integrators and will approximate system degradation

assuming that this timing is independent of the carrier phase reference. Even though this is not always the case in practical receivers, the derivation is of considerable value. Indeed, the result can readily be seen to provide a valid expression for estimation of the increase in error probability for retiming of the detected data. This can be visualized by considering the retiming to be the timing of the decision element at the output of the correlators.

A slightly different expression for the effect on error probability will be obtained if the retimed data is in other than a no-return-to-zero (NRZ) format. This will be discussed later in this chapter.

Differential Phase Shift Keying (DPSK)

Two distinct forms of DPSK will be studied, both of which involve the differential encoding of the digital data prior to PSK modulation. In the first case the demodulation is coherent, while in the second a differential detection process is used.

Differential encoding of a data stream refers to the process of sending a signal based upon the present information bit and the preceding transmitted bit. This is normally accomplished by a modulo two adder (exclusive or gate) and a one bit delay element as shown in Fig. 2.3. In this way a "one" is transmitted if the present information bit differs from the previously transmitted bit, and a zero is transmitted if they are the same.

This encoding process is commonly used in coherent PSK systems where carrier recovery is accomplished at the receiver from a suppressed

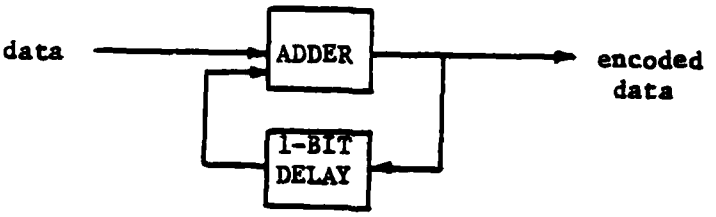

Fig. 2.3. Differential Encoding.

carrier signal. Most such carrier recovery systems will suffer a phase ambiquity of π radians in the binary case. The reason for differential encoding of the data stream is that the decoded output will be correct for either phase, even in the presence of a π radians phase slip (one error will occur).

Coherent Detection

The probability of bit error for the binary case is readily determined from the following logic. Correct decoding of the nth information bit will occur if the nth and the (n-1)th, received bits are correctly detected or if they are both incorrectly detected. Therefore, the probability of error will be the sum of the probability that the nth bit is detected incorrectly and that n-1 was correct plus the probability n is correct and n-1 is incorrect. Assuming that the probabilities of detection error are independent and equal for every bit, the probability of bit error for coherent detection of a differentially encoded signal becomes:

$$P_b = P\{n_c\ (n-1)_e\} + P\{n_e\ (n-1)_c\} = 2\ P_e(1-P_e) \tag{2.39}$$

where P_e is the probability of bit error for binary CPSK:

$$P_e = \text{erfc}\left(\frac{2E}{N_o}\right)^{1/2}$$

then this becomes

$$P_b = 2\ \text{erfc}\left(\frac{2E}{N_o}\right)^{1/2}\left[1 - \text{erfc}\left(\frac{2E}{N_o}\right)^{1/2}\right] \tag{2.40}$$

A general expression of probability of symbol error for an N-phase system can be found in Lindsey (1973). The only other case for which an exact closed form is available is the quadriphase system. The probability of symbol error is:

$$P_s = 4\ \text{erfc}\left(\frac{E_s}{N_o}\right)^{1/2} - 4\ \text{erfc}^2\left(\frac{E_s}{N_o}\right)^{1/2} + 2\ \text{erfc}^3\left(\frac{E_s}{N_o}\right)^{1/2} - \frac{1}{2}\ \text{erfc}^4\left(\frac{E_s}{N_o}\right)^{1/2} \tag{2.41}$$

where E_s/N_o is the symbol signal-to-noise ratio.

The effects of carrier phase reference error and symbol synchronization error for coherent detection of differentially encoded binary PSK are readily obtained from the results derived for CPSK and from Eq. (2.40). For carrier phase jitter, the conditional probability of bit error is (assuming constant error over a symbol duration):

$$P_{b|\theta} = 2\ \text{erfc}\left(\frac{2E}{N_o}\right)^{1/2}\cos\theta\left[1 - \text{erfc}\left(\frac{2E}{N_o}\right)^{1/2}\cos\theta\right]. \tag{2.42}$$

The probability of error conditioned on baud timing jitter is similarly:

$$P_{b|\tau} = 2\ \text{erfc}\left[\left(\frac{2E}{N_o}\right)^{1/2}\left(1 - \frac{2|\tau|}{T}\right)\right]\left\{1 - \text{erfc}\left[\left(\frac{2E}{N_o}\right)^{1/2}\left(1 - \frac{2|\tau|}{T}\right)\right]\right\}. \tag{2.43}$$

Differential Detection

Differential detection of differentially encoded signals is what is normally termed differential phase shift keying (DPSK). In some communications systems it is not desirable to obtain and maintain a coherent phase reference in the receiver. DPSK is an ingenious method of avoiding the problem. Detection is accomplished by phase comparison of successive symbols, thus information is conveyed by the phase transitions between pulses rather than by the absolute phase of the pulses.

Differential detection is implemented very simply by coherently detecting each pulse using the previous pulse delayed one symbol period as the reference signal. This is illustrated in the block diagram of Fig. 2.4. Unfortunately, the analysis of the system to determine the probability of error is nowhere near so simple.

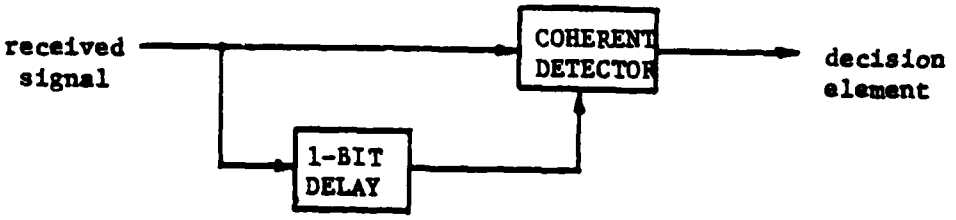

Fig. 2.4. Differential Decoding of PSK.

There are a number of methods (all with the same result) for deriving an expression for error probability. One method, attributed to Stein and Jones (1967), involves the diagonalization of a quadratic form to obtain an expression similar to that which will be integrated to obtain the probability of error for non-coherent FSK in the next section. Another method for calculation of the error rate for a specified signal-to-noise ratio is to obtain the probability density function for the phase of a single pulse (Doob, 1953). The probability that the difference phase deviates by more than 90 degrees from its proper value can then be obtained by graphical integration.

An alternate technique due to Cahn (1959) which provides a closed form solution is only slightly less mathematically complex than Stein and Jones' method but provides some graphical insight into the physical situation.

Suppose that the phase of the noise-distorted first pulse has the value θ with respect to its undistorted position. The probability of error conditioned on θ is then the probability that the phasor representing the noise distorted second pulse will cross the decision boundary indicated in Fig. 2.5. Only the component of noise of the second pulse that is parallel to the distorted position of the first pulse can cause an error. From the figure it can be seen that this conditional probability of error is:

$$P_{b|\theta} = \frac{1}{\sqrt{2\pi N_o}} \int_{\sqrt{2E}\cos\theta}^{\infty} \exp\left[\frac{-x^2}{2N_o}\right] dx \qquad (2.44)$$

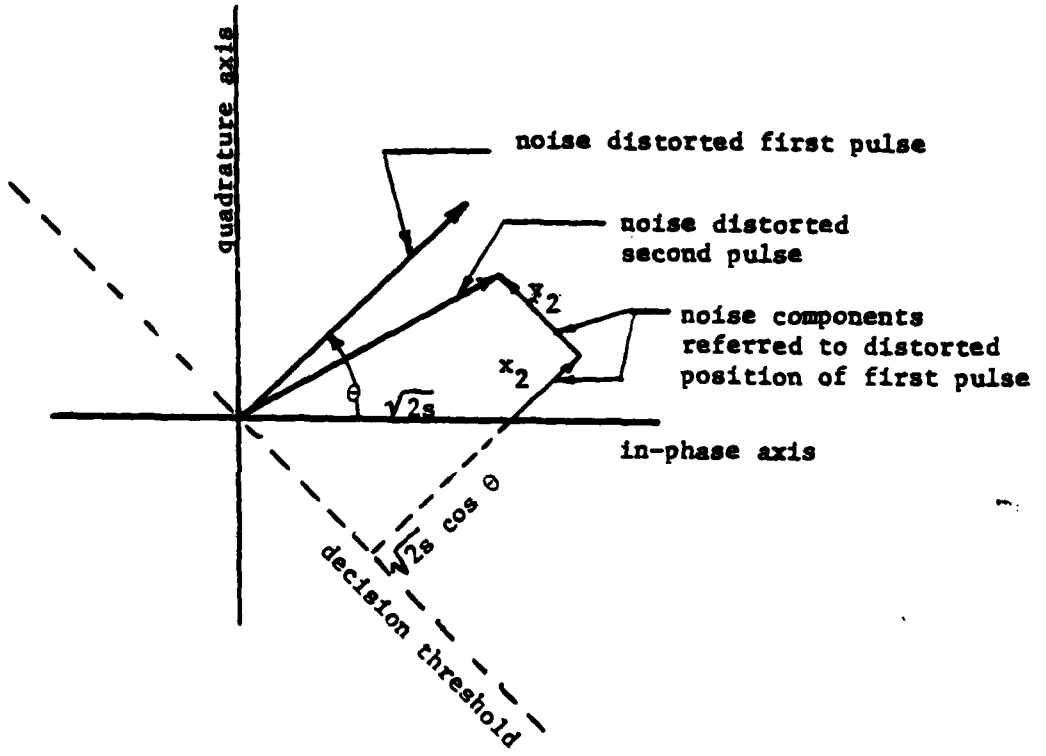

Fig. 2.5. Effects of Noise on Differential Detection of PSK.

Here it has been assumed that the noise is again white and Gaussian and that E is the signal power. The form of Eq. (2.44) is quite familiar and can be expressed as:

$$P_{b|\theta} = \text{erfc}\left[\left(\frac{2E}{N_o}\right)^{1/2}\cos\theta\right]. \tag{2.45}$$

That this expression is identical to that derived for coherent detection with carrier phase reference error is quite revealing. In coherent detection, when the phase reference is perfect, the probability of error is a function only of the magnitude of the signal-to-noise ratio. If there is no phase variance between the pulses used for

differential detection, should not the two processes be equivalent? That this is so is intuitively gratifying. That the effectiveness of the differential detection scheme is diminished by a factor of the cosine of the reference phase error is a logical extension.

It remains then to integrate the conditional function of Eq. (2.45) over the probability density of the phase angle θ to obtain an expression for average probability of error. Rice (1954) has derived an expression for the density of the phase of a sinusoid plus Gaussian noise. The function is quite complex but can be asymptotically approximated by:

$$p(\theta) \doteq \frac{\cos\theta}{\sqrt{\pi N_o/E}} \exp\left(\frac{-E}{N_o}\sin^2\theta\right) \qquad (-\pi \le \theta \le \pi) \ . \tag{2.46}$$

A graphical illustration of this distribution for several values of signal-to-noise ratio is shown in Fig. 2.6.

This expression is then substituted into:

$$P_b = \int_{-\pi}^{\pi} p(\theta)\ \mathrm{erfc}\left[\left(\frac{2E}{N_o}\right)^{1/2}\cos\theta\right] d\theta \ . \tag{2.47}$$

The integration is performed by first expanding the functions in an absolutely convergent power series in $\left(\frac{2E}{N_o}\right)^{1/2}\cos\theta$. All the terms except a single constant term will contain $\cos\theta$ raised to an odd power which integrate to zero over a full cycle. The remaining constant term yields the probability of error for DPSK:

$$P_b = \frac{1}{2}\exp\left(\frac{-E}{N_o}\right) \ . \tag{2.48}$$

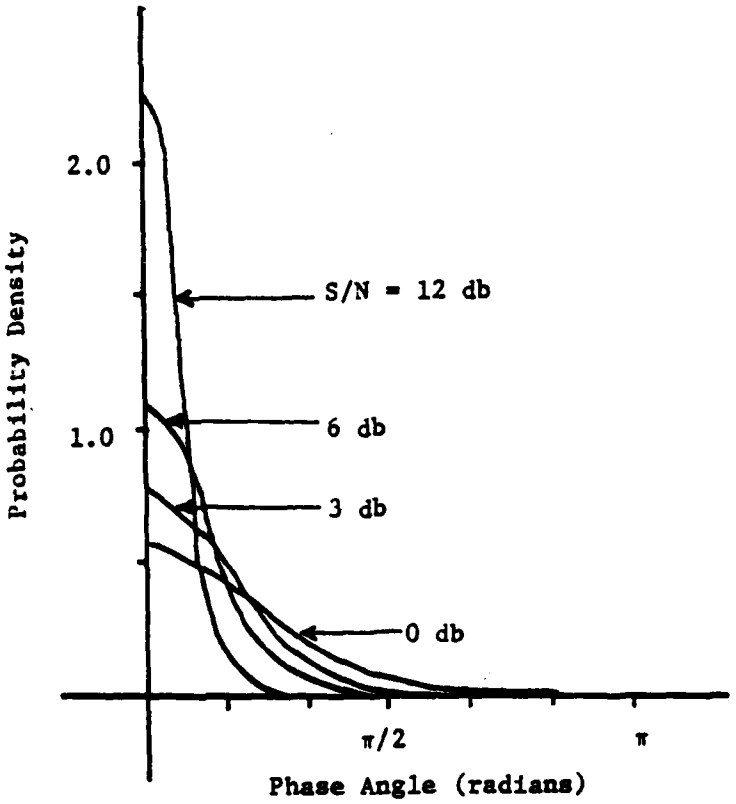

Fig. 2.6. Probability Density of Phase Angle for Sine Wave Plus Gaussian Noise.

A comparison of the characteristic curves of bit error rate (BER) versus signal-to-noise ratio for CPSK, DPSK, and other modulation and detection techniques is contained in Chapter 3.

Improved schemes for differential detection have been devised which utilize the phase of several prior input pulses for reference. It has been shown that tight upper and lower bounds for the probability of error of such systems exist and are exactly those expressions derived above (Lindsey and Simon, 1973). That is:

$$2\ \text{erfc}\left(\frac{2E}{N_o}\right)^{1/2}\left[1 - \text{erfc}\left(\frac{2E}{N_o}\right)^{1/2}\right] \leq P_b \leq \frac{1}{2}\exp\left(\frac{-E}{N_o}\right) \quad . \tag{2.49}$$

For multiple phase shift keying ($N \geq 4$), only approximate expressions can be derived for probability of error. A common expression approximating the symbol error probability due to Cahn (1959) is:

$$P_s = \frac{1}{2}\exp\left(-\frac{E_s}{N_o}\sin^2\frac{\pi}{N}\right) \quad . \tag{2.50}$$

The effects of carrier phase reference error have already been taken into account in the expression for average probability of error in a DPSK system. It is interesting to note from the density function given in Eq. (2.46), for the higher signal-to-noise ratios and for small angular deviations, that the difference angle between successive pulses is approximately Gaussian. As will be seen and discussed in some detail in Chapter 3, this results in an identical approximation to the effects of jitter from a phase-locked-loop upon coherent detection.

The effects of symbol synchronization error upon binary DPSK is analogous to coherent detection of PSK. A timing error at the single

correlator of Fig. 2.1 affects the magnitude of the output by the factor $\left(1 - \frac{2|\tau|}{T}\right)$. The conditional probability of bit error for DPSK in the presence of baud timing jitter is then:

$$P_{b|\tau} = \frac{1}{2} \exp\left[\frac{-E}{N_o}\left(1 - \frac{2|\tau|}{T}\right)^2\right]. \tag{2.51}$$

The density function of the timing error will of course be dependent upon the timing source and the average probability of bit error can be determined by integrating the conditional probability over the function for all values of τ.

Amplitude Shift Keying and Frequency Shift Keying Systems

Amplitude shift keying (ASK) and frequency shift keying (FSK) have been included under the same major heading because of the similarities in the derivations of the error probabilities and the close relationship between the results.

In binary ASK the amplitude of the carrier is switched between two levels, usually between the extremes of full on and totally off. In this case, ASK is most often referred to as on-off keying (OOK). This is the case that will be examined here. The carrier on condition will typically correspond to a binary one and the off condition to zero thereby conveying the digital information.

Switching between two constant but different frequency sources with the carrier selected being dependent upon the binary code is termed FSK. Error probabilities derived for the binary case will be extended

to so-called M-ary systems where M different frequencies (or other orthogonal waveforms) are used to transmit information.

The FSK waveform may be viewed in format as two (or more) interlaced ASK signals at different frequencies. It is this fact that will be used in developing the similarities in the error probabilities. In all cases considered here, it will be assumed that the transmitted pulse envelope is rectangular in shape with no spaces between pulses. Other pulse shapes will be examined later in the discussion of baseband modulation systems.

Coherent Detection of ASK and FSK

In the discussion of the performance of the ideal coherent communications receiver in the presence of additive white Gaussian noise the probability of bit error was shown to be:

$$P_b = \text{erfc}\left[\frac{E}{N_o}(1-\rho)\right]^{1/2} . \tag{2.52}$$

For OOK the average signal energy and correlation coefficient as defined in Eqs (2.10) and (2.11) are:

$$E = \frac{1}{2}\int_0^T s_1^2(t)\,dt \quad \text{and} \quad \rho = 0 . \tag{2.53}$$

The probability of bit error is therefore:

$$P_b = \text{erfc}\left(\frac{E}{N_o}\right)^{1/2} . \tag{2.54}$$

Similarly for FSK:

$$E = \frac{1}{2} \int_0^T [s_0^2(t) + s_1^2(t)]\, dt \quad \text{and} \quad \rho = 0 \tag{2.55}$$

and the probability of bit error is again

$$P_b = \text{erfc} \left(\frac{E}{N_o}\right)^{1/2} . \tag{2.56}$$

So for the same average energy per bit the error probabilities are identical. However, if the signal amplitude in the OOK case is constrained to be no larger than for the FSK signal (which provides a more reasonable comparison), the FSK performance will be 3 db better than the OOK (see Chapter 3 for performance curves).

Jitter Effects on Coherent Detection of ASK and FSK

The effects of carrier phase reference error and symbol synchronization error on coherent FSK detection can readily be seen to be very similar to the effects on coherent PSK as has been described previously.

In the case of carrier phase jitter a derivation similar to that for CPSK can be accomplished to verify the following results. However, it should be intuitively evident that the expected values of the integrator outputs of the ideal correlation detector will be modified by the factor:

$$y = \frac{1}{T} \int_0^T \cos \vartheta(t)\, dt \tag{2.57}$$

and that the variances of the outputs are unaffected by the jitter. If the phase error is assumed constant over a bit period the probability

of bit error conditioned on θ becomes:

$$P_{b|\theta} = \text{erfc}\left[\left(\frac{E}{N_o}\right)^{1/2} \cos\theta\right] . \tag{2.58}$$

The average probability of error is then determined by integrating the conditional probability over the density of θ as was described previously. Similarly, if the phase error is assumed to vary rapidly over a bit period and the process is ergodic, then the time average may be replaced by the statistical mean and y becomes:

$$y = \overline{\cos\theta}$$

a constant, and the average probability of error is:

$$P_b = \text{erfc}\left[\left(\frac{E}{N_o}\right)^{1/2} \overline{\cos\theta}\right] . \tag{2.59}$$

The effects of symbol synchronization error on coherent detection of FSK are not quite the same as for CPSK. As before this is seen by considering the timing of the integrators in the coherent correlators of the ideal CFSK receiver. With a baud timing error of τ seconds the integration takes place over the interval $(\tau, T+\tau)$. If successive symbols are identical, the correlator output will be unaffected by the timing error. However, if transitions occur at every symbol, the period of integration is effectively reduced by τ (since $\rho=0$). This results in an expression for probability of error for CFSK conditioned on symbol synchronization error:

$$P_{b|\tau} = \frac{1}{2}\,\text{erfc}\left(\frac{E}{N_o}\right)^{1/2} + \frac{1}{2}\,\text{erfc}\left[\left(\frac{E}{N_o}\right)^{1/2}\left(1 - \frac{|\tau|}{T}\right)\right] . \tag{2.60}$$

It should be restated that this expression assumes the signal pulses are rectangular and that the baud timing is independent of the carrier phase reference. The average probability of error may then be found by integrating this expression over the probability density function of the timing error τ.

In the case of coherent detection of OOK the effect of carrier phase reference and symbol synchronization errors are slightly different. This is readily visualized by considering the ideal receiver to be a single correlator whose output is compared to a threshhold half the magnitude of the expected value of the output (with no timing error present). Then assume a carrier phase reference error ϑ. Again the variance of the correlator output will be unaffected. The mean value of the output will be affected only when the signal is present. Assuming that signal and no signal are equally probable, the conditional probability of bit error for coherent detection of OOK in the presence of carrier phase reference error is:

$$P_{b|\vartheta} = \frac{1}{2}\,\mathrm{erfc}\left(\frac{E}{N_o}\right)^{1/2} + \frac{1}{2}\,\mathrm{erfc}\left[\left(\frac{E}{N_o}\right)^{1/2}\frac{1}{T}\int_0^T \cos\vartheta\,dt\right]. \quad (2.61)$$

This reduces to expressions similar to Eqs. (2.58) and (2.59) when the phase error is assumed to be constant over a symbol period:

$$P_{b|\vartheta} = \frac{1}{2}\,\mathrm{erfc}\left(\frac{E}{N_o}\right)^{1/2} + \frac{1}{2}\,\mathrm{erfc}\left[\left(\frac{E}{N_o}\right)^{1/2}\cos\vartheta\right] \quad (2.62)$$

and when assumed to vary rapidly over each symbol period:

$$P_{b|\vartheta} = \frac{1}{2}\,\mathrm{erfc}\left(\frac{E}{N_o}\right)^{1/2} + \frac{1}{2}\,\mathrm{erfc}\left[\left(\frac{E}{N_o}\right)^{1/2}\overline{\cos\vartheta}\right]. \quad (2.63)$$

Again, although the derivation of Eq. (2.61) is relatively straightforward, it could not be found in the literature.

A similar reasoning is used to obtain the conditional probability of error for coherent OOK in the presence of baud timing error. In CPSK the period of integration was effectively reduced by 2τ when signal transitions occurred. With OOK since the correlation coefficient is zero as in CFSK rather than minus one, the integration period is reduced by τ when the signals are alternating. The output of the correlator is $\frac{A^2}{2}(T-\tau)$ during a mark and $\frac{A^2}{2}\tau$ during a space. The probability of error assuming a state transition is:

$$P_e = \int_{\frac{A^2T}{4}}^{\infty} \frac{1}{\sqrt{2\pi EN_o}} \exp\left[\frac{-\left(x - \frac{A^2\tau}{2}\right)^2}{2EN_o}\right] dx \ . \qquad (2.64)$$

However, for OOK, $E = \frac{A^2T}{4}$. Then by a change of variables and assuming that the probability of a state transition at any bit is one-half, the overall probability of error conditioned on symbol synchronization error is:

$$P_b = \frac{1}{2}\,\mathrm{erfc}\left(\frac{E}{N_o}\right)^{1/2} + \frac{1}{2}\,\mathrm{erfc}\left[\left(\frac{E}{N_o}\right)^{1/2}\left(1 - \frac{2|\tau|}{T}\right)\right] \ . \qquad (2.65)$$

Non-coherent Detection of ASK and FSK

Non-coherent detection of ASK and FSK is much more commonly used than coherent detection since it is much simpler and less costly to implement and, as shall be seen, is only slightly less effective. However, these benefits do not carry over to the mathematical analysis.

Derivation of the probabilities of error for non-coherent detection are much more complex than for coherent detection and require the evaluation of formidable integrals that in some cases cannot be accomplished in closed form. The attempt here will be to relate the mathematics to a physical understanding of the detection process. References to commonly available literature will be provided for much of the detailed derivation. Sufficient mathematical analysis will be presented to insure an understanding of the effects of jitter and other receiver anomalies on the probabilities of error.

It can be shown [see Whalen (1971) for example] that the optimum receiver for detecting a signal of known amplitude and frequency but unknown phase in the presence of white Gaussian noise is the quadrature receiver. An equivalent and more common receiver utilizes a matched filter and an envelope detector. The output of the envelope detector is compared to a preset threshhold to determine whether a signal is or is not present at the input to the receiver. Obviously a single matched filter and envelope detector will be sufficient for an OOK system, whereas FSK detection will require a number equal to the number of possible signals (2 for binary, etc.). The filter in each case will be matched to one of the possible signal frequencies. For the moment, a single matched filter and envelope detector shall be considered.

The probability of error for the receiver can be calculated if the probability density function of the output can be determined. Remember that in the case of the coherent detector the output was found to be Gaussian and therefore completely determined by the mean and

variance. The output of the non-coherent receiver is not Gaussian, but its density can be determined in terms of the input signal-to-noise ratio.

Assume that if a signal is present at the input to the matched filter, it has the form:

$$r(t) = A \cos (\omega_c t + \theta) + n(t) . \tag{2.66}$$

The amplitude A and frequency ω_c are assumed known and θ is a random variable uniformly distributed $(0, 2\pi)$. The noise, n(t) is assumed to be white Gaussian with zero mean and variance $N_o/2$.

The output of a matched filter with a sine wave input is shown in Fig. 2.7. In a coherent matched filter receiver, the phase of the input would be known so that the filter output could be sampled at precisely the correct time T to correspond to the output of a correlator (maximum output). Since the phase of the input to the non-coherent receiver is unknown it is necessary to determine the distribution of the envelope of the signal plus noise at a specific instant of time.

If n(t) is assumed to be a narrow band process about the frequency ω_c (filters will normally precede the detectors) then it can be expressed in the form (Rice, 1954):

$$n(t) = x(t) \cos \omega_c t - y(t) \sin \omega_c t \tag{2.67}$$

and r(t) is then:

$$r(t) = [A \cos \vartheta + x(t)] \cos \omega_c t - [A \sin \vartheta + y(t)] \sin \omega_c t .$$

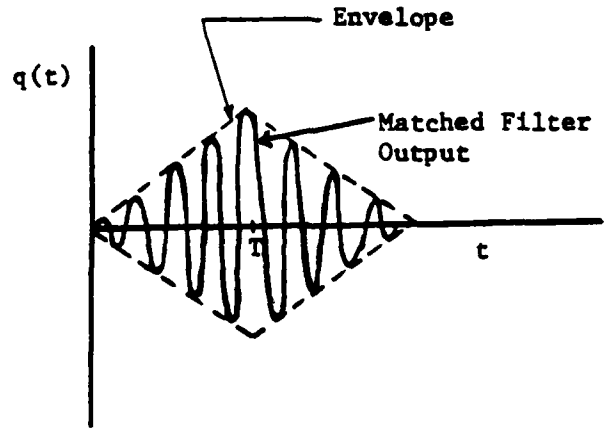

Fig. 2.7. Matched Filter Output and Envelope for Sine Wave Input.

The signal envelope can then be expressed as (Feller, 1957):

$$q(t) = [q_c^2(t) + q_s^2(t)] \tag{2.68}$$

where:

$$q_c(t) = A \cos \theta + x(t)$$

$$q_s(t) = A \sin \theta + y(t) \ .$$

For any given value of θ and considering, for the present, a fixed $t=T$, both q_c and q_s are Gaussian random variables which may be shown to be uncorrelated. Then the means are:

$$E\{q_c\} = A \cos \theta \quad \text{and} \quad E\{q_s\} = A \sin \theta$$

and the variances are equal:

$$\sigma^2 = N_o/2 \ .$$

The joint density function of q_c and q_s conditioned on θ is:

$$p(q_c, q_s|\theta) = \frac{1}{2\pi\sigma^2} \exp\left\{\frac{-1}{2\sigma^2}\left[(q_c - A\cos\theta)^2 + (q_s - A\sin\theta)^2\right]\right\} \tag{2.69}$$

A change of variables to

$$q = (q_c^2 + q_s^2)^{1/2} \qquad q \geq 0$$

and

$$\phi = \arctan q_s/q_c \qquad 0 \leq \phi \leq 2\pi$$

results in the conditional density function:

$$p(q,\phi|\theta) = \frac{q}{2\pi\sigma^2} \exp\left\{\frac{-1}{2\sigma^2}\left[q^2 + A^2 - 2Aq\cos(\theta-\phi)\right]\right\} . \tag{2.70}$$

The marginal density of q given θ can then be found:

$$p(q|\theta) = \int_0^{2\pi} p(q,\phi|\theta)\, d\phi$$

$$= \frac{q}{2\pi\sigma^2} \exp\left\{\frac{-1}{2\sigma^2}\left[q^2+A^2\right]\right\} \int_0^{2\pi} \exp\left[\frac{Aq}{\sigma^2}\cos(\theta-\phi)\right] d\phi \tag{2.71}$$

The integral is recognized as the modified Bessel function of the first kind of order zero:

$$\int_0^{2\pi} \exp\left[\frac{Aq}{\sigma^2}\cos(\theta-\phi)\right] d\phi = 2\pi\, I_o\left(\frac{Aq}{\sigma^2}\right) .$$

The density function of the envelope of the signal plus noise is then independent of θ and is expressed using the subscript 1 to indicate signal is present (this is the Rician density function):

$$p_1(q) = \frac{q}{\sigma^2} \exp\left[\frac{-1}{2\sigma^2}(q^2 + A^2)\right] I_o\left(\frac{Aq}{\sigma^2}\right), \qquad q \geq 0 \tag{2.72}$$

The probability density function for noise only at the input to the detector (subscript 0 indicating no signal present) can be found by letting A = 0. This is the Rayleigh distribution:

$$P_0(q) = \frac{q}{\sigma^2} \exp\left(\frac{-q^2}{2\sigma^2}\right), \qquad q \geq 0 \tag{2.73}$$

The Rician and Rayleigh distributions are shown in Fig. 2.8a. If the decision threshhold for determining the presence of a signal is designated V_T, then the probability of error for OOK will be found from the expression:

$$P_b = \frac{1}{2} \int_{V_T}^{\infty} p_0(q)\, dq + \frac{1}{2} \int_{0}^{V_T} p_1(q)\, dq \quad . \tag{2.74}$$

These integrals may be differentiated with respect to V_T and the result set equal to zero to determine the optimum value for V_T. By Leibnitz's rule it is readily seen that the optimum threshhold must satisfy:

$$\frac{1}{2} [-p_0 (V_T) + p_1(V_T)] = 0 \tag{2.75}$$

which corresponds to the intersection of the two density functions as shown in Fig. 2.8a. Although this appears simple from the diagram, reduction of Eq. (2.75) produces a transcendental equation. An approximate solution given by Stein and Jones (1967) is:

$$V_T = \frac{A}{2} \left(1 + \frac{8N_o}{A^2}\right)^{1/2} \quad . \tag{2.76}$$

That the optimum threshhold is a function of the signal-to-noise ratio is evident from Fig. 2.8b which illustrates normalized Rician densities.

(a)

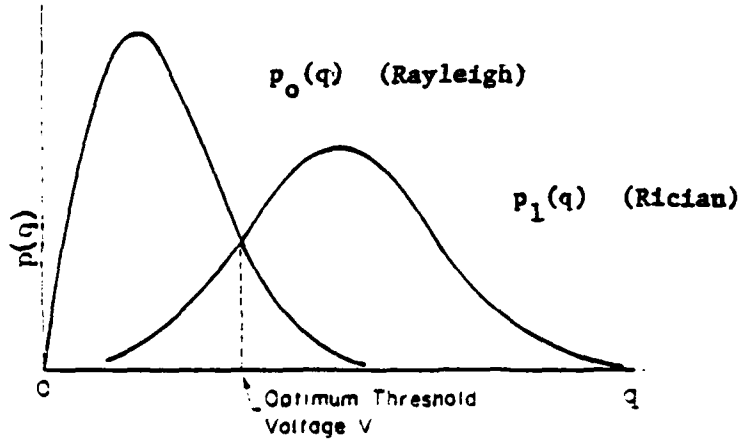

(b)

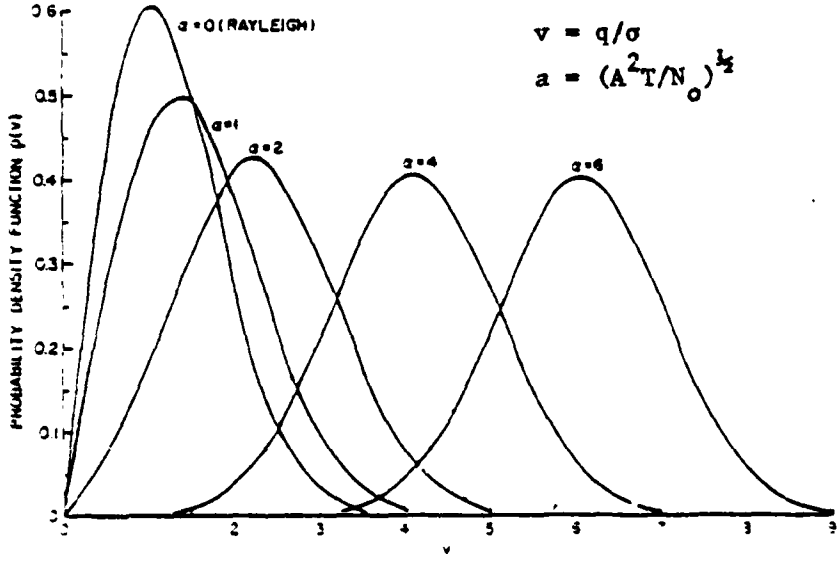

Fig. 2.8. Rayleigh and Rician Probability Density Functions.

a. Optimum threshhold for ASK
b. As a function of signal-to-noise ratio.

If a large signal-to-noise ratio is assumed so that $V_T \simeq A/2$, then the probability of error for non-coherent detection of OOK may be approximated by the expression (Schwartz, Bennett, and Stein, 1966)

$$P_b \simeq \frac{1}{2}\left[1 + \left(\frac{N_o}{\pi E}\right)^{1/2}\right] \exp\left(\frac{-E}{2N_o}\right) \tag{2.77}$$

where $E = \frac{A^2T}{4}$ as previously defined is the long term average signal energy per symbol assuming equally probably zeros and ones.

For non-coherent detection of binary FSK, two matched filters and envelope detectors are required, one matched to each of the two signal frequencies ω_0 and ω_1. The input r(t) is signal plus noise $r(t) = s_i(t) + n(t)$ as previously described. It will be assumed that the signal amplitudes are equal $s_i = A \sin(\omega_i t + \theta)$ where θ is a random variable uniform $(0,2\pi)$ and that the average energy per symbol is $E = AT^2/2$. It will also be assumed that the outputs of the detectors q_0 and q_1 are statistically independent. This is not strictly true since each of the signals are time limited and their true spectra are infinite. However, if the difference $|\omega_0-\omega_1|$ is sufficiently large, the spillover of energy into the wrong filter will be small and may be neglected.

The decision will now be to choose the output that is greater. To determine the probability of error, the density functions of the outputs q_0 and q_1 must again be examined. If signal s_1 is present, the output q_1 will be Rician dependent upon the signal-to-noise ratio and the output q_0 will be Rayleigh distributed. The opposite will be true if signal s_0 is present. From the assumed symmetry it is evident that

the probability of error can be determined by assuming signal s_1 is present and calculating the probability that output q_0 is greater than q_1. The average error probability is found by averaging over all values of q_1:

$$P_b = \int_0^\infty p_1(q_1) \left[\int_{q_1}^\infty p_0(q_0)\, dq_0 \right] d\, q_1 \,. \tag{2.78}$$

This function has been evaluated (Reiger, 1953) with the result for average probability of error for non-coherent detection of binary FSK:

$$P_b = \frac{1}{2} \exp\left(\frac{-E}{2N_o}\right) \,. \tag{2.79}$$

For large values of signal-to-noise ratio it is evident that the probabilities of error for non-coherent ASK and FSK are almost identical for the same average symbol energies. Comparisons of the characteristic BER curves will be made in Chapter 3.

Jitter Effects on Non-coherent Detection of ASK and FSK

Since by definition non-coherent detection implies independence of phase, there will be no effects of carrier phase error. There is, however, a possibility of increased probability of error due to frequency instability of the received signal. An expression for probability of symbol error, conditioned on a fixed normalized frequency error λ_f has been derived by Chadwick (1969) for non-coherent detection of M orthogonal signals:

$$P_{s|\lambda_f} = 1 - \int_0^\infty y \left[1 - \exp\left(\frac{-y^2}{2}\right)\right]^{M-1} \exp\left\{-\frac{1}{2}\left[y^2 + 2\frac{E}{N_o}\left(\frac{\sin\pi\lambda_f}{\pi\lambda_f}\right)^2\right]\right\}$$

$$\times\ I_0\left[\left(\frac{2E}{N_o}\right)^{1/2}\left(\frac{\sin\pi\lambda_f}{\pi\lambda_f}\right) y\right] dy \qquad (2.80)^*$$

The difficulty of evaluating the expression (2.80) places some limitations on the practicality of its use. In addition, the expression assumes an optimum filter, perfect timing, rectangular pulses, and a knowledge of the distribution of the frequency error. More practically, a major effect of anticipated frequency error on the design of the non-coherent receiver is that optimum filters are not necessarily desirable even if they were physically realizable.

It is evident that to quantify the effect of frequency error on average bit error rate requires assumptions that are not totally practical. A qualitative discussion of this effect will be given in Chapter 3.

An expression for the effects of symbol synchronization error has also been derived by Chadwick and Springett (1970). The probability of symbol error conditioned on a fixed normalized timing error λ_t for non-coherent detection of M orthogonal signals is:

$$P_{s|\lambda_t} = 1 - \int_0^\infty 1 - Q\left[\left(\frac{2E}{N_o}\right)^{1/2} \lambda_t y\right] \left[1 - \exp\left(\frac{-y^2}{2}\right)\right]^{M-2}$$

$$\times\ y \exp\left\{-\frac{1}{2}\left[y^2 + 2\left(\frac{E}{N_o}\right)(1 - \lambda_t)\right]^2\right\} I_0$$

$$\times\left[\left(\frac{2E}{N_o}\right)^{1/2} (1 - \lambda_t) y\right] dy \qquad (2.81)$$

---

*In this and several other equations to follow the symbol × is meant to indicate multiplication of additional terms in the integrand.

where $Q[\alpha,\beta]$ is Markum's Q-function which is defined for a normalized Rician distribution in a manner similar to the complimentary error function for a Gaussian distribution (Bennett and Davey, 1965).

$$Q(\alpha,\beta) = \int_{\beta}^{\infty} y \exp\left(\frac{-y^2 + \alpha^2}{2}\right) I_0 (\alpha y)\, dy \quad . \tag{2.82}$$

As was the case for frequency error, the expression (2.81) also assumes an optimum filter and rectangular pulses. A simpler expression similar to that derived for coherent detection in the presence of baud timing error can be obtained under these assumptions by examining the envelope of the output of the matched filter with a sine wave plus a zero mean, white Gaussian noise input. The fact that the noise has zero mean will assure us that the expected value of the envelope will be the same as that for a sine wave input only as was shown in Fig. 2.7. A mathematical proof of this statement is quite difficult, however experimental verification is readily available from most discussions of matched filters [see Gregg (1977) for example].

It can be shown (Whalen, 1971) that near time T the envelope is approximately a linear function of time. The effect of a timing error is then to produce the same modifying factor in the expression for bit error probability as was determined in the coherent detection case. The probability of bit error for non-coherent detection of OOK conditioned on symbol synchronization error is given by:

$$P_{b|\tau} = \frac{1}{4} \exp\left(\frac{-E}{2N_o}\right) + \frac{1}{4} \exp\left[\left(\frac{-E}{2N_o}\right)\left(1 - \frac{2|\tau|}{T}\right)^2\right] \tag{2.83}$$

and for binary FSK is:

$$P_{b|\tau} = \frac{1}{4} \exp\left(\frac{-E}{2N_o}\right) + \frac{1}{4} \exp\left[\left(\frac{E}{2N_o}\right)\left(1 - \frac{|\tau|}{T}\right)^2\right] . \qquad (2.84)$$

Although these are more simple expressions and give us better insight into the physical situation, the same assumptions that other aspects are optimum have been made. It will be illustrated in Chapter 3 that the simplified expressions, which are thought to be original here, produce results that are comparable to Chadwick's.

M-ary Systems

The probability of bit error in a system transmitting an orthogonal set of M signals is a function of the scheme used to encode the information into the symbol set. The amount of information in bits is given by

$$n = \log_2 M . \qquad (2.85)$$

An upper bound for the probability of symbol error in a coherent detection system is given by (Wozencraft and Jacobs, 1965):

$$P_s(M) \leq (M-1)\ \text{erfc}\left(\frac{E_s}{N_o}\right)^{1/2} \qquad M \geq 2 \qquad (2.86)$$

An almost identical expression has been formed (Lindsey, 1965) for an upper bound on the probability of symbol error in a non-coherent detection system:

$$P_s(M) \leq \left(\frac{M-1}{2}\right) \exp\left(\frac{-E_s}{2N_o}\right) \qquad M \geq 2 \qquad (2.87)$$

The effects of jitter on M-ary systems are simple extensions of those found for coherent and non-coherent detection of FSK as given in

the previous sections. However, in the M-ary case the probability that a given symbol will be followed by a like symbol is 1/M (given that all symbols are equally likely). Therefore, the probability of symbol error conditioned on symbol timing error τ is for coherent detection:

$$P_{s|\tau}(M) \leq \frac{(M-1)}{M} \operatorname{erfc}\left(\frac{E_s}{N_o}\right)^{1/2} + \frac{(M-1)^2}{M} \operatorname{erfc}\left[\left(\frac{E_s}{N_o}\right)^{1/2} \left(1 - \frac{|\tau|}{T}\right)\right] \tag{2.88}$$

and for non-coherent detection:

$$P_{s|\tau}(M) \leq \frac{(M-1)}{2M} \exp\left(\frac{-E_s}{2N_o}\right) + \frac{(M-1)^2}{2M} \exp\left(\frac{-E_s}{2N_o}\right)\left[\left(1 - \frac{|\tau|}{T}\right)^2\right]. \tag{2.89}$$

Baseband Systems

Baseband signaling is the process of transmitting information over a frequency band from zero up the maximum of the information bandwidth without (or prior to) the modulation of a higher frequency carrier. Baseband modulation for digital communications is thus the converting of digital information into pulse waveshapes.

Transmission of information at baseband is most often restricted to very short distances where noise is not a factor. However, in some cases (such as the Bell System T-1 Carrier) baseband is used for direct transmission over repeatered cable systems. Although external channel noise (impulse noise) rather than internal receiver noise is generally the limiting factor for probability of error in cable systems, the ordering of digital modulation systems by relative performance in the

presence of Gaussian noise will also be a valid ordering for impulse noise performance (Lucky, Salz, and Weldon, 1968).

In other instances, where a baseband signal is used to key (modulate) a carrier prior to transmission, detection at the receiver is sometimes accomplished at baseband after removal of the carrier (for example, the VICOM T1-4000/FRC-162 system described in Chapter 4. Gaussian noise and other internal receiver anomalies then have significant effects on the baseband detection.

This study will be limited to some representative examples of pulse code modulation (PCM) baseband systems (as differentiated from pulse amplitude, pulse position, or pulse duration modulation) where binary information is conveyed by the presence or absence of a single wave form (pulse) or two wave forms representing a zero and a one. It will not be practical to consider all possible PCM systems, but those that will be discussed are representative and the expressions derived can readily be extended to other less typical systems. For a fairly complete listing of PCM baseband systems see Deffeback and Frost (1971).

Before discussing specific modulation schemes, the theoretical performance of two distinct methods of detection will be examined. These results will then be applied directly to several of the more common PCM signaling formats: no-return-to-zero (NRZ), return-to-zero (RZ), bi-polar, and conditioned di-phase. Special consideration will be given to three-level partial response signalling and to minimum shift keying, a form of continuous phase frequency shift keying.

Methods of Detection

Consider first the problem of detecting two equally probable signal waveforms $s_1(t)$ and $s_0(t)$ which may occur over a duration of T seconds in the presence of additive white Gaussian noise with two-sided spectral density $N_o/2$. Again it can be shown (Whalen, 1971) that the optimum detector is the correlation receiver as was illustrated in Fig. 2.1. Recall that the probability of bit error for such a detector was found to be:

$$P_b = \text{erfc}\left[\left(\frac{E}{N_o}\right)(1-\rho)\right]^{1/2} \tag{2.90}$$

where

$$E = \frac{1}{2}\int_0^T [s_1^2(t) + s_0^2(t)]dt$$

$$\rho = \frac{1}{E}\int_0^T s_0(t)\, s_1(t)dt \quad . \tag{2.91}$$

This expression can then be used for determining the probability of bit error for optimum detection of the different PCM waveforms.

The optimal detection scheme described above would provide a satisfactory basis for comparison of the performance of most PCM systems and to determine the effects of symbol synchronization error. However, since in fact it is seldom used for baseband systems, it will be beneficial to examine the theoretical probability of error for more common detection methods. In general the receiver will interpret the received signal as being either $s_1(t)$ or $s_0(t)$ by means of a simple binary decision threshold. This process normally takes one of two forms.

The first is through the use of "slicers" as shown in Fig. 2.9. The slicing can be accomplished simply by turning a device on or off based upon whether the amplitude of the received signal is above or below a given threshold. The output of the slicer is generally retimed either by a separate clock signal or from timing recovered from the received signal.

The second method is to sample the received waveform near the center of each pulse interval as determined by a local timing source, again either by a separate clock signal or recovered timing. The sampled value is then compared to the preset threshold. Multiple sampling techniques are sometimes used but their analysis would serve no purpose here. In either method (assuming for the moment perfect timing) the probability of error will depend upon the amplitude of the noise at the moment sampled. (The slicer outputs are essentially sampled when retimed.) To illustrate how the probability of error can be calculated, assume the signals are equally probable rectangular pulses with amplitudes $s_1(t) = -s_0(t) = A$ during the entire symbol interval. (Note: this format will soon be termed polar NRZ-level.) The received signal is given by:

$$r(t) = s_1(t) + n(t) \tag{2.92}$$

and the probability of error will be:

$$P_b = \frac{1}{2} P\{n(T_o) \geq A | s_o\} + \frac{1}{2} P\{n(T_o) \leq -A | s_1\} \tag{2.93}$$

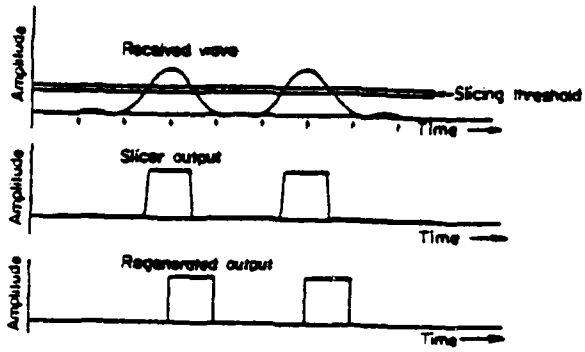

Fig. 2.9. Slicer Detection.

where T_o is the moment of sampling. Since the noise is assumed to be white Gaussian, this value can be obtained by calculating the area of either of the symmetrical error regions as illustrated in Fig. 2.10 where G is the amplitude of the sample.

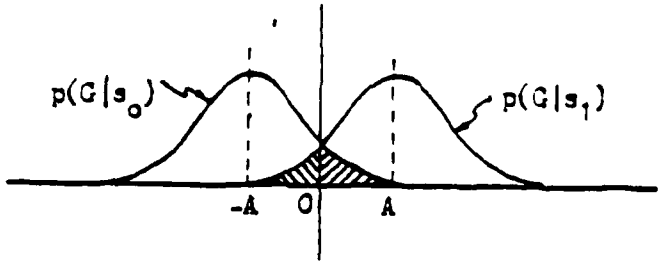

Fig. 2.10. Conditional Probability Density Functions of G, and Error Regions.

This is:

$$P_b = \int_0^\infty \frac{1}{\sqrt{2\pi}\,\sigma} \exp\left[\frac{-(y + A)^2}{2\sigma^2}\right] dy \ . \tag{2.94}$$

Recalling the definition of the complimentary error function:

$$\text{erfc}(x) = \frac{1}{\sqrt{2\pi}} \int_x^\infty e^{-z^2/2}\, dz \tag{2.95}$$

the probability of bit error is:

$$P_b = \text{erfc}\left(\frac{A}{\sigma}\right) . \tag{2.96}$$

For this single sample case it is evident that the error probability is independent of the symbol interval (still assuming perfect timing). So that this expression can be compared with the correlation receiver it is convenient to consider equal symbol intervals for each case. The average energy per symbol is then proportional to A^2 and the probability of error for sampling detection can be written in terms of signal-to-noise ratio as:

$$P_b = \text{erfc}\left(\frac{E}{N_o}\right)^{1/2} \ . \tag{2.97}$$

This derivation and Eq. (2.90) can now be used to determine directly the theoretical error probabilities for the various PCM signals described in the next several sections.

No-return-to-zero (NRZ) Systems

NRZ is the simplest PCM format and the most commonly used internally within digital communications equipment. It is often used for communications between collocated items of equipment, but because of its

power spectrum it is seldom used for transmission over any appreciable distance. [For a concise description of the spectral characteristics of baseband systems see Deffeback and Frost (1971).] NRZ signals, as will be seen, enjoy the greatest immunity to noise of any baseband signals.

The various NRZ signals are shown in Fig. 2.11. The basic NRZ scheme, whereby a binary one is represented by one amplitude level over the entire symbol period and a zero by another amplitude level, has been given the designation NRZ-level or NRZ-L. When binary zero is represented by a zero signal level as in Fig. 2.11(a) the scheme is termed unipolar NRZ. When equal but opposite polarity signals are used as in Fig. 2.11(b) it is called polar NRZ.

For coherent correlation detection as defined by Eq. (2.90) it is readily seen that for unipolar NRZ-L, $\rho=0$, whereas for polar NRZ-L $\rho = -1$. The probabilities of error, therefore, become for unipolar NRZ-L:

$$P_b = \text{erfc}\left(\frac{E}{N_o}\right)^{1/2} \tag{2.98}$$

and for polar NRZ-L:

$$P_b = \text{erfc}\left(\frac{2E}{N_o}\right)^{1/2} . \tag{2.99}$$

Note that in both cases E is the average energy per bit. If the constraint placed upon the systems is that they have the same peak signal power, then the polar performance will be 6 db better than the unipolar. Again these differences will become more evident after the discussion and comparisons of the characteristic BER curves in Chapter 3.

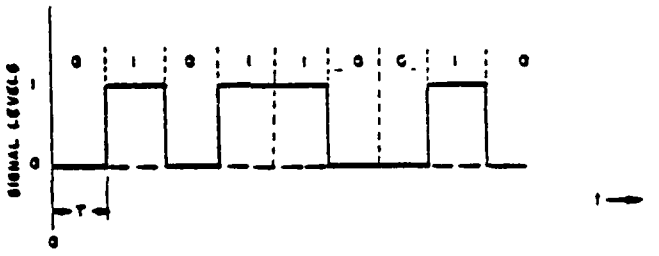

(a) UNIPOLAR NRZ-L

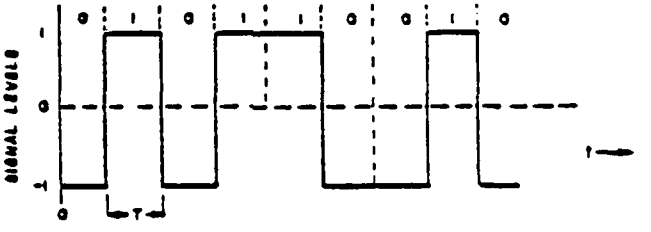

(b) POLAR NRZ-L

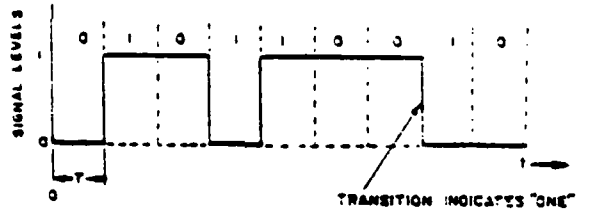

(c) NRZ-MARK

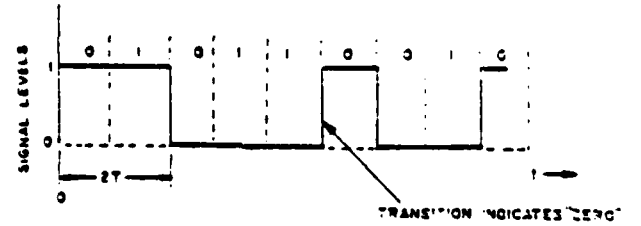

(d) NRZ-SPACE

Fig. 2.11. No-return-to-zero (NRZ) Signals.

For the slicer or sampling method of detection it can be seen from Eq. (2.97) which was derived for a polar NRZ-L signal that this method of detection suffers a 3 db loss from the correlation receiver. The relative performance between the polar and unipolar NRZ-L remains the same, however. For unipolar the detection threshold will be A/2 and the probability of error is readily seen to be:

$$P_b = \int_{A/2}^{\infty} \frac{1}{\sqrt{2\pi}\,\sigma} \exp\left[\frac{-y^2}{2\sigma^2}\right] dy$$

$$= \text{erfc}\ \frac{A}{2\sigma} \qquad (2.100)$$

and since in this case the average energy per bit is proportional to $A^2/2$ this becomes in terms of signal-to-noise ratio

$$P_b = \text{erfc}\left(\frac{E}{N_o}\right)^{1/2} . \qquad (2.101)$$

Again, if the constraint is that the systems have the same peak signal power, the difference in performance levels between the polar and unipolar NRZ-L will be 6 db.

In both NRZ-mark (NRZ-M) and NRZ-space (NRZ-S) [Fig. 2.11(c) and 2.11(d)] the information is encoded in terms of the signal transitions. This is in fact differential encoding of the binary information as was discussed previously for differential phase shift keying (DPSK). As was the case with DPSK the function describing probability of error will depend upon whether the detection is coherent or differentially accomplished. For the case of the correlation receiver and coherent

detection of differentially encoded unipolar signals, the probability of error is the probability that one of two successive symbols is decoded correctly while the other is decoded incorrectly or:

$$P_b = 2\,\text{erfc}\left(\frac{E}{N_o}\right)^{1/2}\left[1 - \text{erfc}\left(\frac{E}{N_o}\right)^{1/2}\right]. \tag{2.102}$$

For differential decoding (using the correlation receiver) the derivation of the expression for error probability will be similar to that for DPSK with the results:

$$P_b = \frac{1}{2}\exp\left(\frac{-E}{2N_o}\right) . \tag{2.103}$$

For the slicer or sampling receiver it is difficult to envision a differential decoding procedure. However, for a differentially encoded signal where each bit is detected by sampling and then decoded, the probability of error would be similar to Eq. (2.102):

$$P_b = 2\,\text{erfc}\left(\frac{E}{2N_o}\right)^{1/2}\left[1 - \text{erfc}\left(\frac{E}{2N_o}\right)^{1/2}\right] \tag{2.104}$$

where E is again the average energy per bit.

Return-to-zero (RZ) Systems

RZ signalling also includes both a unipolar and a polar format as shown in Fig. 2.12 (bipolar signals are considered in the next section). The unipolar format has essentially no advantages over NRZ-L and is seldom used. The primary advantage of the polar RZ format is that it has a fairly large power spectral component at the bit rate which permits easier clock recovery for bit synchronization than do the

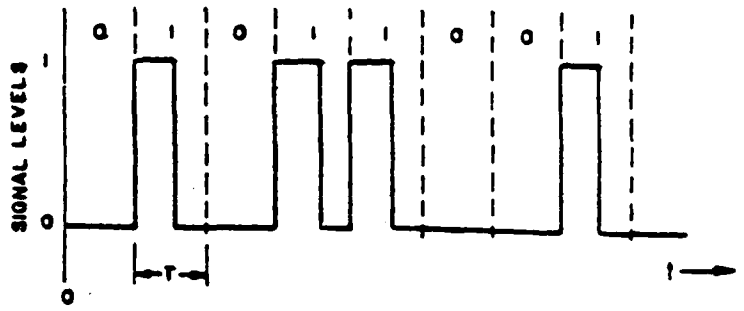

(a) UNIPOLAR RZ

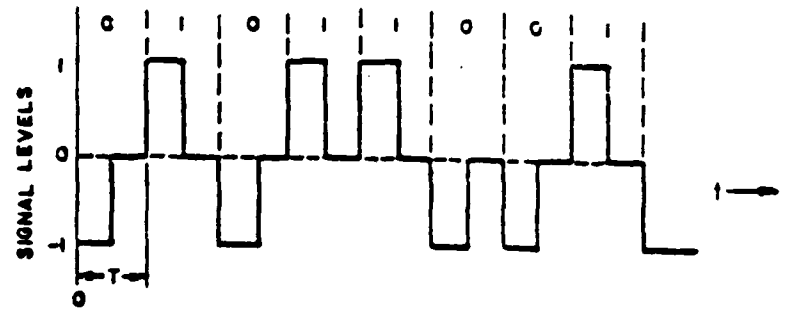

(b) POLAR RZ

Fig. 2.12. Return-to-zero (RZ) Signals.

NRZ signals which have nulls in the power spectral density at integral multiples of the bit rate (Deffeback and Frost, 1971).

For the correlation receiver it can readily be seen that the expressions for bit error probability for RZ signals have exactly the same form as for NRZ for both unipolar and polar formats. For unipolar RZ:

$$P_b = \text{erfc}\left(\frac{E}{N_o}\right)^{1/2} \tag{2.105}$$

and for polar RZ:

$$P_b = \text{erfc}\left(\frac{2E}{N_o}\right)^{1/2} . \tag{2.106}$$

However, it must be noted that if the maximum signal levels are constrained to be the same, the average energy per bit for RZ is half that of the NRZ signal and will, therefore, suffer a 3 db loss of performance in both the unipolar and polar formats. Now a word of caution. This line of reasoning is logical and correct, but it can result in some very misleading conclusions. The basic assumption has been made that the integration occurs over the complete symbol interval (0,T). In the case of the RZ format this assumption does not result in optimum detection and would lead to the conclusion, as will be seen, that sampling detection is in some cases superior to the correlation receiver. This is not so, and the reason is apparent if the integration is assumed to be only over that portion of the interval where a non-zero signal can occur. Then the RZ signals are equivalent to the NRZ but with timing spaces between pulses. The importance of this caution becomes more evident when examining sampling detection.

The expression for probability of error for sampling detection of RZ signals are again identical to those for the NRZ cases. For unipolar RZ:

$$P_b = \text{erfc}\left(\frac{A}{2\sigma}\right) \tag{2.107}$$

and for polar RZ:

$$P_b = \text{erfc}\left(\frac{A}{\sigma}\right) . \tag{2.108}$$

The problem arises in relating these formulae to signal-to-noise ratio. For example in the polar RZ, the average energy per bit is $\frac{A^2T}{2}$. If, as before, this is related to the correlation detection by assuming the symbol periods to be the same, the probability of error becomes:

$$P_b = \text{erfc}\left(\frac{2E}{N_o}\right)^{1/2} \tag{2.109}$$

which is equivalent to the correlation receiver. Again, to maintain the proper perspective, the expressions for probability of error should be left in the form of Eq. (2.107) or (2.108), or else the conversion to the energy ratio form for purposes of comparison should consider only the portion of the symbol interval where energy is possible.

Bipolar Systems

Bipolar systems also take both RZ and NRZ formats; however, they have distinct characteristics that tend to place them in a special category. Bipolar waveforms are three-level signaling methods, whereby a binary zero is represented by a zero signal level and successive ones are represented by equal-magnitude opposite-polarity pulses that are

either one-half bit period wide for RZ or a full bit period wide for NRZ as illustrated in Fig. 2.13.

The primary advantages of bipolar signals are, first that there is no DC component in the power spectrum which permits transmission over repeatered cable systems, and second that there is a built-in error detecting capability which is implemented by detecting violations of the alternating property of the pulses. The bipolar RZ signal is used by the Bell System in the T-1 carrier. This type of signal is also often referred to as AMI, standing for alternate mark inversion.

Correlation detection of bipolar signals could be implemented through the use of two correlators to detect the presence of either the positive or negative signals, or more likely by the use of a full wave rectifier and a single correlator. In either case it is readily seen that the error probabilities will be identical to the results obtained for unipolar RZ and NRZ, respectively. For both bipolar RZ and bipolar NRZ:

$$P_b = \text{erfc}\left(\frac{E}{N_o}\right)^{1/2} . \tag{2.110}$$

The same discussion concerning the average energy per bit and the word of caution mentioned previously are applicable here particularly in the case of the bipolar RZ format.

Sampling detection also produces results that are identical to the unipolar RZ and NRZ. Again the expression is:

$$P_b = \text{erfc}\left(\frac{A}{2\sigma}\right) \tag{2.111}$$

and caution is required to relate this to signal-to-noise ratio.

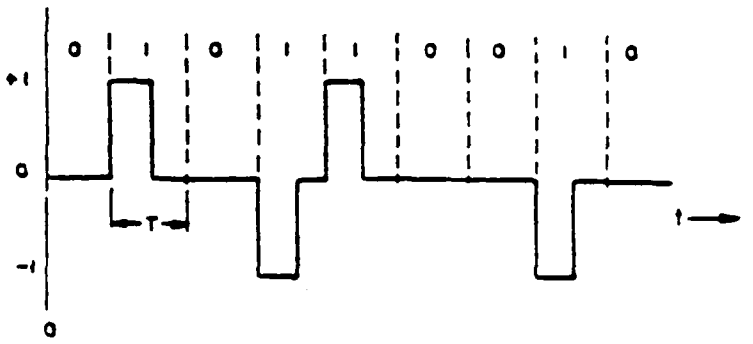

(a) BIPOLAR RZ

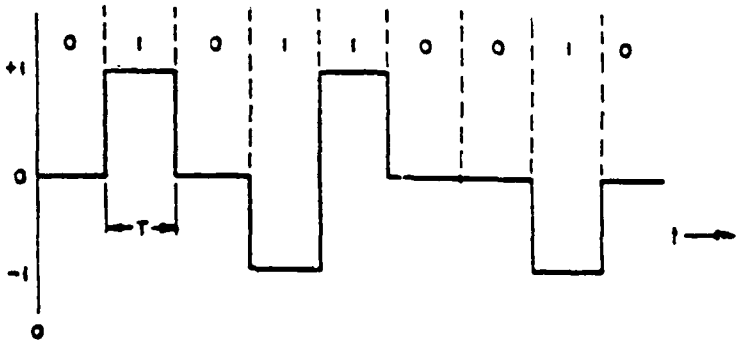

(b) BIPOLAR NRZ

Fig. 2.13. Bipolar Signals.

Conditioned Diphase

Although not commonly found in textbooks or other references on baseband signaling, this mode is singled out because of its predominant usage in the new military tactical communications system. Conditioned diphase is a two-level baseband system that has excellent spectral characteristics for long distance transmission over repeatered cable systems.

Conditioned diphase waveforms are obtained by first converting the binary information in an NRZ-L signal into the signal transitions, i.e., each binary one causes a change of state, whereas the state does not change for a zero. This "conditioned" signal is then modulated by adding a square wave (modulo two) at the timing pulse rate. This process is illustrated in Fig. 2.14. Detection is accomplished by delaying the incoming signal by one baud and modulo two adding this to the undelayed signal. The conditioned diphase waveform will be seen later to be very similar to MSK.

Note that the conditioned diphase signal may be either in polar or unipolar format. In either case it is essentially a differentially encoded signal. The detection, whether it occurs before or after the differential decoding, is not differential. Therefore, the expressions for probability of error will be similar to those obtained for coherent detection of a differentially encoded signal as was previously discussed. That is, an error occurs only if one or the other of two successive bits are erroneous, not if both are incorrect. Since the wave shape is the same as an NRZ-L signal, the probability of error for correlation detection of polar conditioned diphase is:

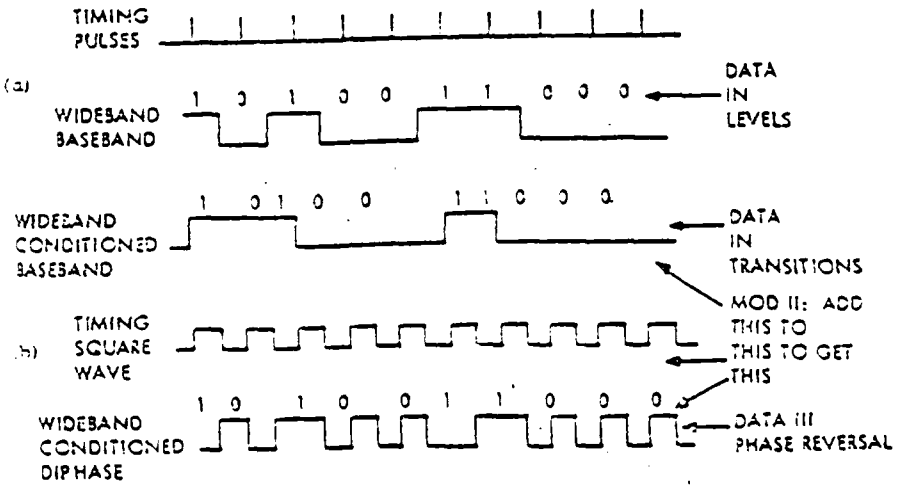

Fig. 2.14. Conditioned Diphase Signals.

$$P_b = 2\,\mathrm{erfc}\left(\frac{2E}{N_o}\right)^{1/2}\left[1 - \mathrm{erfc}\left(\frac{2E}{N_o}\right)^{1/2}\right] \tag{2.112}$$

and if the signals are unipolar:

$$P_b = 2\,\mathrm{erfc}\left(\frac{E}{N_o}\right)^{1/2}\left[1 - \mathrm{erfc}\left(\frac{E}{N_o}\right)^{1/2}\right] . \tag{2.113}$$

The results for sampling detection are extended in a similar fashion. For the polar case:

$$P_b = 2\,\mathrm{erfc}\left(\frac{E}{N_o}\right)^{1/2}\left[1 - \mathrm{erfc}\left(\frac{E}{N_o}\right)^{1/2}\right] \tag{2.114}$$

and for sampling detection of unipolar conditioned diphase

$$P_b = 2\,\mathrm{erfc}\left(\frac{E}{2N_o}\right)^{1/2}\left[1 - \mathrm{erfc}\left(\frac{E}{2N_o}\right)^{1/2}\right] . \tag{2.115}$$

Effects of Symbol Synchronization Error on PCM Signals

As has been done previously, the approach will be to evaluate the error probability for the various baseband systems conditioned upon a constant error in the symbol synchronization (baud timing). The average probability of error can then be obtained by integrating this conditional probability over the probability density function of the baud timing jitter. The general result will be given by:

$$P_b = \int_{-\infty}^{\infty} P_{b|\tau}\, p(\tau)d\tau . \tag{2.116}$$

This integral will be evaluated for typical cases in Chapter 3.

It will be convenient at this point to separate the discussion of the effects of symbol synchronization error on the correlation

receiver from the effects on sampling detection. As will be seen the effects are quite similar, but the derivations require different reasoning. Expressions will first be derived for probability of error for each of the baseband systems described in the preceding paragraphs conditioned on a constant symbol synchronization error τ in a correlation receiver. Although very few of these expressions can be found in the literature, they are for the most part relatively simple extensions of previous work.

Beginning with the polar NRZ waveform, it is evident that baud timing error will have no effect if successive symbols are the same. However, if transitions occur at every symbol, the integration period will be effectively reduced by 2τ. The output of the correlator over the period $(\tau, T + \tau)$ will be

$$A^2(T-|\tau|) - A^2|\tau| = A^2T\left(1 - \frac{2|\tau|}{T}\right) . \tag{2.117}$$

The absolute value sign arises since the effect is the same for both positive and negative τ. Since for polar NRZ the average signal energy per bit $E = A^2T$, the conditional probability of error becomes, assuming equally probable ones and zeros:

$$P_b = \frac{1}{2}\,\mathrm{erfc}\left(\frac{2E}{N_o}\right)^{1/2} + \frac{1}{2}\,\mathrm{erfc}\left[\left(\frac{2E}{N_o}\right)^{1/2}\left(1 - \frac{2|\tau|}{T}\right)\right] \quad |\tau| < \frac{T}{2} . \tag{2.118}$$

For unipolar NRZ it is still true that baud timing error will have effect only when symbol transitions occur. In this case the output of the correlator over the period $(\tau, T + \tau)$ will be simply $A^2(T-\tau)$.

However, the average energy per bit is now $E = \frac{A^2T}{2}$ so the expression for conditional probability of error for unipolar NRZ is also:

$$P_b = \frac{1}{2}\,\mathrm{erfc}\left(\frac{E}{N_o}\right)^{1/2} + \frac{1}{2}\,\mathrm{erfc}\left[\left(\frac{E}{N_o}\right)^{1/2}\left(1 - \frac{2|\tau|}{T}\right)\right] . \qquad (2.119)$$

The effect of baud timing error on RZ signals will be dependent upon whether the integration is assumed to take place over the entire symbol period or just that portion during which a signal level other than zero may occur. First, assume the integration is over the entire symbol period $(\tau, T + \tau)$ with fixed timing error τ. Then, for polar RZ the correlator output with alternating symbols will be

$$A^2\left(\frac{T}{2} - |\tau|\right) - A^2|\tau| = \frac{A^2T}{2}\left(1 - \frac{4|\tau|}{T}\right) \qquad |\tau| \le \frac{T}{4} \qquad (2.120)$$

and since the average energy per bit is $\frac{A^2T}{2}$, the conditional error probability is:

$$P_b = \frac{1}{2}\,\mathrm{erfc}\left(\frac{E}{N_o}\right)^{1/2} + \frac{1}{2}\,\mathrm{erfc}\left[\left(\frac{E}{N_o}\right)^{1/2}\left(1 - \frac{4|\tau|}{T}\right)\right] \quad |\tau| \le \frac{T}{4} \qquad (2.121)$$

For unipolar RZ the correlator output will be:

$$\frac{A^2T}{2}\left(1 - \frac{2|\tau|}{T}\right) .$$

However, in this case the average energy per bit is $\frac{A^2T}{4}$ and the conditional probability of error is:

$$P_b = \frac{1}{2}\,\mathrm{erfc}\left(\frac{E}{2N_o}\right)^{1/2} + \frac{1}{2}\,\mathrm{erfc}\left[\left(\frac{E}{2N_o}\right)^{1/2}\left(1 - \frac{4|\tau|}{T}\right)\right] \quad \tau \le \frac{T}{4} \qquad (2.122)$$

Although this is probably not a typical case, it should be instructive to examine the results if the period of integration is assumed to be $(\tau, \frac{T}{2} + \tau)$. In both the polar and unipolar RZ instances the correlator output will now be affected the same whether or not a transition occurs and will be the same for both polar and unipolar. However, when the effect is reflected on the average energy per bit the results become, for polar RZ

$$P_b = \text{erfc}\left[\left(\frac{E}{N_o}\right)^{1/2}\left(1 - \frac{2|\tau|}{T}\right)\right] \qquad |\tau| \leq \frac{T}{2} \tag{2.123}$$

and for unipolar RZ:

$$P_b = \text{erfc}\left[\left(\frac{E}{N_o}\right)^{1/2}\left(1 - \frac{4|\tau|}{T}\right)\right] \qquad |\tau| \leq \frac{T}{4} \quad . \tag{2.124}$$

Symbol synchronization error will have a different effect on bipolar waveforms depending upon whether two correlators are used or if the input waveform is full wave rectified prior to detection. If a full wave rectifier is used, and this is certainly the most likely case, the results will be identical to the unipolar NRZ and RZ, respectively. That is, for bipolar NRZ:

$$P_b = \frac{1}{2}\,\text{erfc}\left(\frac{E}{N_o}\right)^{1/2} + \frac{1}{2}\,\text{erfc}\left[\left(\frac{E}{N_o}\right)^{1/2}\left(1 - \frac{2|\tau|}{T}\right)\right] \qquad |\tau| < \frac{T}{2} \tag{2.125}$$

and for bipolar RZ:

$$P_b = \frac{1}{2}\,\text{erfc}\left(\frac{E}{2N_o}\right)^{1/2} + \frac{1}{2}\,\text{erfc}\left[\left(\frac{E}{2N_o}\right)^{1/2}\left(1 - \frac{4|\tau|}{T}\right)\right] \qquad |\tau| < \frac{T}{4} \tag{2.126}$$

Although the use of two correlators for detection of bipolar signals is very unlikely, it will be instructive to examine the results which might be usefully extended to some other baseband formats. Now the effects on the correlator outputs will be different depending upon whether successive symbols are alternate ones and zeros, two zeros, or two ones. Obviously baud timing error has no effect if successive symbols are both zeros. However, the effect on successive ones is twice that upon alternating ones and zeros. Again, assuming equally probable and independent ones and zeros for each symbol, the conditional error probability for bipolar NRZ becomes:

$$P_b = \frac{1}{4}\,\mathrm{erfc}\left(\frac{E}{N_o}\right)^{1/2} + \frac{1}{2}\,\mathrm{erfc}\left[\left(\frac{E}{N_o}\right)^{1/2}\left(1 - \frac{2|\tau|}{T}\right)\right]$$

$$+ \frac{1}{4}\,\mathrm{erfc}\left[\left(\frac{E}{N_o}\right)^{1/2}\left(1 - \frac{4|\tau|}{T}\right)\right] \qquad |\tau| \le \frac{T}{4} \quad . \tag{2.127}$$

For bipolar RZ assuming the integration takes place over the entire symbol period the result is:

$$P_b = \frac{1}{4}\,\mathrm{erfc}\left(\frac{E}{N_o}\right)^{1/2} + \frac{1}{2}\,\mathrm{erfc}\left[\left(\frac{E}{2N_o}\right)^{1/2}\left(1 - \frac{4|\tau|}{T}\right)\right]$$

$$+ \frac{1}{4}\,\mathrm{erfc}\left[\left(\frac{E}{2N_o}\right)\left(1 - \frac{8|\tau|}{T}\right)\right] \qquad |\tau| \le \frac{T}{8} \quad . \tag{2.128}$$

For conditioned diphase signals, the effect of symbol synchronization error will be the same as for NRZ signals depending upon whether the waveforms are polar or unipolar. The results may be readily seen to be, for polar conditioned diphase:

$$P_b = \operatorname{erfc}\left(\frac{2E}{N_o}\right)^{1/2}\left[1 - \operatorname{erfc}\left(\frac{2E}{N_o}\right)^{1/2}\right] + \operatorname{erfc}\left[\left(\frac{2E}{N_o}\right)^{1/2}\left(1 - \frac{2|\tau|}{T}\right)\right]$$
$$\left\{1 - \operatorname{erfc}\left[\left(\frac{2E}{N_o}\right)^{1/2}\left(1 - \frac{2|\tau|}{T}\right)\right]\right\} \qquad |\tau| \le \frac{T}{2} \qquad (2.129)$$

and for unipolar conditioned diphase:

$$P_b = \operatorname{erfc}\left(\frac{E}{N_o}\right)^{1/2}\left[1 - \operatorname{erfc}\left(\frac{E}{N_o}\right)^{1/2}\right] + \operatorname{erfc}\left[\left(\frac{E}{N_o}\right)^{1/2}\left(1 - \frac{2|\tau|}{T}\right)\right]$$
$$\left\{1 - \operatorname{erfc}\left[\left(\frac{E}{N}\right)^{1/2}\left(1 - \frac{2|\tau|}{T}\right)\right]\right\} \qquad |\tau| \le \frac{T}{2} \quad . \qquad (2.130)$$

In summary, then, we have shown that, for correlation detection of typical PCM baseband signaling, the theoretical effects of symbol synchronization error on the probability of bit error result in the same types of expressions that were derived for coherent PSK and FSK systems. The fact that these expressions result in lateral shifts of the curves of BER versus signal-to-noise ratio for small values of jitter variance will be demonstrated later in Chapter 3.

In all the previous discussions it has been assumed that the waveshapes are rectangular. Obviously if this is so, symbol synchronization error will have no effect upon sampling detection unless it is so severe as to cause bit slippage. Such tolerance to baud timing errors is, of course, one reason that sampling detection is commonly used where the baseband communications are between collocated or close proximity devices.

When baseband transmission is over considerable distances, received waveforms are no longer rectangular. Indeed, the pulses are

most often purposely shaped prior to transmission to obtain desirable spectral characteristics and to reduce intersymbol interference. There is considerable information in the literature on the optimization of filters for pulse shaping at the transmitter and the receiver prior to detection [see Lucky, Salz, and Weldon (1968), for example]. This will be discussed further in the section that follows on partial response and in Chapter 3. At the present it will suffice to use as an example pulses with a raised cosine shape as shown in Fig. 2.15.

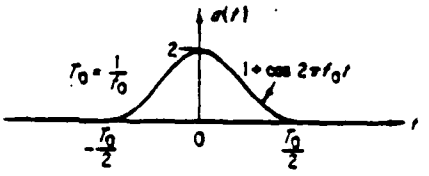

Fig. 2.15. Raised Cosine Pulse.

Here it is readily seen that the sample timing will have a definite effect on the error probability. A first approximation to the effect on the amplitude of the sample with a fixed timing error τ would be proportional to $\cos \frac{\pi\tau}{T}$. Using this approximation, the expression for conditional probability of error for a polar NRZ system, for example, would be

$$P_b = \operatorname{erfc}\left[\frac{A}{\sigma}\cos\left(\frac{\pi\tau}{T}\right)\right] . \tag{2.131}$$

Too many assumptions are required to attempt to define precise expressions in terms of signal-to-noise ratio and their usefulness would be doubtful. Equation (2.131) does, however, serve the purpose of illustrating that the effects of symbol synchronization errors do result in a familiar type of expression.

Quantitative effects of this type will become more evident in the detailed discussion in Chapter 5 of the effects of baud timing jitter on the detection of a specific three-level partial response system.

Partial Response Signaling

It can be shown (Bennett and Davey, 1965) that the theoretical limit for the rate at which pulses can be transmitted without intersymbol interference is equal to twice the bandwidth of the transmission media. This limit, known as the Nyquist rate, is not directly attainable since it requires perfect filtering. This will be discussed further in the section on intersymbol interference in Chapter 3.

Partial response signaling, sometimes referred to as duobinary, is a baseband transmission technique developed by Lender (1963) which uses a controlled amount of intersymbol interference in order to achieve data transmission at the Nyquist rate. A number of multilevel partial response signaling techniques have been developed and are described by Kretzmer (1966). The class I, three-level partial response system will be described here.

The class I, three-level partial response waveform is obtained by passing a polar NRZ signal through a cosine filter whose characteristics are shown in Fig. 2.16. In practice half of the filtering is

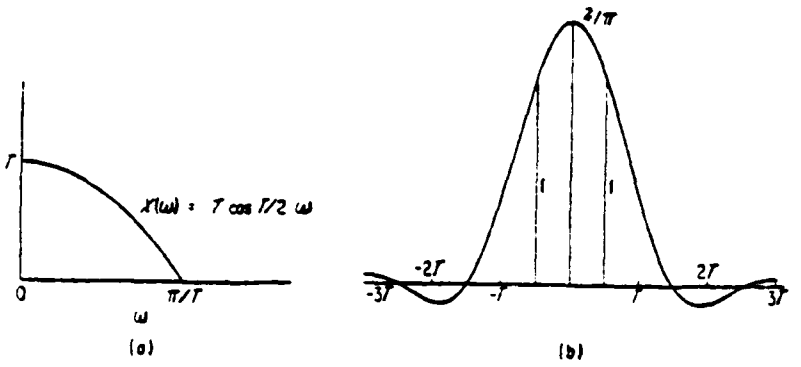

Fig. 2.16. Partial Response Filter Characteristics.

accomplished at the transmitter and half at the receiver. The transfer function and impulse response of the composite filter are:

$$X(\omega) = T \cos \frac{\omega T}{2} \qquad |\omega| \leq \frac{\pi}{T} \qquad \text{(0 elsewhere)} \qquad (2.132)$$

$$x(t) = \frac{2}{\pi} \left[\frac{\cos \pi t/T}{1 - 4\, t^2/T^2} \right]$$

It can readily be seen that if the sampling time is at nT - T/2 rather than at nT, the response is the sum of equal values from adjacent symbols, but that other symbols have zero effect.

In practice, to eliminate the possibility of error propagation, the data is differentially encoded at the transmitter; that is, each transmitted bit is the sum of the input plus (modulo 2) the previously transmitted bit. The encoding, filtering, and detection schemes are illustrated in Fig. 2.17. In the detection, if the received signal level exceeds either the high or the low slicer threshholds in absolute

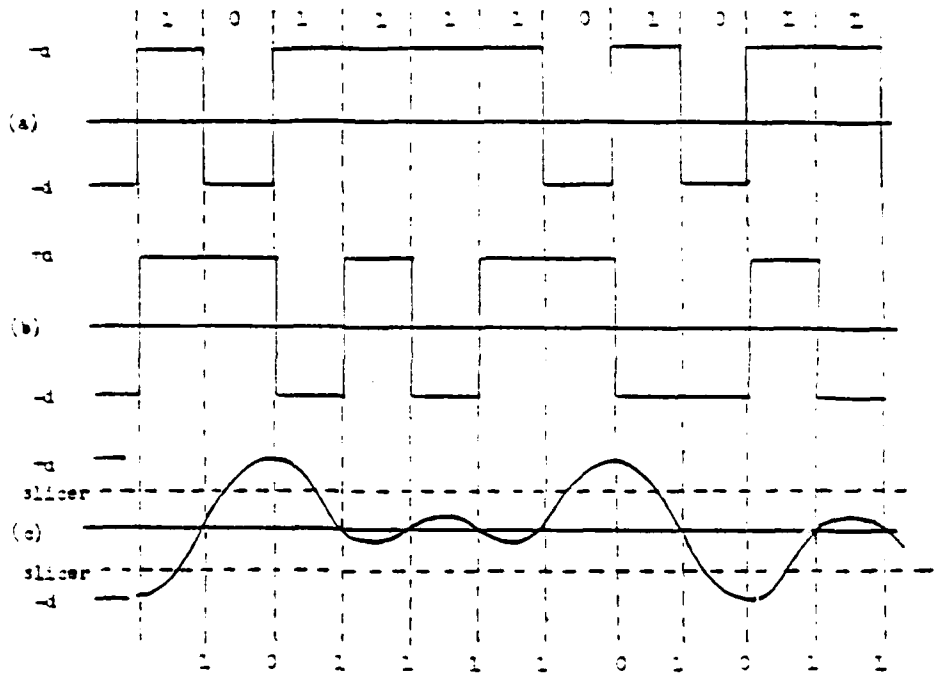

Fig. 2.17. Generation of Three-level Partial Response.

(a) Input NRZ
(b) Differentially Encoded NRZ
(c) Partial Response Signal

magnitudes at the sample time, the bit is decoded as a zero. If not, then the bit is decoded as a one. As can be seen, this decoding process results in the original input data stream.

To determine the probability of error for sampling detection of a three-level partial response signal it will be assumed as usual that zeros and ones are equally probable in the input data stream. The noise is assumed to be additive white Gaussian with zero mean and spectral density $N_o/2$. In the absence of noise, the received signal at the sampling instant can then assume the three values +A, 0, and -A with probabilities 1/4, 1/2, and 1/4, respectively. The probability of detection error with the slicer threshholds at $\pm$ A/2 is then:

$$P_b = \frac{3}{2} P \{N \geq A/2\} \tag{2.133}$$

where N is the noise level at the sampling instant. If the noise variance is σ_N^2 this becomes:

$$P_b = \frac{3}{2} \int_{A/2}^{\infty} \frac{1}{\sqrt{2\pi}\ \sigma_N} \exp\left[\frac{-x^2}{2\sigma_N^2}\right] dx \tag{2.134}$$

$$= \frac{3}{2} \operatorname{erfc}\left(\frac{A}{2\sigma_N}\right) .$$

It remains then to evaluate this expression in terms of the energy per bit and the noise variance after the nominal filtering. The average energy per bit of the polar NRZ signal is A^2T. After filtering this will be:

$$E = \frac{A^2}{\tau} \int_{-\pi/T}^{\pi/T} |X^{1/2}(\omega)|^2 \, d\omega \tag{2.135}$$

which after substituting the expression (2.132) for $X(\omega)$ and evaluating becomes:

$$E = \frac{2A^2}{\pi} \quad . \tag{2.136}$$

Similarly evaluating the noise variance:

$$\sigma_N^2 = \frac{1}{2} \int_{-\pi/T}^{\pi/T} N_o \left| X^{1/2}(\omega) \right|^2 d\omega = \frac{2N_o}{\pi} \quad . \tag{2.137}$$

The probability of bit error in terms of signal-to-noise ratio is then obtained as:

$$P_b = \frac{3}{2} \operatorname{erfc} \left[\frac{\pi}{4} \left(\frac{E}{N_o} \right)^{1/2} \right] \quad . \tag{2.138}$$

This is approximately a loss of 2.1 db in noise performance over the polar NRZ signal; however, it is a small sacrifice for doubling the practically achievable data rate over the same bandwidth.

Detection of the three-level partial response waveform has been shown to be relatively insensitive to the sample timing. However, determining a closed analytical expression for the effect of symbol synchronization error is not practicable. If the sample time is slightly offset, the noiseless signal can then assume eight different levels, instead of three, and interference occurs from symbols other than the adjacent one.

The literature contains several variations of methods for calculating the effect of baud timing jitter in the detection of partial response systems. Since the results are more readily presented in terms of the effects on the characteristic curve of BER versus signal-to-noise ratio, the discussion of the methods will be deferred to Chapter 3.

Minimum Shift Keying (MSK)

Minimum shift keying is a data transmission technique which is very difficult to define since it can be considered as variations of several different modulation techniques and can be detected in a variety of ways. As a baseband modulation system it normally will take the format shown in Fig. 2.18. In this case a data one is represented by a half cycle sinewave of one-half the data rate frequency. A data zero is represented by one full cycle sinewave at the data rate. The signals are constrained to be continuous in phase.

In general, MSK may be considered as a continuous phase frequency shift (CPFSK) carrier modulation technique where the frequency shift is exactly ± 1/4 the bit rate with the requirement that the mark and space frequencies be exact, even multiples of the shift frequency. Datran was one of the early users of this technique in a microwave system described by Sullivan (1972). In that system, MSK modulation was

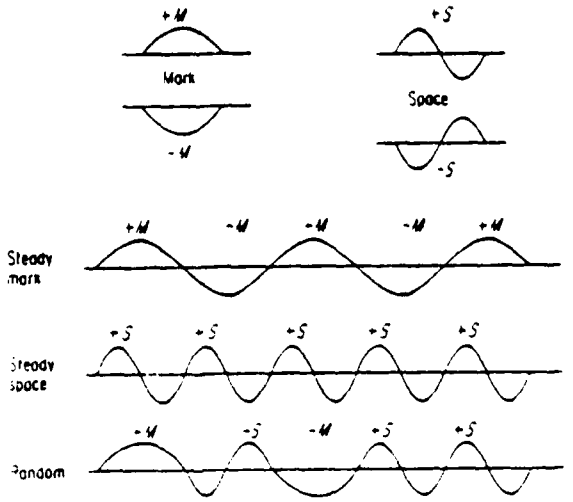

Fig. 2.18. MSK Format.

AD-A097 123 ARIZONA UNIV TUCSON ENGINEERING EXPERIMENT STATION F/G 17/2
DIGITAL COMMUNICATIONS SYSTEMS: TEST AND EVALUATION STUDIES, VO--ETC(U)
AUG 79 L C SCHOOLEY, G R DAVIS DAEA18-74-A-0271
UNCLASSIFIED NL

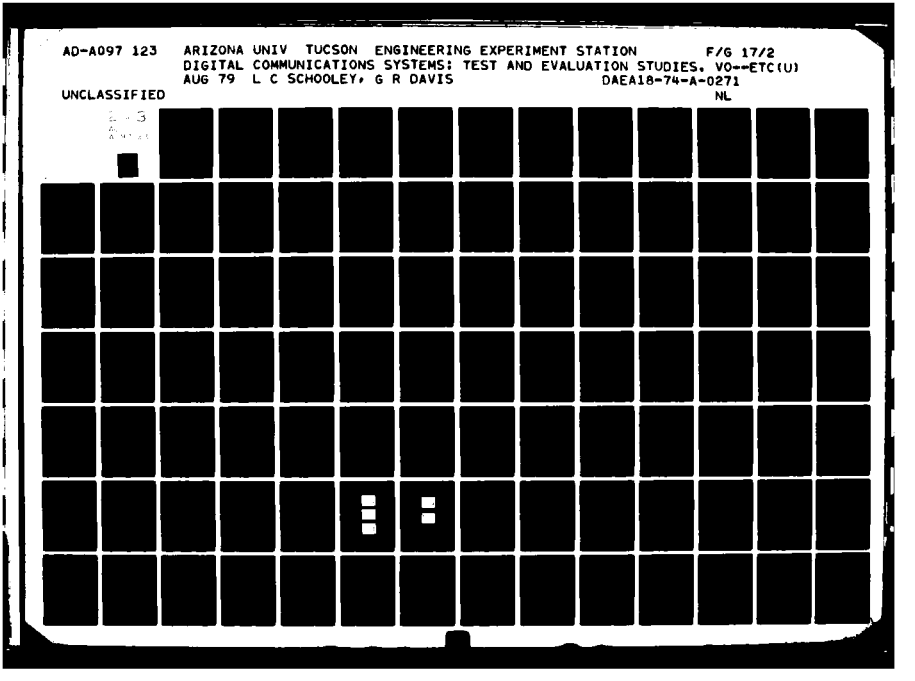

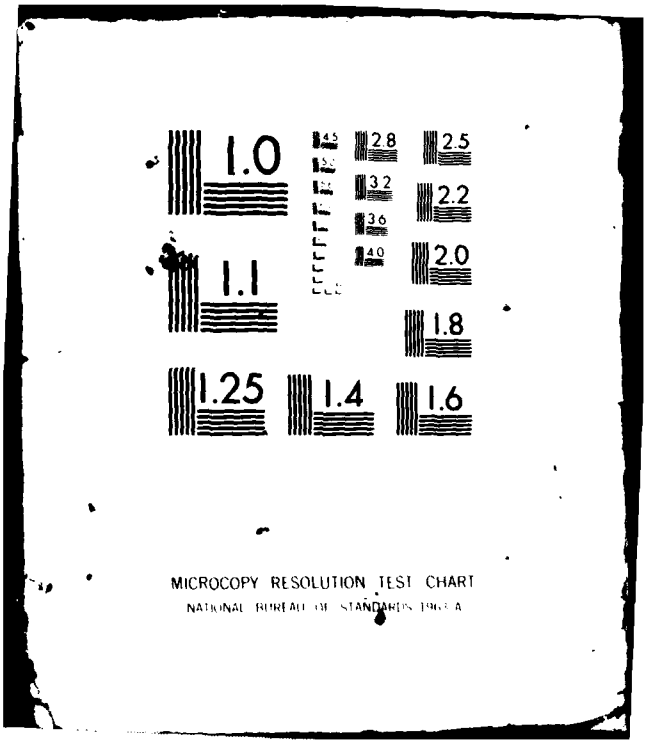
1.0
1.1
1.25
1.4
1.6
1.8
2.0
2.2
2.5
2.8
3.2
3.6
4.0
MICROCOPY RESOLUTION TEST CHART
NATIONAL BUREAU OF STANDARDS 1963 A

accomplished at the intermediate frequency of the transmitter. With a bit rate of 21.504 Mbps the mark and space frequencies were 64.5 MHz and 75.3 MHz, respectively.

MSK can also be viewed as a special case of offset keyed quaternary phase shift keyed modulation (OK-QPSK)(Gronemeyer and McBride, 1976). This viewpoint is apparent if one considers the mark and space frequencies as quadrature (orthogonal) carriers, each of which is phase shifted 180° depending upon the previous outputs. It is indeed from this point of view that MSK can be seen to provide an error rate performance equivalent to coherent PSK.

The primary advantage of MSK is that, when coherently detected, its performance in additive white Gaussian noise is equivalent to CPSK, while it can be transmitted in 0.75 of the bandwidth (De Buda, 1972). That is, for coherent detection of MSK:

$$P_b = \text{erfc}\left(\frac{2E}{N_o}\right)^{1/2} . \tag{2.139}$$

MSK can also be non-coherently detected by use of a discriminator (Bennett and Salz, 1963) whereby its performance is equivalent to non-coherent detection of FSK, i.e.,

$$P_b = \frac{1}{2}\exp\left(\frac{-E}{N_o}\right) . \tag{2.140}$$

An interesting modification of MSK, which is described in some detail in the experimental results, is used in the GTE Lenkurt 261A data set. In this case the signal is duo-binary encoded prior to MSK

modulation. At the receiver the signal is passed through a discriminator to produce a three-amplitude level signal, similar to a three-level partial response waveform, which is then sample (slicer) detected. The result of this detection process will be similar to that for partial response where:

$$P_b = \text{erfc}\left(\frac{A}{2\sigma}\right) . \tag{2.141}$$

The filter characteristics and effect of the discriminator would then have to be taken into account to redefine this expression in terms of signal-to-noise ratio.

For CPFSK in general, advantage can be taken of the memory imposed upon the waveform by continuous phase transitions. By using several symbols upon which to base detection decisions the performance can be further improved. It has been shown (Schonhoff, 1976) for a three bit observation period, the performance over CPSK is improved approximately 1.1 db. Non-coherent detection of CPFSK using a five bit observation time can also be made to outperform CPSK.

With normal coherent and noncoherent detection, it can be expected that the performance of MSK in the presence of carrier phase and baud timing errors would be similar if not identical to those for CPSK and noncoherent FSK. Although there appears to be no specific references to this, it certainly would be expected that multiple observation detection would reduce susceptibility to both carrier phase and baud timing jitter. Rhodes (1974) has shown in the case of OK-QPSK that the susceptibility to carrier phase error is considerably less than for CPSK.

The overall conclusion that can be drawn from the above discussion is that MSK, when considered in all its forms and possible detection schemes, still results in common expressions for probability of error. Internal receiver anomalies will have the same type of effects, although possibly of different order, as those previously discussed.

Summary

This chapter has shown the commonality of expressions for probability of error for a wide variety of modulation techniques and detection methods. Although it was not possible to consider every variation, a sufficiently broad base has been established so that the desired conclusions may be reached, with a high degree of confidence.

The expressions that have been derived here will be examined closely in Chapter 3 to determine the effects of the variations upon the characteristic curves of BER versus signal-to-noise ratio. Chapter 3 also contains discussions of the anomaly effects for which closed analytical expressions could not be obtained.

Table 2.1 has been prepared to provide a ready reference to the equations that have been derived for probability of error for each modulation technique. A blank entry indicates that that particular anomaly is not applicable.

Table 2.1. Index of Equations.

	Ideal	Phase Jitter	Baud Timing Jitter
CPSK (binary)	2.19	2.33 - 2.35	2.38
(quadrature)	2.20	2.36 - 2.37	*
(N-phase)	2.23	*	*
DPSK (coh det)	2.40	2.42	2.43
(diff det)	2.48		2.51
ASK (coh det)	2.54	2.62	2.65
(non-coh)	2.77		2.83
Binary FSK (coh det)	2.56	2.58	2.60
(non coh)	2.79		2.84
M-ary FSK (coh det)	2.86	*	2.88
(non-coh)	2.87		2.89
NRZ-L unipolar (coh)	2.98		2.119
(sample)	2.101		**
NRZ-L polar (coh)	2.99		2.118
(sample)	2.97		**
NRZ-M&L	2.104		
RZ unipolar (coh)	2.105		2.122
(sample)	2.107		**
RZ polar (coh)	2.106		2.121
(sample)	2.108		**
Bipolar NRZ (coh)	2.110		2.125
(sample)	2.111		**
Bipolar RZ (coh)	2.110		2.126
(sample)	2.111		**
Conditioned Diphase			
unipolar (coh)	2.113		2.130
unipolar (sample)	2.115		**
polar (coh)	2.112		2.129
polar (sample)	2.114		**

Table 2.1. Index of Equations (Con't.)

	Ideal	Phase Jitter	Baud Timing Jitter
Partial Response	2.138		*
MSK (coh det)	2.139	2.58	2.60
(non-coh)	2.140		2.84
(sample)	2.141		*

* no closed form expression available
**dependent upon wave shape

CHAPTER 3

CALCULATED RESULTS

In Chapter 2 it was shown that there was a high degree of commonality among the expressions derived for probability of error for a wide variety of modulation techniques and detection methods. In this chapter these expressions will be used to calculate and plot curves of bit error rate versus signal-to-noise ratio. (From here on these will be referred to simply as BER curves.) The purpose is to show that not only do the equations for ideal detection of the various modulation schemes result in similarly shaped BER curves, but that the predicted effects of internal receiver anomalies are to shift these curves laterally while the theoretical shape is essentially preserved.

The approach will be to first examine the effects of constant factors and additive terms in the expressions for probability of error upon the BER curves. These will then be related to the specific modulation techniques and detection methods described in Chapter 2.

Before proceeding to the effects of carrier phase reference error and symbol synchronization error on the BER curves there is a need to investigate briefly how the errors occur and to summarize their behavior. Therefore a short discourse will be presented on the probability distribution of phase errors at the output of a typical second order phase-locked-loop (PLL).

The probability density function of the PLL phase error will be used to evaluate the equations for conditional probability of error with carrier phase and baud timing jitter derived in Chapter 2 to determine the effects upon the BER curves. This will be accomplished for a number of different values of mean and variance. The calculations are essentially an extension of work done previously by Stiffler (1964) and Lindsey (1972). However, as will be seen in Chapter 4, the calculated curves published in these two widely quoted references do not agree in one very important aspect with experimental results. A simple but satisfying solution that resolves this disparity will be presented in the comparison of calculated and experimental results in Chapter 5.

The effects of jitter on non-coherent detection of ASK and FSK and on three-level partial response systems are then examined. These are discussed separately since in the one case the expressions for probability of error are considerably different from the common format, and in the other case no closed form expression could be obtained.

The chapter concludes with a discussion of intersymbol interference and non-linearities of frequency response in receivers. Again these have been deferred since closed form expressions for probability of error are not obtainable and these anomalies are more readily discussed in terms of their effects upon BER curves.

Effects of Constant Factors

The expressions derived in Chapter 2 for probability of error were in all cases either error functions or exponentials, depending upon the method of detection. Error functions were obtained for coherent and sampling detection and exponentials for non-coherent and differential detection. In the discussions that follow calculation of effects on BER curves will be illustrated for one or the other but generally not both. That the effects on both are the same (or at least very similar) is readily apparent from the fact that error function curves are asymptotically exponential. For values of $x > 1$ the error function is very closely approximated by the expression:

$$\text{erfc}(x) \approx \frac{2 \exp(-2x^2)}{\sqrt{2\pi}\ x} \quad . \tag{3.1}$$

That the x in the denominator of the right hand function has very little effect on the shape of the curve is proven in Haykin (1978), and is illustrated by comparing the BER curves for coherent and non-coherent detection of FSK. These are shown in Fig. 3.1. Note that, although coherent detection is considerably more complex than non-coherent detection, it only results in approximately one db improvement in performance.

The most common variation in expressions for probability of error is the appearance of a constant multiplier of the signal-to-noise ratio. This is invariably a function of the modulation scheme. Take for example the probability of error for a binary noncoherent FSK system:

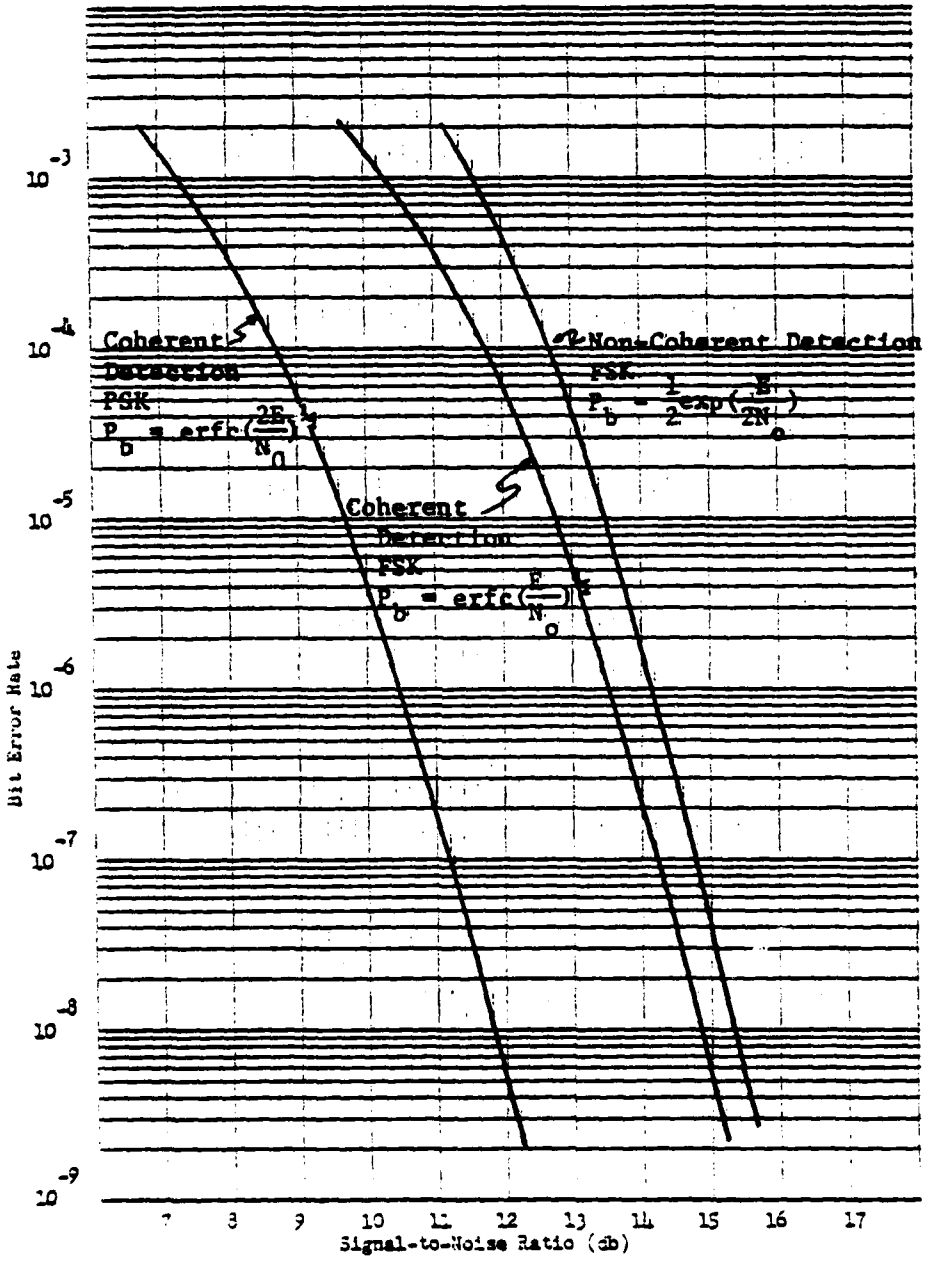

Fig. 3.1. Comparison of Coherent and Non-coherent Detection of FSK and CPSK.

$$P_b = \frac{1}{2} \exp\left(\frac{-E}{N_o}\right) \quad . \tag{3.2}$$

For convenience let $E/N_o = R$. Now suppose some other system has a probability of error:

$$P_b = \frac{1}{2} \exp\left(\frac{-R}{2}\right) \quad . \tag{3.3}$$

The exercise is to show that this error curve will be shifted exactly 3 db from the first. This is demonstrated by determining the required values of R for equal P_b. This means that for every P_b:

$$\frac{1}{2} \exp\ (-R_1) = \frac{1}{2} \exp\left(\frac{-R_2}{2}\right) \tag{3.4}$$

or

$$R_1 = R_2/2 \quad .$$

But since the BER curves are plotted versus R in db, this means:

$$10 \log R_1 = 10 \log R_2 - 10 \log 2 \tag{3.5}$$

or in decibels

$$R_1 = R_2 - 3 \text{ db} \quad .$$

A little reflection shows that this is true whether the function is an exponential or a complementary error function. Multiplying the signal-to-noise ratio by a constant shifts the error curve by 10 times the log of the constant in db. That is:

$$P_b = \text{erfc}\left(\frac{KE}{N_o}\right)^{1/2} \tag{3.6}$$

results in a curve that is 10 log K decibels to the left of the curve:

$$P_b = \text{erfc}\left(\frac{E}{N_o}\right)^{1/2} . \tag{3.7}$$

This is illustrated by comparing the curve for coherent detection of PSK which is also shown in Fig. 3.1 with that for coherent detection of FSK. The curves have exactly the same shape but are separated by 10 log 2 = 3 db.

Another common variation is a constant multiplier in front of the error expression, such as:

$$P_b = \frac{3}{2}\,\text{erfc}\left(\frac{KE}{N_o}\right)^{1/2} \tag{3.8}$$

which occurs in the detection of a three-level partial response system. The pre-multiplier 1/2 appears continually in expressions for the effect of baud timing jitter. Since P_b is plotted on a logarithmic scale, these factors result in constant upward or downward shifts of the characteristic curve. In the areas of normal interest, i.e., for the error rates less than 10^{-4}, these will be almost indistinguishable from lateral shifts. This is illustrated in Fig. 3.2. Curves have been plotted in this figure with multiplicative constants of 1/2, 1, 3/2, and 10. Note that even with the factor of 10, which is much more extreme than normally encountered, the shape of the curve at low error rates is altered very little.

Constant multipliers also occur in the expressions for upper bounds on the probability of error in both coherent and noncoherent

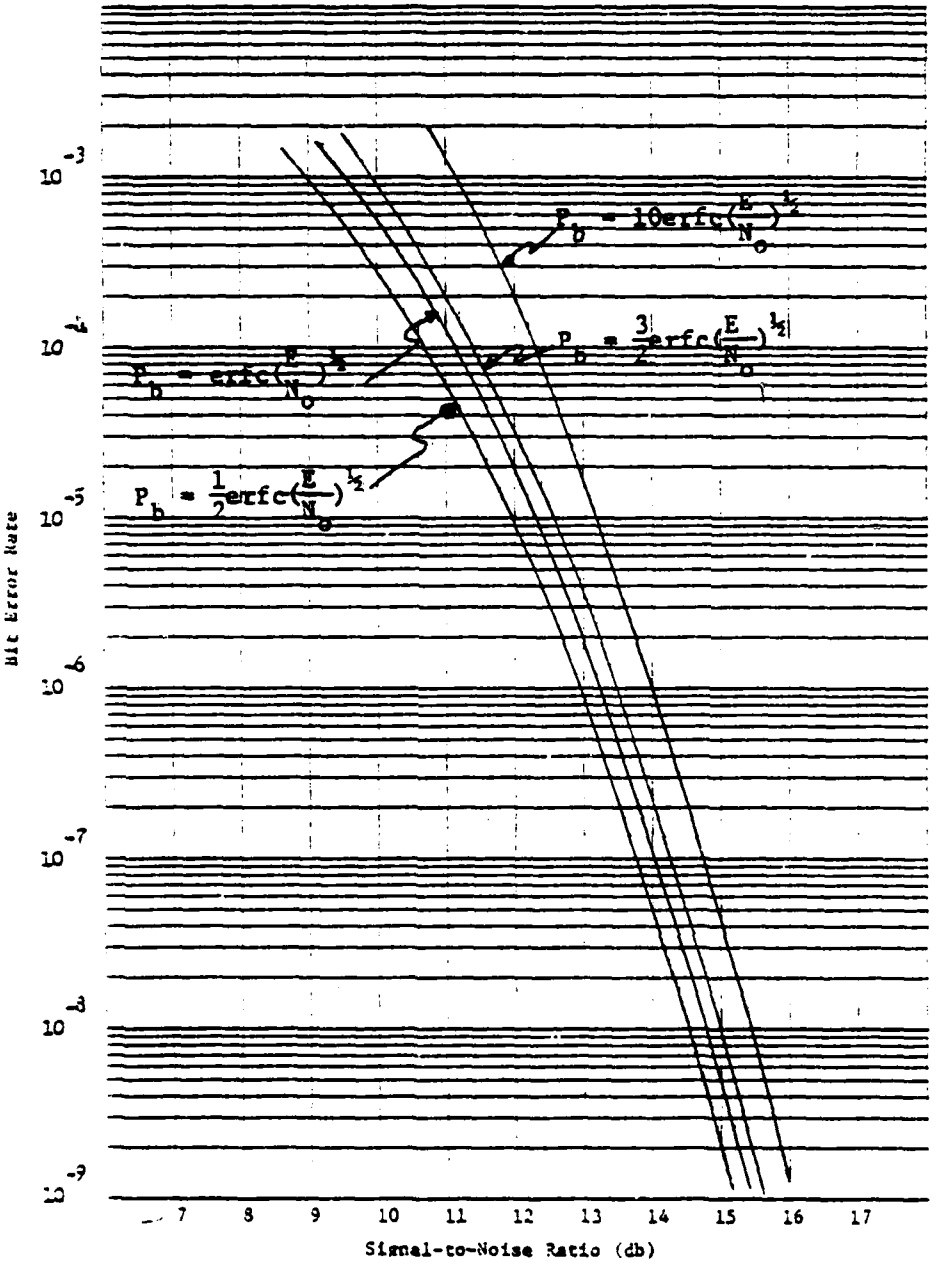

Fig. 3.2. Effects of Constant Multiplier on BER.

detection of M-ary modulation schemes [Eqns. (2.91) and (2.92)]. Note however, that these expressions are for symbol error in terms of symbol energy-to-noise ratio. A probably more meaningful illustration of the performance of M-ary systems is given in Fig. 3.3 taken from Viterbi (1961) which shows bit error rate as a function of bit signal energy-to-noise ratio for a number of values of $n = \log_2 M$. Similar results can be shown for non-coherent detection (Lindsey, 1965).

Another variation that occurs is the summing of two error functions such as is found from the effects of baud timing jitter.

$$P_b = \frac{1}{2}\,\mathrm{erfc}\left(\frac{E}{N_o}\right)^{1/2} + \frac{1}{2}\,\mathrm{erfc}\left[\left(\frac{E}{N_o}\right)^{1/2}\left(1 - \frac{2|\tau|}{T}\right)\right] . \qquad (3.9)$$

To determine the effects on the curve shape, it will be instructive to graphically examine an extreme case, for example let $1 - \frac{2|\tau|}{T} = \frac{1}{\sqrt{2}}$. The curves to be summed are shown graphically in Fig. 3.4. Note that in this case the first term in the sum can be completely neglected and becomes less significant with increasting $|\tau|$. On the other hand, if $|\tau|$ becomes smaller, the pair of curves on the right would shift to the left while maintaining their relative spacing. The summation would always lie between these two right most curves reaching the limiting case of $P_b = \mathrm{erfc}\left(\frac{E}{N_o}\right)^{1/2}$ for $\tau = 0$. This demonstrates that for constant values of τ the curves shift but essentially retain their shape.

The final variation of the common expressions for probability of error is for coherent detection of a differentially encoded PSK signal as given by Eq. (2.40). This involves the difference of an error

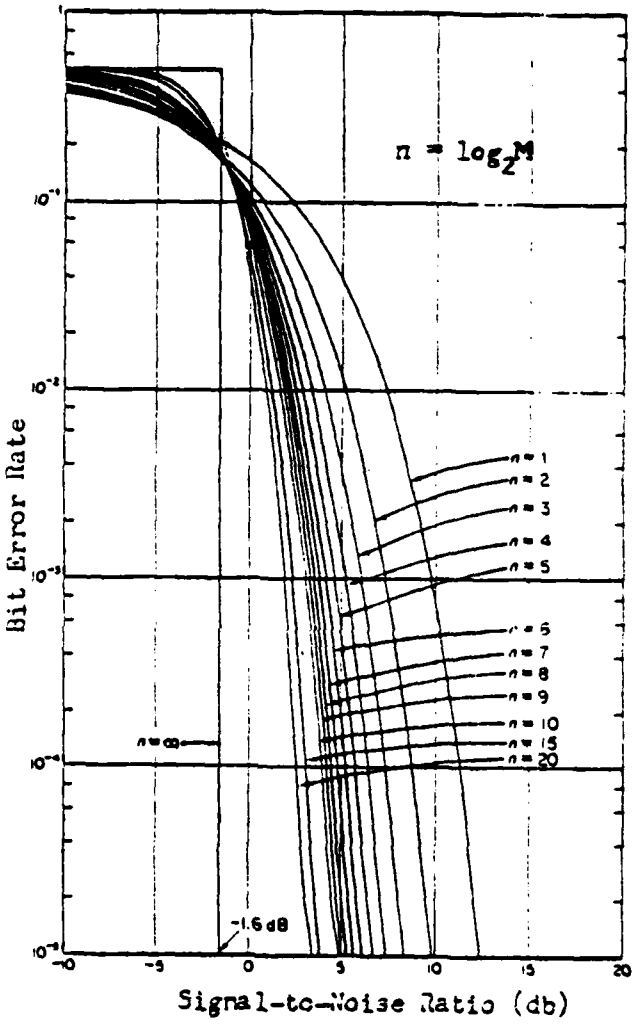

Fig. 3.3. BER vs. Bit Signal-to-noise Ratio, Coherent M-ary FSK.

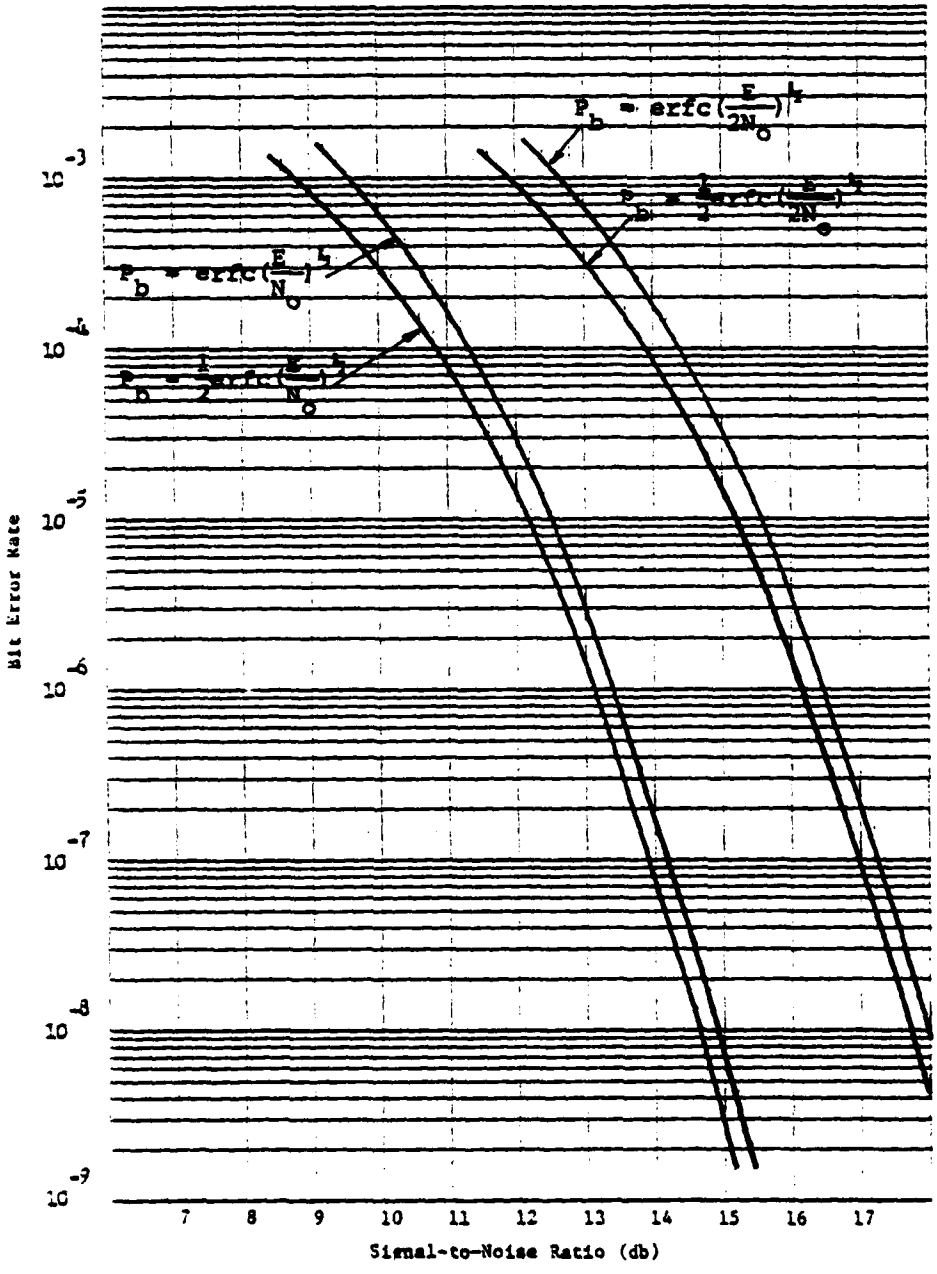

Fig. 3.4. Effects of Constant Symbol Synchronization Error.

function and an error function squared. The BER curve for this expression is shown in Fig. 3.5 as compared to CPSK and DPSK (differential detection). Note that the curve for coherent detection of a differentially encoded signal falls directly between those for CPSK and DPSK, and recall that it serves as a lower bound for any differential detection scheme as shown by Eq. (2.49).

The variations of the functions for probability of error described above completely encompass those normally found for different modulation schemes and ideal detection methods. As mentioned previously, the examples cited for error function curves are equally applicable for exponential functions. In all cases the variations by constant factors and by summation cause shifts in the curves but alter the shape a negligible amount for low error rates.

Phase Error from Phase Locked Loops (PLL)

In later paragraphs the effects of carrier phase error and baud timing error on the performance of different systems will be considered. Before doing so, however, there is a need to investigate briefly how the errors occur and to summarize the characteristics of them.

The use of PLL's for obtaining coherent references for both phase detection and baud timing is almost universal. PLL's in general are non-linear devices and their analysis is highly complex. The initial work in obtaining a probability density function for the phase error of a PLL was accomplished by Tikhonov (1959) and Viterbi (1963).

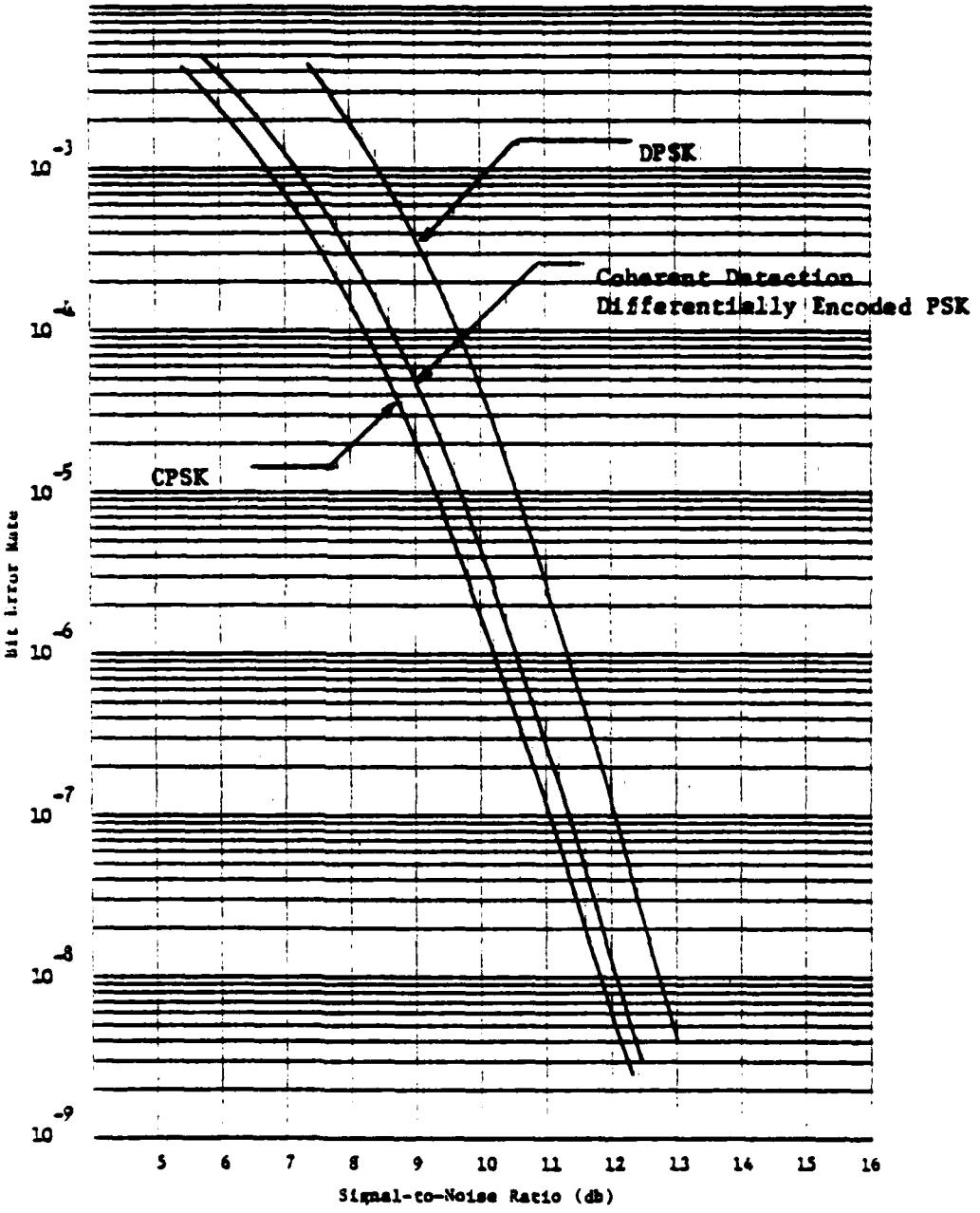

Fig. 3.5. Comparison of CPSK and DPSK.

Excellent textbooks for detailed analysis of PLL's are Viterbi (1966), Stiffler (1971), and Lindsey (1972).

The Tikhonov distribution is widely accepted as the most precise characterization of the phase error of second-order PLLs which are in general use. When the quiescent frequency (no control signal) of the voltage controlled oscillator (VCO) of the PLL is tuned to be equal to the frequency of the received signal, the probability density function of the phase error θ is given by:

$$p(\theta) = \frac{\exp(\alpha \cos \theta)}{2\pi I_0(\alpha)} \qquad -\pi \leq \theta \leq \pi \tag{3.10}$$

where α is the band limited signal-to-noise ratio at the input to the loop and I_0 is the modified zeroth order Bessel function.

Figure 3.6, taken from Viterbi (1963), shows this expression plotted for several values of α. For large values of signal-to-noise ratio and small error, the distribution closely resembles the Gaussian. That a Gaussian density is a very close approximation can be seen from Eq. (3.10) by using the asymptotic expression for the zeroth order modified Bessel function:

$$I_0(\alpha) = \frac{\exp \alpha}{(2 \pi \alpha)^{1/2}} \quad . \tag{3.11}$$

Then expanding cos θ in a Taylor series the function becomes:

$$p(\theta) = \frac{\exp[(-\alpha\theta^2/2)(1 - 2\theta^2/4! + 2\theta^4/6! - \cdots)]}{(2\pi/\alpha)^{1/2}} \quad . \tag{3.12}$$

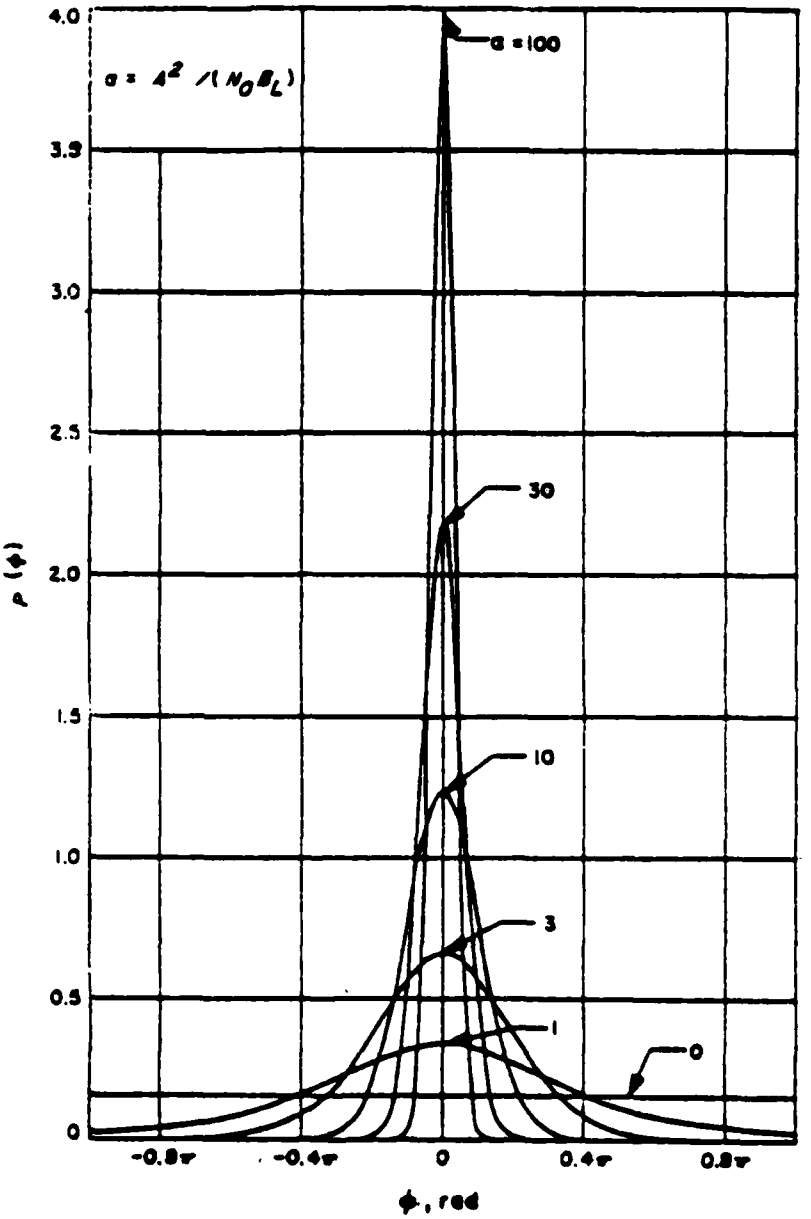

Fig. 3.6. Tikhonov Distribution with Zero Frequency Offset.

For large values of α where θ is small, the higher orders of the Taylor series can be neglected and the density is Gaussian, with mean zero and variance $1/\alpha$. The approximation is valid so long as the phase error variance is sufficiently small [less than about 1/4 rad^2 for sinusoidal signals (Stiffler, 1971)]. In most cases of interest, the phase error variance will be small enough to justify this assumption; if it were not, the loss-of-lock probability would be unacceptably large.

Further justification for the assumption of a Gaussian phase error is needed when the tracking loop involves, or is preceded by, non-linear elements. Because of the non-linearities the noise would then be no longer Gaussian. Nevertheless, if the loop bandwidth is narrow relative to the bandwidth of the filters preceding the non-linear devices, which is generally true, the phase error at any instant is due to the weighted average of a large number of effectively independent noise contributions. The central limit theorem can then be used to argue that the phase error is approximately Gaussian even in this case (Stiffler, 1971).

We have seen that the approximation of Eq. (3.12) and the accepted linear model of a first order PLL result in the variance of the phase error σ_θ^2 being related to the signal-to-noise ratio by:

$$\sigma_\theta^2 = \frac{1}{\alpha} \quad . \tag{3.13}$$

It can also be shown that the variance of the phase error changes very little if the quiescent frequency of the VCO is off-tuned from the received frequency. The mean value, however, is shifted from zero as

an almost linear function of the amount of frequency offset (Lindsey and Simon, 1973), and is almost independent of signal-to-noise ratio over the interval of significance to the BER curves. This is illustrated in Fig. 3.7, which was abstracted from Viterbi (1963).

The density function of the phase error can then be related directly to jitter measurements if the rms and the average values can be determined. If it can be assumed that the phase error is ergodic (this should not create significant problems if the phase error is small enough to insure that bit slippage does not occur), then the variance will be equal to the square of the rms jitter value minus the square of the average. There is always a finite probability of bit slippage, but detection of this phenomenon can be incorporated into jitter meter design.

Calculated Effects of Jitter

In the previous paragraphs the effects of constant multipliers on the derived expressions for probability of error were examined. It was seen that for the most part the results shifted the BER curves but had very little effect on their shape. However, the modifying factors that result from carrier phase reference error and symbol synchronization error, in general, involve random variables. It was found that these errors were normally due to the jitter in the output of a phase-locked loop (PLL) whose probability density function is Tikhonov, but which, in general, can be closely approximated by a Gaussian distribution.

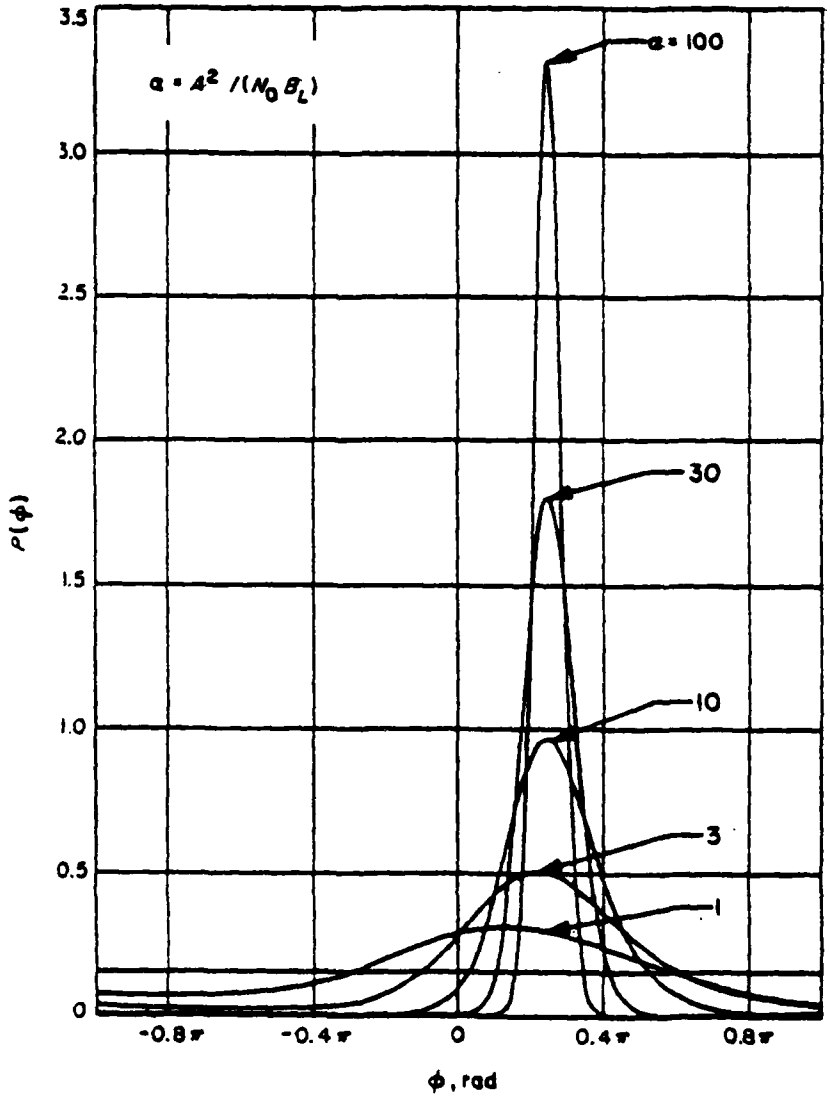

Fig. 3.7. Tikhonov Distribution with Frequency Offset.

To determine the average probability of bit error, the conditional expressions derived for constant timing errors must be integrated over the probability density functions of these errors. For purposes of illustration the expressions derived for CPSK will be used. For the probability of error conditioned on carrier phase jitter the expression is:

$$P_b|\theta = \text{erfc}\left[\left(\frac{2E}{N_o}\right)^{1/2} \cos\theta\right] \tag{3.14}$$

and for symbol synchronization error:

$$P_b|\tau = \frac{1}{2}\,\text{erfc}\left(\frac{2E}{N_o}\right)^{1/2} + \frac{1}{2}\,\text{erfc}\left[\left(\frac{2E}{N_o}\right)^{1/2}\left(1 - \frac{2|\tau|}{T}\right)\right]. \tag{3.15}$$

Numerical evaluation of these expressions integrated over the Tikhonov distribution has been accomplished by Lindsey (1972) and over the Gaussian distribution by Stiffler (1964) with similar results. Graphical representations of Stiffler's results are shown in Figs. 3.8 and 3.9.

In order to have complete information upon which to base conclusions about the effects of carrier phase and baud timing jitter it was necessary to extend the results of Stiffler and Lindsey in four areas. First, these curves are plotted only to a BER of 10^{-5}, whereas results to 10^{-7} or 10^{-8} are of interest to this study and to many practical applications.

Second, Stiffler's and Lindsey's results are similar, but not sufficiently alike to judge absolutely the extent of the validity of

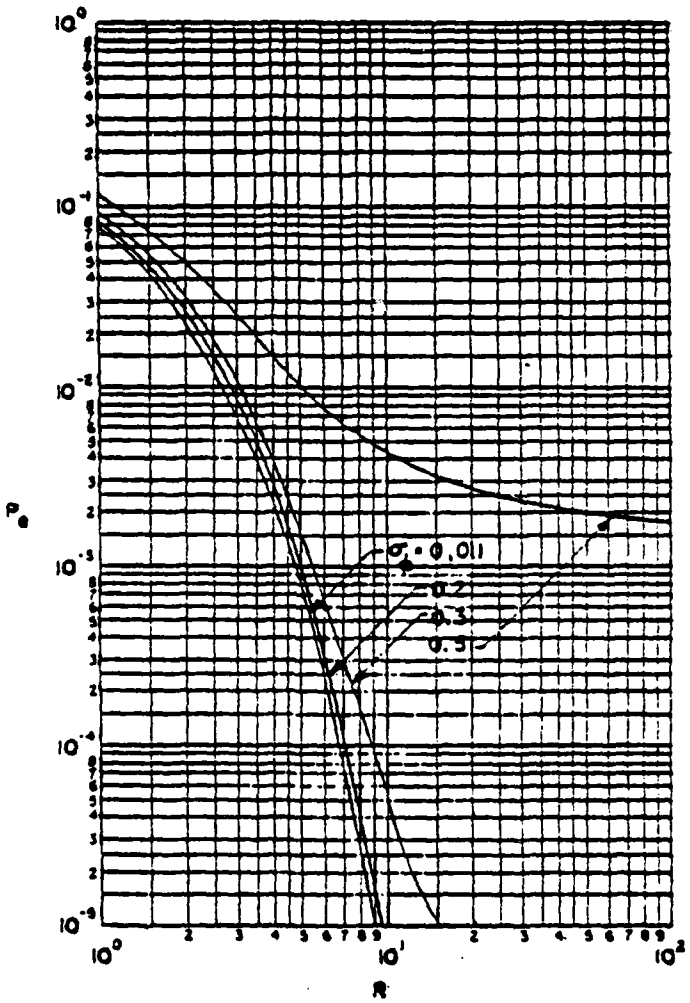

Fig. 3.8. BER Curves with Gaussian Carrier Phase Error, Zero Mean, Standard Deviation as Indicated (Stiffler, 1964).

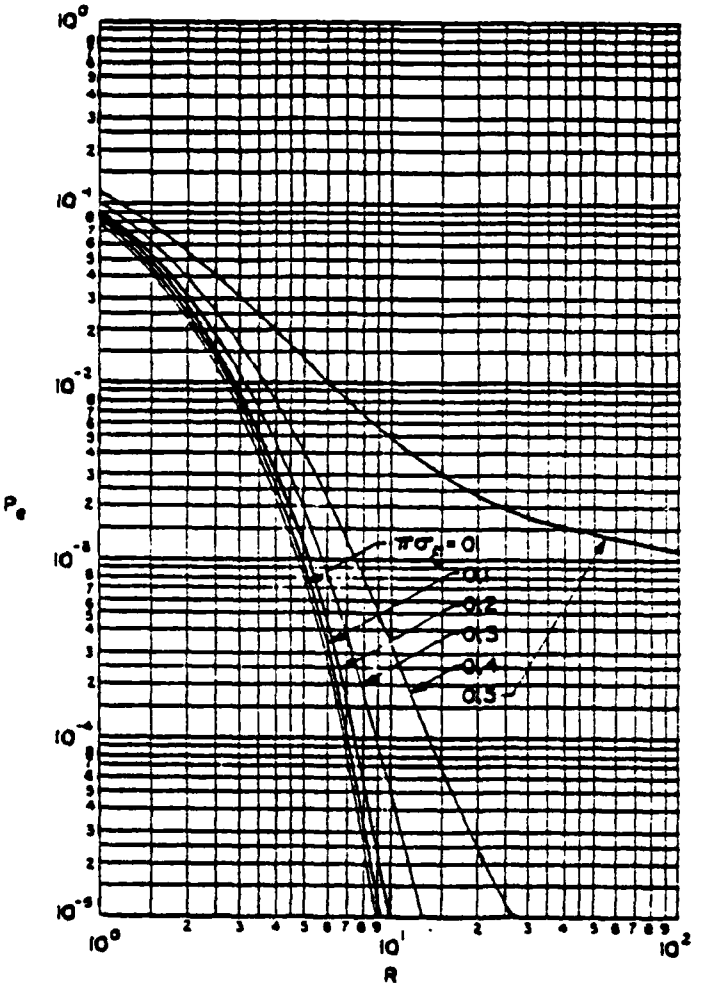

Fig. 3.9. BER Curves with Gaussian Baud Timing Error, Zero Mean, Standard Deviation as Indicated (Stiffler, 1964.

the Gaussian approximation. A suitable basis for comparison was established by the use of the same parameters for both distributions and of course by using the same program for numerical integration.

The third extension was to obtain curves for the effects of jitter with non-zero mean. Although it is very easy to misconceive the term jitter as referring to a purely oscillatory phenomenon, it is a random variable having both a mean and a variance. Indeed, as will be seen in Chapter 4, in most of the experiments it was possible to adjust the mean value of the jitter by phase offset, but little could be done to change the variance.

The last extension involved the extreme tails of the phase error density functions. Both the Tikhonov distribution and the Gaussian approximation are valid only on the interval $(-\pi/2, \pi/2)$ which assumes no bit slippage. The question to be answered was: how significant are the so-called irreducible bit errors? These are the errors that result from the probability that the jitter exceeds $\pi/2$ in magnitude.

In order to answer these questions a computer program for the CDC Cyber 175 was written to evaluate error probabilities for a wide range of parameters. The first step was to attempt to duplicate the curves of Lindsey and Stiffler to insure that a common basis was being used and to establish the validity of the program.

Carrier Phase Jitter

Figures 3.10 and 3.11 are the results obtained by integrating Eq. (3.14) for carrier phase reference error over the Tikhonov and Gaussian probability density functions respectively with zero mean and constant standard deviation as indicated. The results agree closely with those of Lindsey and Stiffler and have been extended to lower bit error rates where applicable. The differences between the Tikhonov and Gaussian curves are only very slight at the extreme tails. For most purposes these differences would be completely insignificant. It should be noted here that, as expected, for small values of jitter variance the curves are shifted laterally while essentially retaining the characteristic error function shape. However, for the large values of standard deviation in excess of 0.2, the shifts become more pronounced and the tails of the curves tend to flare outward. This phenomenon will be discussed in detail in Chapter 5 in comparison with the experimental results.

Figures 3.12 and 3.13 are the results of carrier phase jitter calculations assuming constant variance and non-zero mean with the Gaussian distribution. In Fig. 3.12 where the variance is small the curves are very well behaved and maintain their theoretical shape while shifting laterally with increased mean value. However with the larger variance in Fig. 3.13 the curves again begin to flare outward at the tails as the mean value is increased.

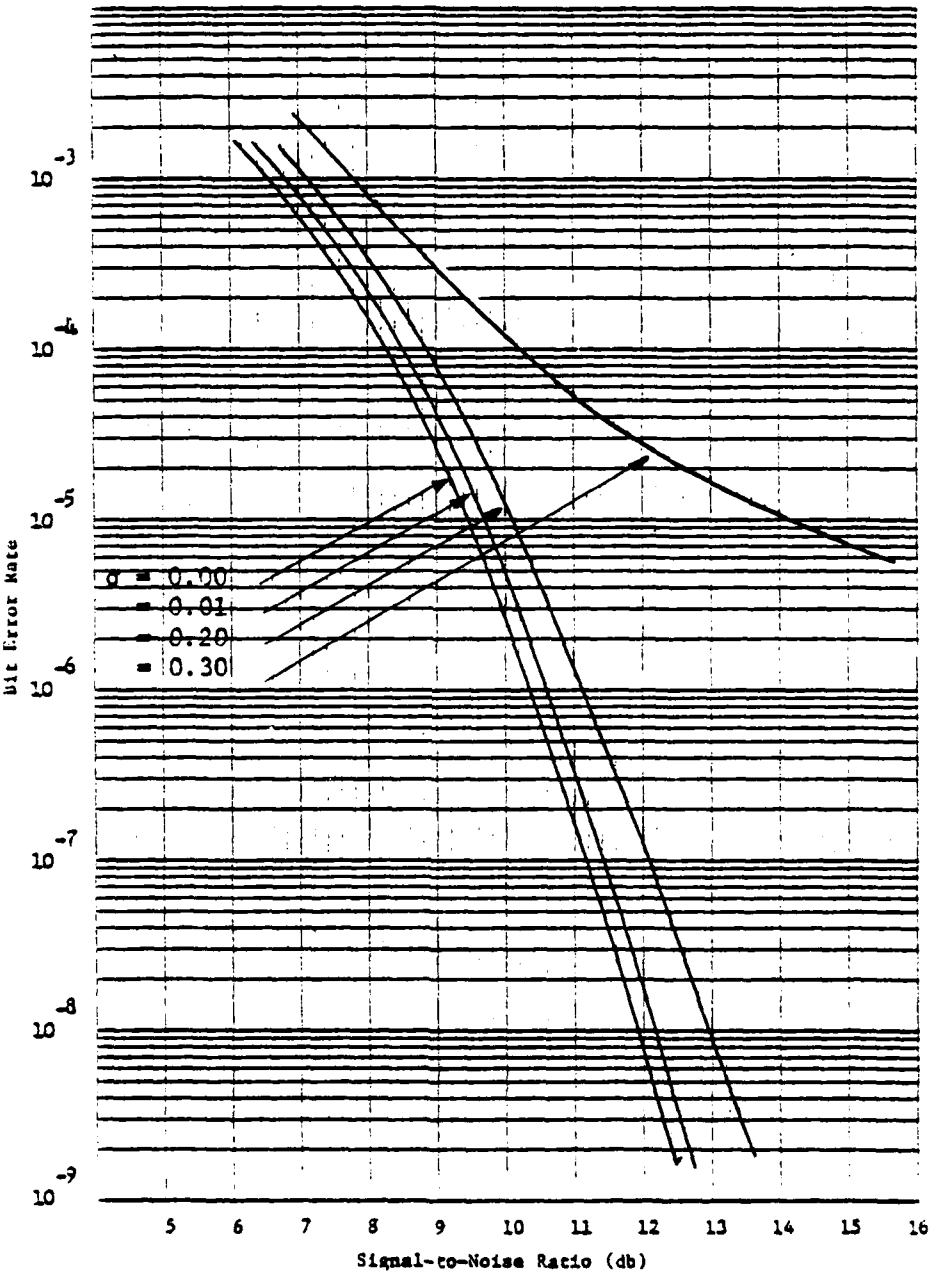

Fig. 3.10. Carrier Phase Jitter, Tikhonov Distribution, Zero Mean, Constant Standard Deviation as Indicated.

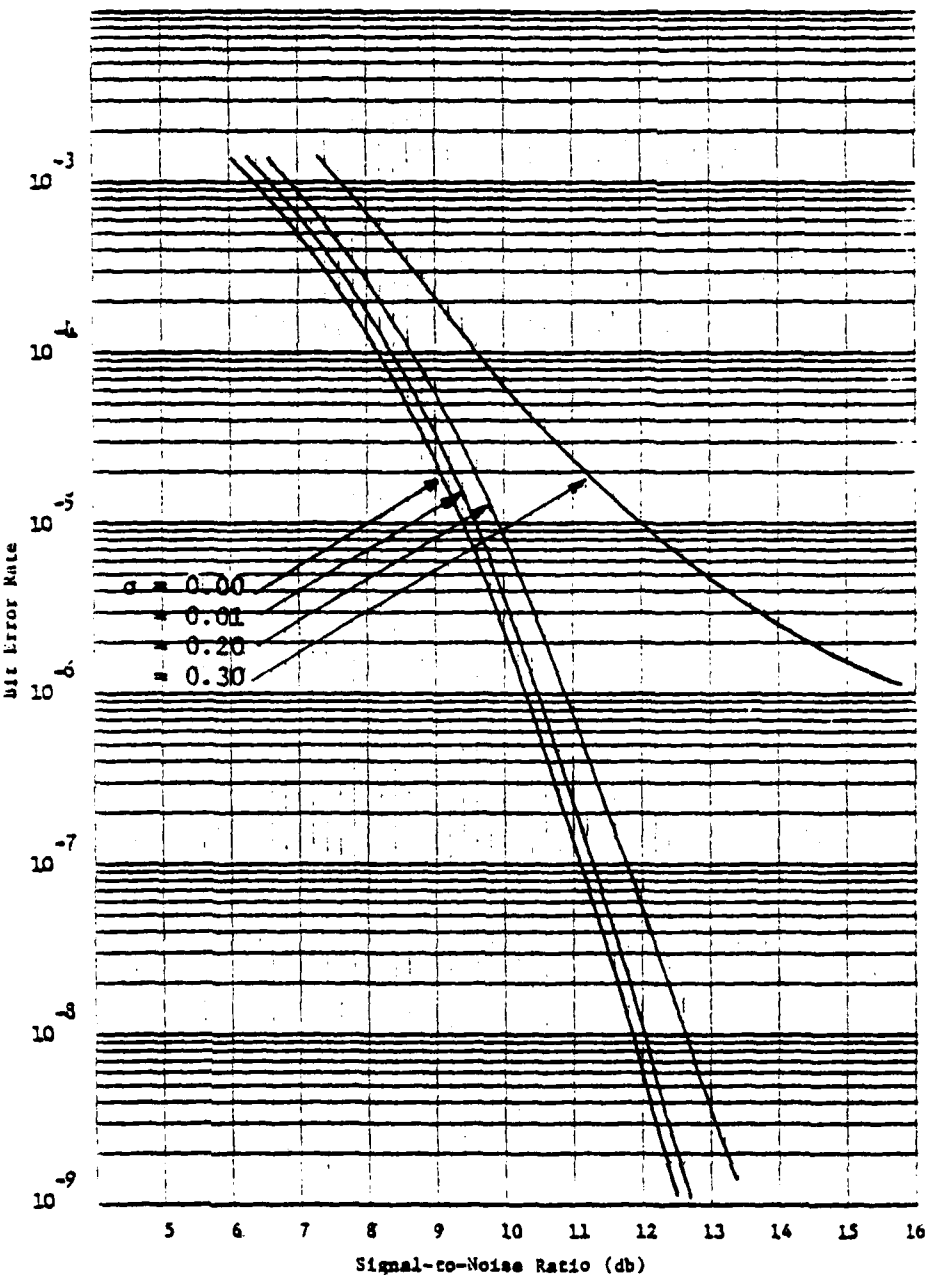

Fig. 3.11. Carrier Phase Jitter, Gaussian Distribution, Zero Mean, Constant Standard Deviation as Indicated.

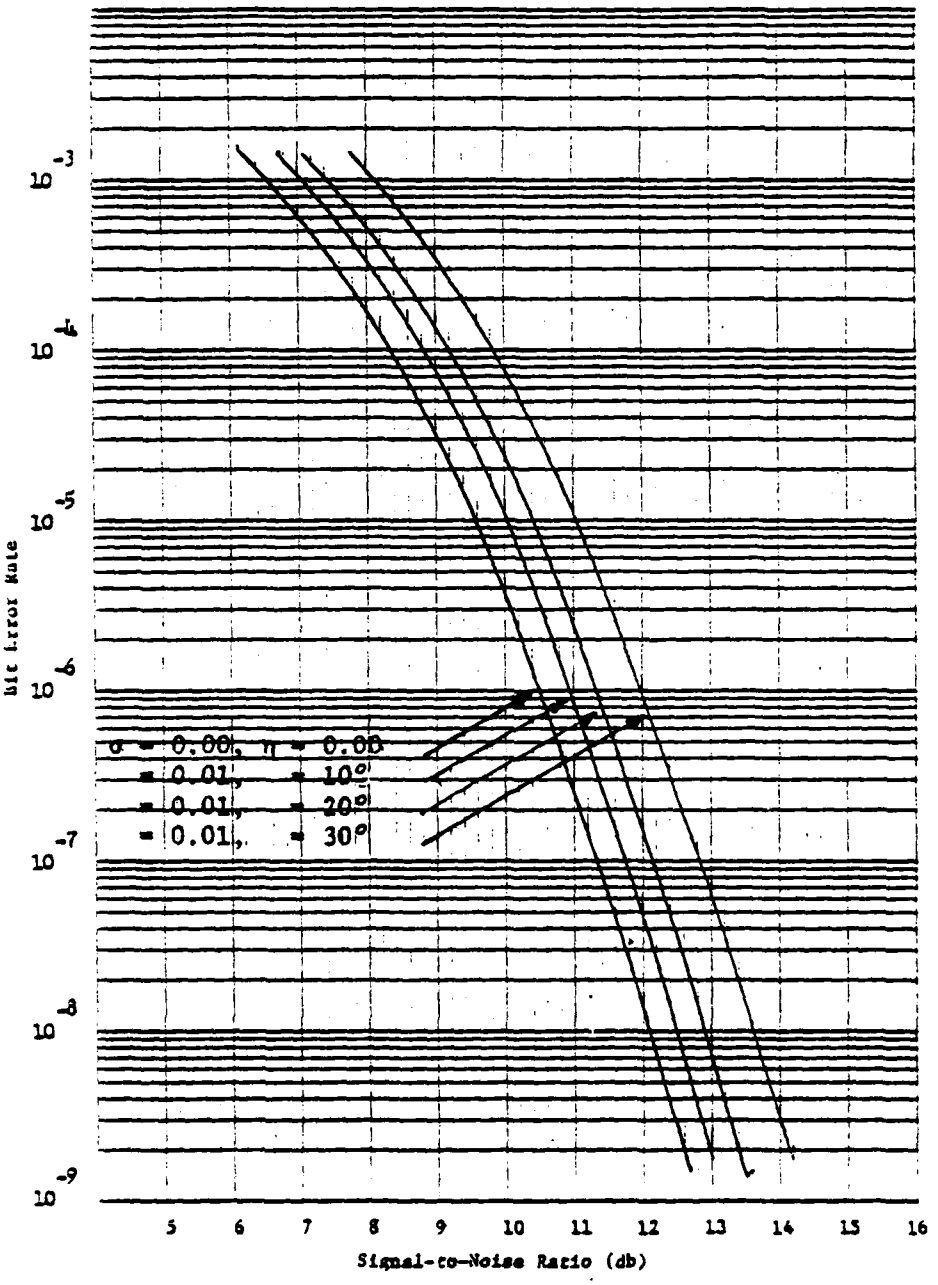

Fig. 3.12. Carrier Phase Jitter, Gaussian Distribution, Non-zero Mean, 0.01 Constant Standard Deviation.

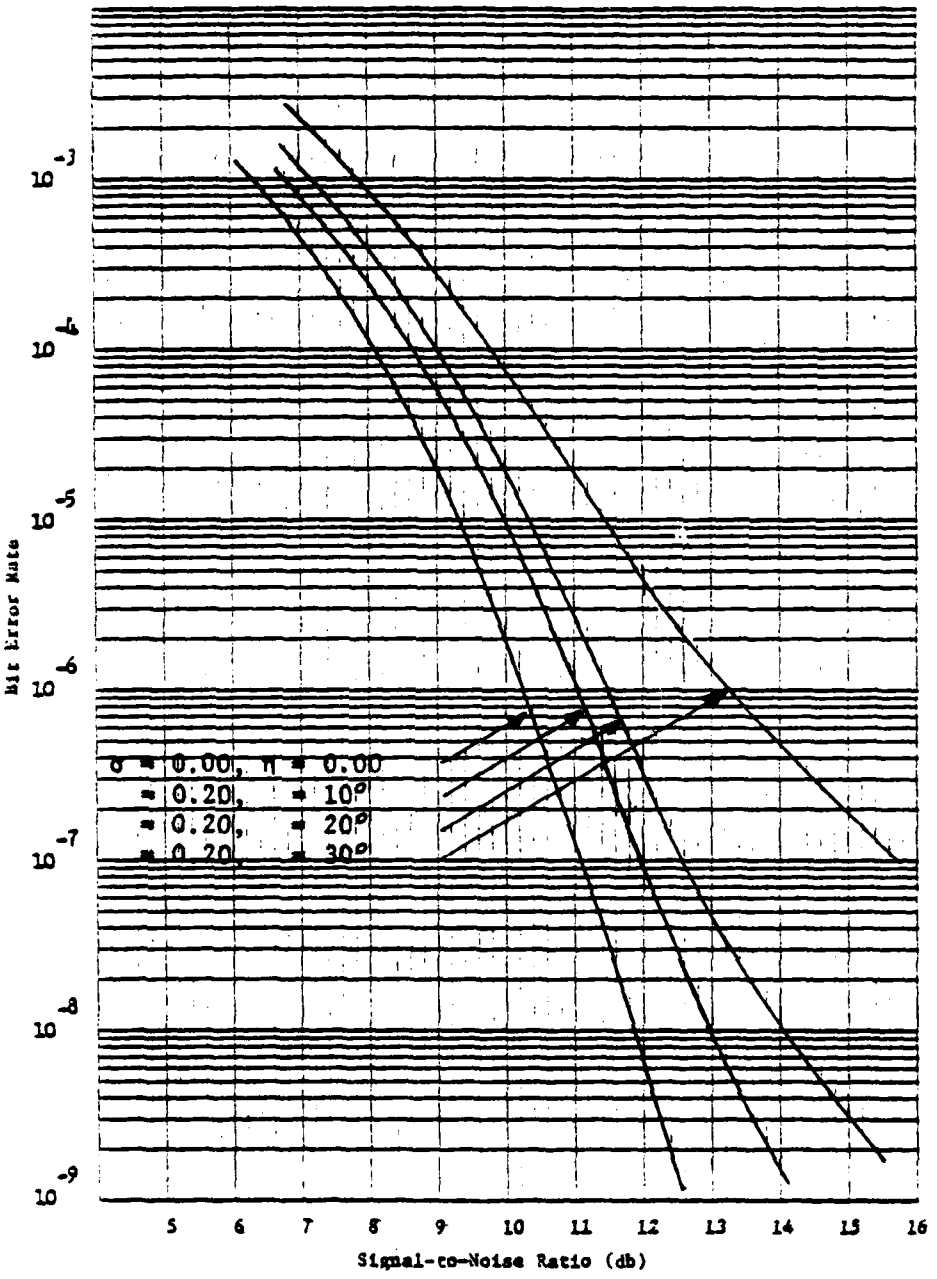

Fig. 3.13. Carrier Phase Jitter, Gaussian Distribution, Non-zero Mean, 0.20 Constant Standard Deviation.

Baud Timing Jitter

Figures 3.14 and 3.15 are the results for symbol synchronization error obtained by integrating Eq. (3.15) over the Tikhonov and then Gaussian distributions with zero mean and constant variance. These curves again show the results to be consistent with those of both Lindsey and Stiffler and demonstrate that the Gaussian approximation is indeed valid. The differences between the Tikhonov and Gaussian curves are very slight at the extreme tails and for most purposes can be neglected. The curves shift as expected for increases in variance but again the tails flare out for the larger values.

The next two sets of curves, Figs. 3.16 and 3.17 have been obtained for baud timing jitter with non-zero mean Gaussian distributions and with constant standard deviations of 0.03 and 0.05 respectively. As can be seen, the non-zero mean acts similarly to a constant multiplier of the argument and although the curves are shifted considerably, there is only a slight tilting, in these cases, but no flareout. Based on the previous results flareout would be expected for a larger value of constant variance. This is discussed in Chapter 5 in comparison with experimental results.

Irreducible Errors

Table 3.1 lists the irreducible errors for a number of mean values and standard deviations. These are the probabilities that the magnitude of the phase error exceeds $\pi/2$ using the Gaussian distribution. The significance of the irreducible errors is a result of their

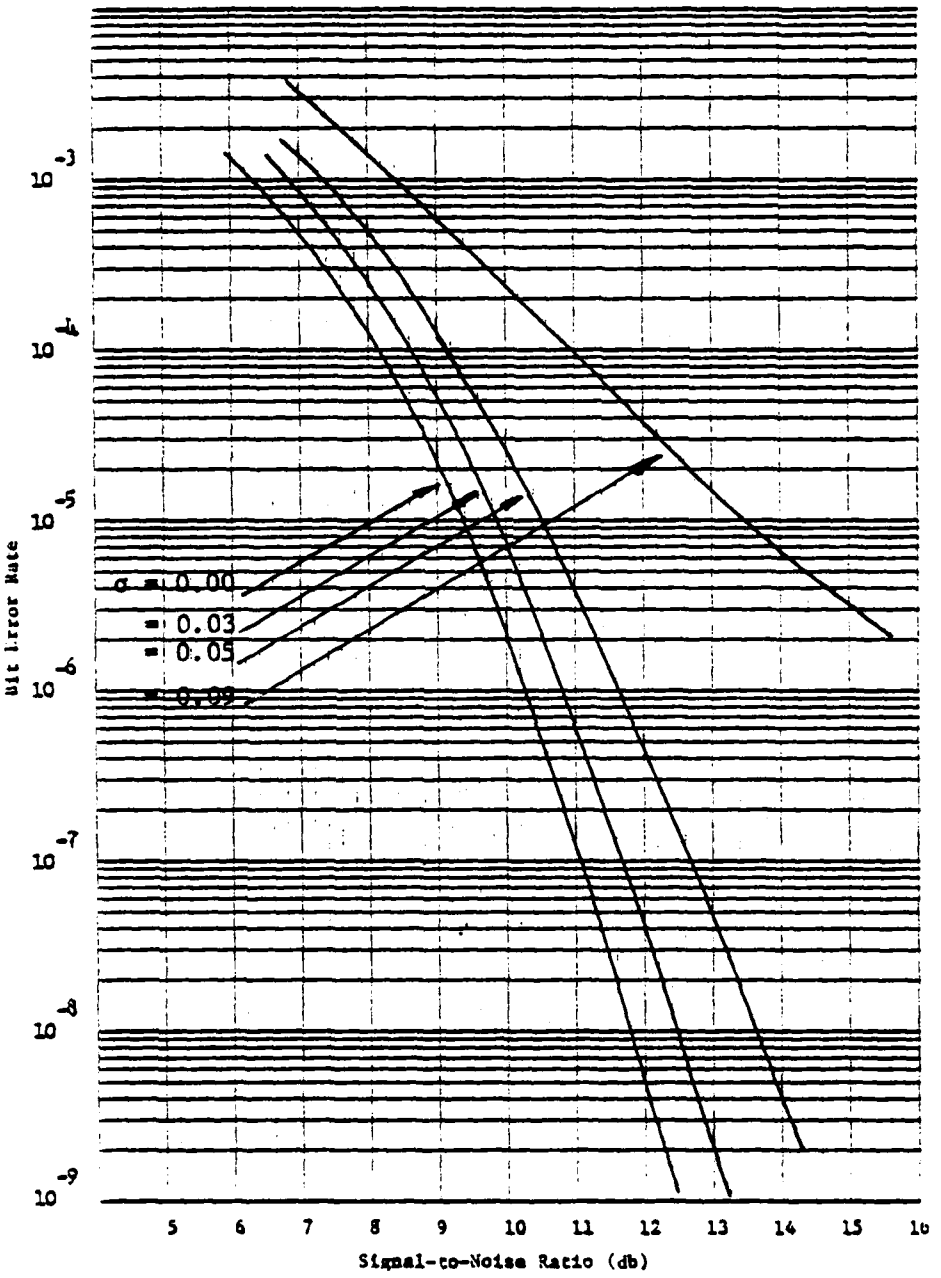

Fig. 3.14. Baud Timing Jitter, Tikhonov Distribution, Zero Mean, Constant Standard Deviation as Indicated.

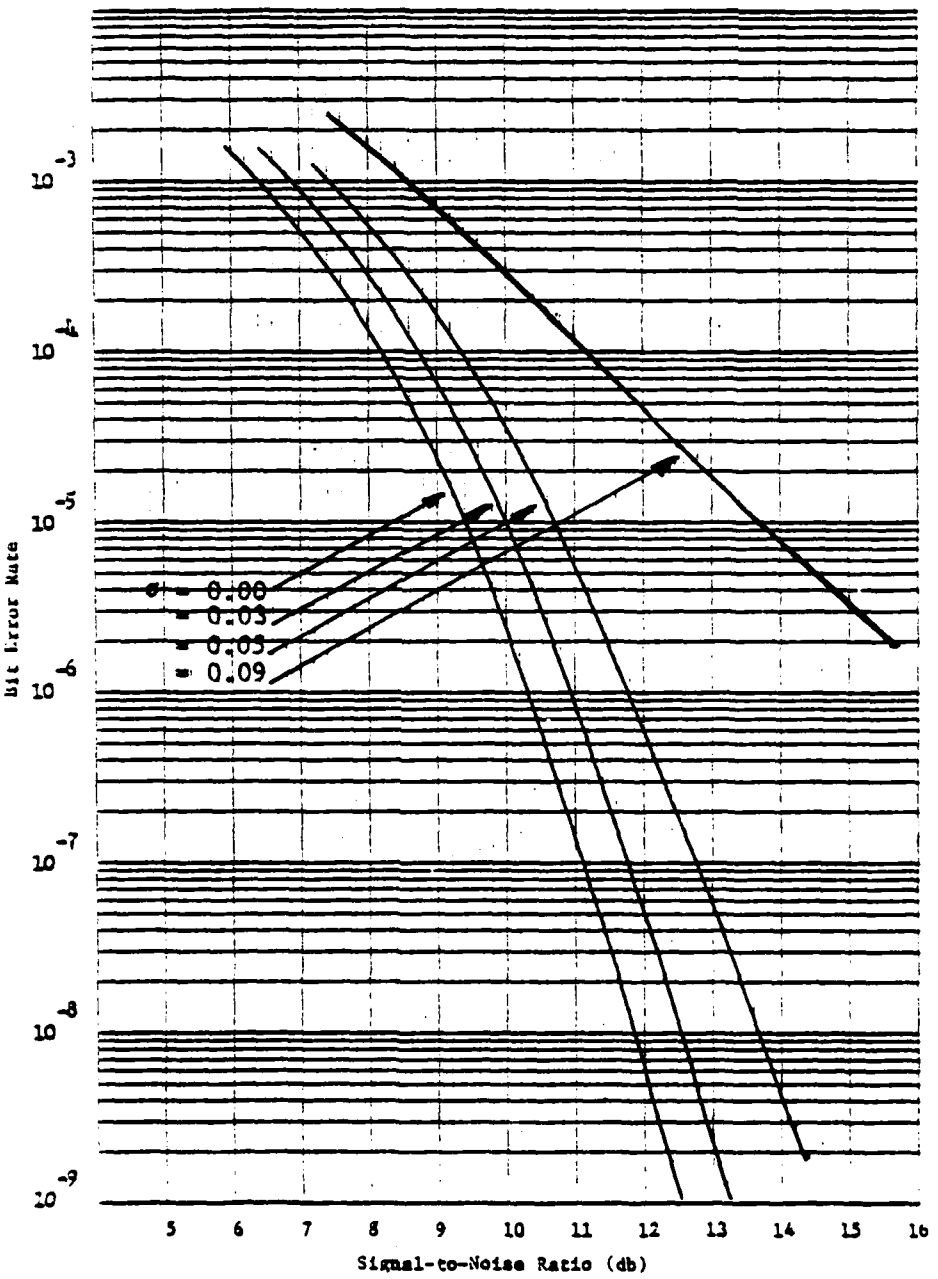

Fig. 3.15. Baud Timing Jitter, Gaussian Distribution, Zero Mean, Constant Standard Deviation as Indicated.

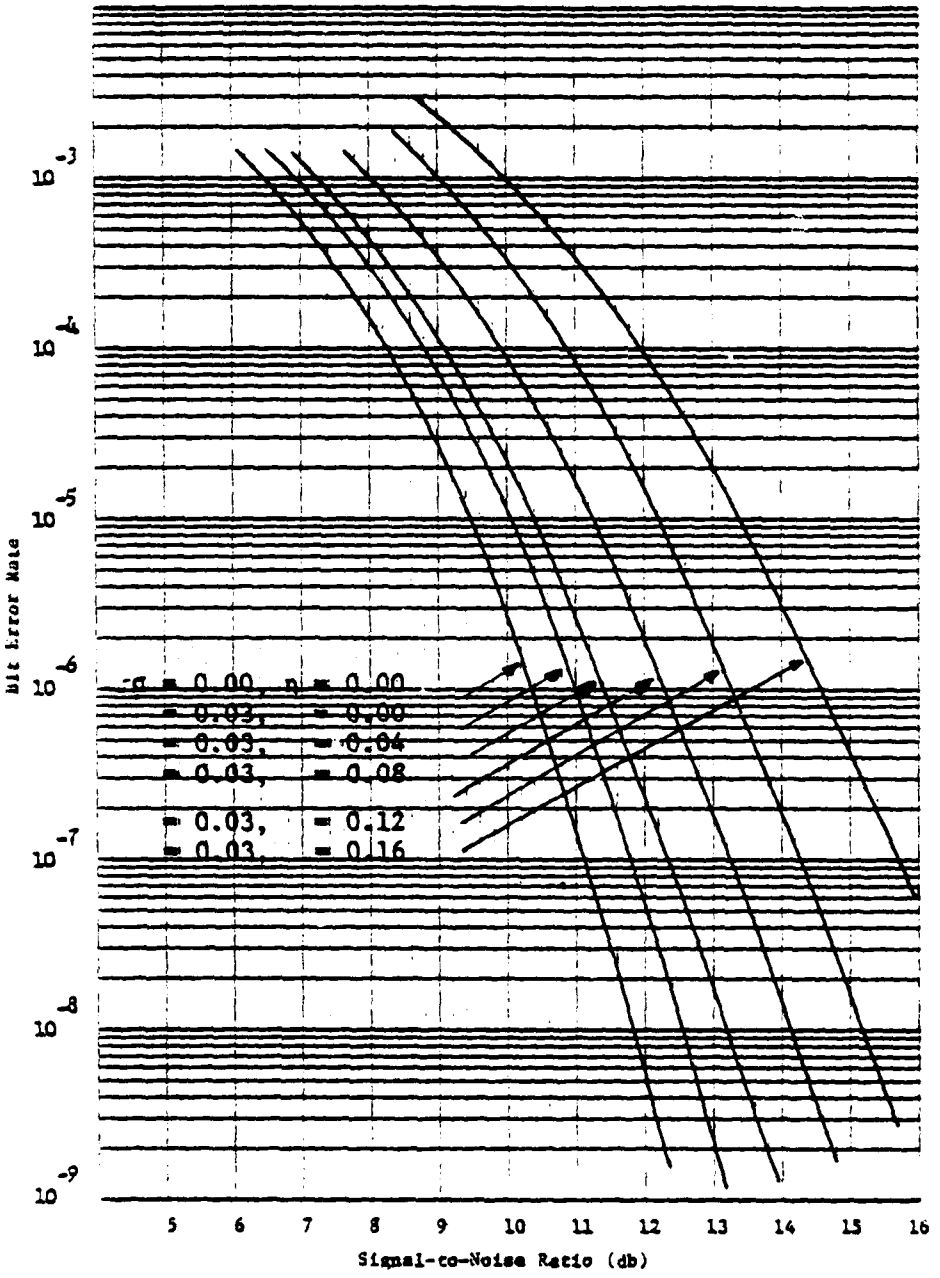

Fig. 3.16. Baud Timing Jitter, Gaussian Distribution, Non-zero Mean, 0.03 Constant Standard Deviation.

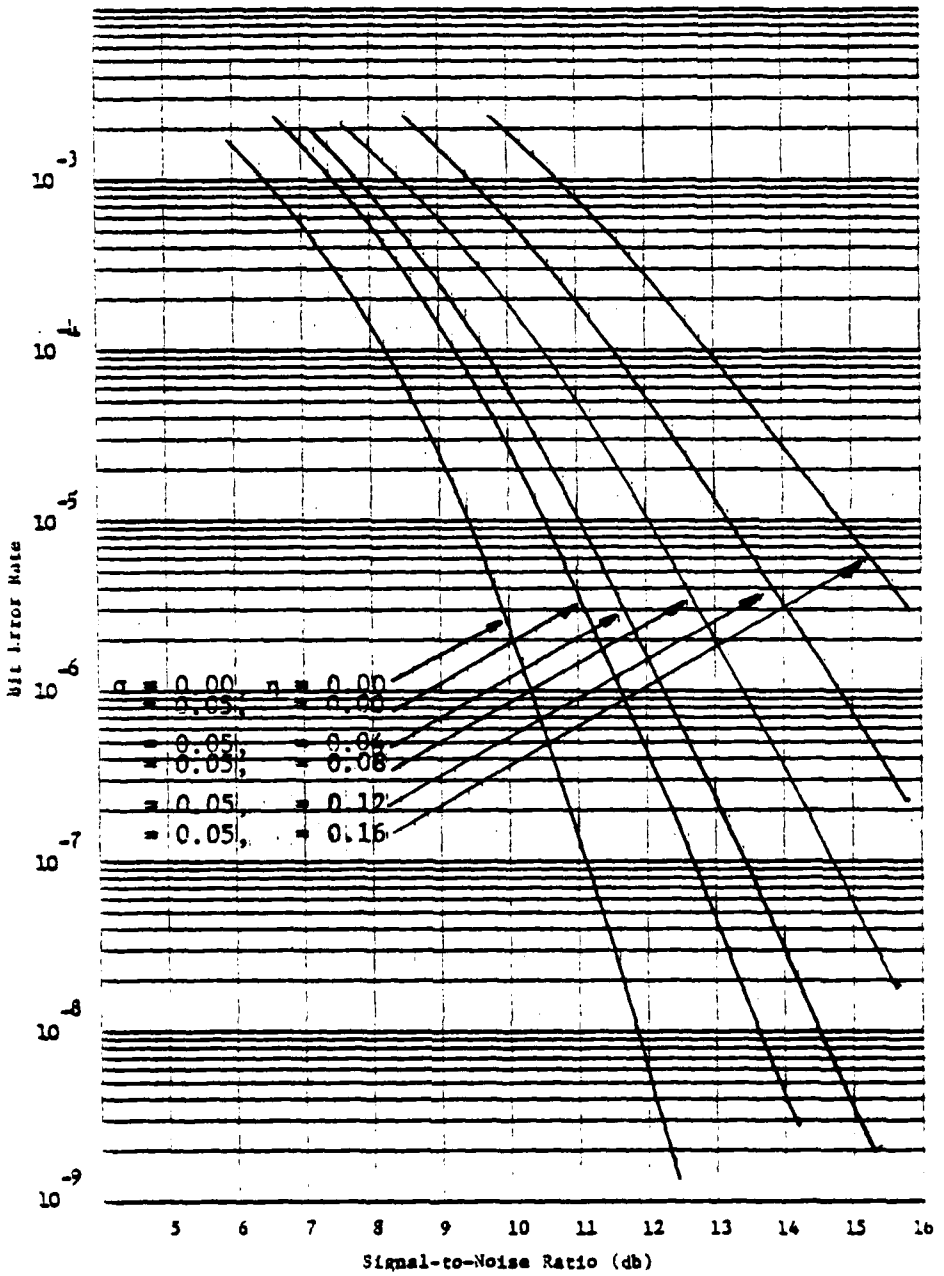

Fig. 3.17. Baud Timing Jitter, Gaussian Distribution, Non-zero Mean, 0.05 Constant Standard Deviation.

Table 3.1. Irreducible Errors.

η	σ		
	0.01	0.2	0.3
0	$< 10^{-50}$	$< 10^{-50}$	1.6×10^{-7}
5°	$< 10^{-50}$	6.0×10^{-14}	4.3×10^{-7}
10°	$< 10^{-50}$	1.4×10^{-12}	1.7×10^{-6}
20°	$< 10^{-50}$	5.0×10^{-10}	2.3×10^{-5}
30°	$< 10^{-50}$	8.2×10^{-8}	2.4×10^{-4}

being constant for given values of mean and variance of the jitter. They are irreducible in that they are independent of signal-to-noise ratio and the BER curves will flatten out and become asymptotic to that error rate. Fortunately as seen from the table these probabilities will be negligible except in the cases of large variance or large phase offset. These conditions are not normally found in real systems since small constant variance is a PLL design objective and phase offset can be eliminated to a great extent by proper alignment.

Other Effects of Jitter

It was found in Chapter 2 that the effects of jitter upon some modulation schemes could not be expressed in closed form or the forms were considerably different from those used in the calculations of the previous section. These will be discussed here in terms of their effects upon the BER curves.

Non-coherent Detection of ASK and FSK

An expression for probability of symbol error conditioned on a fixed normalized frequency error in the non-coherent detection of M orthogonal signals was given in Eq. (2.80). This expression was evaluated for several fixed values of frequency error by Chadwick (1969). His results are shown in Fig. 3.18. Since the curves are plotted only for relatively large symbol error rates the results are not too conclusive. However, to the extent that is shown, the curves shift but retain their characteristic shape for increases in frequency error.

A similar expression was given in Eq. (2.81) for the effect of symbol synchronization error on non-coherent detection of M orthogonal signals. This was also evaluated by Chadwick (1969) for several constant values of normalized timing error with the results shown in Fig. 3.19. Again the results are not too conclusive, but illustrate that at least for small values of timing error the curves essentially retain their shape.

Simplified expressions for probability of bit error in non-coherent detection of binary ASK and FSK similar to those for other systems were derived and given in Eqns. (2.83) and (2.84) respectively. To illustrate that the simplified expressions are comparable to Chadwick's, several points (indicated by x's in Fig. 3.19) have been calculated using Eq. (2.84) with a normalized timing error of 0.1.

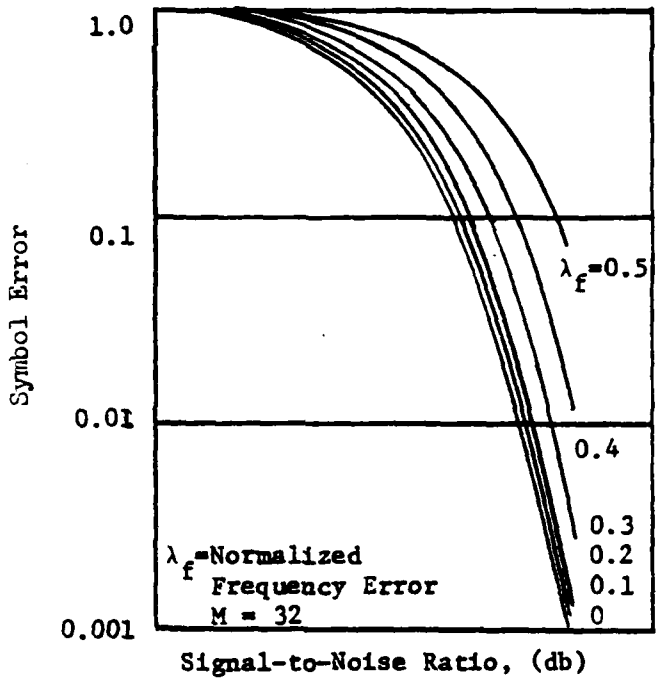

Fig. 3.18. Probability of Symbol Error vs. Signal-to-noise Ratio, with Frequency Deviation, Noncoherent FSK.

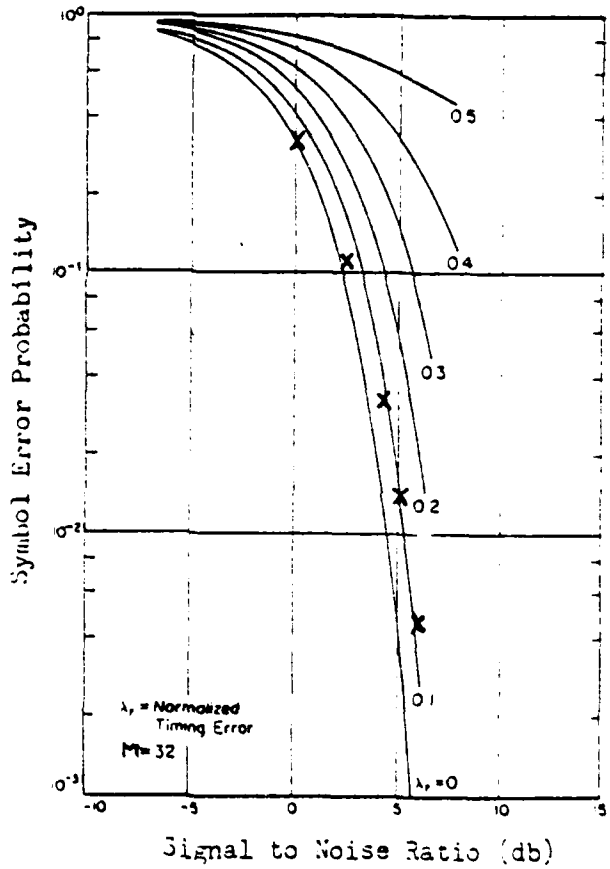

Fig. 3.19. Probability of Symbol Error vs. Signal-to-noise Ratio with Normalized Timing Error, Non-coherent FSK.

Three-level Partial Response Systems

The literature contains several variations of methods for calculating the effects of baud timing jitter in the detection of partial response systems. All of the methods observed resulted in a shift of the theoretical BER curve as a function of timing offset without substantial variation in the shape of the curve; however, none considered jitter as a random variable possessing both a mean and a variance. Two of the results will be described.

Craig (1975) utilized equations describing the eye openings of partial response systems to determine the effect of error in sample time. He calculated the additional signal power necessary (assuming constant noise) to maintain a given error rate for a given timing error. The results illustrate the point that a given timing error causes a lateral shift of the characteristic curve of BER versus signal-to-noise ratio without alteration of the shape.

Smith (1973) proposed a performance monitoring scheme for a class I, three-level partial response system by monitoring pseudo-errors generated by offsetting the sampling time. To prove the validity of the performance monitoring scheme, he set out to show that the pseudo-errors tracked the actual error rate. He calculated the resulting signal level for given values of offset by summing the contributions of all interfering signals. Curves illustrating the results of the calculations for several values of timing offset Δ which are fractions of T/2 are shown in Fig. 3.20. As can be seen, the curves are shifted but are essentially

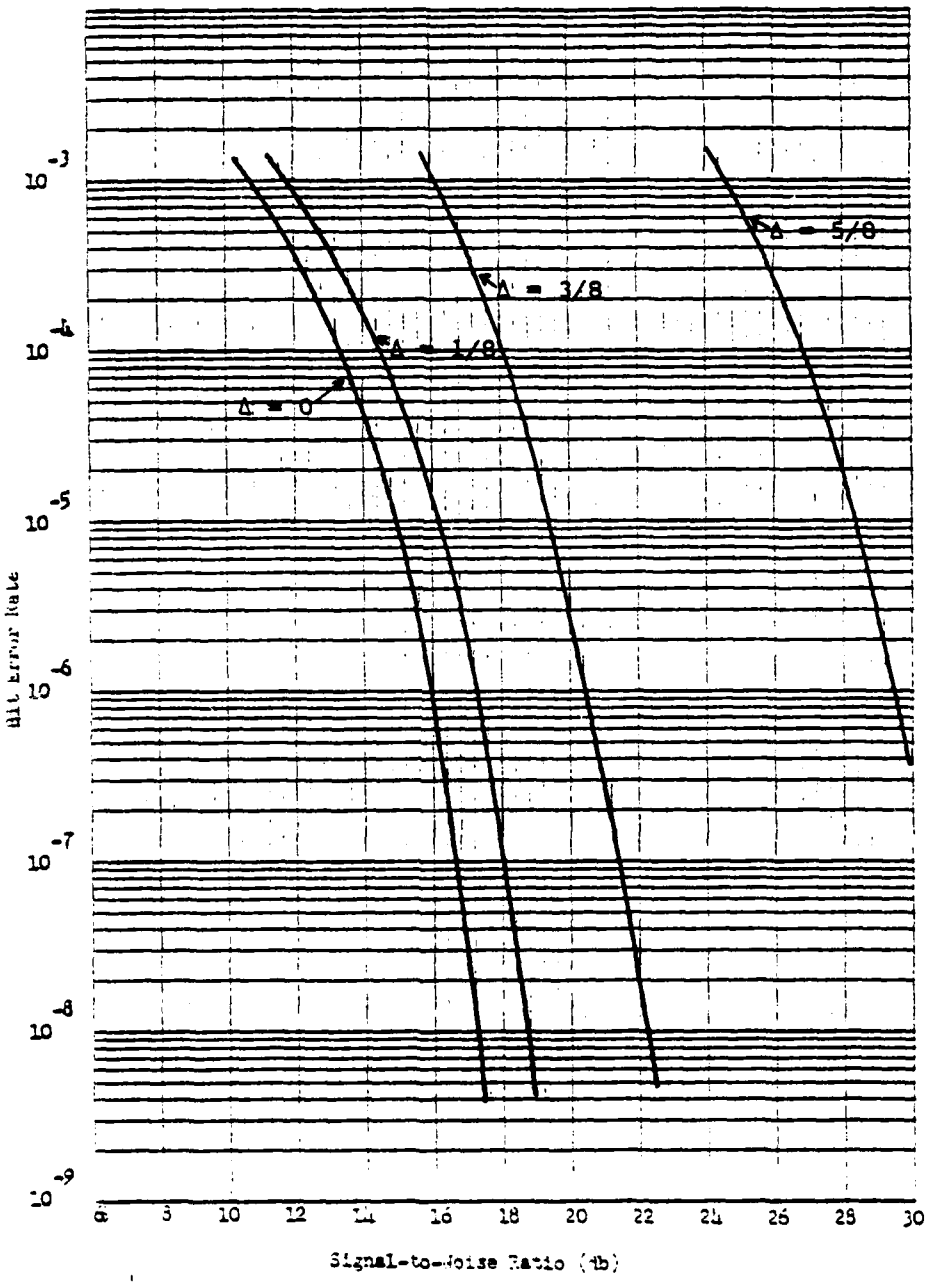

Fig. 3.20. Calculated BER Curves with Sampling Offset, Three-level Partial Response (Smith, 1973).

parallel at error rates less than 10^{-4}. An interpolation of these curves will be used in Chapter 5 in a comparison with experimental results.

Intersymbol Interference

In any real channel transmitting digital data there will be present during the detection of any given pulse an overlapping of the tails of other pulses, which in general will degrade the detection process and add to the probability of error. This undesirable characteristic is called intersymbol interference. Although it is equally present in carrier modulation systems, the discussion of intersymbol interference has been deferred until after the description of baseband systems since it is primarily a function of the pulse shape, regardless of the presence or absence of a carrier.

The classical design problem of a digital data system is to manipulate the transmitting and receiving filter characteristics in order to minimize the combined effects of intersymbol interference and Gaussian noise and thereby achieve minimum probability of error. [For detailed discussions of this problem see Lucky, Salz, and Weldon, 1968) or Bennett and Davey (1965)]. The conditions upon the shape of the received signal, as the overall result of the channel characteristics and the filters, which results in elimination of intersymbol interference were first derived by Nyquist.

If the received signal r(t) is a series of pulses a_i, then the detection sample of the kth pulse will be

$$r_k = a_k + \sum_{m \neq k} c_m a_m + n_k \tag{3.16}$$

where c_m represents the interference factor from other pulses a_m, and n_k is the noise at the kth sampling instant. The probability of error is the probability that the amplitude of the interference plus noise exceeds a_k. Obviously, intersymbol interference can only be eliminated by making all $c_m = 0$. This can be accomplished if the tails of all pulses pass through zero at T-second intervals where 1/T is the data rate. An example of such a pulse is the Nyquist shape shown in Fig. 3.21.

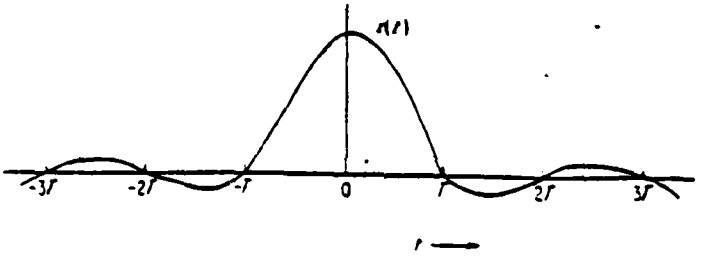

Fig. 3.21. Nyquist Pulse.

This criterion for removal of intersymbol interference does not uniquely specify the spectrum of the received pulse unless the bandwidth is limited to the Nyquist band 1/2T as will be seen. Unfortunately, the filter characteristics that are necessary to achieve the desired overall characteristic are in general not physically realizable and can only be approximated. One class of Nyquist characteristics which has been extensively used and studied is the raised-cosine response illustrated in Fig. 3.22. A raised-cosine frequency characteristic consists

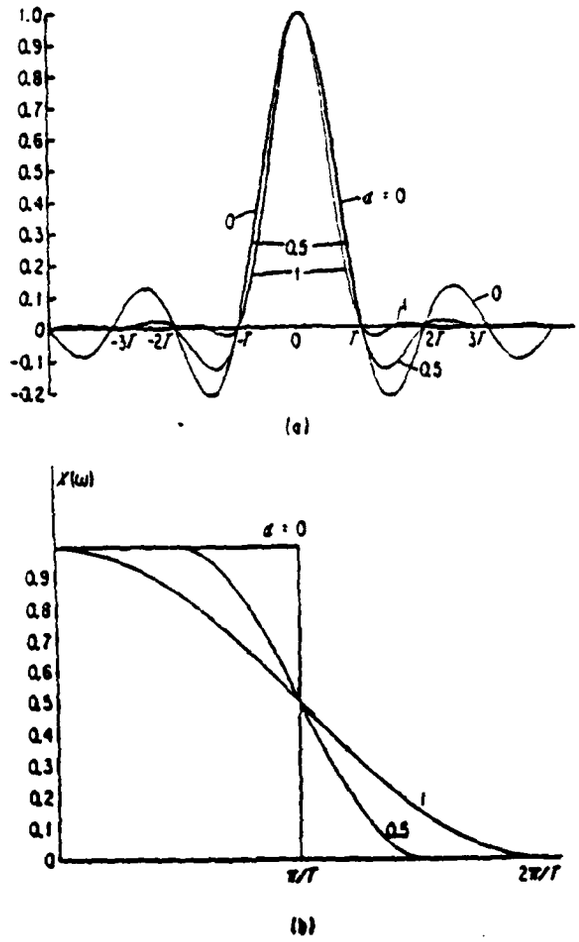

Fig. 3.22. Raised Cosine Spectrum.

of a flat amplitude and a roll-off portion which has a sinusoidal form as shown in Fig. 3.22(b). The roll-off factor is the proportionate amount of excess bandwidth used over the Nyquist bandwidth. The characteristic for $\alpha = 0$, corresponding to an ideal low-pass filter, would result in a data rate of two bits per Hz of bandwidth, with no intersymbol interference as has been mentioned previously. Unity roll-off represents a one bit per Hz characteristic.

Although the overall pulse spectrum in digital data transmission systems is generally selected to meet the Nyquist criterion as closely as possible, this assumes a predictable channel and perfect timing conditions. Since these conditions can only be approached in any real system, it is necessary to examine the effects of significant amounts of intersymbol interference.

Exact calculation of the probability of error in a digital data system with intersymbol interference is theoretically possible by directly enumerating all possible values that the interference can take at the sampling instant (Lucky et al., 1968). This direct approach is computationally extremely complex and usually impractical. Extensive efforts have been expended in the search for practical alternative methods.

The alternative methods for estimating the effects of intersymbol interference have generally taken the form of upper and lower bounds or of truncated pulse train approximations. The results have for the most part been confined to pulse amplitude modulated (PAM) baseband systems and CPSK systems, but as was mentioned above, the

pulse shape is the most significant factor and the results can readily be extended to other modulation schemes.

As an illustration of the results that are obtainable from the method of establishing upper and lower bounds, Fig. 3.23 has been extracted from McLane (1974). These curves were obtained by assuming a Gaussian pulse shape which was introduced by Lugannani (1969). It can be seen that the bounds are quite tight. Figure 3.24 also from McLane, shows similar results when the pulse shape is assumed to be Chebyshev [also introduced by Lugannani (1969)].

Shimbo, Celebiler, and Fang (1971 and 1973) claim to have an exact method for calculation of the effects of intersymbol interference. Actually the method uses a truncated pulse train approximation which can be extended to obtain results as accurate as desired. Their results for a quaternary PSK system with a double-pole filter and several values of time-bandwidth product is shown in Fig. 3.25 as compared to Prabhu's upper bound. Figure 3.26 shows their results considering the effect of intersymbol interference on binary CPSK and DPSK systems with seven-pole Butterworth filters with a time-bandwidth product of 1.2.

The effect of intersymbol interference is a discrete random variable dependent upon the pulse sequence. Its distribution becomes continuous in the limit if an infinite number of symbols are considered; however, it can be shown that even in the limit, the density function is bounded (Lucky et al., 1968). The tails are, therefore, non-Gaussian. Errors due to intersymbol interference alone would be independent of signal-to-noise ratio and would, therefore, distort the shape of the

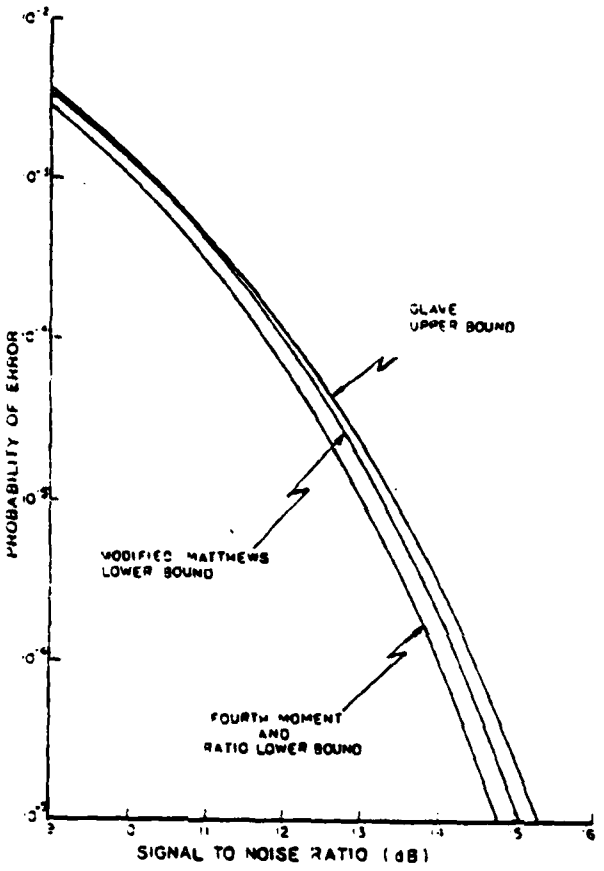

Fig. 3.23. Intersymbol Interference, Upper and Lower Bounds, Gaussian Pulse (McLane, 1974).

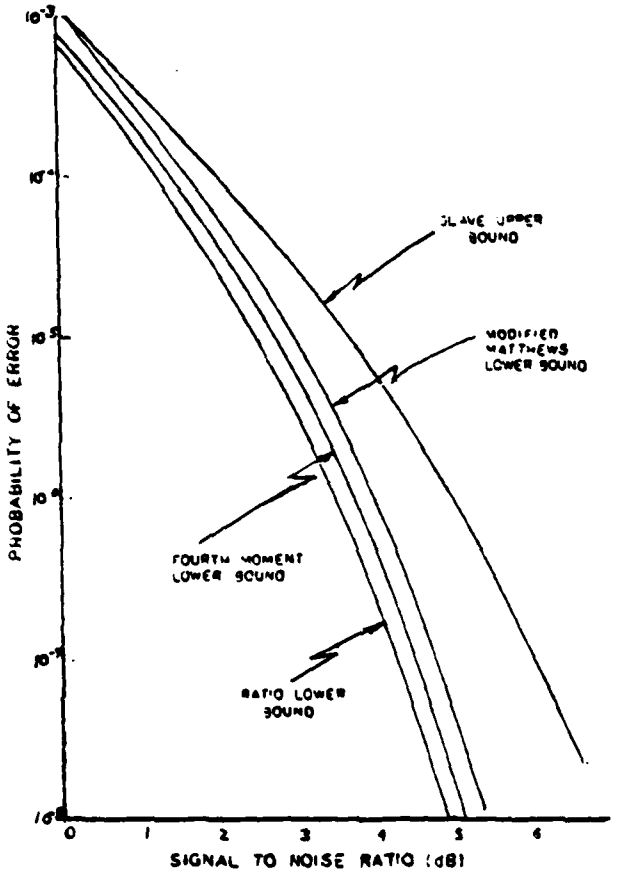

Fig. 3.24. Intersymbol Interference, Upper and Lower Bounds, Chevyshev Pulse (McLane, 1974).

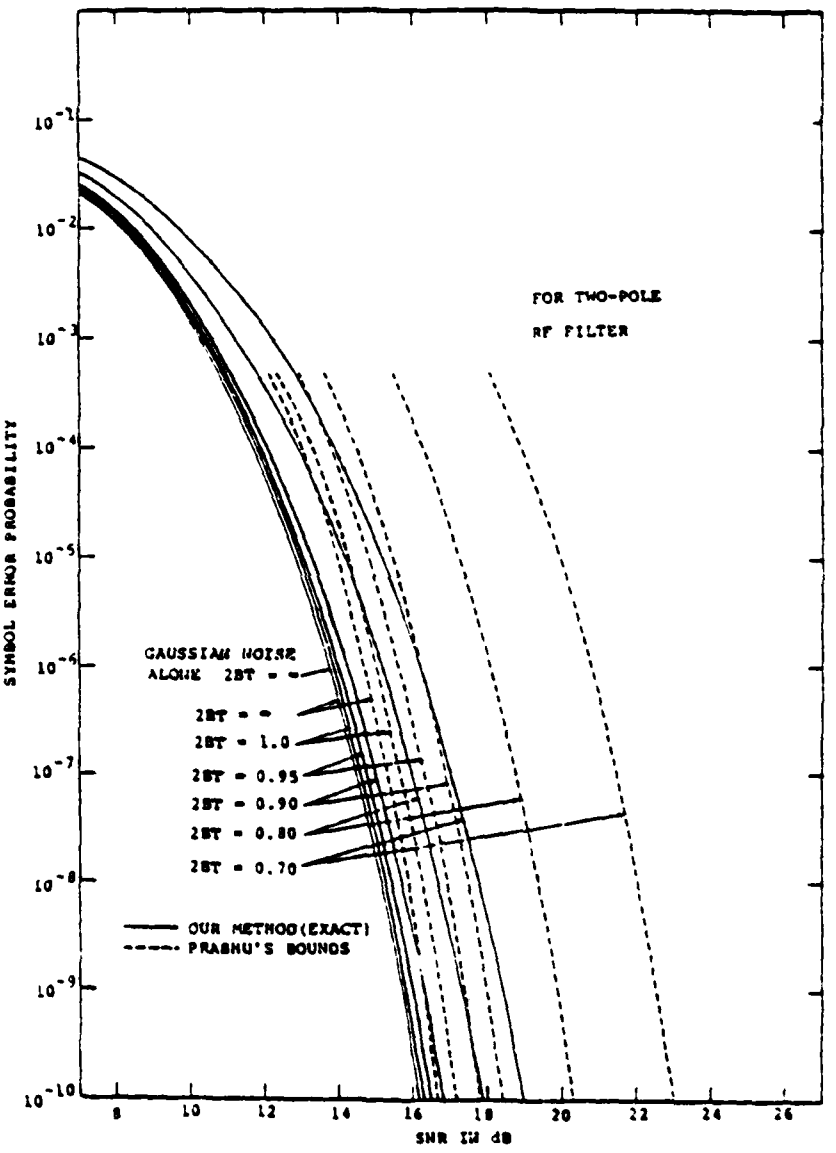

Fig. 3.25. Intersymbol Interference, Truncated Pulse Train, Two-pole Filter (Shimbo et al., 1973).

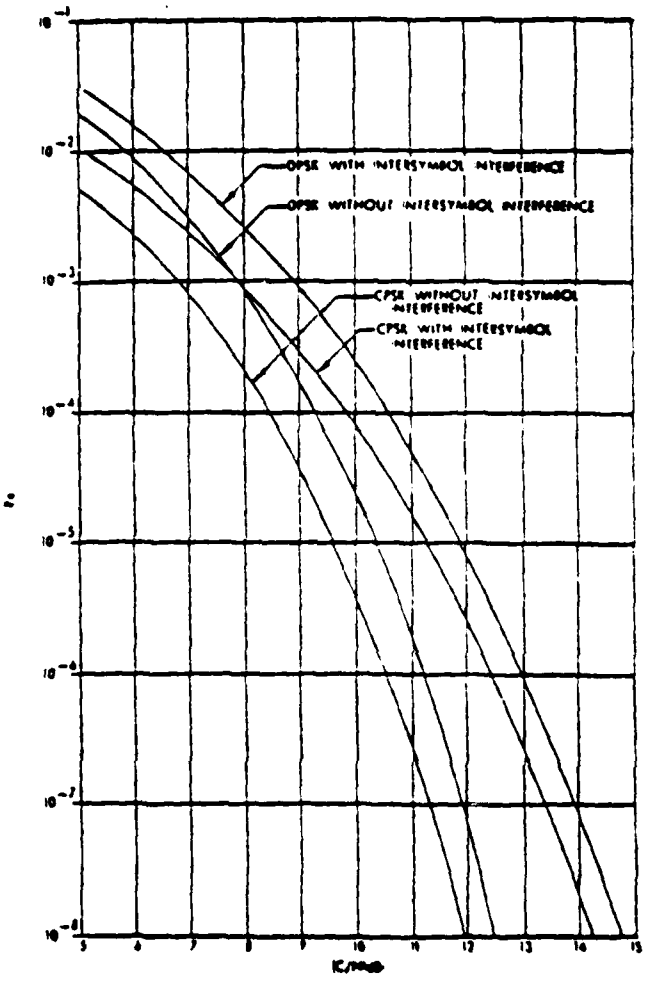

Fig. 3.26. Intersymbol Interference, Truncated Pulse Train, Seven-pole Butterworth Filter (Shimbo et al., 1971).

BER curves. However, since most systems are designed to minimize the effect of intersymbol interference, errors are generally not caused directly by the interference. The average effect is to reduce the expected value of signal-to-noise ratio and thereby shift the curves of BER but not significantly distort the characteristic shape.

Receiver Non-linearities

The type of non-linearities that will be discussed here are those that occur in the frequency response of the receiver and generally distort the pulse waveform from the desired shape. This phenomenon, which is present in all receivers, is commonly referred to as distortion. Distortion internal to the receiver can result from imperfect filters, non-linear frequency response of discriminators as will be described in the experimental results, and from a variety of other causes.

The above is emphasized to differentiate non-linearities in frequency response from a non-linear element or circuit. A linear element or circuit is defined as one for which the superposition principle applies. An example of a non-linear circuit is a square-law detector. Real elements and circuits always display a certain amount of non-linear properties; however, the effect of these non-linearities is a highly complex subject which would require extensive treatment. For this reason and since most non-linearities are undesirable and are eliminated as much as possible, their effect will not be discussed further here. The results of intentional imposition of non-linearities as in a square-law detector have been discussed under noncoherent detection of ASK and FSK.

This very brief discussion of non-linearities in frequency response has been deferred to this point since, as with intersymbol interference, the primary effect is on the pulse waveshape. Indeed, in many cases the greatest effect on receiver performance is reflected in increased intersymbol interference.

Other than the increase in intersymbol interference the effect of distortion on both correlation and sampling type detection is to reduce the signal to Gaussian noise ratio. This is clearly seen from the fact that, although the frequency response of the circuits causing the distortion are non-linear, the circuits are assumed to be linear circuits as defined above. This assures that the response to signal plus noise is equal to the response to signal plus the response to noise. That is, if L denotes the circuit transformation (response) then:

$$L\,[s(t) + n(t)] = L\,[s(t)] + L\,[n(t)] \quad . \tag{3.17}$$

But the output of a linear system with a Gaussian input is Gaussian (Papoulis, 1965). Therefore, the overall response to the frequency non-linearity is a distorted signal plus Gaussian noise.

It can, therefore, be concluded (unless intersymbol interference is drastically increased) that non-linearities in frequency response in receivers will cause lateral shifts of the BER curves with little or no alteration in shape. The amount of shift caused by distortion cannot be formulated in general, but can be calculated in specific instances. An example is shown in Fig. 3.27 taken from Jones (1971) which compares

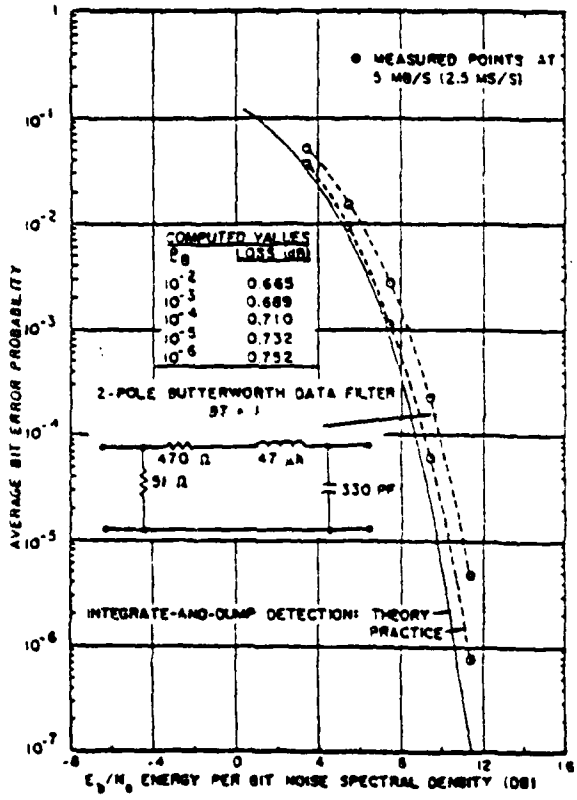

Fig. 3.27. BER Curves with Imperfect Filtering (Jones, 1971).

calculated losses from a two-pole Butterworth filter with measured results.

Summary of Calculated Results

It was shown in this chapter that, when expressions for probability of error are varied by constant factors or a summation of the common functions, the BER curves are shifted but the basic shape is essentially retained at low error rates. This was also found to be true for the calculated effects of jitter for small mean values and variances. However, when the amount of jitter was substantial, the curves were seen to flare outward at the tails. This phenomenon will be examined more closely in Chapter 5 in comparison with experimental results. It was then shown that, in one case where a closed form expression was not available and in another where the expressions were not in the common format, the effect of jitter on the BER curves was predictably to shift them but not distort their shape. Intersymbol interference and non-linearities of frequency response were discussed with the common conclusion that, as long as the anomalies are not so large as to cause errors by themselves, the overall effect is an equivalent reduction of signal-to-noise ratio.

CHAPTER 4

EXPERIMENTAL RESULTS

The experimental work for the most part was conducted at the Digital Transmission Evaluation Program (DTEP) test facility at Fort Huachuca during June and July, 1978, with some additional work at Bell Aerospace in Tucson during the first part of August. The jitter measurements on the T1-4000 and the experiment on combined effects were performed at DTEP in May, 1979. The delay was caused first by the lack of an instrument to measure jitter and then by other commitments of the test facility.

The objective was to experimentally verify the hypothesis that small variations in the internal anomalies which contribute to errors in digital demodulators cause a lateral displacement of the characteristic curve of bit error rate versus received signal-to-noise ratio, while the curve retains its theoretical shape at the higher levels of signal-to-noise ratio.

Toward this objective, in each of the experiments described below, the equipment was first tested as it was found at the test facility to establish a base or reference curve of BER versus signal-to-noise ratio [in some cases, received signal level (RSL)]. Attempts were then made to induce increased jitter in the demodulators or to simulate the effects of increased jitter by offsetting the timing of

the receiver. Data were then taken to determine the effect of these perturbations on the equipment performance, as related to the reference curve. In one case nonlinearities in frequency response were introduced to determine their effect on the BER curve.

The organization of this chapter is as follows. First the tests of each of the four digital communications equipments are described in some detail. The operational characteristics of the items tested and the major items of test equipment are noted. The test procedures are explained and the results are summarized. More detailed descriptions of the tests and complete data are contained in Schooley and Davis (1978), and have not been included here for the sake of brevity. The chapter is concluded with an analysis of the results of the tests from the points of view of accuracy and consistency. Discussions of the deviations of the experimental BER curves from the theoretical shape, and of the amount of displacement of the curves that was induced will be included in Chapter 5 in a comparison with calculated results.

VICOM T1-4000--Initial Tests

The VICOM T1-4000 is primarily a digital time division multiplexer which converts from two to eight non-synchronous T1 channels into a single 12.5526 Mbps data stream for transmission over a coaxial cable or radio facility. The T1 inputs (Bell System Standard) are 1.544 Mbps signals in a return to zero (RZ) bipolar format (also termed AMI, alternate mark inversion). The high level output can either be a serial binary no return to zero (NRZ) or a three level

partial response signal. It is in the three level partial response mode that the multiplexer acts as a modulator/demodulator converting this external signal from/to the internal NRZ format.

Since the T1-4000 is essentially a multiplexer it must be operated with a nominal input signal level which is too high for the inherent front end noise to effect the error rate. Therefore, external noise had to be added to the signal to establish the error curves. A random noise generator with a reasonably flat spectrum over the required bandwidth (approximately 8 MHZ) that would produce the necessary noise power was not available. To obtain the desired result, a microwave radio set (the AN/FRC-162) was utilized as a transmission facility. The input signal to the radio receiver could then be attenuated to a low enough level for the receiver front end noise to produce the necessary range of signal-to-noise ratios.

The AN/FRC-162, manufactured by Collins Radio, is a frequency modulated line-of-sight microwave radio which operates in the 8 GHZ band. The radio has been modified to accept the 12.5526 Mbps three-level partial response output of the T1-4000. The AGC features of the radio provide a constant level output signal to the T1-4000, regardless of the signal level at the input to the receiver.

The HP-3780A Error Measuring Set is a pattern generator/error detector in one instrument for measurement of loop errors with data rates from 1 Kbps to 50 Mbps. Error count is indicated on a front panel LED display. Alternatively BER is calculated and displayed every 10^6, 10^8 or 10^{10} bits, as desired. An indication is given if the

error count is less than 100 errors in any period. Signal output is either AMI or NRZ.

Test Procedure

The equipment configuration for the test is shown in Fig. 4.1. The HP-3780A Error Measuring Set was used to generate a pseudo-random T1 signal which was connected to a single channel of T1-4000. The T1-4000 three level partial response signal was then connected to the FRC-162 transmitter. The transmitter radio frequency output was connected to the receiver via waveguide which contained two calibrated attenuators for adjustment of the signal level. After demodulation in the FM receiver the three-level partial response signal was fed back through the T1-4000 to the 3780A for detection of errors.

Three separate T1-4000 multiplexers were tested in this configuration. In each case BER versus RSL curves were plotted and compared with a theoretical (error function) curve. Readings were taken on several different T1 channels to verify that the same error rates were present on each channel. Baud timing jitter was induced as described below and BER versus RSL curves were obtained for each system with several levels of perturbation. Finally, as further described below, the frequency response of the receiver discriminator was purposely distorted to determine the effect of receiver nonlinearities upon the bit error rate. BER curves were determined for several observable aberrations of the discriminator response curve.

The automatic gain control (AGC) voltage of the receiver was calibrated to establish the received signal level (RSL). To accomplish

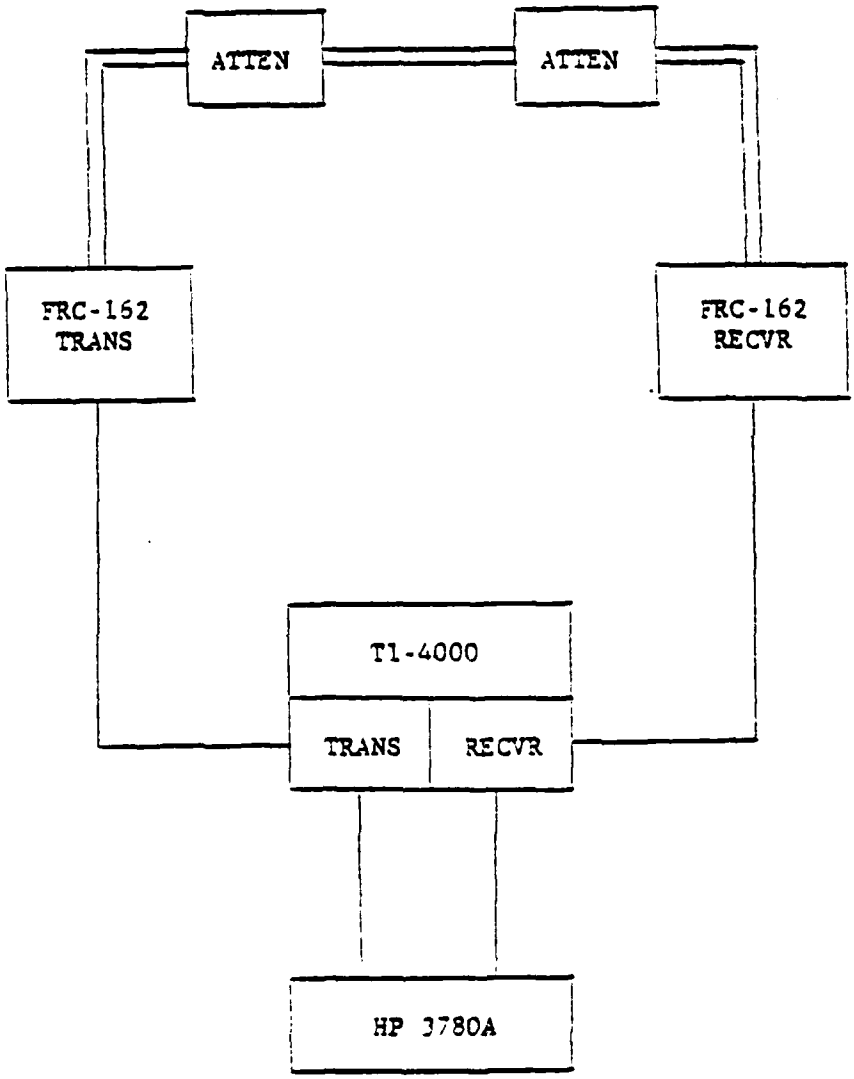

Fig. 4.1. Equipment Configuration: Vicom Tests.

this, the output of an SHF signal generator was first calibrated with a power meter. This output was then connected directly to the input port of the receiver mixer with the waveguide from the transmitter cut off. Readings were then taken of the AGC voltage for input power levels from -10.5 to -64.5 dbm which when considering the input loss at the mixer port of 19.5 db corresponded to RSLs of from -30 to -84 dbm. That portion of the resulting curve of AGC voltage versus RSL over which BER statistics were taken and the data for the AGC curve are contained in Schooley and Davis (1978).

A complete description and mathematical formulation of the detection process of a three-level partial response demodulator is contained in Chapter 2. For the purpose of understanding the inducement of baud timing jitter it will suffice to note that the detection is accomplished by "slicing" the received signal. The slicer outputs are converted to NRZ signals via logic circuits that are timed by the output of a phase-locked-loop (PLL). Baud timing jitter can thus be introduced by jittering this timing signal.

A complete description of the operation of the phase comparator and PLL circuitry of the TI-4000 can be found in Schooley and Davis (1978). The effects of various PLL circuit parameters on the output jitter was discussed in Chapter 3. However, it should be restated here that the term "jitter" as used herein refers to a random variable whether it is carrier phase reference error or symbol synchronization error. As such it has both a mean value and a variance. For the most

part the induced jitter to be described will take the form of a phase or timing offset which affects the mean of the jitter but not the variance.

To induce changes in the amount of baud timing jitter present in the T1-4000 receiver, the natural frequency of the voltage controlled oscillator was offset from its nominal value of 6.276 MHz. This was accomplished by varying an inductor in the oscillator tuned circuit. The free running oscillator was found to be too unstable to permit meaningful measurements of the natural frequency; therefore, the effects of the adjustment were noted by recording the corresponding variation of the quiescent value of a dc bias voltage which could be monitored at the PLL test point.

No method was available during the original experiments for quantitatively measuring the amount of baud timing jitter that was induced. However, a qualitative estimate was obtained by observing the receiver clock signal on an oscilloscope using the transmit clock as an external reference and with the transmitted signal looped directly to the receiver. The result was not completely satisfactory and led to the later experiments that were conducted when a jitter measuring device became available.

To determine the effects of nonlinearities in frequency response upon the BER curve, the linearity of the response of the discriminator of the FRC-162 FM receiver was purposely distorted. The linearity was observed by connecting a sweep signal generator to the discriminator input and observing the output on an oscilloscope with the frequency

varying ± 25 MHz about the 70 MHz IF center frequency. Operation of the FRC-162 with the nominal 45 MHz bandwidth discriminator is apparently normal practice even though the signal bandwidth of the T1-4000 is approximately 8 MHz. This fact accounts for what may appear to be a disparity between the linearity and the error rates, since the only meaningful portion of the observed curve is ± 4 MHz from the 70 MHz center frequency. Variations were made on the settings of the discriminator tuning capacitors and inductors while the linearity distortions were observed on the oscilloscope. Data were then taken to determine the effects of several different distortions on the BER curve.

Results

Complete data for the T1-4000 tests are contained in Schooley and Davis (1978) as are complete sets of curves for all models tested. Only representative curves will be included here. In general only the results are presented at this time. Analysis and comparisons with calculated results are deferred until Chapter 5. However, in some of the figures theoretically shaped curves have been included with the experimental results for ready reference. These have been placed for convenient comparisons of shape without regard for absolute lateral location.

The initial BER curves obtained from the three separate models of the T1-4000 were quite consistent with the differences among the three curves being less than one db. The initial curve for model 11H0009 is shown in Fig. 4.2 with a theoretical error function curve placed for convenient reference.

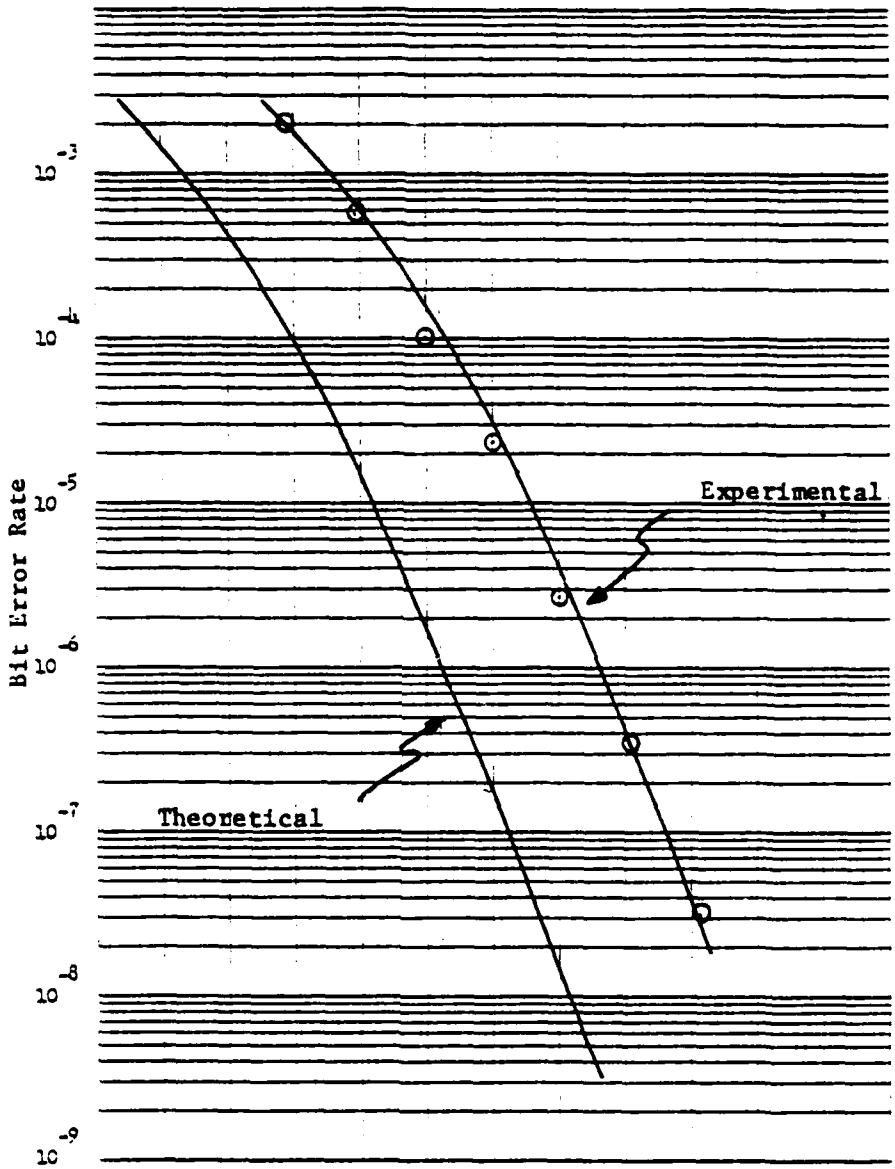

Fig. 4.2. BER vs. RSL, Experimental and Theoretical, Vicom T1-4000, Model 11H009.

The results of the baud timing experiments for all three models were essentially the same. Curves for one model are shown in Figs. 4.3 and 4.4. It should be noted here that for small amounts of offset the BER curves are shifted laterally but closely retain their initial shape. However, as the displacements become larger the curves begin to tilt outward as shown in Fig. 4.4 for PLL voltages of 4 and 3 volts. This phenomenon and the relationship between the amount of shift and the timing variations will be discussed in detail in Chapter 5.

An easily observable fact from these experimental results is that, even when the curves do distort somewhat from the theoretical shape, they never cross. This observation, which will be further supported by the results of the other experiments, leads to a conclusion which has potentially greater benefit than the saving of test time. BER measurements of this kind can be extremely useful in new techniques for equipment alignment!

To illustrate this fact, curves have been plotted from the data which show BER as a function of the PLL voltage for fixed received signal levels. Figures 4.5, 4.6, and 4.7 are plots of BER versus PLL voltage for RSL's of -69, -70, and -71 dbm for each VICOM T1-4000 model tested. Two highly significant features are revealed. First, the PLL setting which provides optimum performance (lowest BER) is different for each model. The curves show that small variations in this alignment can easily impair performance by an order of magnitude or more. There appear to be no other methods of determining the optimum setting. Secondly, the optimum value of PLL voltage for each model is the same

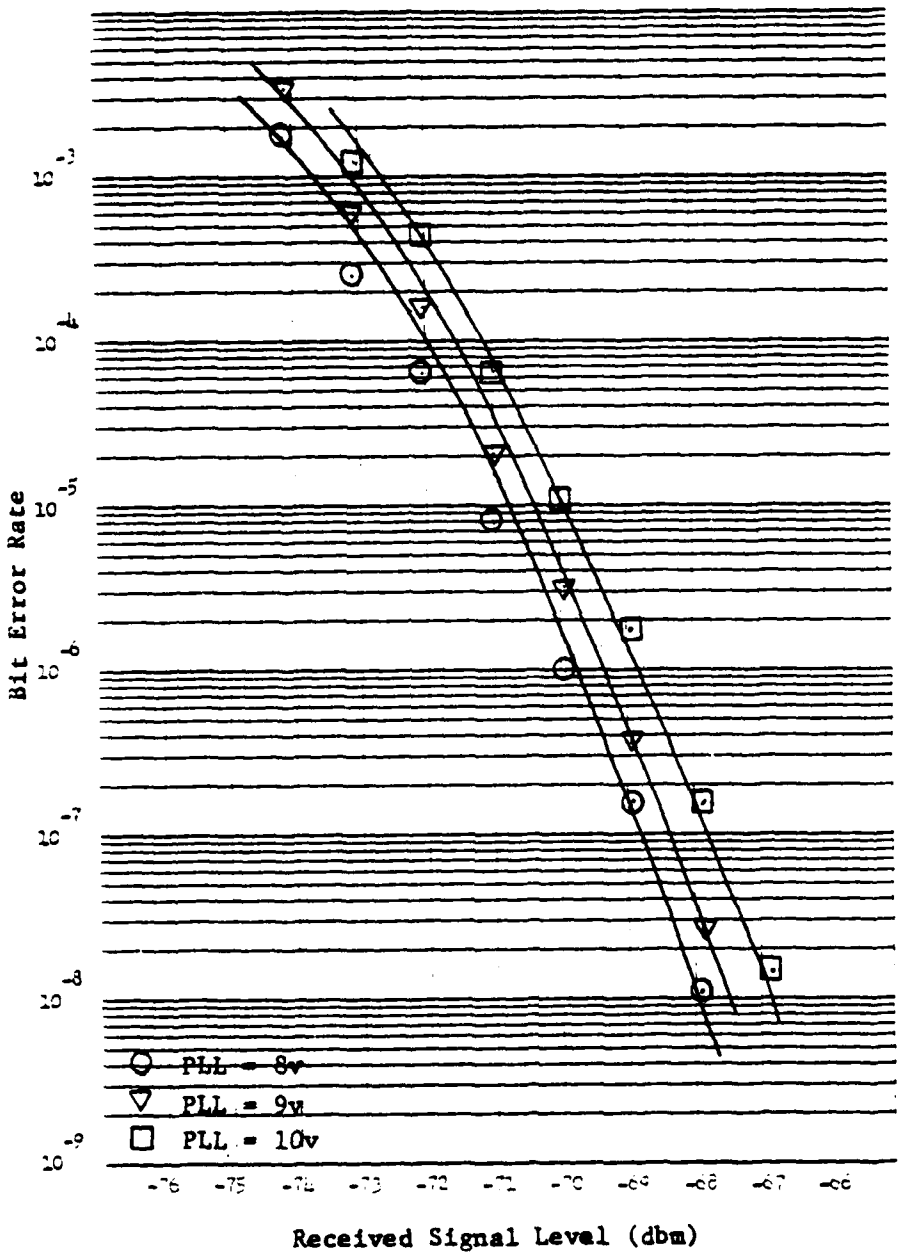

Fig. 4.3. BER vs. RSL with PLL Variations Vicom T1-4000, Model 11H0009.

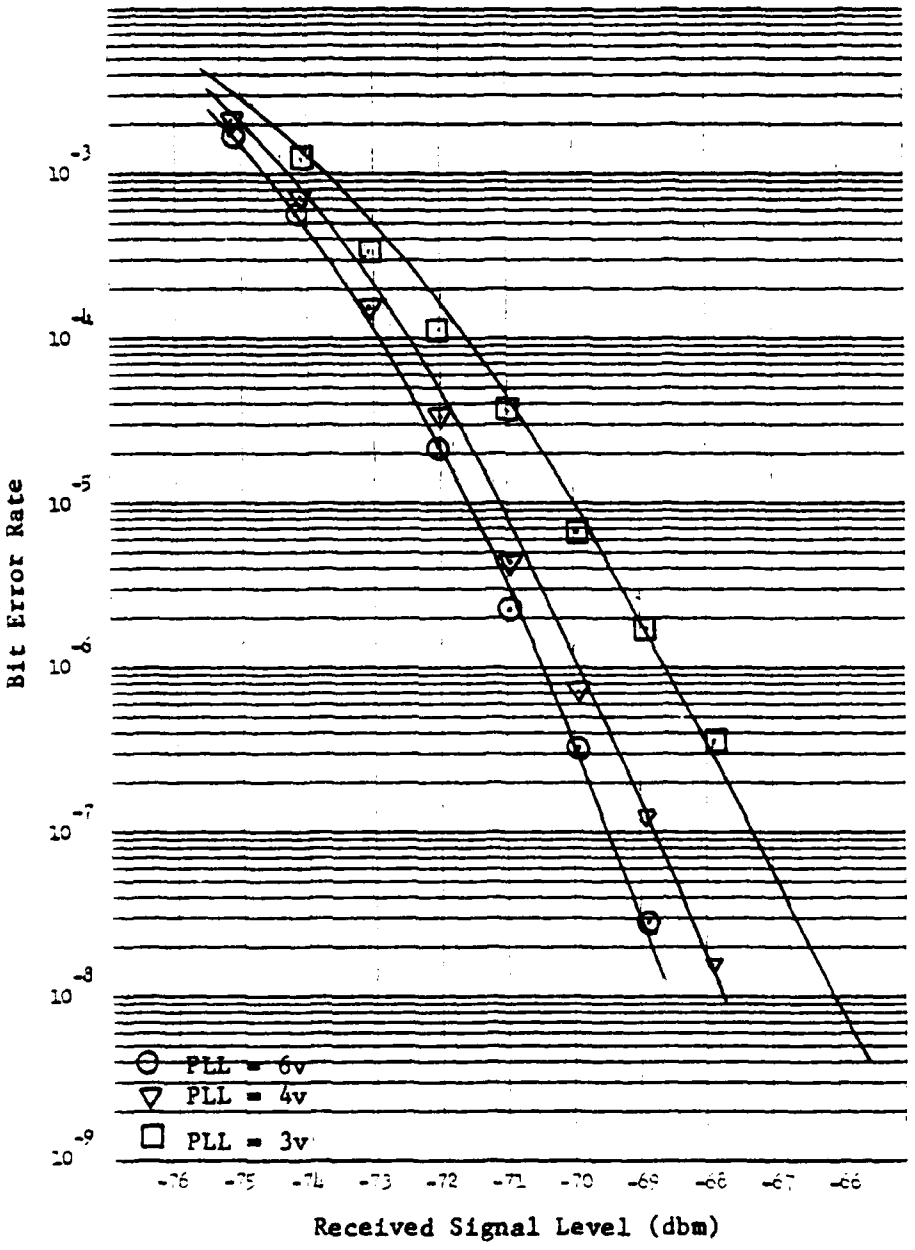

Fig. 4.4. BER vs. RSL with PLL Variations (2), Vicom T1-4000, Model 11H0009.

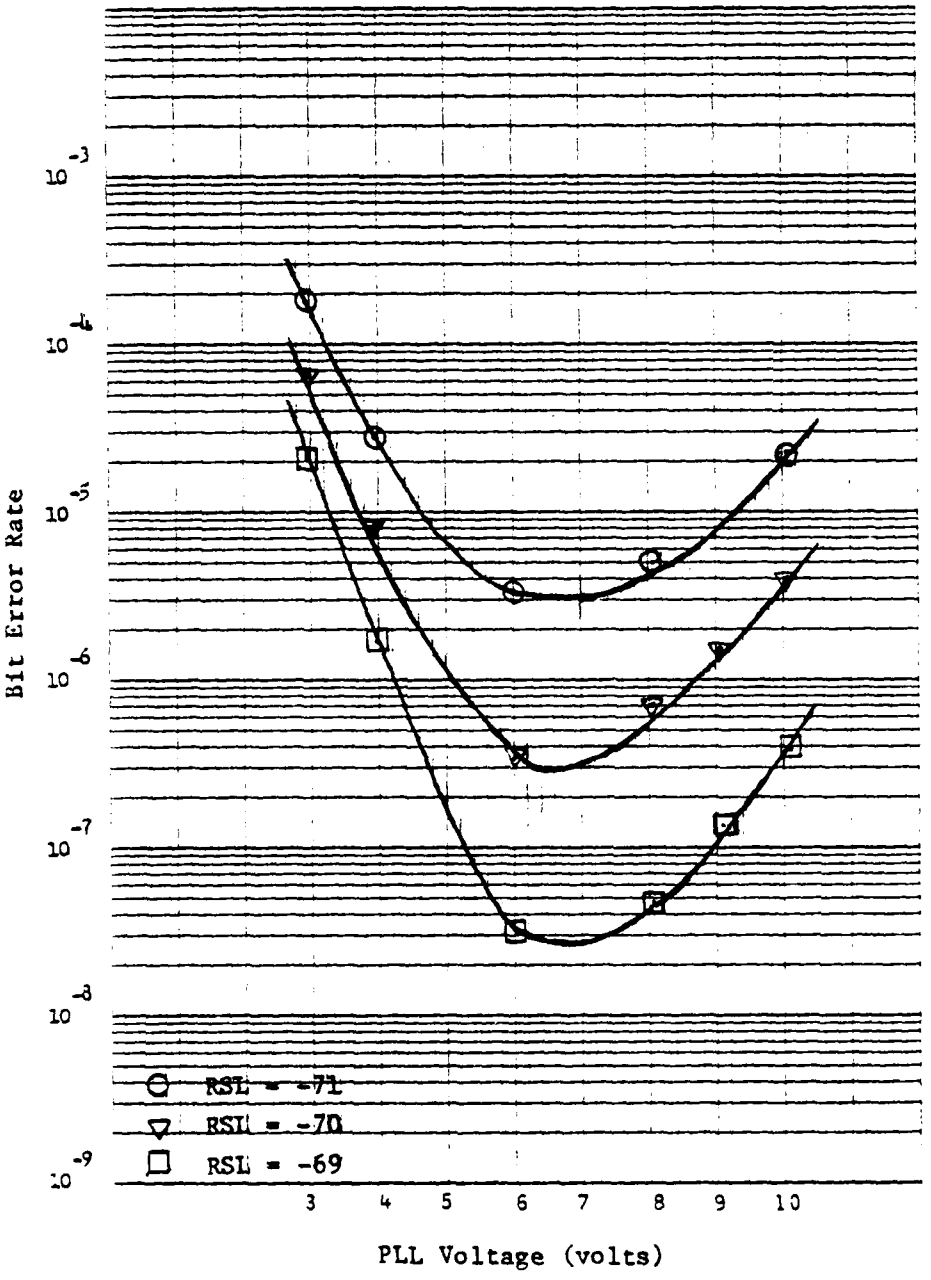

Fig. 4.5. BER vs. PLL Voltage Vicom T1-4000, Model 11H0004.

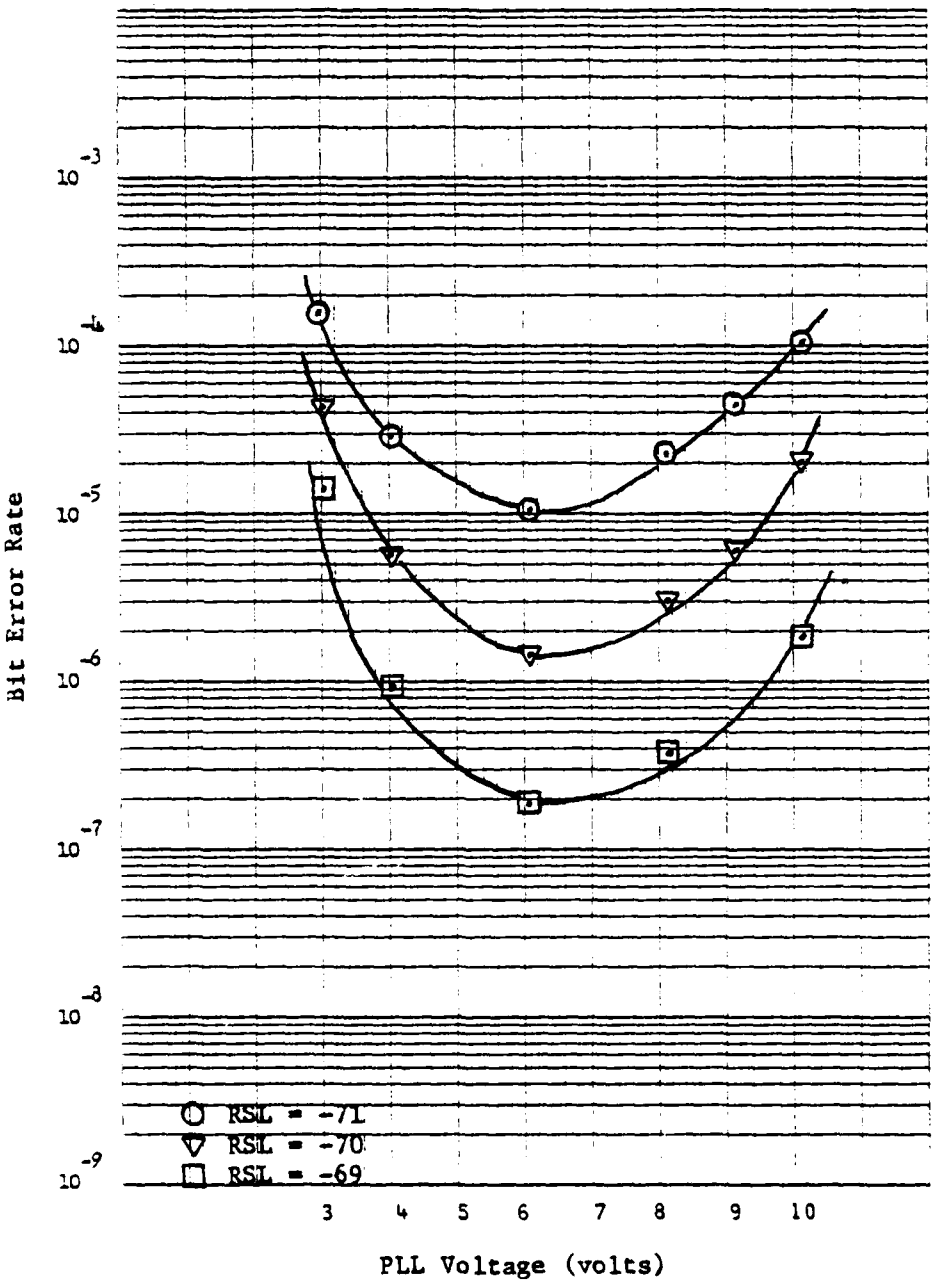

Fig. 4.6. BER vs. PLL Voltage Vicom T1-4000, Model 11H0006.

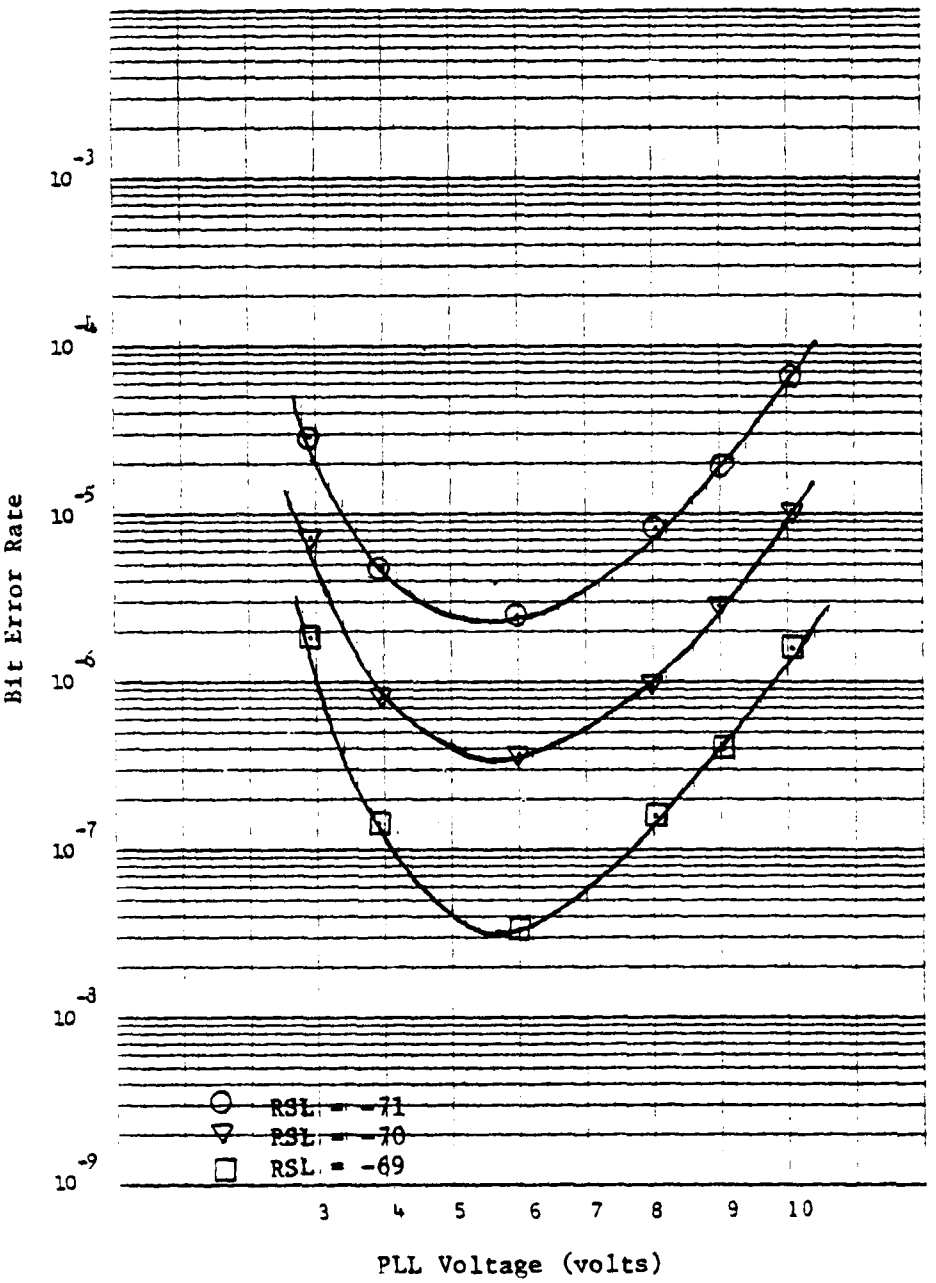

Fig. 4.7. BER vs. PLL Voltage Vicom T1-4000, Model 11H0009.

for each value of RSL. This indicates that the alignment can be accomplished at nominal values of RSL (where BER readings are easily obtained) with the assurance that the setting so determined will be truly optimum.

Figures 4.8 and 4.9 are the error curves obtained from variations of the FM receiver discriminator linearity utilizing model 11H0009 with approximately optimal baud timing. Figures 4.10 and 4.11 are oscilloscope pictures of the discriminator response curves. The scope was calibrated to 5 MHz per horizontal unit, so that the 50 MHz sweep covers the entire scope face with 70 MHz at the center.

As can be observed from the curves, the distortions of the discriminator linearity caused lateral shifts but no significant tilt or additional deviation from the theoretical shape. That this is a predictable effect will be discussed in Chapter 5.

Probably the most significant result of the discriminator linearity experiments was the surprise effect obtained from variation B. Variation A was the result of an attempt to improve the linearity from observation of the oscilloscope display, as shown in Fig. 4.11. This did in fact provide a slight improvement in the BER curve (less than 1/3 db shift to the left). Variation B on the other hand was a deliberate attempt to distort the linearity as shown in Fig. 4.10, but resulted in approximately 3/4 of a db improvement over the initial curve. As was mentioned previously this apparent disparity was due to the fact that the only meaningful portion of the displayed linearity response was a small segment in the center. Nevertheless, it does demonstrate

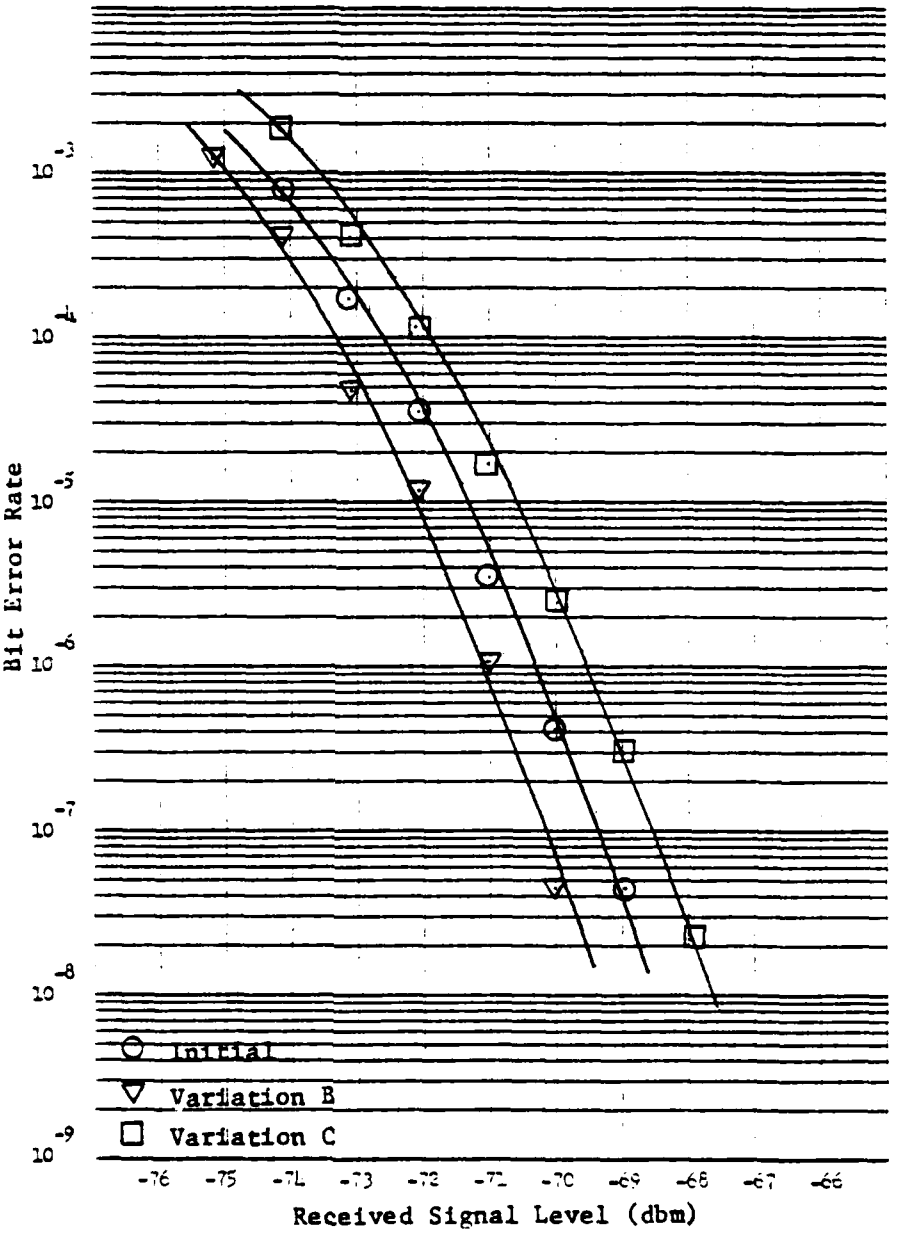

Fig. 4.8. BER vs. RSL with Discriminator Variations, Vicom T1-4000, Model 11H0009.

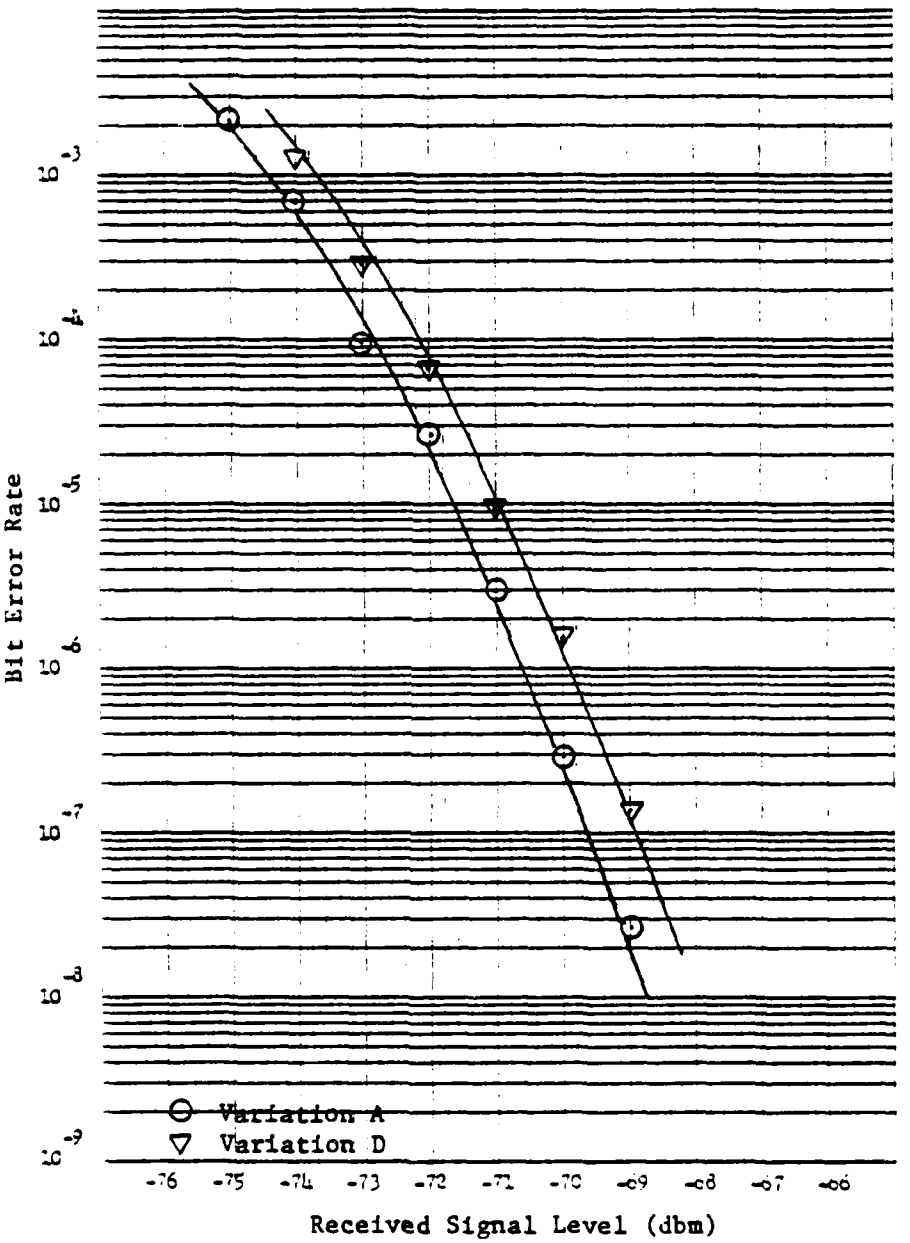

Fig. 4.9. BER vs. RSL with Discriminator Variations (2), Vicom T1-4000, Model 11H0009.

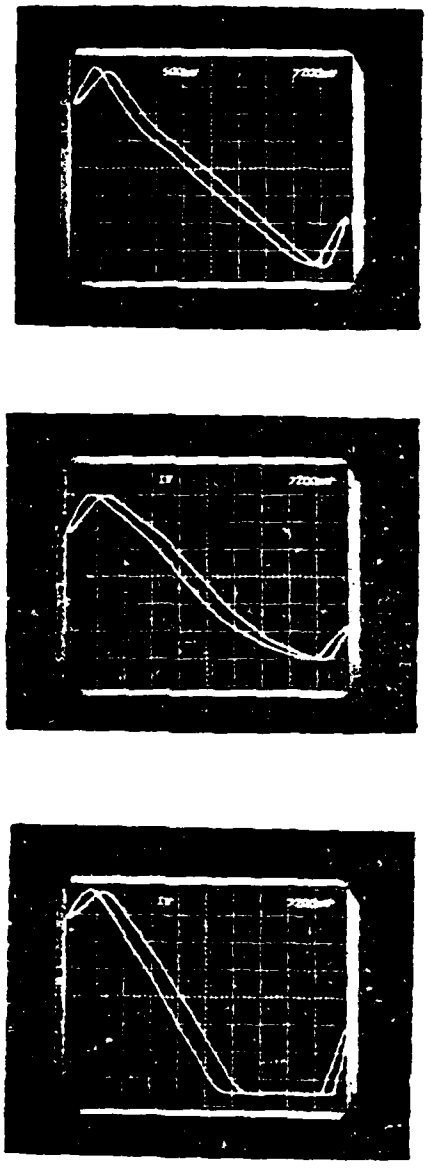

Fig. 4.10. Discriminator Linearity Variations, Vicom T1-4000, Model 11H0009.

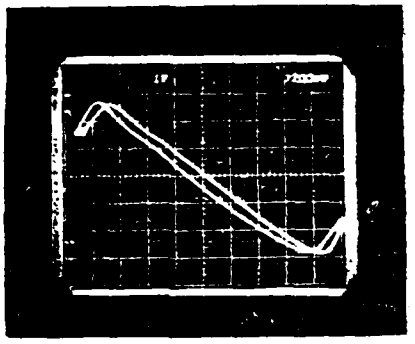

Variation A

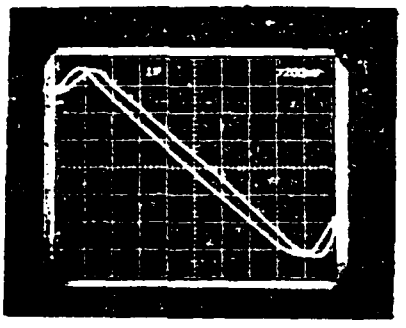

Variation D

Fig. 4.11. Discriminator Variations (2), Vicom T1-4000, Model 11H0009.

that the BER readings give a much better indication of the true alignment than does the analog display technique.

Again, this result and others described led to the realization that alignment of equipment can be accomplished much more accurately in some cases by monitoring BER at low signal-to-noise ratios than by other existing techniques.

VICOM T1-4000--Additional Tests

The objectives of this later experimental work with the T1-4000 were twofold. First, it was desirable to repeat the baud timing jitter experiment while measuring the induced jitter so that comparisons could be made between experimental and calculated results. Secondly, the initial experiments had raised the question of combined effects. That is, could greater shifts of the BER curves be obtained without additional distortion of their shape by simultaneously stimulating two separate error causes?

Test Procedure

The test configuration was essentially the same as for the initial tests as shown in Fig. 4.1. The FRC-162 radios were not available, but Terracom radios which have a different physical configuration but the same electrical characteristics were substituted. The three T1-4000 models originally tested were also not available and a slightly newer, but essentially unchanged, model was used.

The Hewlett-Packard HP 5370A, Universal Time Interval Counter, was used to measure jitter. In the mode of operation employed, the meter measures the time interval between the leading edges of the nearest pulses of two separately applied signals at the moment the reference switch is activated. Readings may then be taken of the mean value and the standard deviation of the difference between the reference interval and the time interval between the signals averaged over a preset number of samples.

The procedure for the baud timing experiment was essentially the same as in the initial tests. Jitter was induced in the symbol synchronization circuitry by offsetting the quiescent frequency of the VCO in the PLL. BER curves were obtained for a number of frequency variations spread between the extremes where the system lost synchronization.

To measure the amount of jitter induced, the output of the PLL was compared to the transmitter timing signal. The VCO adjustment that resulted in minimum error rate was assumed to produce a zero offset and was used as a reference. The mean value of the induced phase offset was then measured corresponding to the PLL voltages for which BER curves were taken. These measurements were repeated for several values of RSL. The same procedure was used to obtain data on the standard deviation for the various values of PLL voltage and RSL.

A procedure similar to that used for the discriminator variation tests was applied to determine combined effects. Two different degrees of distortion were made to the linearity of the discriminator

response of the FM receiver. In this case, error data were taken for both the optimum setting of the PLL voltage and for an extreme value. In this manner the combined effects of baud timing jitter and receiver non-linearities could be determined.

Results

The BER versus RSL curves for the several values of PLL voltage are shown in Figs. 4.12 and 4.13. The results are very similar to those obtained previously except that the range of PLL voltage and the optimum setting are shifted approximately 2 volts lower than the three sets initially tested. The curve for the near optimum setting of 4 volts is very close to the theoretical. As before, the curves for the high voltage settings are closely spaced with no additional deviation in shape from the theoretical, whereas the lower voltage settings produced wider spacings and the curves tilt outward.

The measurements of the mean and standard deviation of the jitter are contained in Table 4.1. The mean was found to remain essentially constant with variations of RSL and therefore only one value is given. The meter readings were in nano-seconds which have been converted to fractions of a bit period for the table entries. The frequency of the timing signals was 12.55 MHz. These values will be used in Chapter 5 to determine calculated BER curves for comparison with the experimental results described above.

Figure 4.14 shows curves of BER versus PLL voltage for constant values of RSL. It is interesting to note that the optimum setting of PLL voltage is approximately 4.2 volts. According to test site personnel,

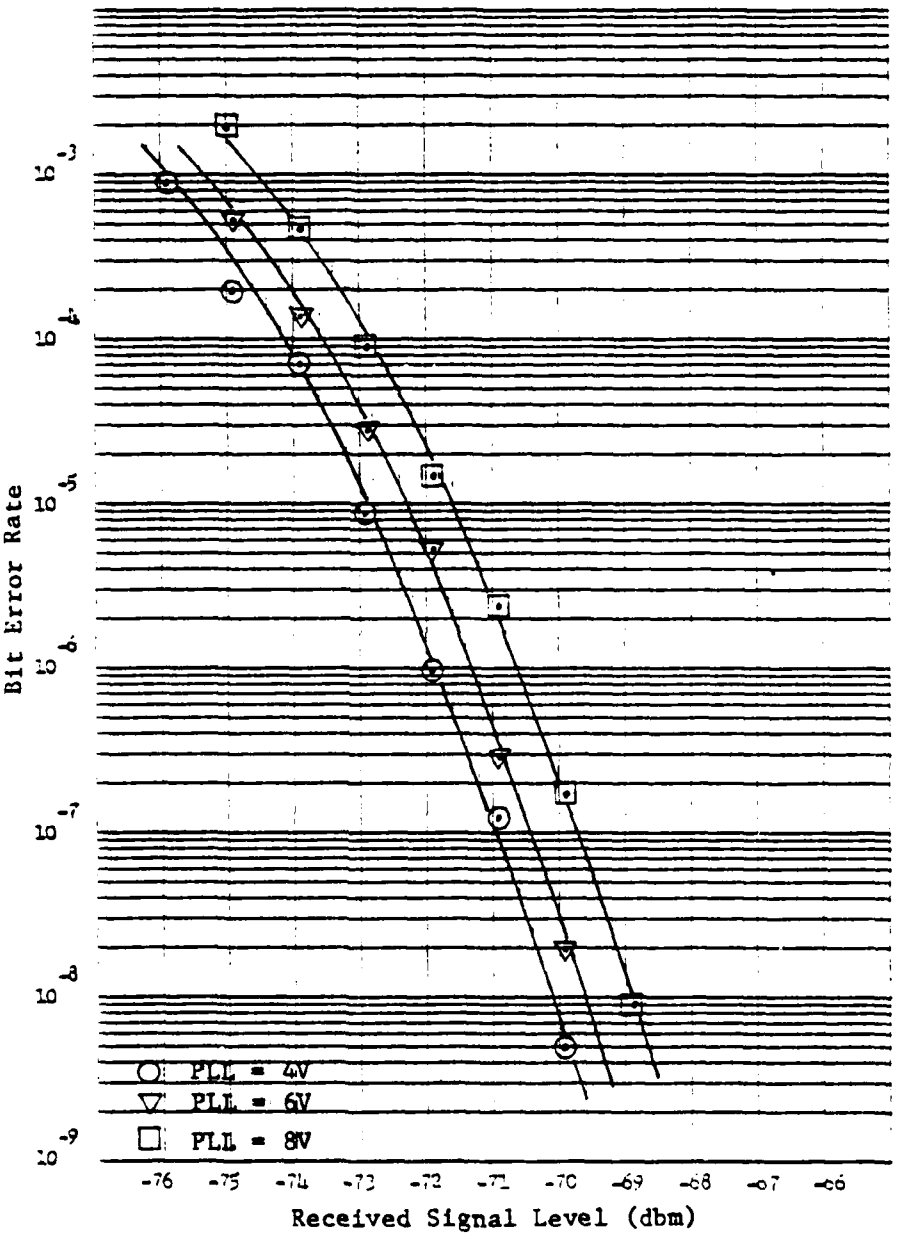

Fig. 4.12. BER vs. RSL with PLL Variations, Vicom T1-4000, Model 01J0033.

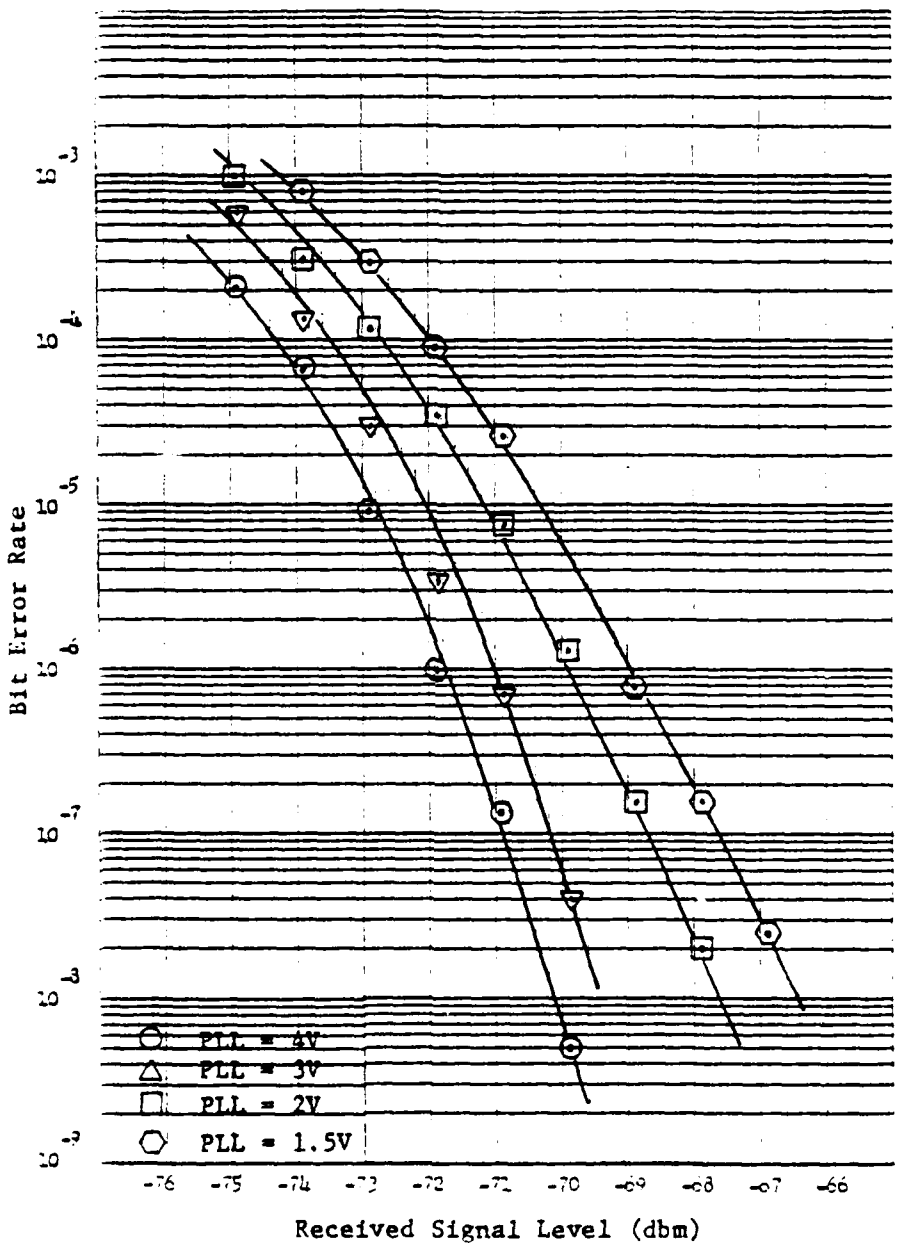

Fig. 4.13. BER vs. RSL with PLL Variations (2), Vicom T1-4000, Model 01J0033.

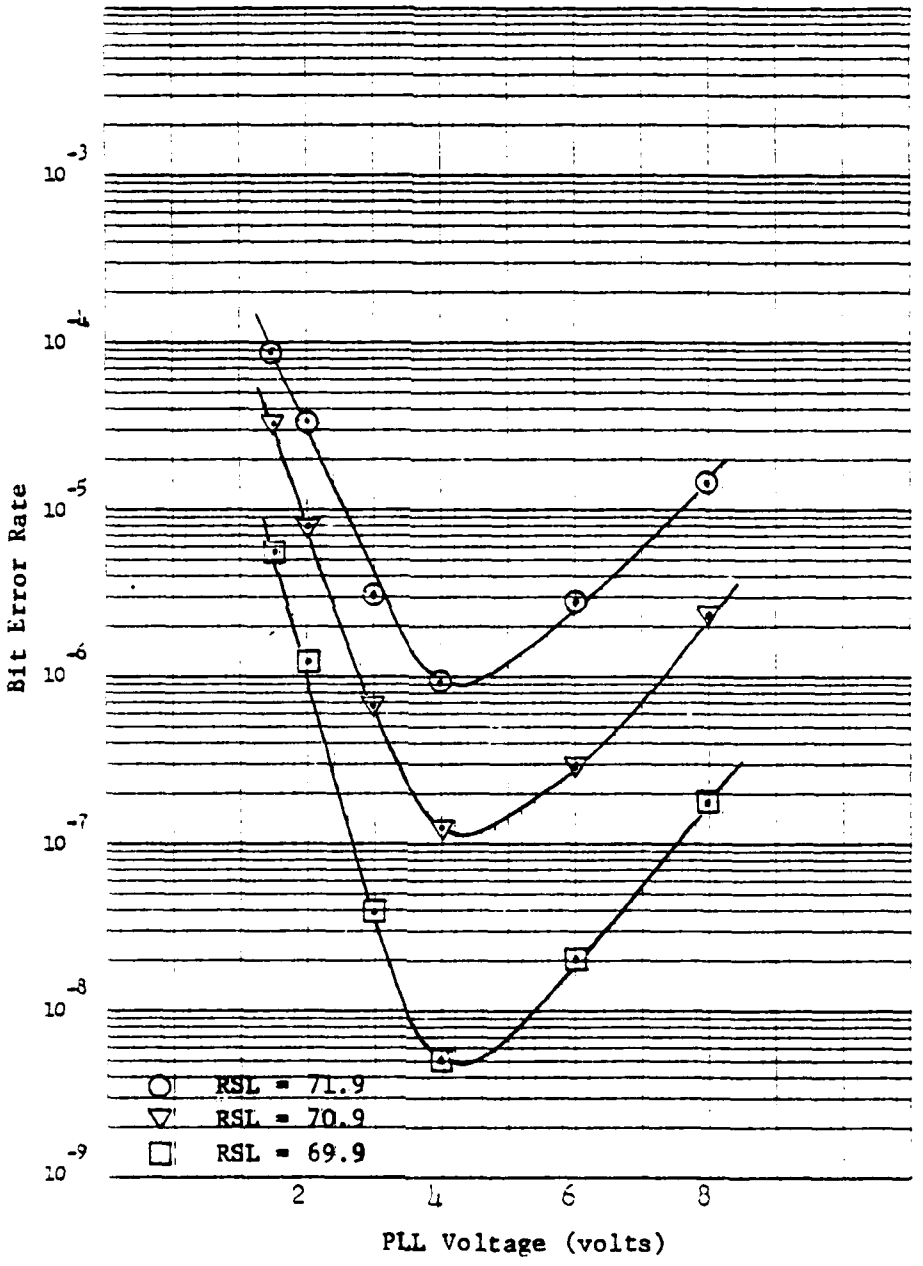

Fig. 4.14. BER vs. PLL Voltage (Module A), Vicom T1-4000, Model 01J0033.

Table 4.1. Measured Mean and Standard Deviation.

		PLL Voltages				
		1.5 v	2 v	4 v	6 v	8 v
Mean Value		0.11	0.083	0.0	0.038	0.064
Standard	-73	0.099	0.099	0.095	0.095	0.095
Deviation	-71	0.086	0.086	0.083	0.083	0.083
at	-69	0.076	0.076	0.070	0.070	0.070
Given RSL	-67	0.070	0.070	0.064	0.064	0.064

the VCO had not been adjusted since having been received from the manufacturer. Yet this factory setting was found to produce a PLL voltage of 2.44 volts corresponding to a BER curve shifted approximately 1.3 db from the optimum.

Two additional receiver input modules were on hand whose VCO alignments had not been altered since receipt from the factory. These modules were placed in the same multiplexer used for the above experiments. The PLL voltage for the manufacturer's alignment was first determined and then data was taken for each module to determine curves of BER versus PLL voltage for two values of RSL. The results are shown in Figs. 4.15 and 4.16. In the case of module B the manufacturer's setting produced a PLL voltage of 5.5 volts whereas the optimum setting is slightly less than 4 volts. This corresponds to a shift of the characteristic BER curve of approximately 0.6 db.

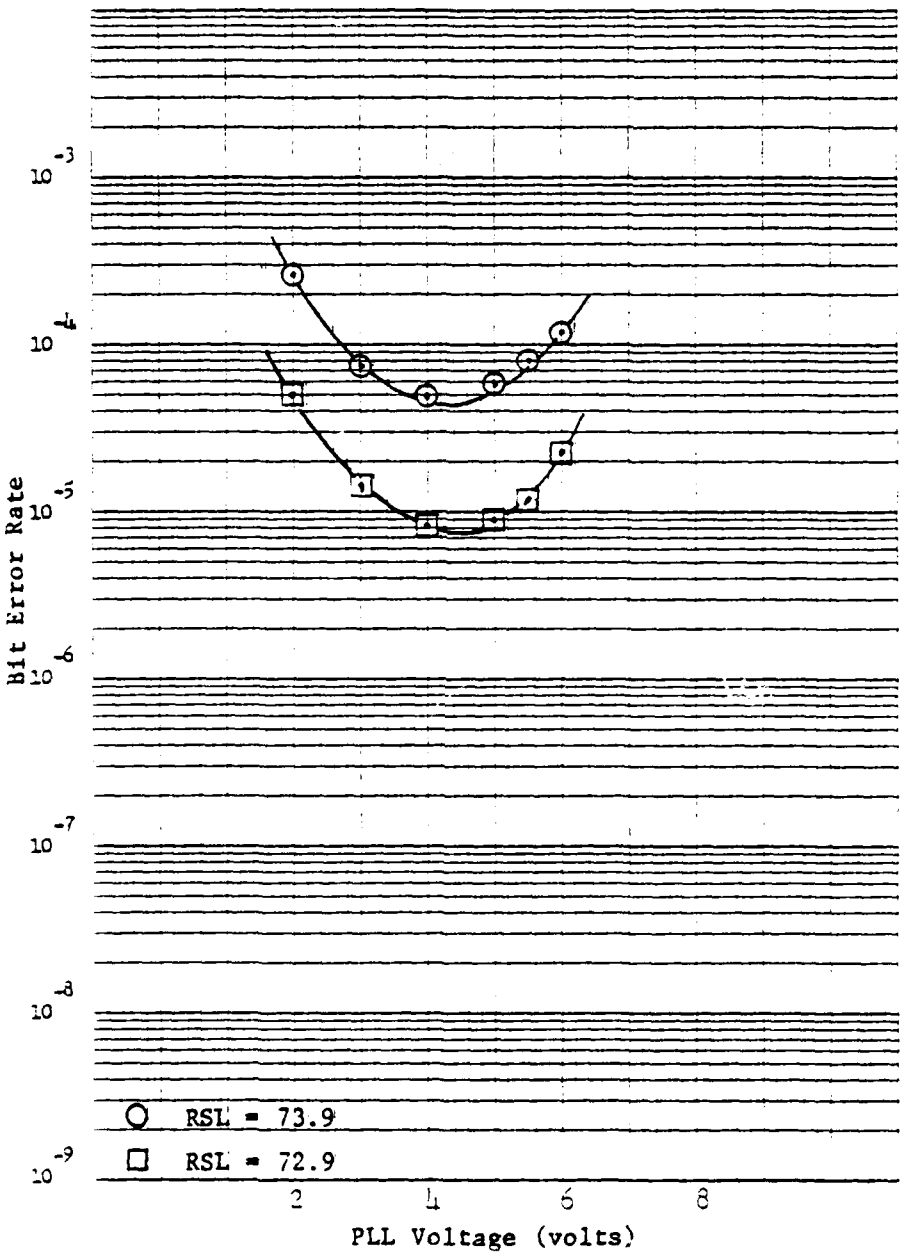

Fig. 4.15. BER vs. PLL Voltage (Module B), Vicom T1-4000, Model 01J0033.

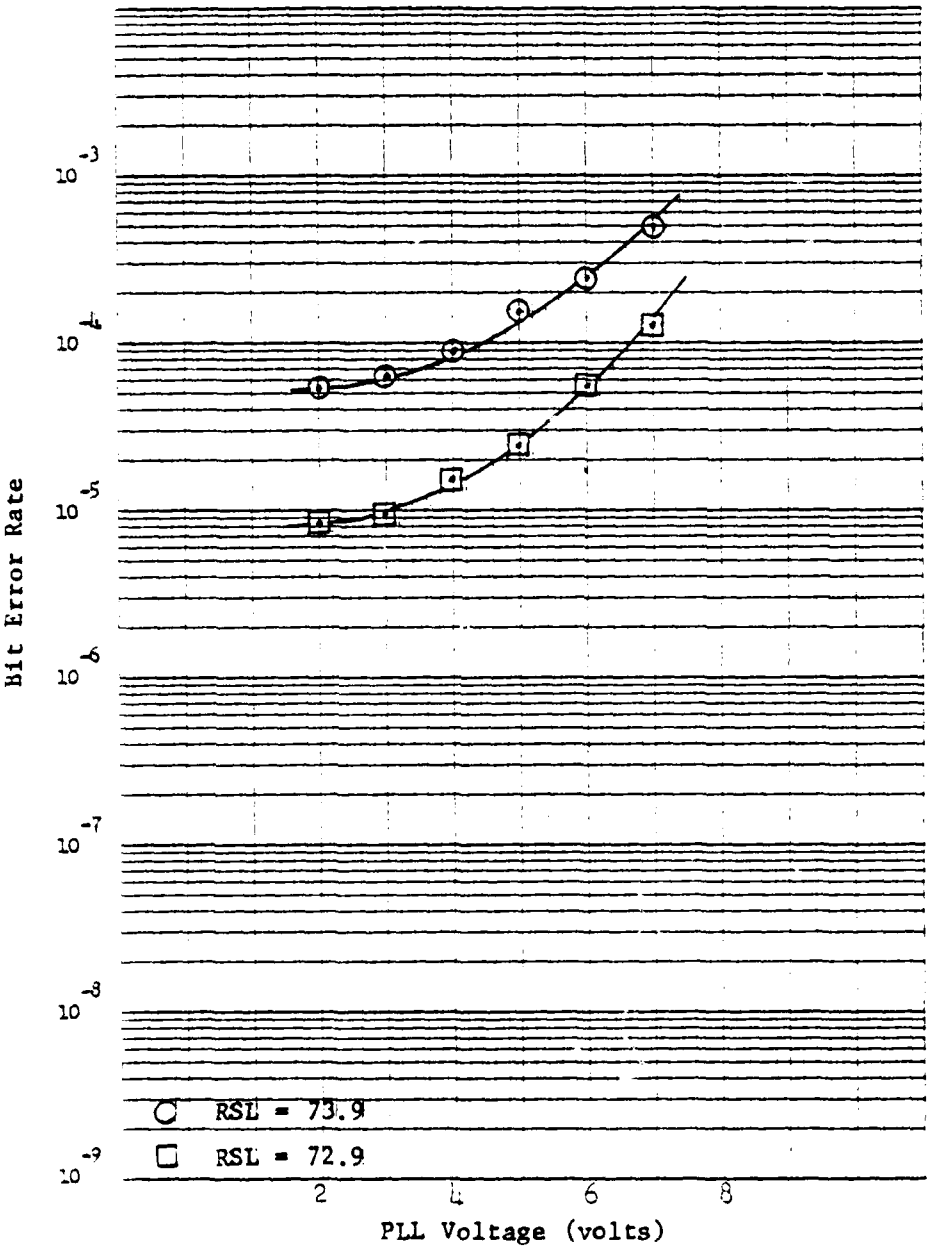

Fig. 4.16. BER vs. PLL Voltage (Module C), Vicom T1-4000, Model 01J0033.

For module C the initial PLL voltage was 4 volts. Interestingly, the optimum setting was at 2.3 volts which was obtained with the core removed from the tuning inductor. To check this last result the module was retested in a different multiplexer. The voltage readings were slightly different but the optimum error rate was still obtained with the core all the way out. This probably indicates that one or more of the other components in the tuned circuit were out of tolerance. The difference between the manufacturer's alignment and the optimum resulted in a shift of the BER curve of approximately 0.5 db.

The major significance of these latter results is that, whatever alignment technique was used by the manufacturer, it did not produce optimum tuning of the VCO. The technique of alignment while monitoring the BER can be readily applied and will result in optimum performance.

The results of the combined effects experiment are illustrated in Fig. 4.17. The curves occur in pairs with PLL voltages of 4 and 8 volts, first with no discriminator distortion, and then with two levels of distortion. Distortion level A shifted the pair of curves approximately 2.2 db yet the curves retained their original shape and spacing of about 1.2 db. Distortion level B shifted the pair approximately 3.8 db. Again the original shape and spacing have been maintained. In neither case did the curves have any appreciable additional deviation from the theoretical (tilt). This result will be discussed further in Chapter 5.

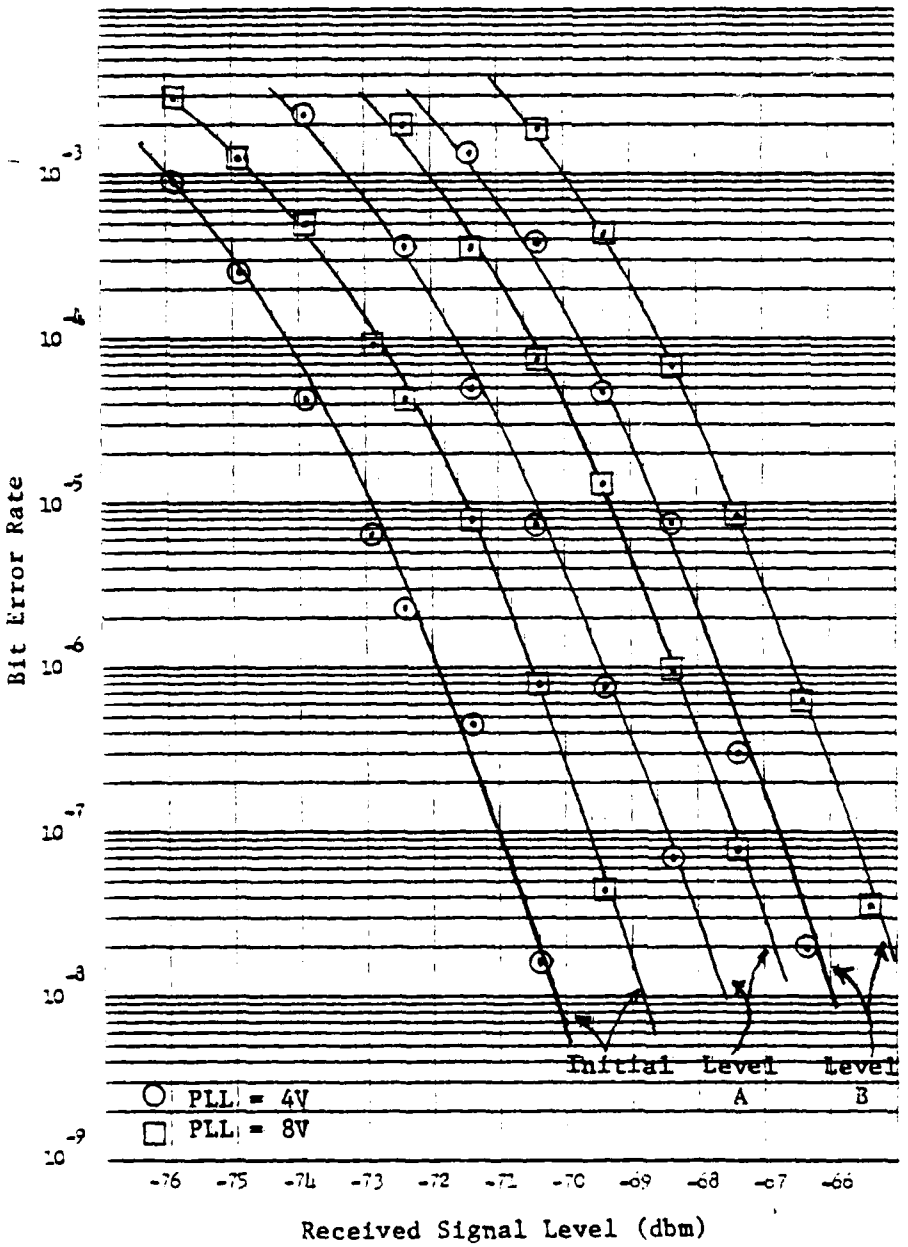

Fig. 4.17. Combined Effects, Vicom T1-4000, Model 01J0033.

Lenkurt 261A

The Lenkurt 261A is a digital data transmission set designed to operate at 2400 bps over a conditioned voice frequency channel. It is designed to accept 2400 bps data from business machines, computers, and other digital terminal equipment provided with EIA Standard RS-232C interfaces. The line side output is a combination of a synchronous duobinary encoding technique with frequency shift keying (FSK) modulation.

The transmitted signal of the 261A is a synchronous (continuous phase) frequency modulated duobinary waveform. The upper and lower levels of the duobinary signal (1200 and 2400 Hz) represent mark, and the center level (1800 Hz) represents space. The mark frequency depends upon the pattern of previous signals. At the receiver the incoming signal is passed through a discriminator which produces a 3-level amplitude signal similar to the 3-level partial response signal of the T1-4000. This signal is then detected by slicers and the outputs are combined, sampled, and retimed by the receive clock.

Although the transmitted signal is synchronous, zero-crossing detection is used in the receiver for timing recovery to allow operation over circuits that exhibit significant error in frequency translation. Before detection, the signal is modulated up in frequency to facilitate separation of the recovered baseband signal from the line signals, which may have suffered frequency translation in transmission.

The method of deriving the receive clock is described in Schooley and Davis (1978). The functions are similar to a phase-locked-loop, however, the phase corrections are discrete in 2.6 μsec steps at each data transition.

The Lenkurt 26C Data Set is end-to-end compatible with the 261A and is essentially the same in electrical characteristics; however, it has been physically configured for rack mounting.

The General Radio Company Type 1390-B Random Noise Generator is capable of providing high level noise, essentially Gaussian distributed, which has a relatively flat frequency content over a bandwidth of 20 KHz (500 KHz and 5 MHz bandwidths may be selected). The set uses a gas-discharge tube as its noise source. The noise output is amplified, filtered and equalized to attain the relatively flat spectrum over the desired bandwidth.

The HP 1645A Data Error Analyzer generates a pseudo-random bit stream to loop through the equipment under test, and return for analysis. Errors are counted and displaced on the front panel. The equipment can be operated with an external timer and recorder. This was the only error measuring set that was available which had an RS-232 interface capability.

Test Procedure

A block diagram of the test configuration is shown in Fig. 4.18. The pseudo-random data generated by the HP 1645A was transmitted to the modulator section of the data set over the RS-232 connection. Since

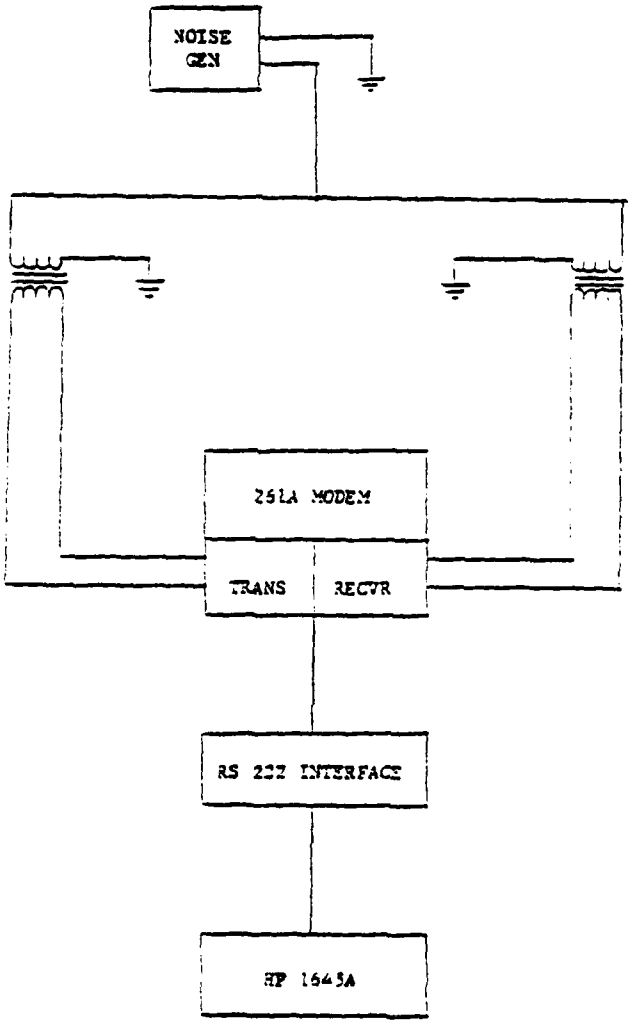

Fig. 4.18. Equipment Configuration: Lenkurt 261A Tests.

the modem line side was a balanced 600 ohm nominal output impedance and the noise generator (and the power measuring device) were both unbalanced, audio transformers were used to add the signal and noise. The demodulator output was looped back to the HP 1645A for comparison with the generated signal and the detection of errors. In the normal mode of operation, the modem provided the timing for the data generator. This situation was altered during one of the test modes and will be described in the following paragraphs.

An adjustment factor of -7.7 db was used on the signal-to-noise ratio to compensate for the apparent bandwidth of the measured noise. The noise generator bandwidth is nominally 20 kHz whereas the receiver input is filtered to 3.4 kHz. Assuming the signal is totally within the receiver bandwidth, the adjustment factor is then 10 log 3.4/20 = -7.7 db. The validity of this factor was not established to the extent of measuring the actual signal and noise bandwidth nor was it verified that the noise was truly white within the band as claimed by the manufacturer. However, since the adjustment factor merely shifts the error curves laterally without effecting the shape, the matter was not considered to be greatly significant. Since the tests were conducted at voice frequencies, the effects of the mismatch, metering, and loading were also considered negligible for the purposes of demonstrating the desired phenomena. This assumption was born out by the results.

Bit error rate versus signal-to-noise ratio curves were plotted for three 261A modems and one 26C operating in the most common mode. Normally both the transmit and the receive timing of the modem are

derived from a 1.92 MHz internal oscillator. The transmit timing signal is provided via the RS 232 interface to the data terminal being serviced (in this case the HP 1645A). The receive timing is aligned with the received data by means of a variable ratio divider driven by data transitions.

In order to determine the effects of baud timing jitter, efforts were made to offset the actual timing of the received data and the internal receive timing prior to alignment with the received data. This was accomplished by using a separate external timing source for the HP 1645A.

Both the internal oscillator of the 261A and the square wave generator used for external transmit timing appeared very stable when checked with a frequency counter and when displayed on an oscilloscope. Unfortunately, when the timing was offset by as much as 2 Hz, the 1645A lost synchronization even though the modem appeared to operate satisfactorily. When the external timing was set for precisely 2400 Hz the error analyzer maintained synchronization and an error curve was plotted. Even though, as mentioned above, both oscillators appeared quite stable and the timing was not deliberately offset, timing the transmit and receive sections from separate sources resulted in a shift in the error curve of approximately one db. The curve using internal timing for both transmit and receive was repeated in this same time frame to insure that the shift was not caused by external (test setup or other environmental) factors.

Results

Complete data and curves for all the Lenkurt 261A models tested are contained in Schooley and Davis (1978). Figure 4.19 is the experimental BER curve obtained from 261A model #1 as compared to a theoretically shaped curve. Figure 4.20 is the experimental curve for the Lenkurt 26C. The three models of the 261A modem tested provided very consistent results. The error curves were all well within 1/2 db of each other. On the other hand, the curve for the 26C was shifted approximately 2.5 db to the right but with very little deviation in shape. This will be commented on further in Chapter 5.

Figure 4.21 shows the results of utilizing separate transmit and receive timing for 261A model #1 as compared with results using the single internal source. This also will be discussed in Chapter 5.

MW-518

The MW-518 tested here is an engineering model of a modification to the commercial MW-518 FDM-FM radio set manufactured by Collins Radio. This is essentially the same radio equipment as the AN/FRC-162 modified for quadrature phase shift keying operation (QPSK). The radio set accepts a 12.5526 Mbps MECL logic signal and performs the QPSK modulation and detection internally at the IF level. Although the data is differentially encoded prior to modulation, the detection scheme is coherent (nondifferential).

The HP 3760A Data Generator and HP 3761A Error Detector are used in combination for the generation of a pseudo-random data stream and for the detection of errors. The data generator can be triggered either

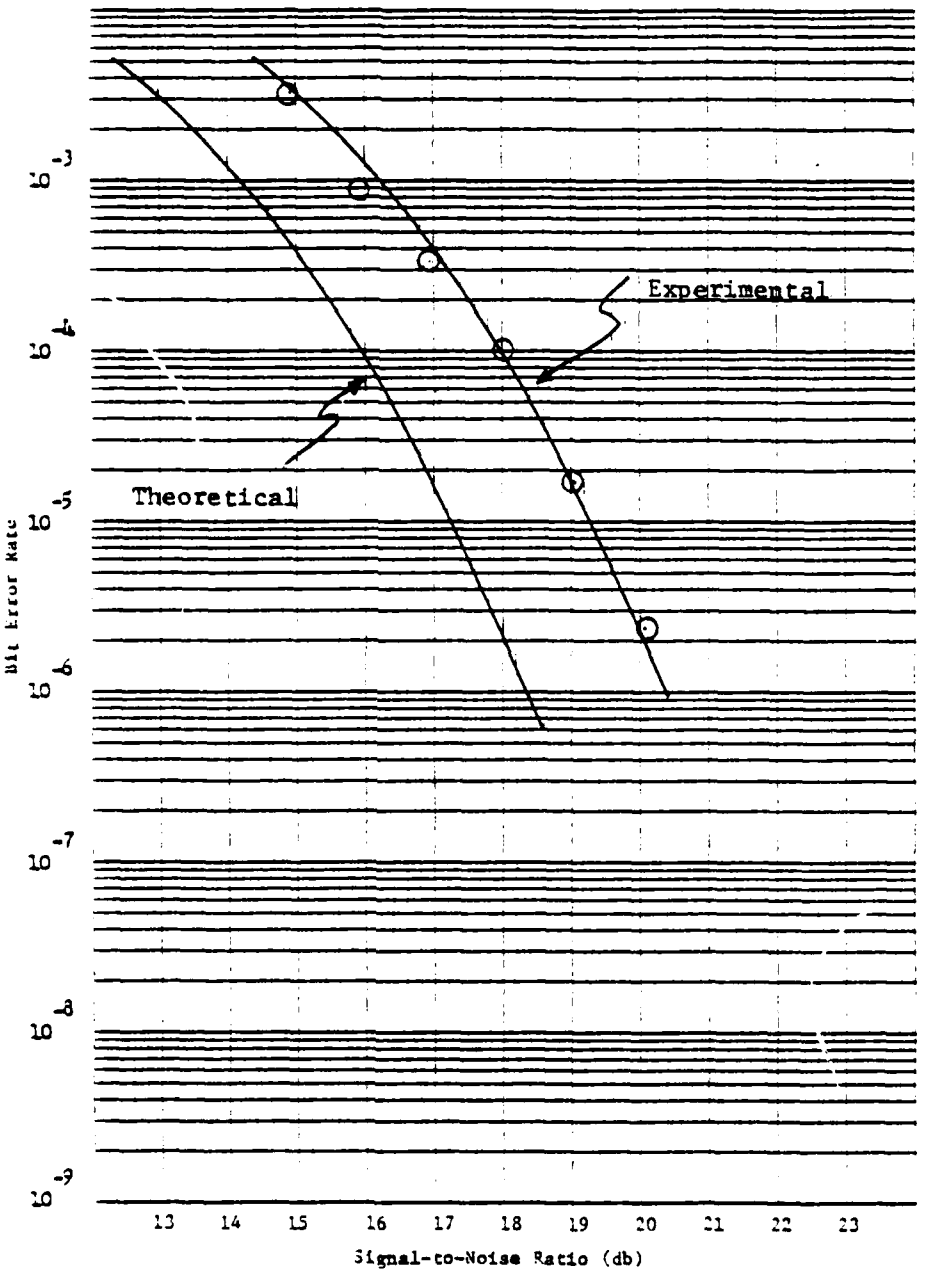

Fig. 4.19. BER vs. S/N, Lenkurt 261A, #1.

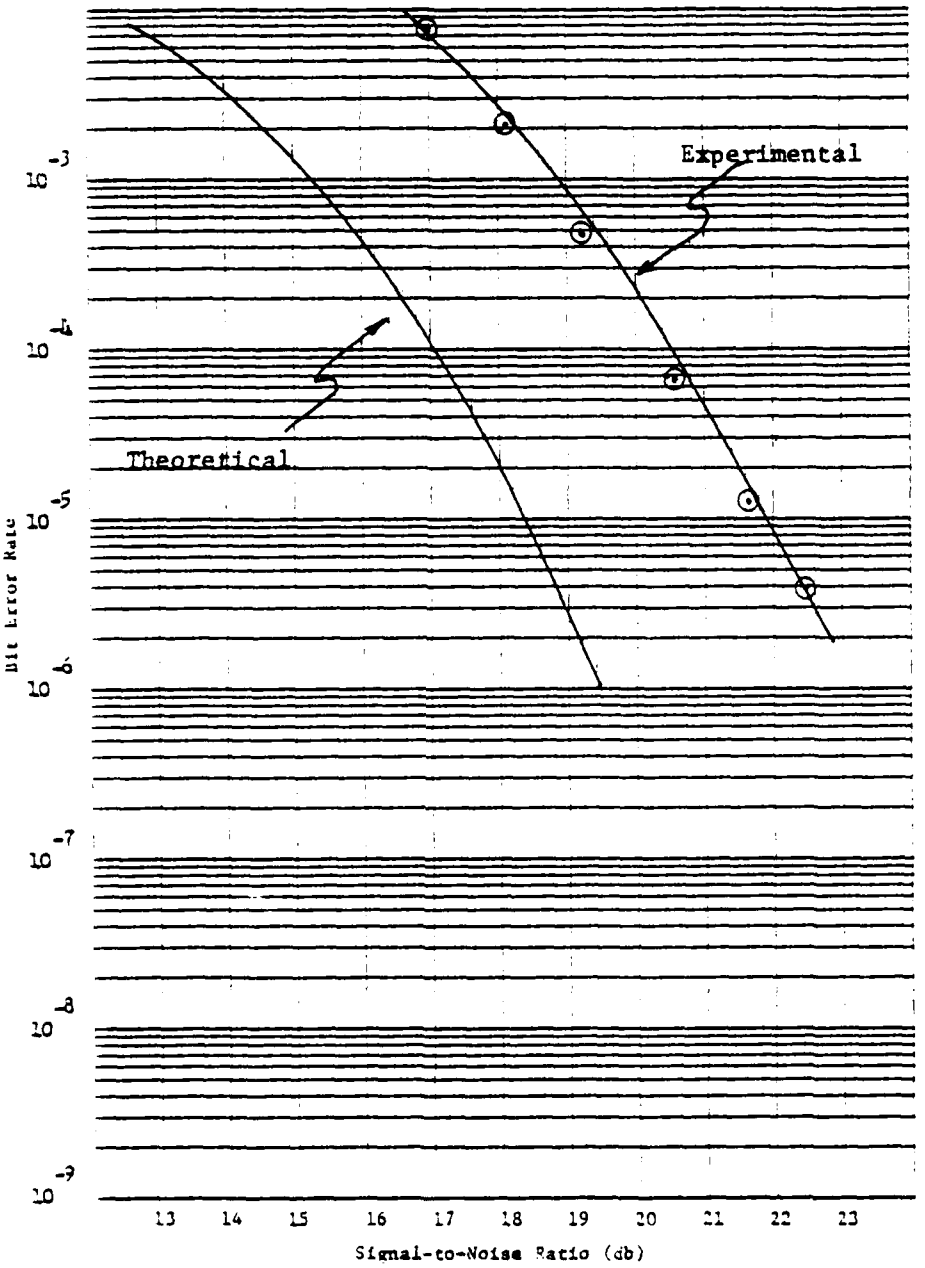

Fig. 4.20. BER vs. S/N, Lenkurt 26C.

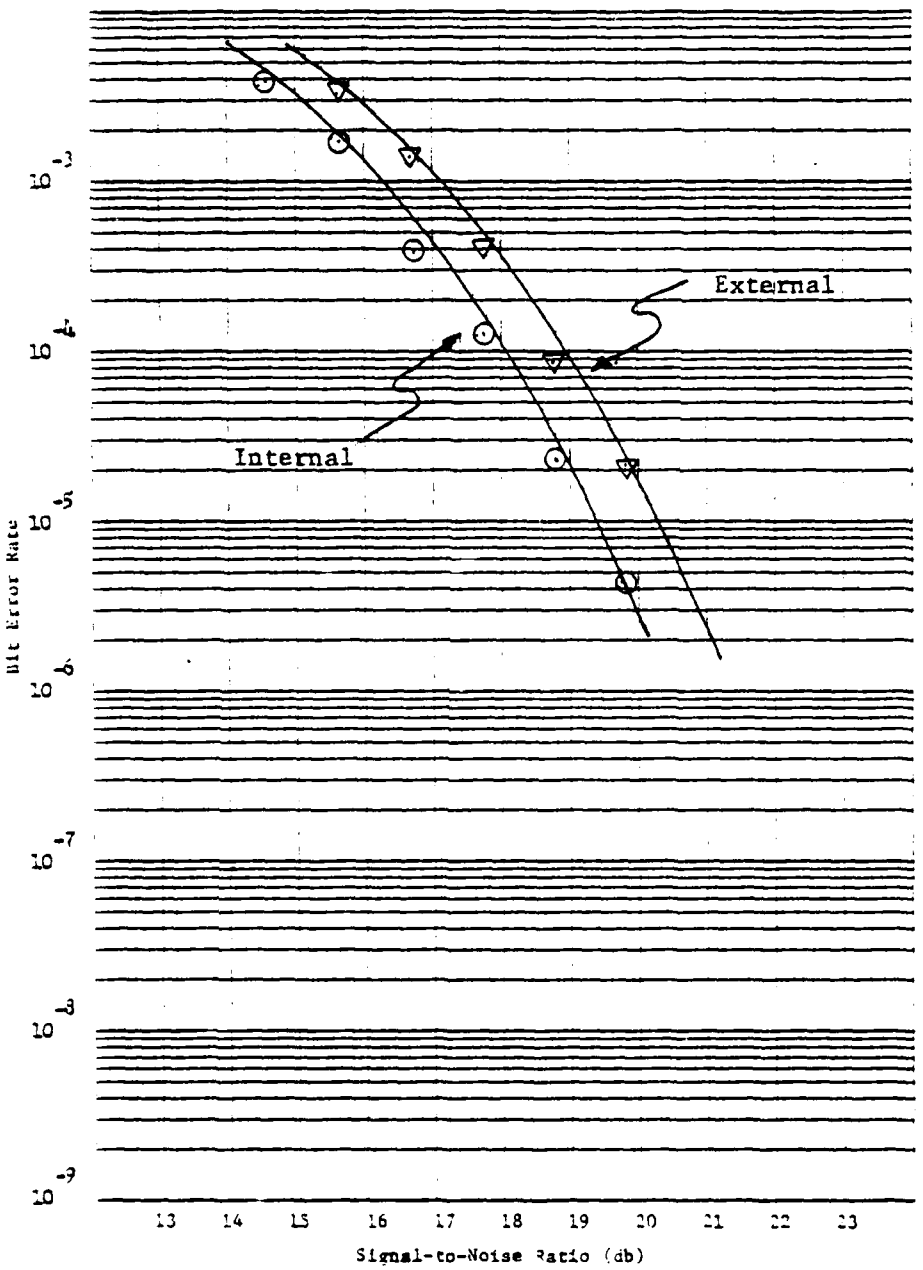

Fig. 4.21. BER vs. S/N, Internal and External Timing: Lenkurt 261A, #1.

internally or externally. The output can be either NRZ or RZ, with the level variable from 0.1 to 3.2 volts (50 ohm output impedance). The 3761A is specifically designed to receive the data stream of the 3760A and to count errors after comparison with an internal closed loop reference sequence synchronized by a sync pulse generated every sequence by the 3760A. Errors may be counted over a gating period or BER can be calculated and displayed upon the receipt of 100 or more errors.

Test Procedure

The test configuration is shown in Fig. 4.22. The interface box was a locally fabricated device to convert the TTL logic of the 3760/3761 to the MECL logic of the MW-518. The interface box also provided clock to both the data set and the modulator section of the MW-518. Data was transmitted at 19.804 Mbps. As in previous tests, the AGC voltage of the receiver was calibrated to determine the receive signal level. Attempts were made to record BER at signal levels from -70 to -80 dbm.

As before, the first step was to obtain a BER versus received signal level curve as a base for comparison prior to attempting any alterations of the internal timing, or other parameters. However, the considerable difficulties encountered in efforts to obtain consistent (repeatable) BER data precluded any attempts to directly demonstrate the effects of jitter, or other anomalies. These difficulties are described below.

The received QPSK modulated 70 MHz signal which is input to the phase demodulator of the MW-518 may assume any one of four phases during

AD-A097 123 ARIZONA UNIV TUCSON ENGINEERING EXPERIMENT STATION F/G 17/2
DIGITAL COMMUNICATIONS SYSTEMS: TEST AND EVALUATION STUDIES, VO--ETC(U)
AUG 79 L C SCHOOLEY, G R DAVIS DAEA18-74-A-0271
UNCLASSIFIED NL

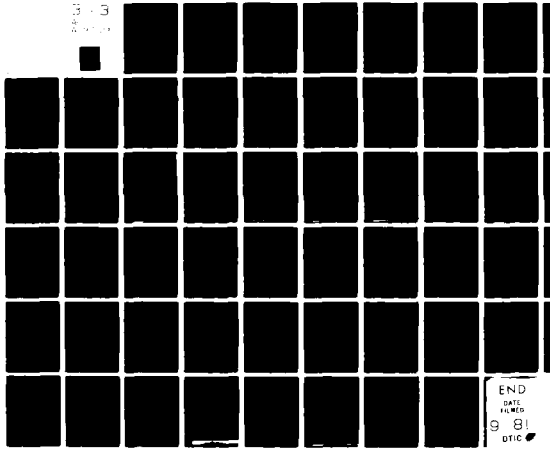

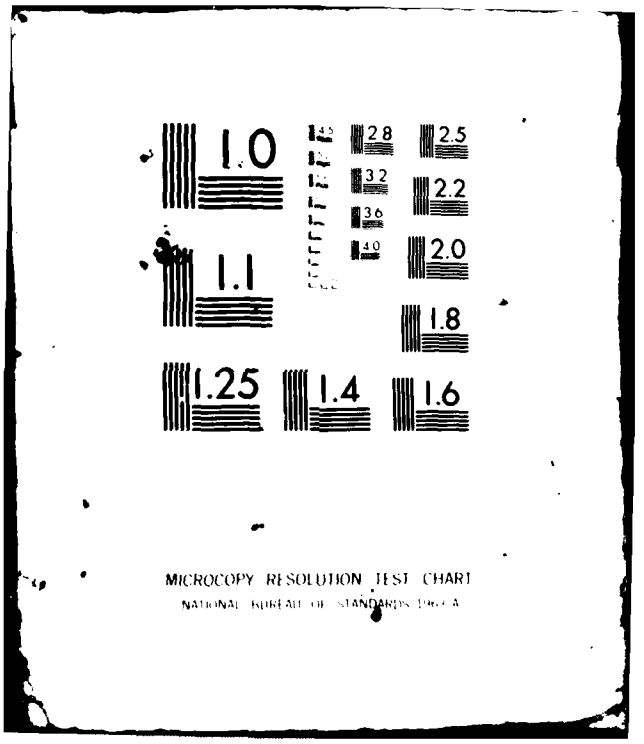
1.0
1.1
1.25
1.4
1.6
2.8
3.2
3.6
4.0
2.5
2.2
2.0
1.8
MICROCOPY RESOLUTION TEST CHART
NATIONAL BUREAU OF STANDARDS 1963-A

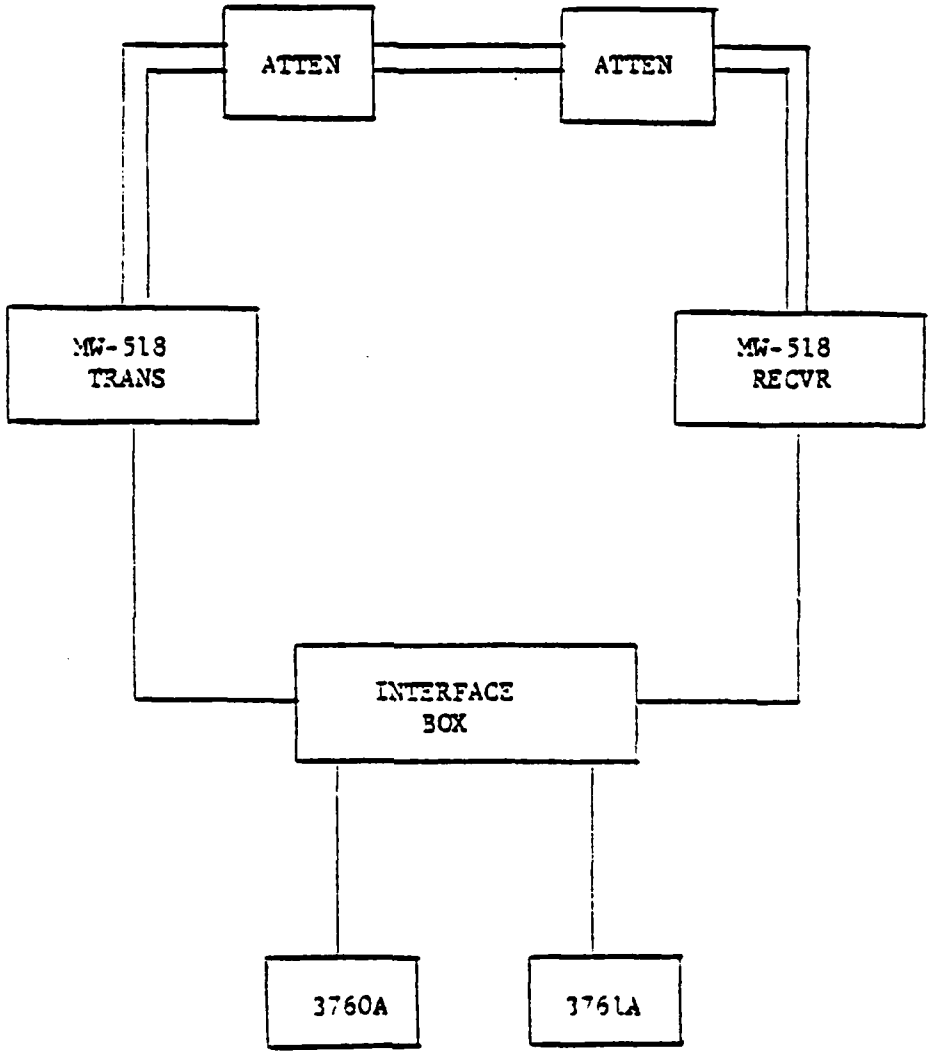

Fig. 4.22. Equipment Configuration: MW-518 Tests.

any one bit period of the modulating waveform. The function of the phase demodulator is to detect the QPSK modulation and provide a 70 MHz output signal.

The input signal is routed to both the carrier recovery circuitry and the phase detector. An input times-four frequency multiplier in the carrier recovery section raises the signal to 280 MHz. This signal, with phase discontinuities removed, is the reference to the phase detector. The other phase detector input is the output of an identical multiplier driven by a 70 MHz voltage-controlled oscillator. The phase detector output is amplified and filtered to provide a dc voltage which phase-locks the 70 MHz VCO to the 280 MHz reference signal. However, since the loop phase comparison is performed at 280 MHz, the 70 MHz recovered carrier will assume any one of four, static phase states separated by 90°. This four state possibility of the carrier phase introduces an ambiguity in the detected QPSK signal which must be removed by the radio system.

The frequency deviation of the FM on the input signal is multiplied by a factor of four along with the carrier frequency in the reference multiplier as is the level of any noise present with the input signal. However, the FM modulating frequency is not changed, and at the 70 MHz VCO output, the deviation is again the same as that on the 70 MHz input signal. The loop may be viewed as a narrow band tracking filter (noise BW 1 MHz wide) which filters the 280 MHz signal, followed by a factor of four divider to restore the original deviation. Because the filter is a phase-locked loop however, it can only function as long

as the loop remains locked. For modulating frequencies small compared to the 135 KHz loop bandwidth, the loop will remain locked for arbitrarily large deviations. At frequencies outside the loop bandwidth, the loop will remain locked only if the carrier is present, and if the equivalent phase deviation is less than 90° peak. Low carrier-to-noise ratios at the 70 MHz input generate large phase deviations at the 280 MHz multiplier output and the loop unlocks. A reduction in the noise level is necessary for the loop to regain phase lock.

This method of carrier recovery results in a family of four distinct bit error rate curves depending upon which static phase state has been assumed. Attempts were made to identify the phase states by observing the I and Q channels on an oscilloscope. To note any changes it was necessary to provide a data input of alternating ones and zeros. Three distinct states were identified in this manner. The fourth state either did not occur or it was not noted. Unfortunately, it was not possible to relate the observed states with specific BER curves, since, when the data input was changed from alternating ones and zeros to a pseudo-random sequence, the system would lose synchronization (the phase-locked-loop unlocked) and there was no way of determining which state was regained.

Information from persons involved in the initial acceptance testing of this equipment indicates that the Collins technicians had photographs of eye patterns of the I and Q channels which permitted them to discern the several phase states while pseudo-random data was being input; however, these photographs were not available.

The second problem was the extreme sensitivity of the MW-518. The receiver repeatedly lost synchronization without apparent cause, even at relatively high signal levels (-76 -77 dbm). At no time was lock maintained at a signal level of -80 dbm, or less, for a sufficient period to obtain a BER reading. At each loss, the signal levels had to be increased to approximately -70 to -72 dbm to regain synchronization. Unfortunately, upon each resynchronization the system had the opportunity to lock on different phases of the carrier.

Compounding the situation was the apparent sensitivity of the system to heat. The AGC versus RSL curves were found to vary by as much as 1 db between the morning and afternoon (and from day to day). This was attributed to temperature variations, since the test site air conditioning was not working properly during the period of the tests and ambient temperatures varied by at least 10 degrees. The demodulator module of the receiver was noted to operate at a very high temperature. Although this did not necessarily affect the AGC voltage, it probably contributed to the instability of the system.

It appeared that there would be no possible way to discriminate between variations in BER intentionally induced and those due to the above-described phase and heat problems. For this reason, no attempts were made to induce jitter, or other anomalies, into the operation of the system.

Results

After many attempts, two separate curves of BER versus signal-to-noise ratio were obtained during a single short time period

(approximately one hour), while the ambient temperature was essentially constant. The data points of each curve were obtained without loss of synchronization, but the system was resynchronized between the two groups of data. The differences in the curves were, therefore, attributed to the system having locked onto different phases of the recovered carrier. Complete data for the MW-518 tests are contained in Schooley and Davis (1978). Figure 4.23 shows the two curves that were obtained. The phases were arbitrarily numbered one and two. The curves do adhere reasonably to the theoretical shape and are consistent with the results of previous tests. The shift of approximately 1/2 db between the two curves is attributed to an increase in carrier phase jitter caused by the resolution of the ambiguity in the detection process.

RDS-80

The RDS-80 is a QPSK radio system manufactured by Raytheon. The multiplexer accepts up to 25 T1 (1.544 Mbps) lines and delivers a 40.15 Mbps data stream to the quadrature phase modulator. Modulation is accomplished at the IF (70 MHz) level and the signal is then up converted to the 11 GHz band. Demodulation is coherent from a recovered carrier.

The HP 3780A error measuring set was described previously.

Test Procedure

The equipment configuration for the test is shown in Fig. 4.24. The RDS-80 transmitter timing was utilized to key the 3780A at 40.18 Mbps. This signal was then fed directly to the radio modulator section

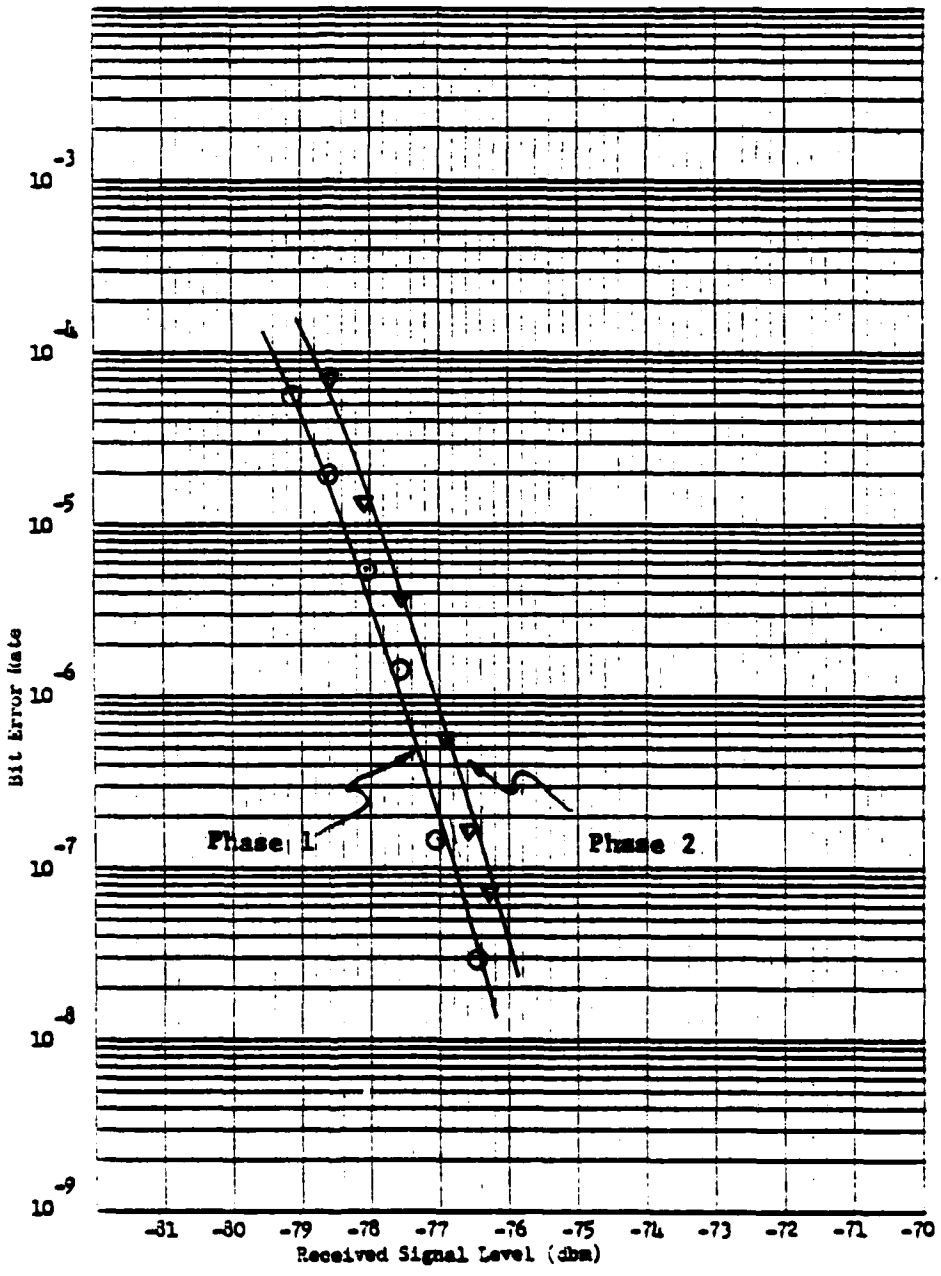

Fig. 4.23. BER vs. RSL, MW-518.

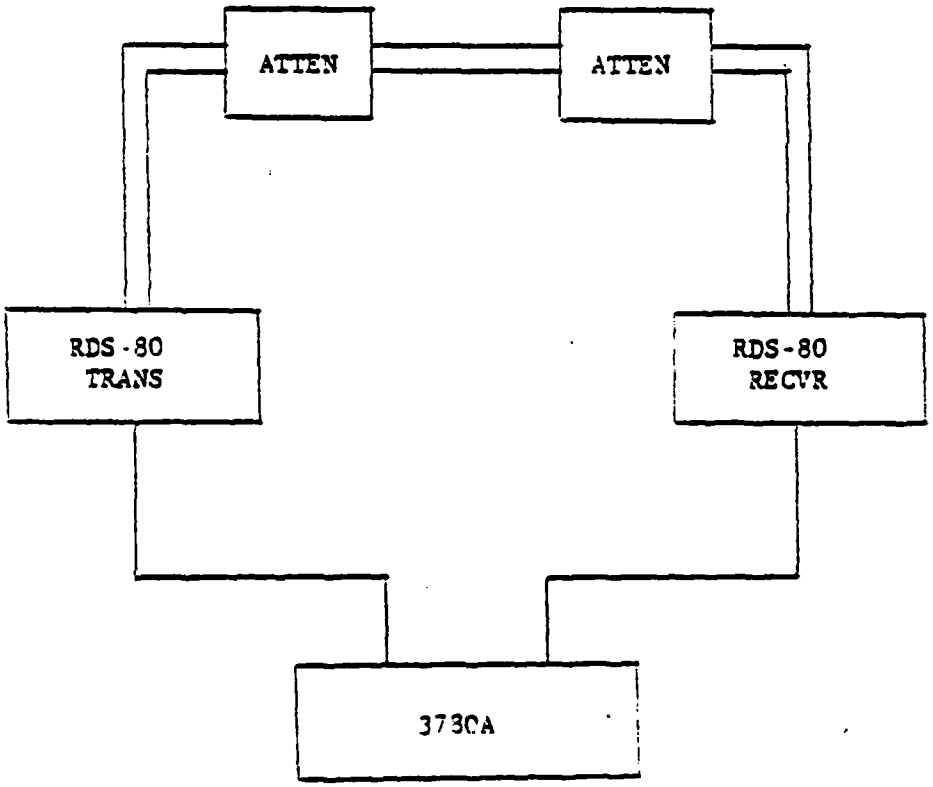

Fig. 4.24. Equipment Configuration: RDS-80 Tests.

of the RDS-80 bypassing the multiplexer. The attenuators in the waveguide were calibrated so that the received signal level could be read directly. The HP 382A attenuator that was varied during the tests had been calibrated on June 1, 1978. The 40.15 Mbps NRZ signal was returned directly from the demodulator to the 3780A, again bypassing the multiplexer so that errors were detected at the high data rate.

Data was taken for an initial curve of BER versus received signal level to serve as a basis for future comparisons. Data points were taken for signal levels in the range of -71 to -81 dbm.

Carrier phase jitter was simulated by offsetting the phase of the recovered carrier used for the QPSK demodulation. This was accomplished by varying an inductor in the output of the carrier recovery circuit. The amount of adjustment to this coil was used to identify the states for which BER curves were plotted. Operation of the carrier recovery and demodulator are described in some detail in Schooley and Davis (1978).

Baud timing jitter was simulated by adjusting the phase of the 20 MHz timing signal which is used in the regeneration of the output data stream after detection. This was accomplished by adjustment of a trimming capacitor in the output of the phase-locked-loop. Operation of the phase-locked-loop and the data regeneration module also are described in Schooley and Davis (1978). The orientation of the trimming capacitor was used to identify the several states for which BER curves were plotted.

Results

Complete data for the RDS 80 tests are contained in Schooley and Davis (1978). Figure 4.25 shows a comparison of the experimental BER curve of the RDS 80 prior to any adjustments with a theoretical error function curve. Figures 4.26 and 4.27 are the experimental BER curves obtained as a result of varying the carrier phase offset. Figures 4.28 and 4.29 are the experimental curves obtained as a result of offsetting the baud timing.

In general, the data taken on the RDS-80 was not as consistent as that for the other items of equipment. The cause of this is not known. However, the smooth curves drawn through the data points did produce predictable results. This will be shown in the comparisons with calculated curves in Chapter 5.

Figures 4.30 and 4.31 are curves of BER versus the coil and trimmer capacitor settings for the RDS-80 operating at RSL's of -75, -76, and -77 dbm. The coil setting is obviously quite critical whereas the capacitor alignment has a considerably broader range in the optimum area. Still, once away from the center of this optimum area, small variations could cause startling changes in the BER. Again the optimum settings are independent of the RSL. These curves again demonstrate the facility with which equipment alignment can be accomplished while monitoring the BER at very low signal-to-noise ratios.

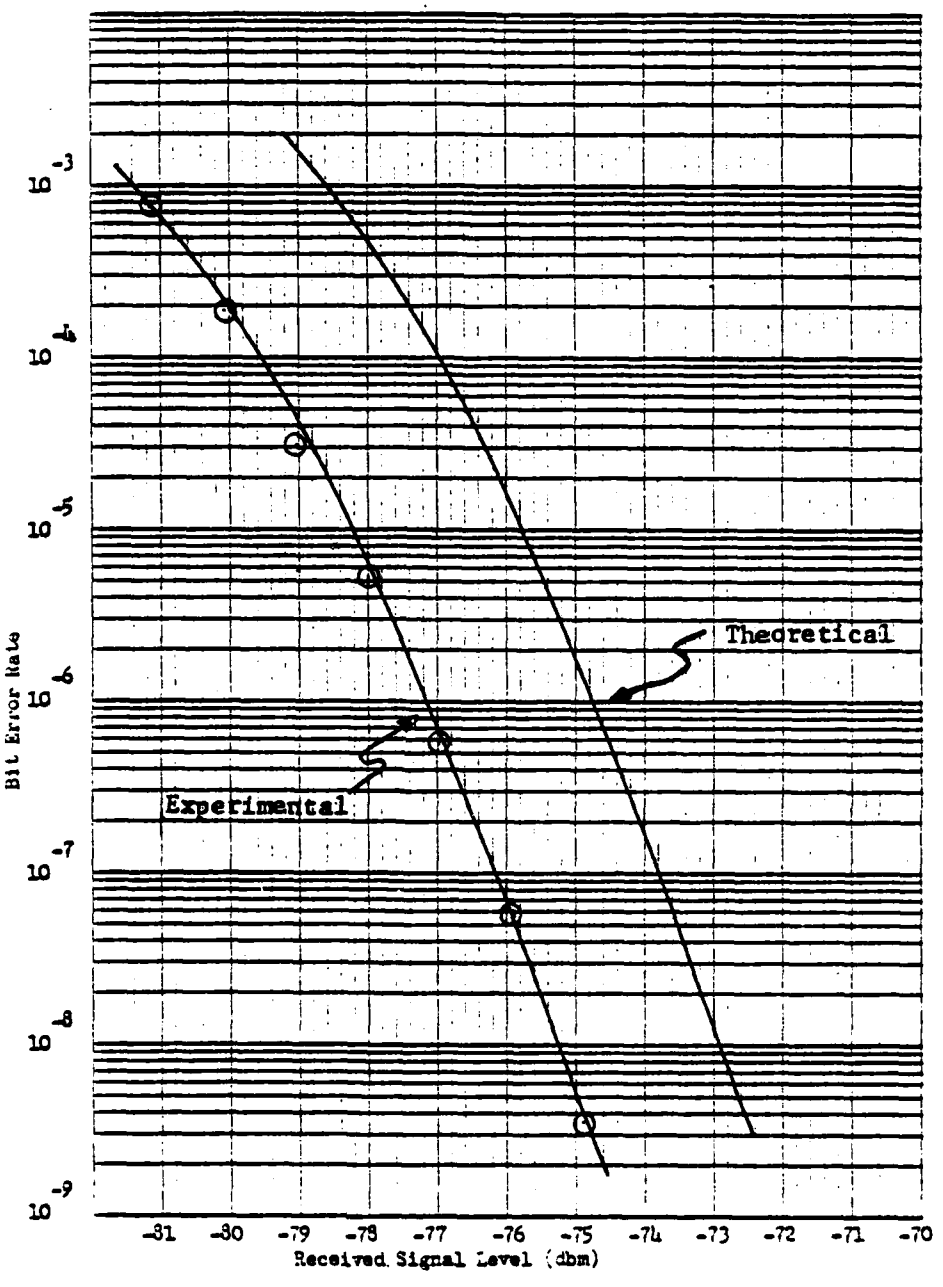

Fig. 4.25. BER vs. RSL, RDS-80.

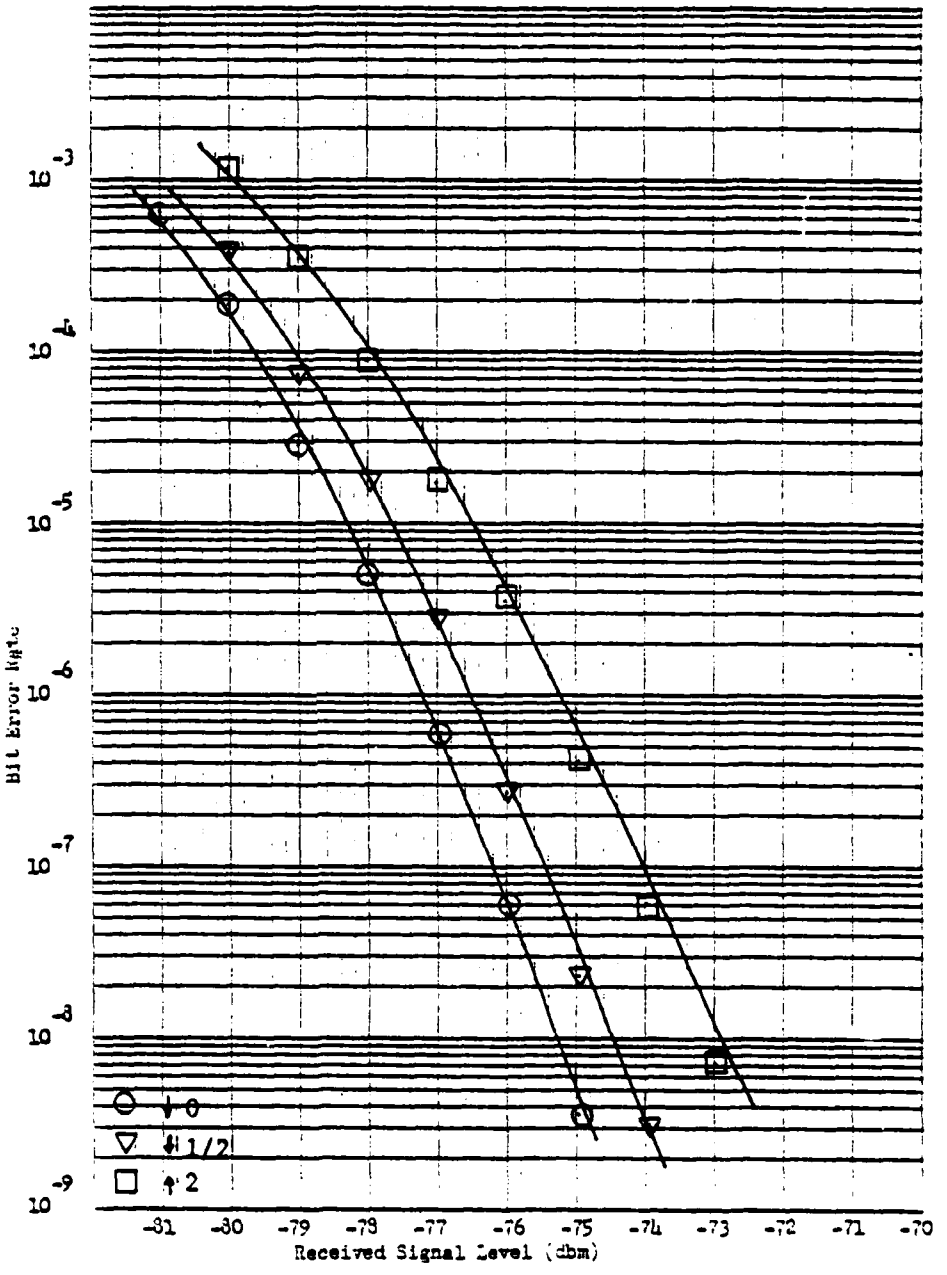

Fig. 4.26. BER vs. RSL, with Carrier Phase Offset, RDS-80.

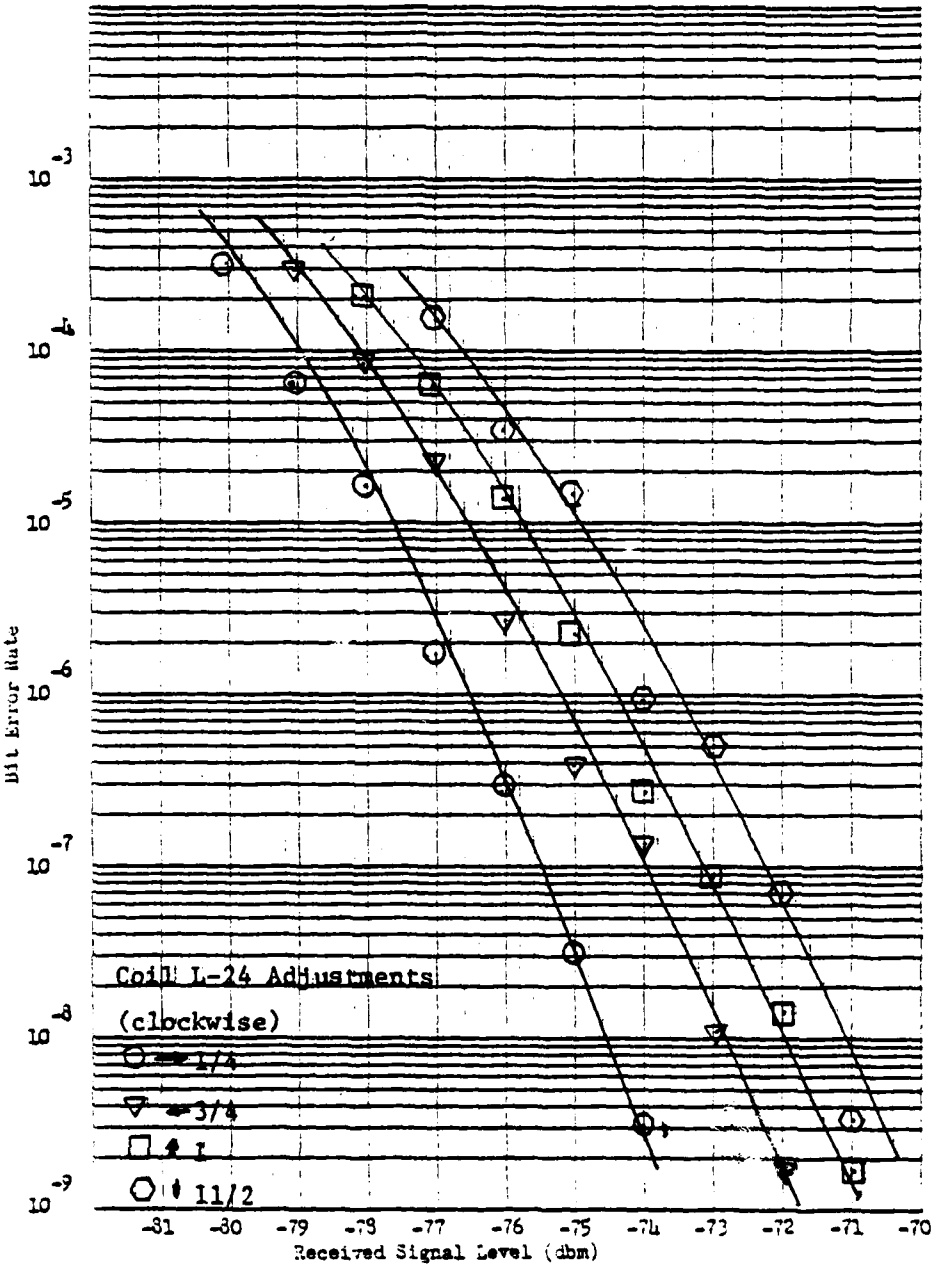

Fig. 4.27. BER vs. RSL, with Carrier Phase Offset (2), RDS-80.

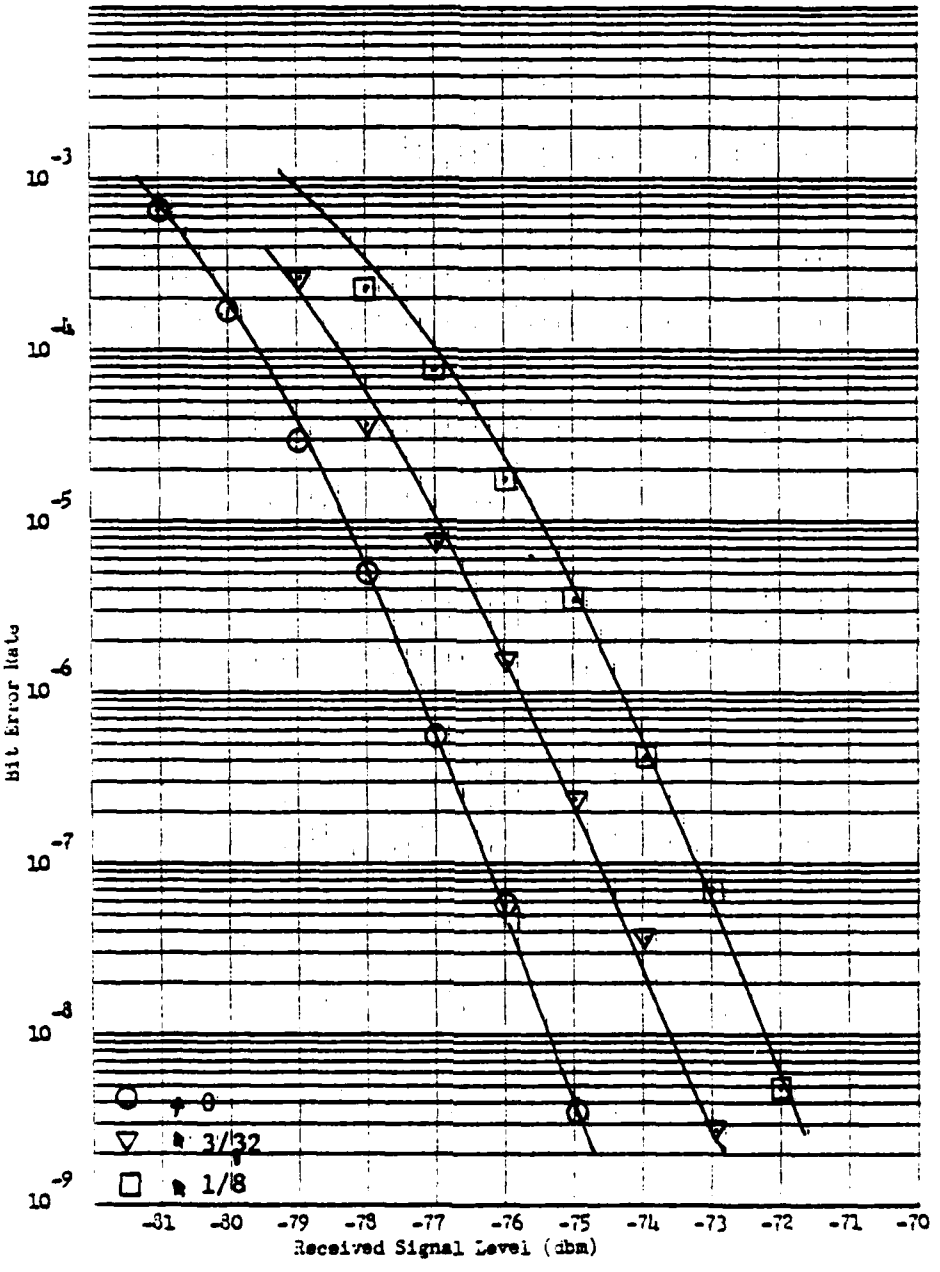

Fig. 4.28. BER vs. RSL, with Baud Timing Offset, RDS-80.

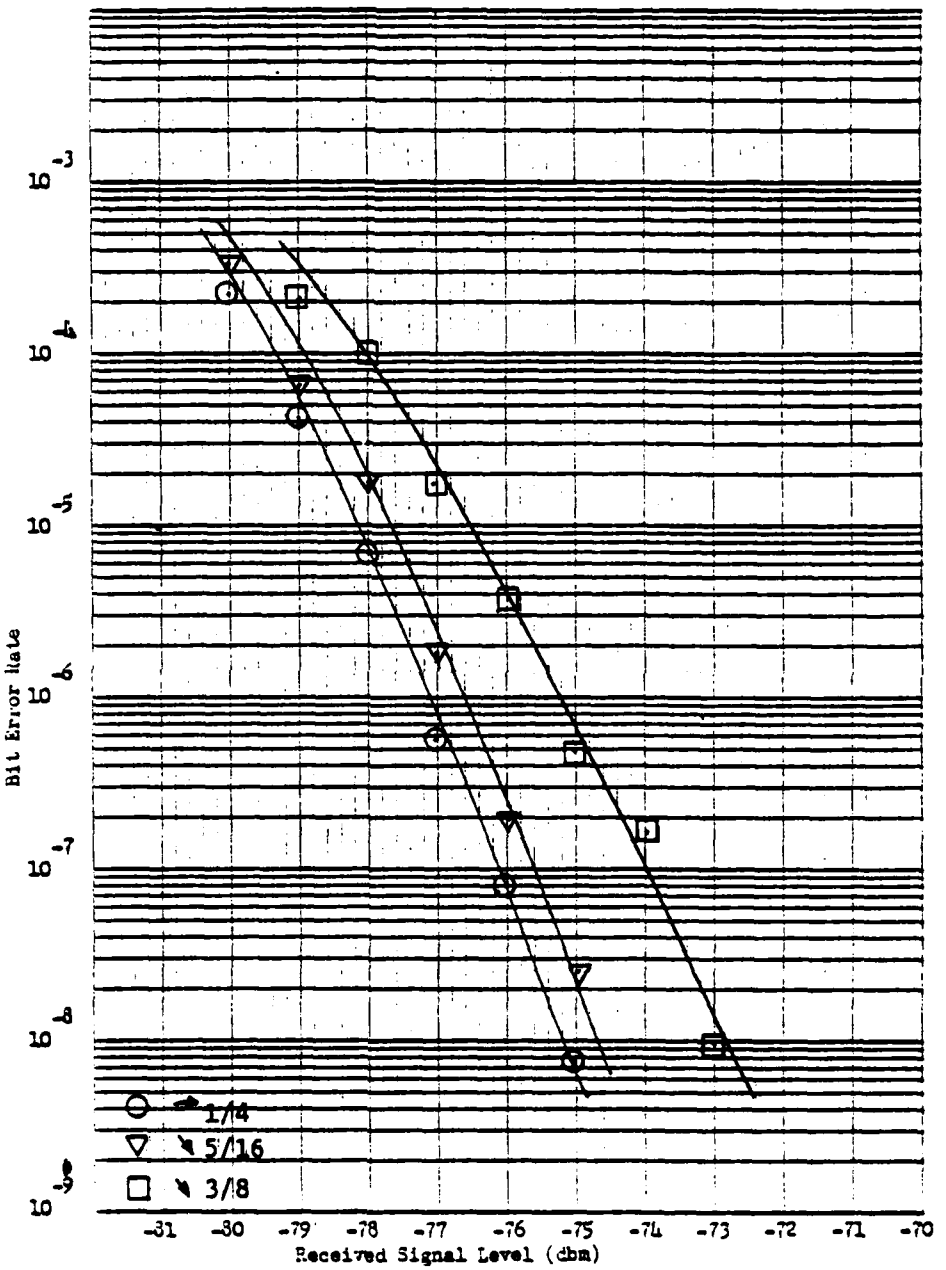

Fig. 4.29. BER vs. RSL, with Baud Timing Offset (2), RDS-80.

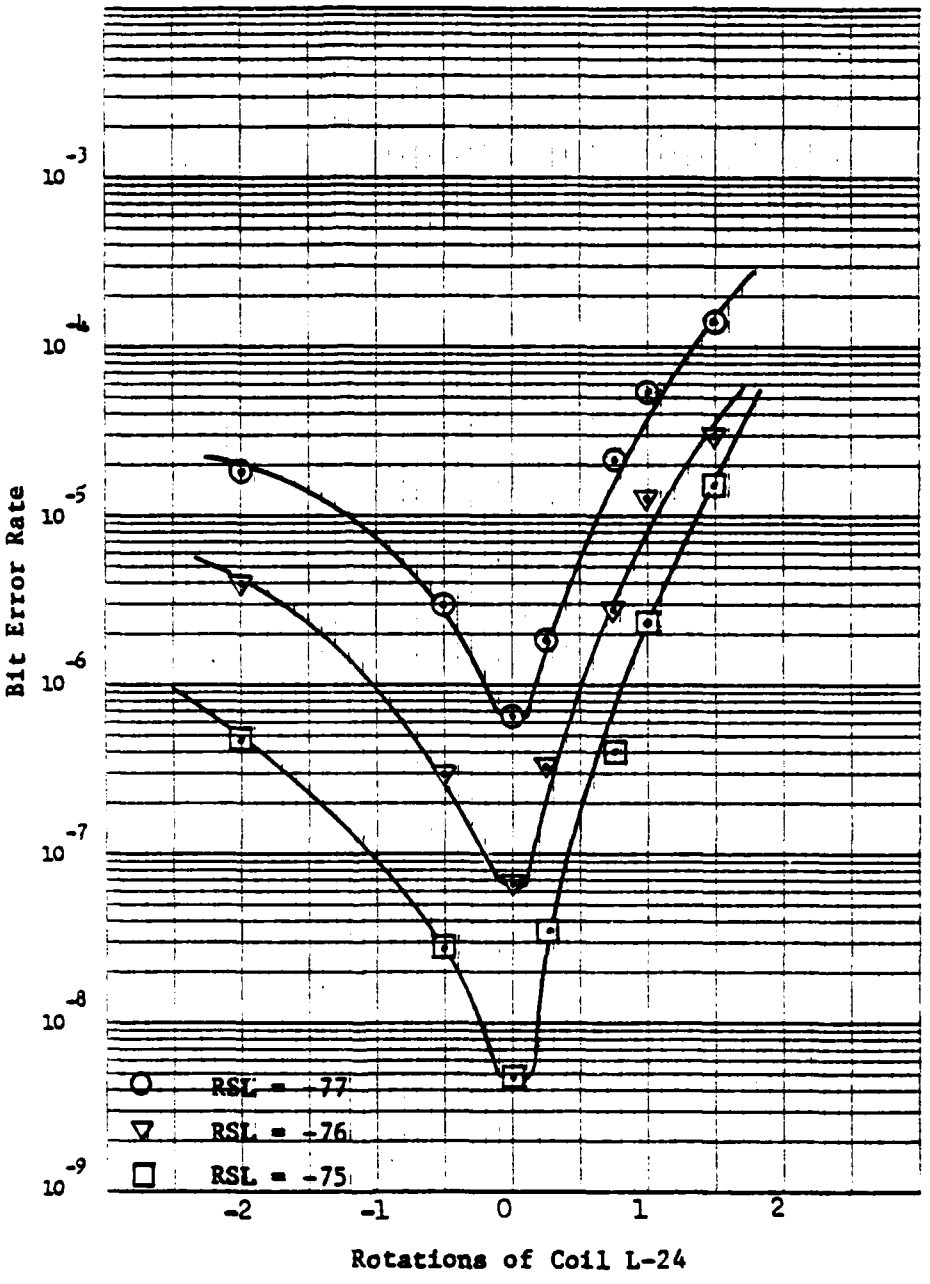

Fig. 4.30. BER vs. Coil Position (Carrier Phase Offset), RDS-80.

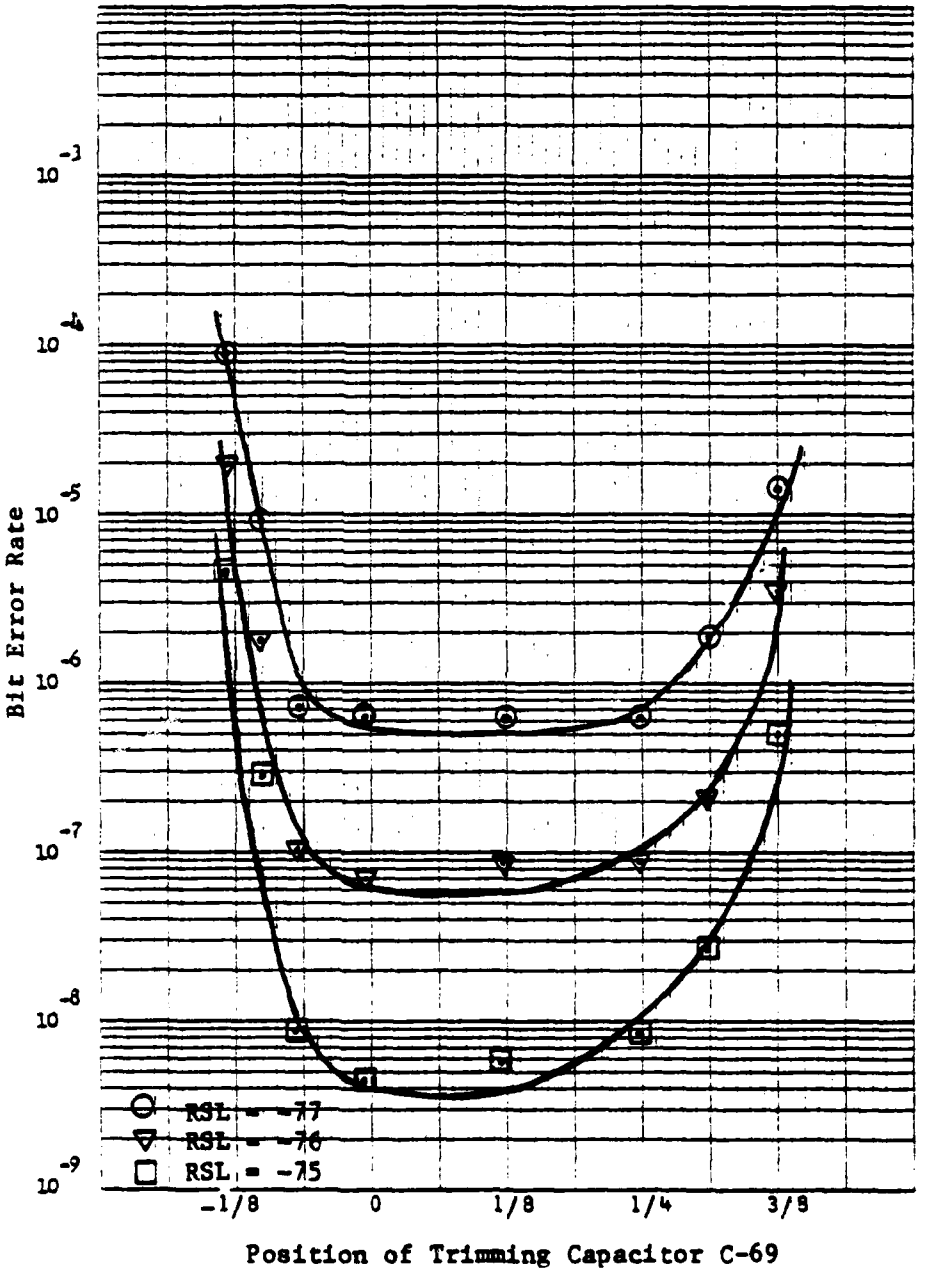

Fig. 4.31. BER vs. Capacitor Orientation (Baud Timing Offset), RDS-80.

Variance and Consistency of Experimental Data

Considerable care was taken during the experiments to obtain reliable consistent data. In those cases where data appeared inconsistent with that previously taken or deviated from what could reasonably be expected, the experiments were halted and complete data for that curve were retaken after the source of difficulty had been resolved. The results for the most part appear to be reliable and consistent.

It must be remembered that the BER measurements are actually estimates of the mean value of a random variable. Where it was practical to do so, the experiments were allowed to run for a sufficient length of time to insure that the variance of the estimates could be neglected. To show that this is in fact a reasonable assumption, the variances for each point of an example curve for each item of equipment were calculated.

The variance is calculated by first assuming that the true value of the mean remained constant during the period the errors were counted. Assuming x errors are counted in an interval of n total received bits, the unbiased estimate of the BER for direct binomial sampling is:

$$\hat{p} = x/n \; . \tag{4.1}$$

Recalling that x is a random variable with a binomial distribution, i.e.,

$$P(x=k) = \binom{n}{k} p^k (1-p)^{n-k} \tag{4.2}$$

the mean and variance of x are (Korn and Korn, 1968)

$$\eta_x = np$$

$$\sigma_x^2 = np(1-p). \tag{4.3}$$

Then to find the mean and variance of $\hat{p}$:

$$\eta_{\hat{p}} = E\{\hat{p}\} = E\{\frac{x}{n}\} = \frac{np}{p} = p$$

$$\sigma_{\hat{p}}^2 = E\{(\hat{p} - \eta_p)^2\} = E\{\frac{1}{n^2}(x^2 - n^2 p^2)\} = \frac{1}{n^2}\sigma_x^2 \tag{4.4}$$

$$\sigma_{\hat{p}}^2 = \frac{p(1-p)}{n}.$$

Complete tables of the calculated variances for each data point of example curves can be found in Schooley and Davis (1979). In all cases the variances were very small, most ranging from 10^{-11} to 10^{-18}. The largest was 1.1×10^{-8} for one point on the Lenkurt 261A curve.

To relate this result to the variance in RSL (or signal-to-noise ratio) necessary to produce a given BER, it can be shown (Papoulis, 1965) that an approximate evaluation can be obtained from:

$$\sigma_{RSL}^2 = [g'(\hat{p})]^2 \sigma_{\hat{p}}^2 \tag{4.5}$$

where $g'(\hat{p})$ is the slope of the BER curve (considering RSL as a function of BER) at the point of interest.

As can be seen at a glance, for BER's of 10^{-4} or less, the slopes of the curves are slowly decreasing, and very much less than unity. Squaring the slope and multiplying by an already very small number does indeed produce a variance which can easily be neglected.

A sample value of this variance was calculated for each example curve. These variances ranged on the order of 10^{-11} to 10^{-19}. Again the largest was for the same point on the Lenkurt 26lA curve which was 2.3 x 10^{-11} db.

For an additional estimation of the data reliability, 90% confidence intervals which were defined by Crow and are described in Schooley and Davis (1977b) were calculated for sample points. The intervals are in terms of the BER variation. Since each interval is a function of the standard deviation, the 90% confidence interval in terms of RSL for a given BER is directly proportional to the slope.

Even for the worst cases, the confidence intervals were found to be less than 1/2 db. Because of this it can be concluded that isolated irregularities in the data are due primarily to experimental procedures, drifting signals, or other external influences rather than to the variance of the estimates of the random variable so long as sufficient time is allowed for the estimates.

CHAPTER 5

COMPARISON OF CALCULATED AND EXPERIMENTAL RESULTS

In the previous chapters expressions were derived for the effects of carrier phase jitter and baud timing jitter on the probability of error in digital communications systems for a variety of modulation techniques and detection methods. These expressions were then used to calculate characteristic curves of long term bit error rate versus signal-to-noise ratio. Other internal receiver anomalies whose effects could not be derived in closed form were studied directly in terms of calculated BER curves. With some notable exceptions that will be discussed further in this chapter, it was found that, in theory, small variations of these internal receiver anomalies caused shifts of the BER curves without significant distortion of the shape.

Chapter 4 presented the results of experiments that were performed in an attempt to directly verify the theoretical predictions. In this chapter the BER curves obtained from these experiments will be analyzed to determine how closely they conform to the calculated results. The analysis will be in terms of the amount of deviation of the experimental curves from the theoretical shape, and where measurements have made comparative calculations possible, in terms of the amount of shift.

The approach in this chapter will be to first correct the misconception about detection behavior in the presence of jitter that has

apparently occurred based upon the wide acceptance of the theoretical curves of Lindsey and Stiffler that were presented and extended in Chapter 3. These calculated results showed a dramatic flareout of the tails of the BER curves for relatively large values of both carrier phase and baud timing jitter. In the experimental results described in Chapter 4 and in all those observed in the literature, the BER curves tend to tilt outward with large disturbances, but the predicted flareout of the tails does not occur. A simple but satisfying resolution of this apparent disparity is presented.

Before proceeding with the comparisons of the results, a brief description is given of the calculations that were performed to provide a quantitative measure of the "goodness of fit" of the experimental curves to the theoretical. Then the results obtained from each item of equipment are compared with calculated curves to determine their deviations from the theoretical shape. In the cases of the T1-4000 and the RDS-80 measured values of jitter and phase offset are used to compare the amount of shift that can be theoretically predicted to that obtained experimentally.

The Flareout Question

Examination of the curves in Chapter 3 that were calculated for the effects of both carrier phase and baud timing jitter raises a significant question. Why don't these analytically derived curves agree more closely with the experimental results? Much larger shifts of the error curves were obtained experimentally without the dramatic flareout

shown in the calculated curves. True, for the most part, the experimental results were obtained by phase and timing offsets which shifted the mean value of the jitter but essentially left the variance unchanged. However, since such a shift in the mean is relatively unaffected by the signal-to-noise ratio over the range of interest, it would be expected that the irreducible errors (probability that the magnitude of the jitter is greater than $\pi/2$) would be increased significantly, causing an even more dramatic flareout of the error curves. In addition to the experiments performed in support of this work, a search of the literature revealed no experimental results where internal equipment anomalies caused the BER curves to be so distorted.

The answer to this question lies in the fact that the theoretical curves of Lindsey and Stiffler were plotted for constant variances over the complete range of signal-to-noise ratios. However, it was shown in the discussion of phase error from PLLs in Chapter 3 that, in the linear approximation to PLL operation, if the phase of the input signal is constant, the variance of the output jitter due to additive white Gaussian noise is inversely proportional to the signal-to-noise ratio within the PLL bandwidth. That is:

$$\sigma_n^2 = \frac{N_o B}{A^2} \tag{5.1}$$

where $N_o/2$ is the two-sided noise spectral density, B is the loop bandwidth, and A is the signal amplitude.

It must be noted that σ_n^2 is the variance of the phase jitter due only to the noise. Although this is generally the most significant

factor, random oscillator fluctuations and other transient phenomena, are always present causing relative variations between the received signal and VCO output phases (Stiffler, 1971). The design of the loop filter of the PLL is normally a compromise between tracking the phase variations and eliminating the effects of the additive noise. For this reason the jitter variance will contain both constant and varying (functional) components depending upon the particular filter design and the stabilities of the transmitter and VCO oscillators (disregarding other transient phenomena as being primarily due to the external channel).

There appears to be no prescribed method available to formulate the specific relationship between the constant and functional components of variance of the output phase of a PLL. Although this would be an interesting investigation, it is not within the scope of this study. That such components do exist in a definite relationship will be shown from the experimental measurements made with the T1-4000. For the present purposes of examining the effect upon the BER curves several possible relationships will be assumed.

The results in Chapter 3 were obtained with only a constant component of variance. It should be instructive to examine the other extreme of a purely varying component. In all of the following examples the mean will be assumed to be zero. Figure 5.1 is BER curves calculated from the expression for probability of error conditioned on carrier phase jitter with a zero mean and the variance equal to 0.8, 1.0, and 1.4 times the inverse of the signal-to-noise ratio. Similar results are

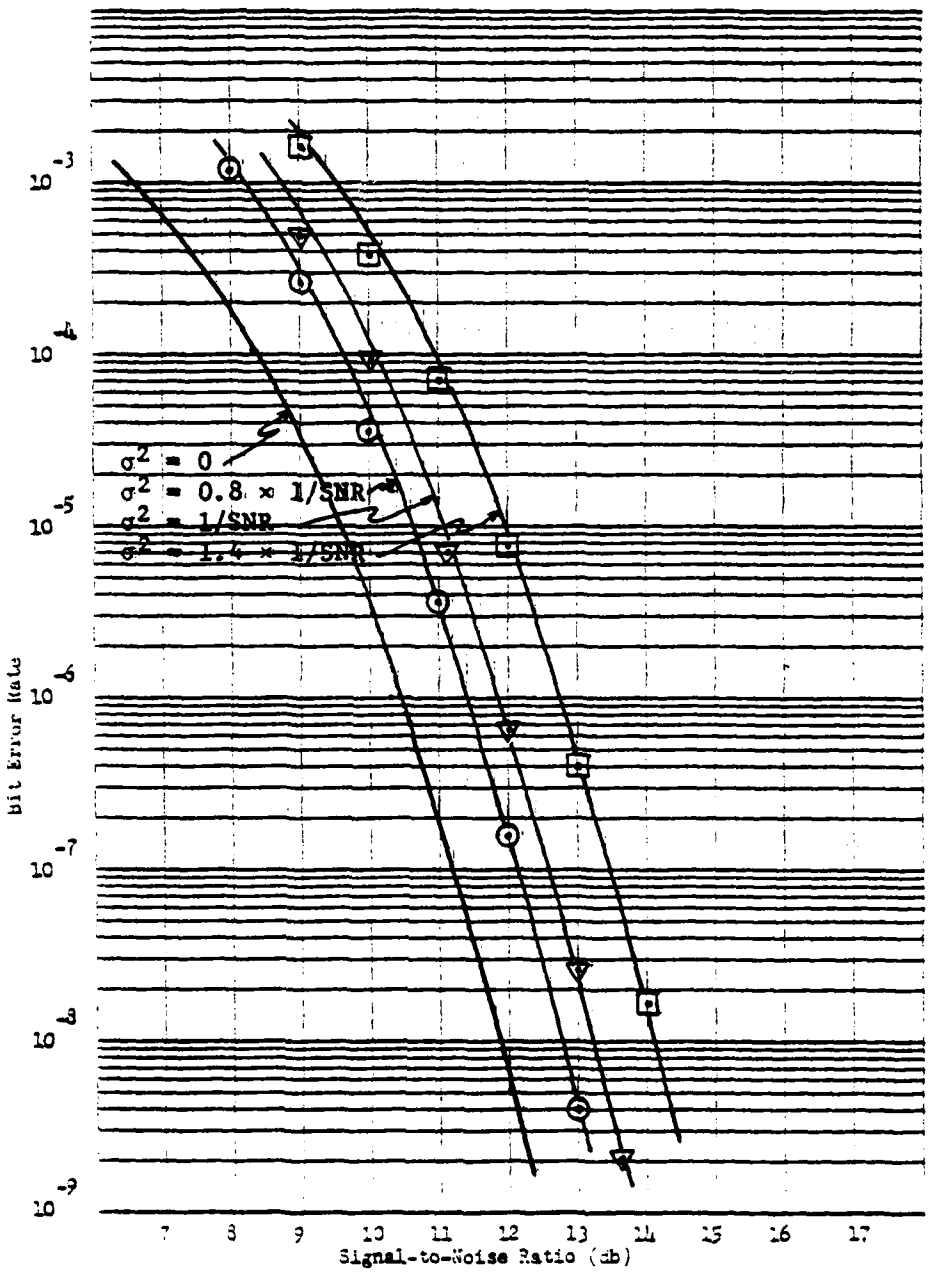

Fig. 5.1. Carrier Phase Jitter, Zero Mean, Variance as Indicated.

shown in Fig. 5.2 for baud timing jitter where the variance was made equal to 0.08, 0.2, and 0.3 times the inverse of the signal-to-noise ratio. The proportionality constants are used since the loop bandwidth of the PLL is generally kept very narrow and the PLL signal-to-noise ratio will in general be larger than that at the point of detection. Although these results are not too realistic since the curves tilt inward slightly, they certainly demonstrate that the functional component of variance does not cause a flareout of the tails of the curves.

In a real system the results will be somewhere between the two extremes of the constant and the functional variance. Figure 5.3 shows an example for carrier phase jitter with variance $\sigma^2 = 0.02 + 1/SNR$. Figure 5.4 is for baud timing jitter with a standard deviation $\sigma^2 = .003 + 0.1/SNR$. As can be seen, these relationships cause the curves to shift and tilt slightly, but there is no flareout of the tails.

The above examples demonstrate that the flareout of the tails of the curves calculated by Lindsey and Stiffler was due to the assumption of constant variance. When the variance is assumed to have both a constant and a functional component, the curves were in much closer agreement with the experimental results. This conclusion will be verified further by the calculations using the measured values of jitter in the discussions of the T1-4000 test results that follow.

Deviation of Experimental Curves from the Theoretical

So far in the discussion, the shapes of the experimental BER curves have been compared graphically to the theoretical error function

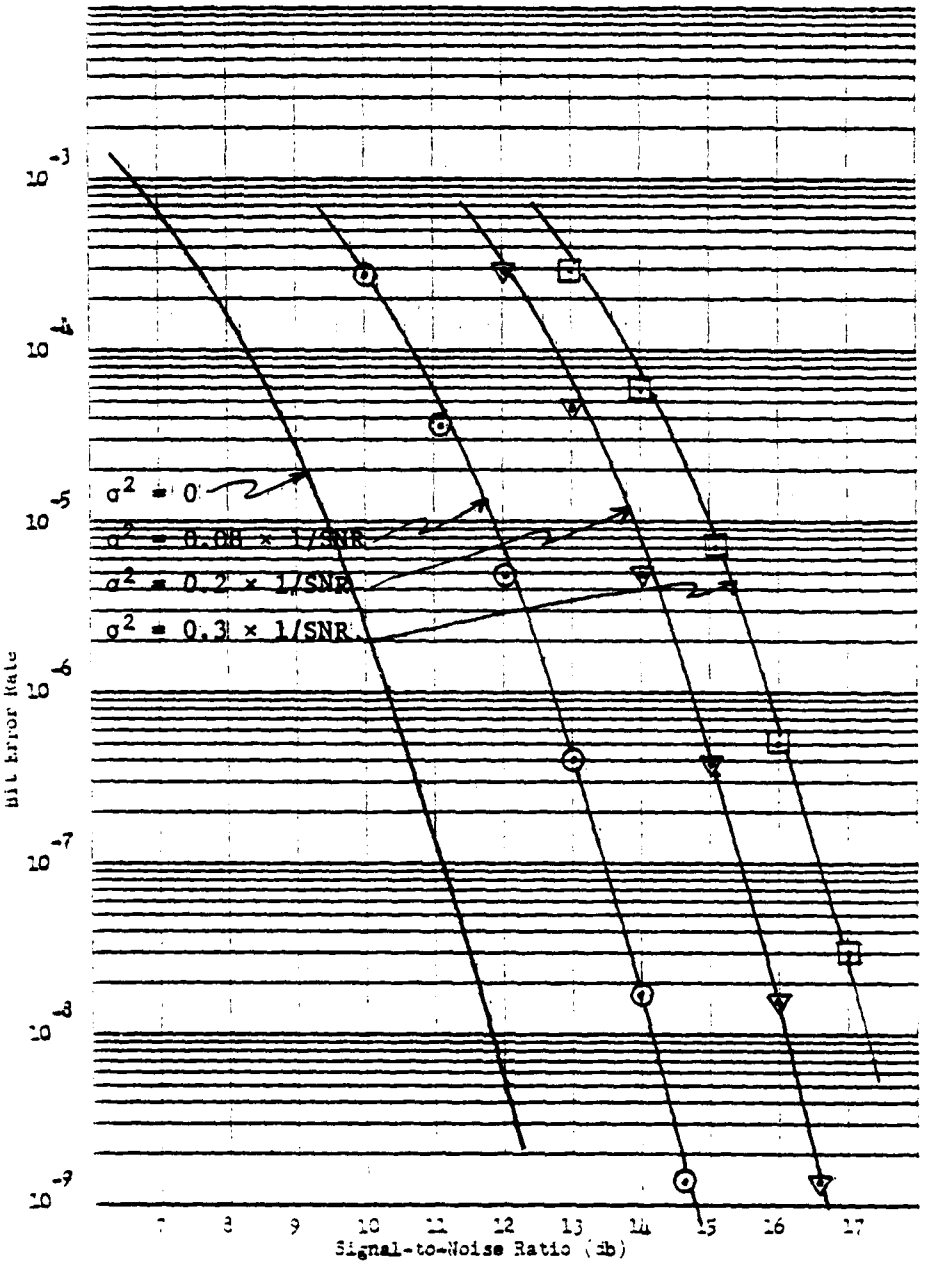

Fig. 5.2. Baud Timing Jitter, Zero Mean, Variance as Indicated.

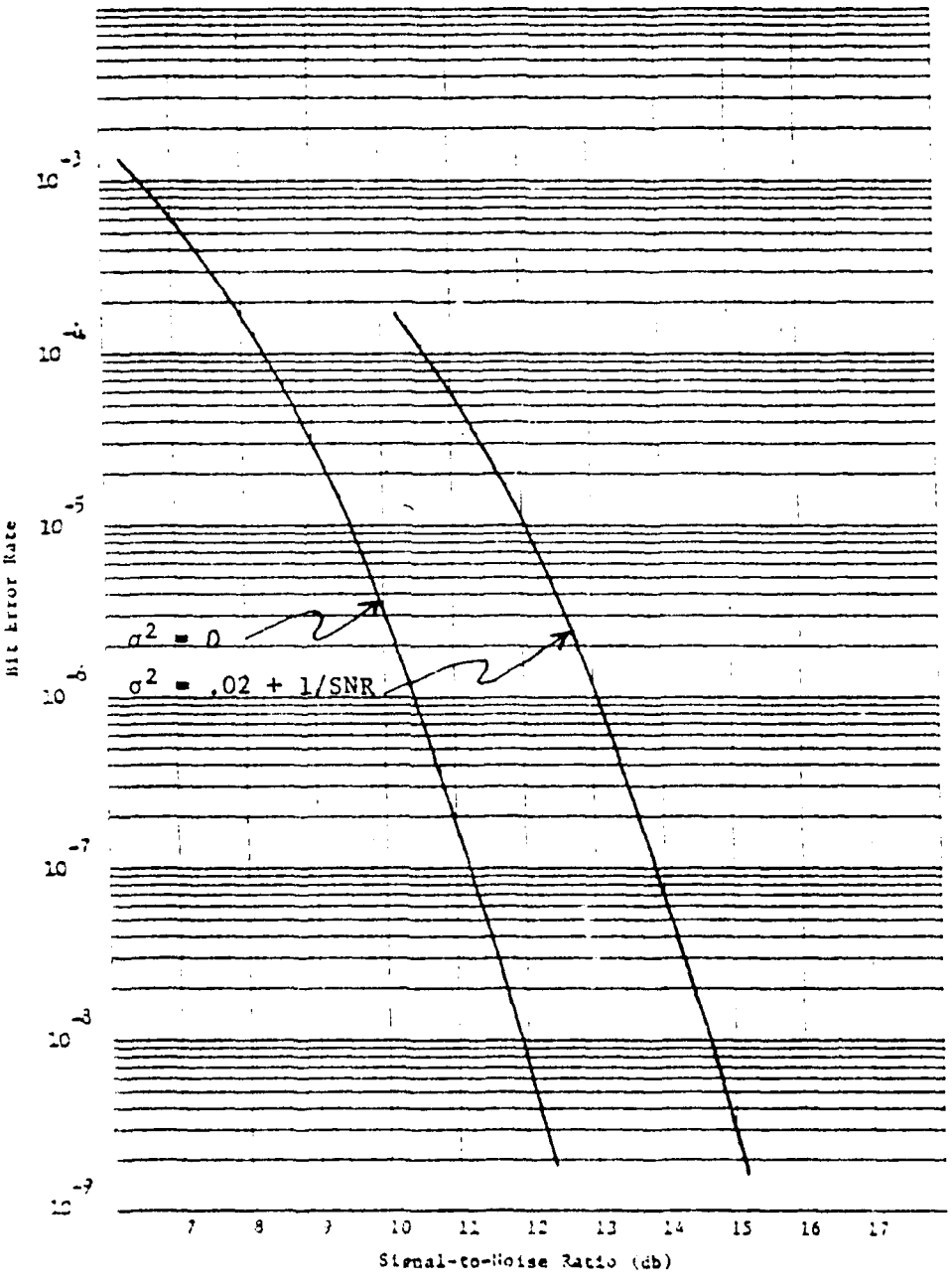

Fig. 5.3. Carrier Phase Jitter, Zero Mean, Constant Plus Functional Component of Variance.

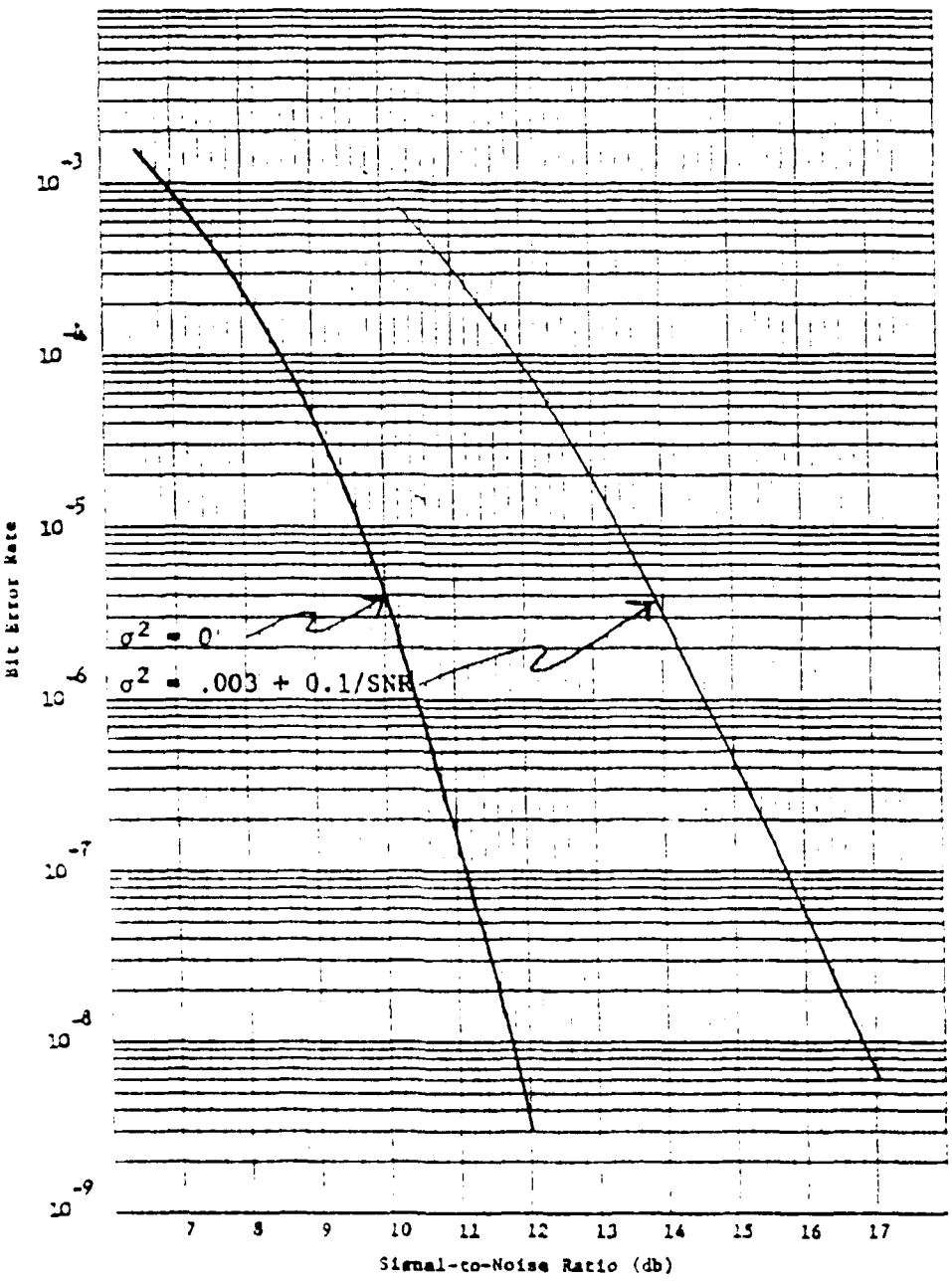

Fig. 5.4. Baud Timing Jitter, Zero Mean, Constant Plus Functional Component of Variance.

by sketching curves through the experimental data and examining their appearance relative to a theoretically shaped curve drawn through some convenient reference point. This "sight" comparison is of considerable value, but does not provide a quantitative measure of how valid the theoretical approximation is.

To provide a quantitative measure of "goodness of fit" of the experimental curves to the theoretical, a computer program was written to perform the following calculations. The experimental data point closest to a BER of 10^{-4} for each error curve was selected as reference. The signal-to-noise ratio necessary to produce this BER was then calculated from the theoretical expression for CPSK:

$$\operatorname{erfc}\left(\frac{2E}{N_o}\right)^{1/2} = 10^{-4} \tag{5.2}$$

(not precisely 10^{-4} in each case). Then using the RSL that experimentally produced this BER as the average signal energy E, an overall noise figure N_o for the receiver was determined. Using this noise figure as a constant for the receiver, an RSL was then calculated for each data point on the experimental curve using the theoretical expression. The theoretical values were then compared with the experimental RSLs that produced the data points.

In other words, the program mathematically drew a theoretical curve through the experimental data point nearest a BER of 10^{-4} for each experimental curve. Then for each data point on the experimental curve, the theoretical RSL (or signal-to-noise ratio) required to produce that BER was calculated and compared with the measured value. This provides

a quantitative measure of the deviation of the experimental curve from the theoretical at every level.

A second set of calculations was performed in a similar manner but using the experimental data point closest to 10^{-5} as a reference.

The complete results of the calculations are contained in Schooley and Davis (1979). A close check was made to insure that the graphical comparisons shown are consistent. The significant calculations are cited in the discussions of results for each item of equipment that follow.

TI-4000 Initial Tests

As was mentioned in Chapter 4 the initial curves obtained from the three models of the TI-4000 tested were very consistent. The data points were found to lie on or near smooth curves which were within one db of one another. The maximum deviations from the theoretical were between 0.9 and 1.1 db. This indicated that the receivers were reasonably well-aligned, although the fact that the alignment was not optimum, at least for model 11H009, became evident from the results of the discriminator variation tests.

The results of the baud timing experiments for the three models were again essentially the same. Figure 4.3, which shows the curves for PLL voltages of 8, 9, and 10, illustrates that for small variations the curves are shifted slightly laterally but retain their theoretical shape within one db. Recall that the variations in baud timing were obtained by offsetting the quiescent value of the VCO frequency of the

PLL. The theoretical result of this offset is to increase the mean value of the jitter without much effect on the variance. These experimental curves are then in complete agreement with the calculated results for small jitter variance and small increases of the mean.

On the other hand, the curves for PLL voltages of 4 and 3 volts in Fig. 4.4 show a larger displacement and a slight tilting outward. This would indicate that the VCO becomes slightly less stable for these adjustments. However, the maximum deviation from the theoretical shape was less than 2 db in the worst case and there was no flareout of the tails of the curves. It will be most significant to note that these results were very consistent with those of the additional T1-4000 tests that were performed when it was possible to measure the amount of jitter induced by the VCO variations.

Probably the most significant aspect of the discriminator response tests, which supported the technique of alignment while monitoring BER, was discussed in detail in Chapter 4. The results of the distortions of the discriminator linearity were to shift the BER curves (Figs. 4.8 and 4.9) with no additional deviations from the original shape. This is in complete agreement with the theoretical prediction that such non-linearities of frequency response cause a reduction in the effective signal-to-noise ratio but the noise itself remains Gaussian.

T1-4000: Additional Tests

The additional tests of the T1-4000 for baud timing jitter produced results very similar to the initial tests. The optimum PLL setting of approximately 4 volts resulted in the curve shown in Fig. 4.12, which has a maximum deviation from the theoretical shape of 0.4 db at a BER of 10^{-8}. The BER curves produced by the VCO offsets indicated by PLL voltages of 6 and 8 volts also in Fig. 4.12 were shifted approximately 0.7 and 1.5 db respectively from the optimum 4 volt setting with no additional deviation from the theoretical shape. The curves for voltage readings of 3, 2, and 1.5 volts were shifted approximately 0.6, 1.8, and 2.6 db respectively at a BER of 10^{-6} with some additional tilt. The 1.5 volt curve deviates approximately 1.4 db from the theoretical shape at 10^{-4}.

Measured Jitter

Table 4.1 contains measurements of the jitter mean and standard deviation that correspond to the various PLL voltage readings. The mean was found to remain essentially constant for different values of RSL while the standard deviation varies. This was consistent with the PLL theory previously discussed. The standard deviation was found to vary slightly for the VCO adjustments corresponding to 2 and 1.5 volts. Although this is not predicted by the theory, it is consistent with the effects on the BER curves which are shifted more and tend to tilt outward slightly. This correspondence will become more evident from the calculations that follow.

The standard deviation measurements certainly support the contention made earlier in this chapter that the jitter variance contains both a constant and a functional (varying) component. Some quick calculations using the standard deviation measurements corresponding to zero mean produce the approximate relationship for the variance:

$$\sigma^2 = .0026 + 0.1/SNR \qquad (5.3)$$

where a signal-to-noise ratio of 14 db is taken to correspond to an RSL of -71 dbm. The reason for assuming this correspondence will be shown by later calculations. The relationship for the other set of standard deviation measurements is approximately the same with a slight increase in the constant component. This would appear to be caused by the VCO becoming less stable for these adjustments.

BER Curves from Measured Jitter

Unfortunately, as was discussed in Chapter 3, there is no simple method for formulating the complete effects of baud timing jitter on the detection of a three-level partial response signal. Both methods discussed considered only constant timing offset and did not take into account the effects of jitter variance. However, to obtain some means of comparing theoretical and experimental results, the calculations of Smith (1973) were interpolated to determine the amount of relative shift of the BER curves that could be anticipated from the measured mean values. These results are shown in Figs. 5.5 and 5.6. The shifted curves were assumed to retain the shape of the zero mean curve.

Although this method does not account for the additional tilt of the curves resulting from the extreme variations, the amount of shift

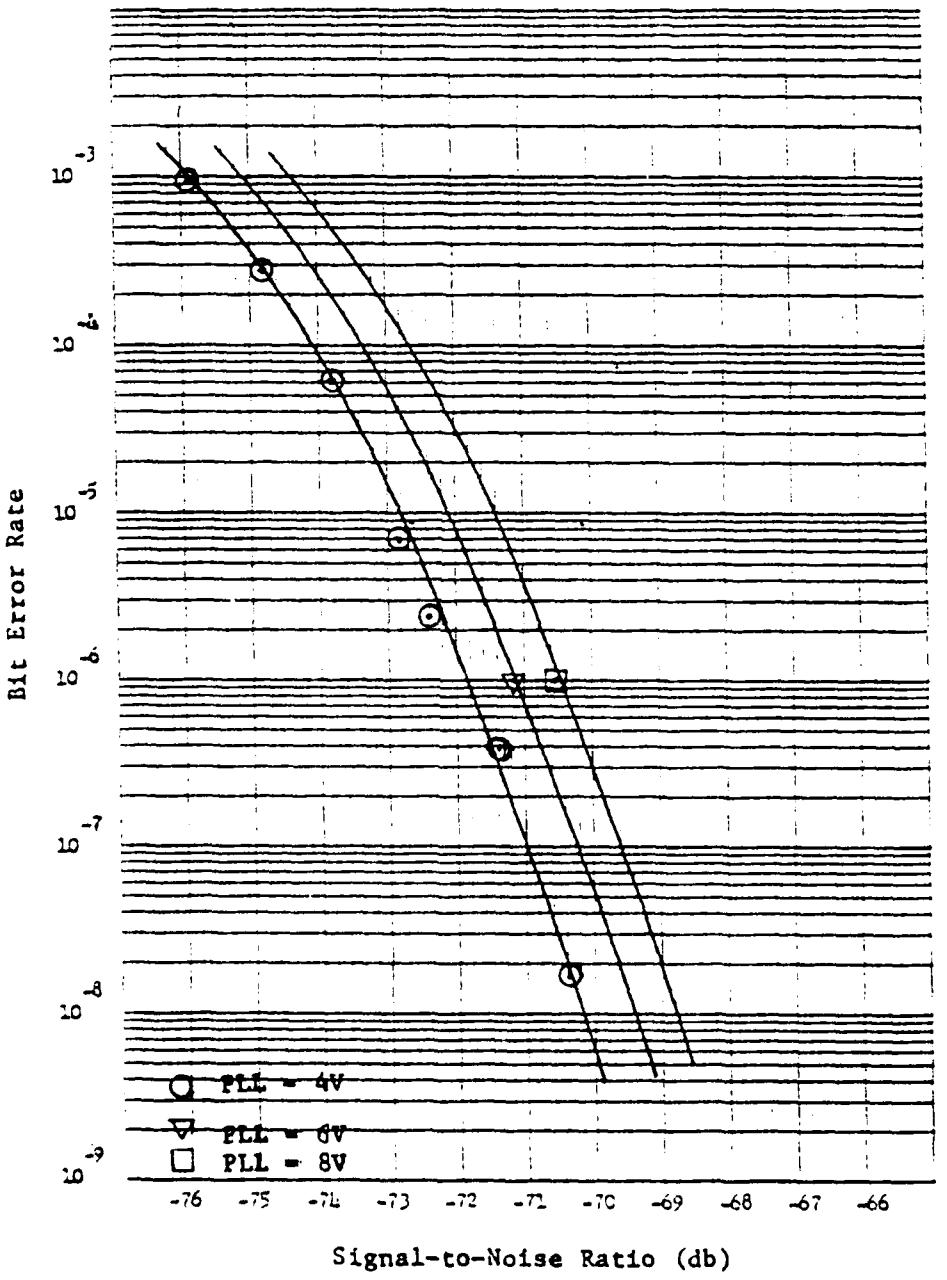

Fig. 5.5. Calculated BER vs. RSL, Smith's Method, Baud Timing Jitter, T1-4000.

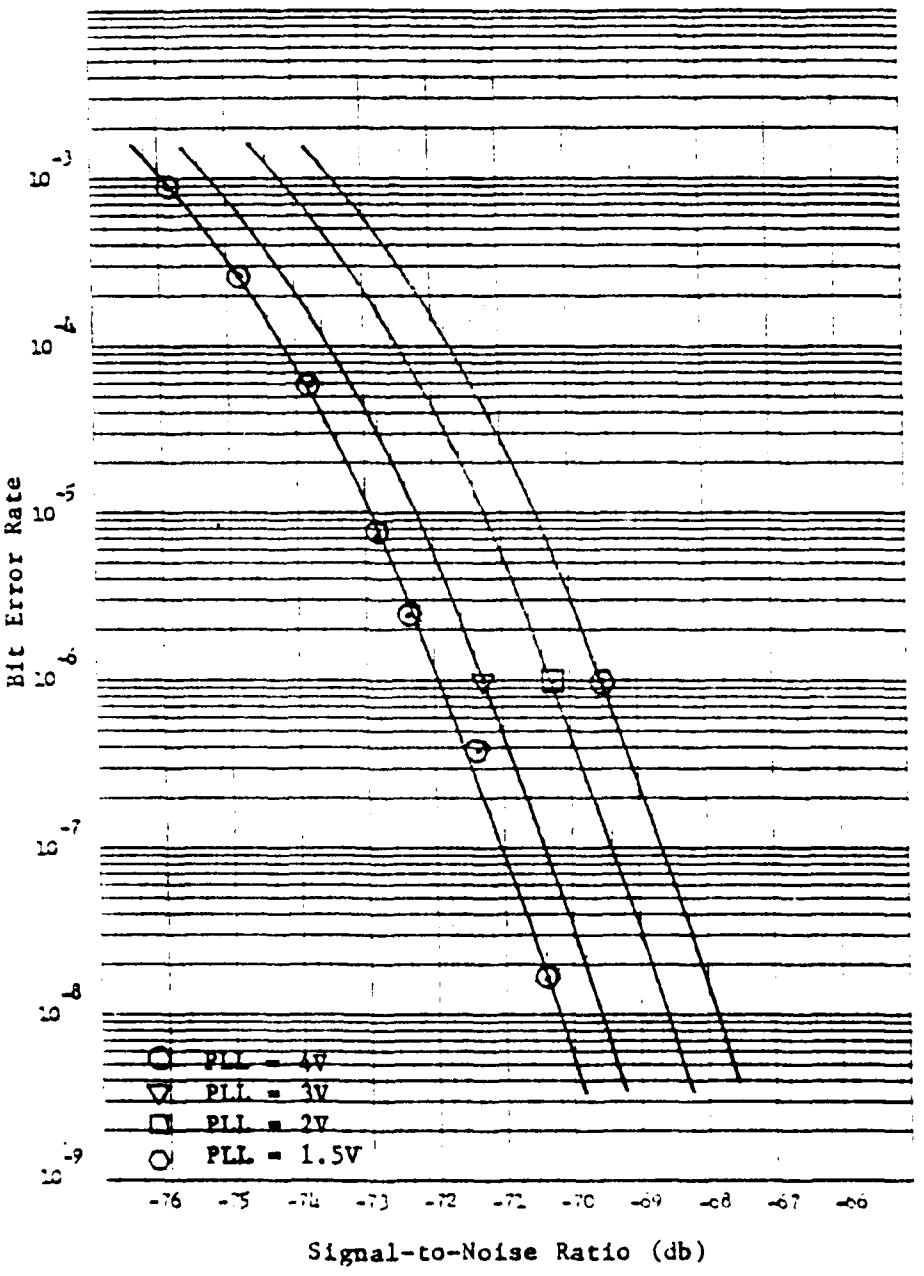

Fig. 5.6. Calculated BER vs. RSL, Smith's Method, Baud Timing Jitter (2), T1-4000.

is quite accurately predicted. This can be seen by comparing the calculated curves with the experimental results in Figs. 4.12 and 4.13. The amount of shift was calculated at the 10^{-6} point relative to the 4 volt curve where the jitter was assumed to have zero mean. The amount of shift calculated from Smith's predictions and from the cosine approximation in the following paragraphs are compared with the experimental results in Table 5.1.

In an attempt to further verify the experimental results and take into account the jitter variance, a cosine approximation was assumed for the effect of the timing error. With some physical, if not strictly mathematical justification, the conditional probability of bit error was assumed to be:

$$P_{b|\tau} = \operatorname{erfc}\left(\frac{KE}{N_o}\right)^{1/2} \cos(\pi\tau) \qquad (5.4)$$

where τ is assumed to be a Gaussian random variable with mean and standard deviation as given in Table 4.1. The constant factor K is necessary so that the curves of zero mean coincide in lateral position. It was in these calculations that the correspondence of 14 db signal-to-noise ratio to an RSL of -71 dbm was established.

The results of integrating this conditional expression over the Gaussian density function with the measured values of mean and standard deviation are shown in Figs. 5.7 and 5.8. The calculated curve for the zero mean essentially superimposes the experimental result with an almost identical shape. The calculated curves corresponding to 6 and 8 volts in Fig. 5.7 are also almost identical to their experimental counterparts, being shifted 0.5 and 1.3 db respectively at 10^{-6} with no additional tilt. The calculated results for 2 and 1.5 volts vary

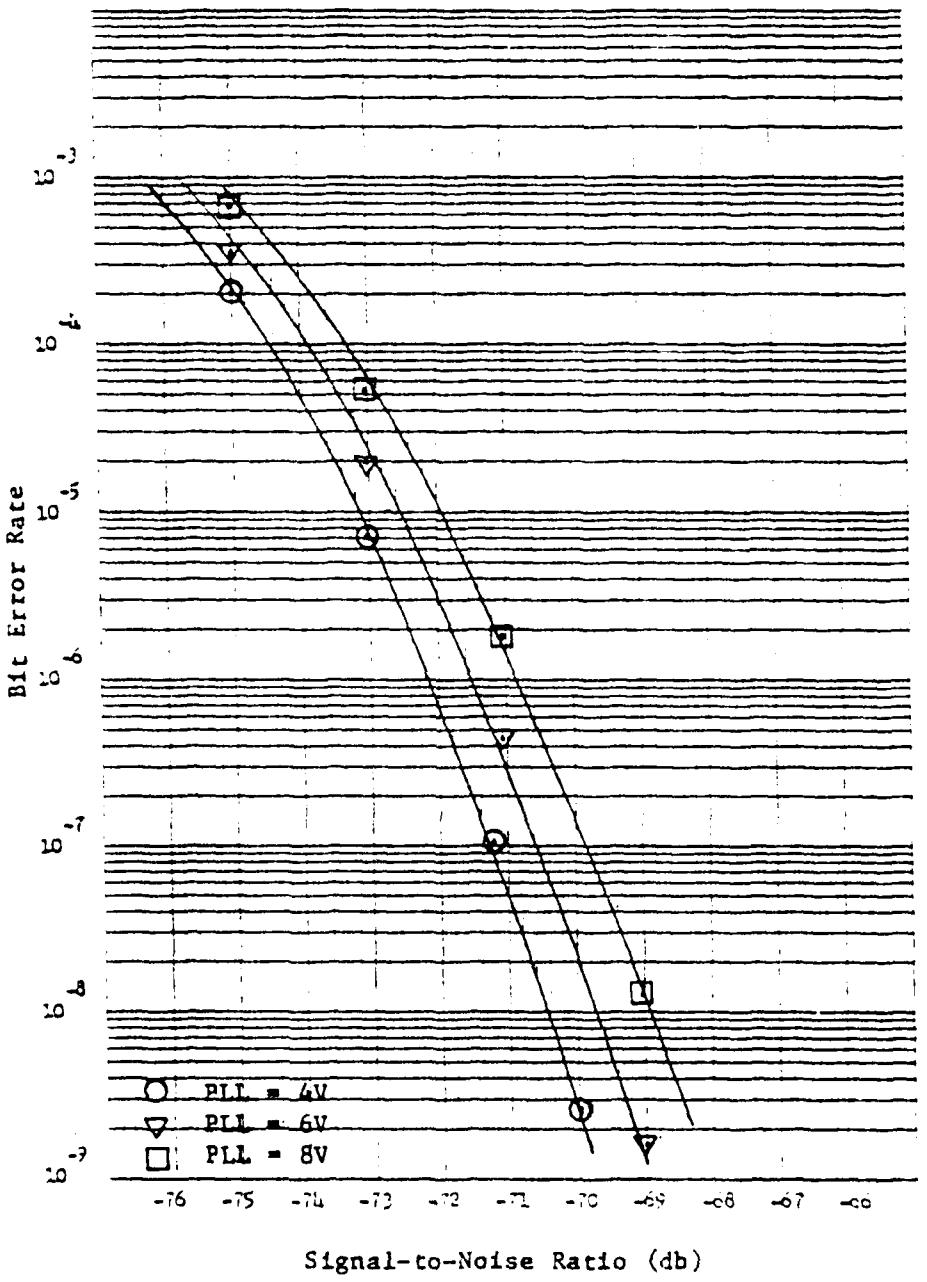

Fig. 5.7. Calculated BER vs. RSL, Cosine Approximation, Baud Timing Jitter, T1-4000.

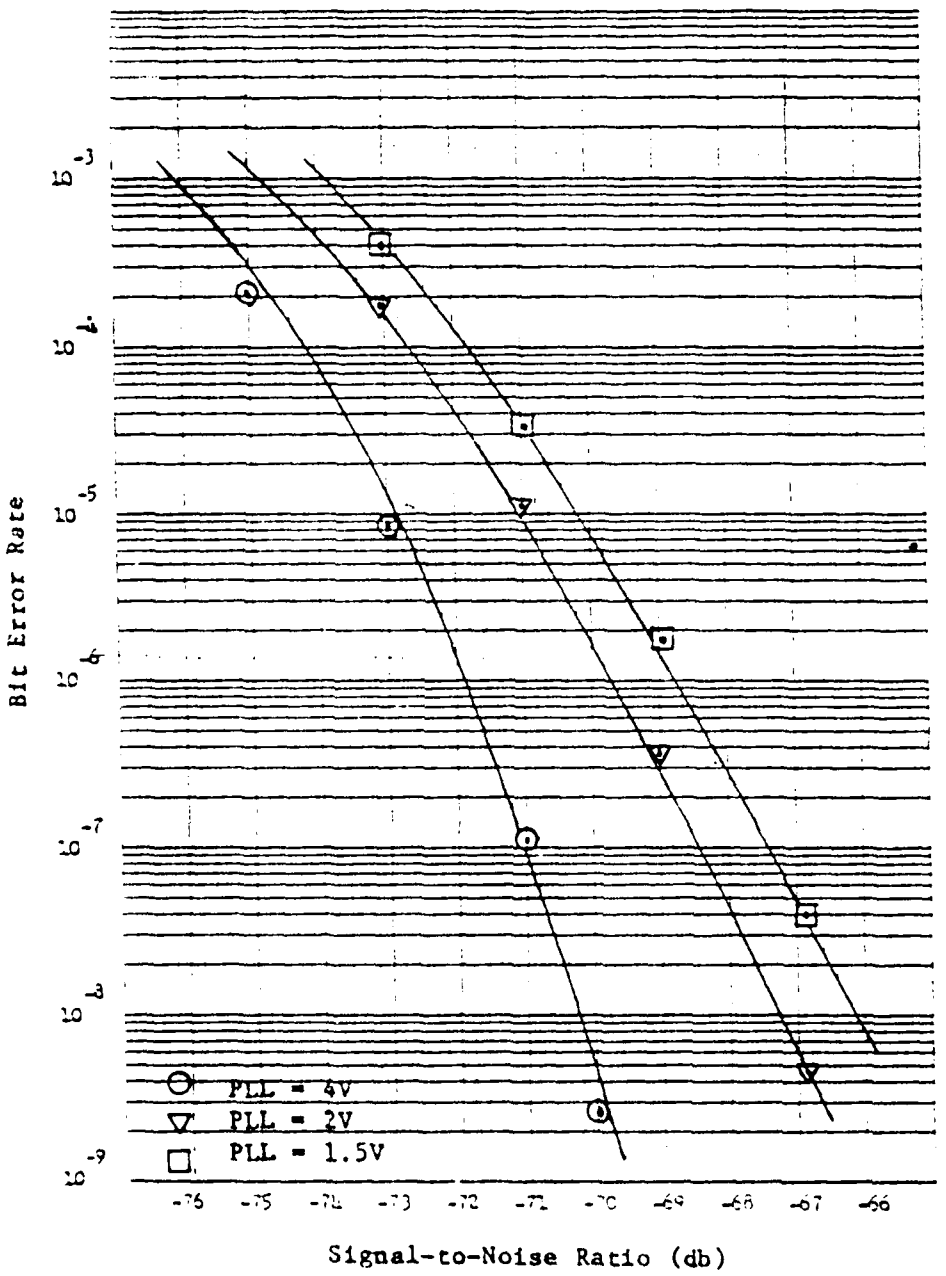

Fig. 5.8. Calculated BER vs. RSL, Cosine Approximation, 3aud Timing Jitter (2), T1-4000.

slightly from the experimental curves, the shifts at 10^{-6} BER being 2.1 and 3 db respectively instead of 1.9 and 2.7 db. The outward tilt of both curves is essentially the same as was found experimentally.

Table 5.1 summarizes the above results by showing the amounts of shift in db at the 10^{-6} BER point which were found experimentally and which were calculated by both methods.

Combined Effects

Combined effects were observed by simultaneously distorting the discriminator response while offsetting the quiescent frequency of the VCO. This resulted in much larger shifts of the BER curves with no additional deviation from the theoretical shape as is shown in Fig. 4.16. The significance of this result is to illustrate that, as long as no single error cause becomes predominant, the central limit theorem will govern and the effects become more nearly Gaussian. The curves therefore retain their characteristic error function shape.

Lenkurt 261A—26C Tests

As can be seen from the example curve of Fig. 4.18, the BER curves for the 261As tested, which were almost identical, adhered very closely to the theoretical shape. The maximum deviation of the three models was 0.6 db at a BER of 10^{-5}. The curve for the 26C (Fig. 4.19) was shifted approximately 2.5 db laterally from those of the 261As and yet the maximum deviation was the same 0.6 db. The large shift with no increased tilt could be attributed to a number of different factors. Although the electrical design of the two sets are supposedly the same,

Table 5.1. Shift in db at 10^{-6} BER.

	PLL Voltage					
	1.5	2	3	4	6	8
Experimental	2.7	1.9	0.6	0	0.6	1.3
Smith's Method	2.4	1.7	0.6	0	0.6	1.2
Cosine Approximation	3.0	2.1	0.5	0	0.5	1.3

there could be a difference in the channel filtering which would result in a decreased signal-to-noise ratio in the 26C. If not due to filter response the effect is probably from a combination of several factors. In general, such large shifts without distortion would not be the result of a single anomaly such as baud timing.

The additional baud timing jitter that was induced by timing the transmitter and receiver from separate sources resulted in a lateral shift of the BER curve of approximately one db without any significant additional deviation from the theoretical shape as is shown in Fig. 4.20. Both timing sources appeared quite stable and were measured to be precisely 2400 Hz. However, each reading of the frequency meter averages the frequency over a fairly large (selected) number of cycles. Variations from cycle to cycle will not appear in the measurement but will provide an increased variance to the baud timing jitter. Although there was no method available at the time to verify this through measurements, the shift of the BER curve is attributed to this increase in baud timing jitter.

MW-518 Tests

Little additional comment can be made in analysis of the MW-518 tests. The two curves (Fig. 4.21) were consistent with other results and matched the theoretical almost exactly (coherent detection of a differentially encoded signal; see Fig. 3.5).

The two separate curves were obtained by the carrier recovery circuit locking onto different phases of the reference signal. The shift of approximately 1/2 db between the two curves is attributed to an increase in carrier phase jitter caused by the resolution of this ambiguity in the detection process.

RDS-80 Tests

The initial BER curve taken for the RDS-80 as shown in Fig. 4.24 had a maximum deviation from the theoretical shape of 0.9 db at a BER of 4×10^{-9}. This performance was the best produced during the tests indicating that the set was well aligned at least so far as the phase and timing adjustments used to simulate jitter were concerned.

As was described in Chapter 4, carrier phase jitter was simulated by offsetting the phase of the recovered carrier prior to the QPSK demodulation. The amount of shift of the BER curves that occurred will be discussed in detail in comparison with calculated results in the section that follows. It is readily seen from Figs. 4.25 and 4.26 that small offsets shifted the curves slightly with very little additional deviation from the theoretical shape, whereas with larger shifts the curves began to tilt outward. The maximum additional

deviation from the initial curve was approximately 1.1 db. These results are in close agreement with the theoretical predictions for the effects of phase offset.

Baud timing jitter was simulated in a similar manner by offsetting the phase of the timing signal used for data regeneration. Again small variations caused very little additional deviation from the theoretical shape while a slight tilting occurred with the larger offsets as is shown in Figs. 4.27 and 4.28. The maximum additional deviation from the initial curve was 1.1 db at a BER of 10^{-8}. The amount of shifting of the curves will be compared with calculated results in a later section.

Carrier Phase Jitter

In the RDS-80 system, carrier phase jitter was simulated by offsetting the phase of the recovered carrier used for QPSK demodulation. This was accomplished by varying an inductor at the output of the carrier recovery circuit. Figure 5.9a is a simplified circuit diagram of the carrier recovery output showing the phase adjustment and quadrature hybrid. The total circuit operation is described in detail in Schooley and Davis (1978). Inductor L-24 was the component adjusted to provide the phase offset.

Because of the physical configuration of the equipment it was not practical to measure the amount of phase offset induced by the variation of the inductor during the conduct of the tests. The ideal procedure for off line measurement with the effected module removed

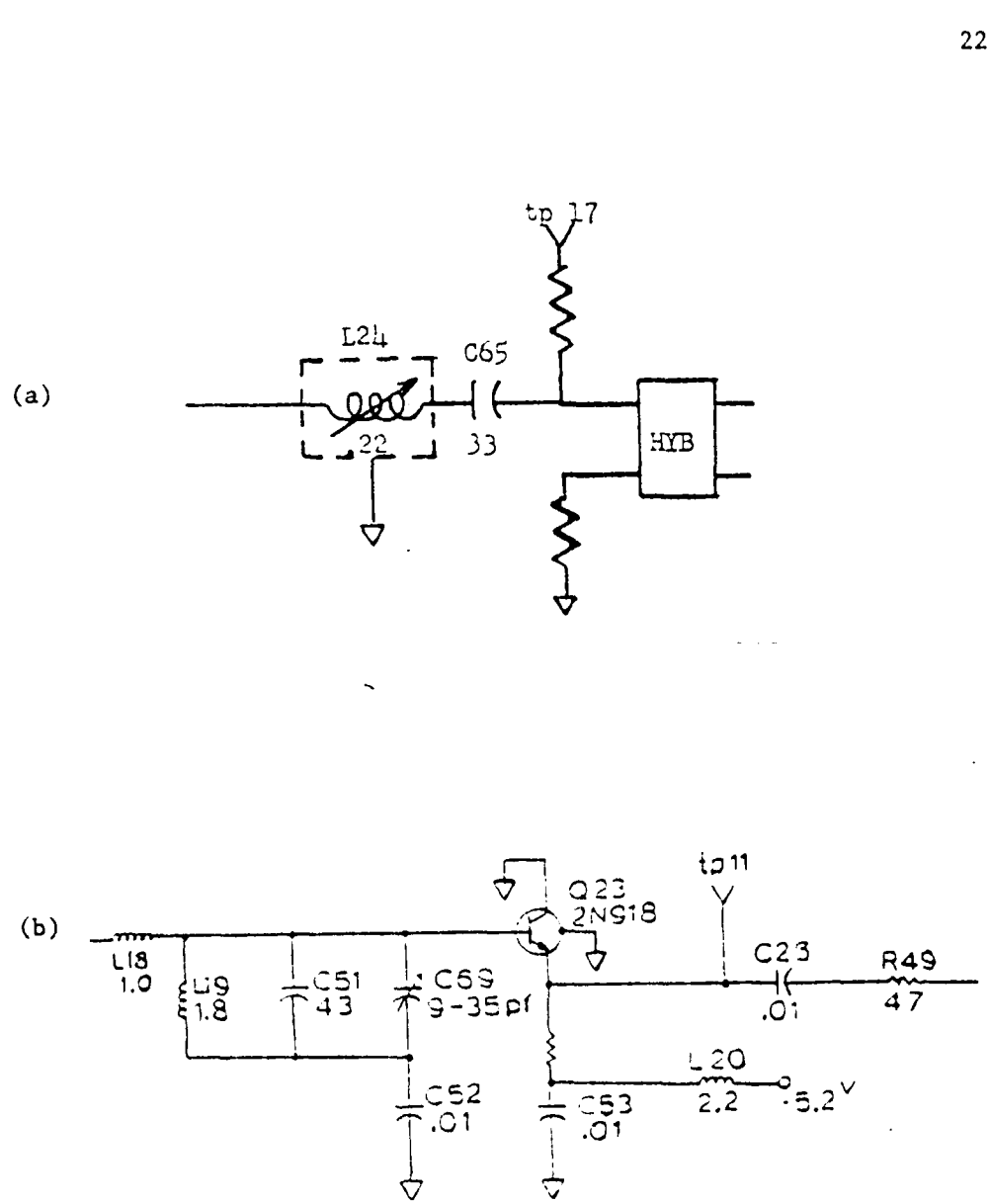

Fig. 5.9. RDS-80 Circuits.

(a) Recovered Carrier Phase Adjustment.
(b) Baud Timing Phase Adjustment.

from the receiver would have been to inject a 70 MHz signal at an appropriate point and directly measure the phase offset. Here again the efforts were thwarted, this time by a lack of instrumentation suitable for operation at 70 MHz.

As a substitute procedure, it was decided to remove the inductor from the circuit and to measure its inductance with various core adjustments. The circuit was then analyzed to determine the amount of phase shift caused by the variations of the inductance.

Since the core adjustments resulted in small variations of a very small inductance (0.16 to 0.21 microhenries) it was not possible with available instrumentation (impedance bridges) to perform the measurements directly. The inductor was first shunted with a suitable capacitor (255 pf) and a VHF signal generator and oscilloscope were used to determine the resonant frequency of the parallel combination. The inductance values were then calculated.

The circuit analysis presented other difficulties. No information was available on the input impedance to the hybrid and again no method was available for measuring this at 70 MHz. At this high frequency the wiring and other stray impedences have considerable effect, and measurements at lower frequencies do not present a true picture. However, since in this instance the primary interest is in relative effects, certain simplifying assumptions were possible.

First the inductor and capacitor in series (L-24 and C-65), if operating into a resistive load, will have a transfer function:

$$T(j\omega) = \frac{R}{R + j\omega L + \frac{1}{j\omega c}} = \frac{j\omega RC}{(1 - \omega^2 LC) + j\omega RC} \qquad (5.5)$$

The phase shift will then be:

$$\theta = \frac{\pi}{2} - \arctan\left[\frac{\omega RC}{1 - \omega^2 LC}\right] \quad . \qquad (5.6)$$

The stray capacitances of the circuit and the input reactance of the hybrid will definitely affect the absolute value of the phase shift, however, the relative phase adjustment will be primarily governed by the predominant pair of poles formed by the series capacitor and inductor as described above.

It seems reasonable to assume that the circuit was properly designed so that zero phase offset occurs at the center frequency of the transfer function of Eq. (5.5). The value of inductance that produced minimum BER was found to be 0.1723 microhenries. If the total series capacitance is assumed to be 30 pf (within 10% of the 33 pf value of C-65) then the resonance occurs at 70 MHz. Note that this assumption is convenient but that the same relative results would be obtained so long as the variations occur within the relatively linear portion of the transfer function phase response.

The second assumption is based upon the fact that, when the inductor L-24 was adjusted two full turns clockwise (corresponding to approximately 0.202 microhenries) irreducible errors were very evident. The BER remained approximately 10^{-3} to 10^{-4} even with signal levels as high as -30 dbm. This was assumed to be at the edge of the passband

(3 db point) of the transfer function where the phase shift was 45° from that of the center frequency. This is the point at which:

$$1 - \omega^2 LC = \omega RC \ . \tag{5.7}$$

This value for ωRC was calculated and then used to determine the relative phase shift for the other measured values of the variable inductor using Eq. (5.6). The complete details of the above calculations are contained in Schooley and Davis (1979).

These results were then used with the theoretical expression derived in Chapter 2 to compare theoretical predictions with the experimental results. The experimental curves of BER versus coil position for constant values of RSL shown in Fig. 4.29 were redrawn using the calculated values of relative phase as an abcissa. The zero phase values of BER for each curve were used to establish a reference value of $\left(\frac{E}{N_o}\right)^{1/2}$. The expression:

$$\text{BER} = \text{erfc}\left(\frac{E}{N_o}\right)^{1/2} \cos\theta \tag{5.8}$$

was then used to determine theoretical curves for comparison. Since the phase was offset directly, the value of θ was a constant for each calculation rather than a random variable. The effects of the true phase jitter are inherent in the calculated value of $\left(\frac{E}{N_o}\right)^{1/2}$.

The results of the above calculations and the experimental curves are shown in Figs. 5.10, 5.11, and 5.12. The results are quite consistent. The differences between the measured and calculated values can be attributed to a number of factors, not the least of which are

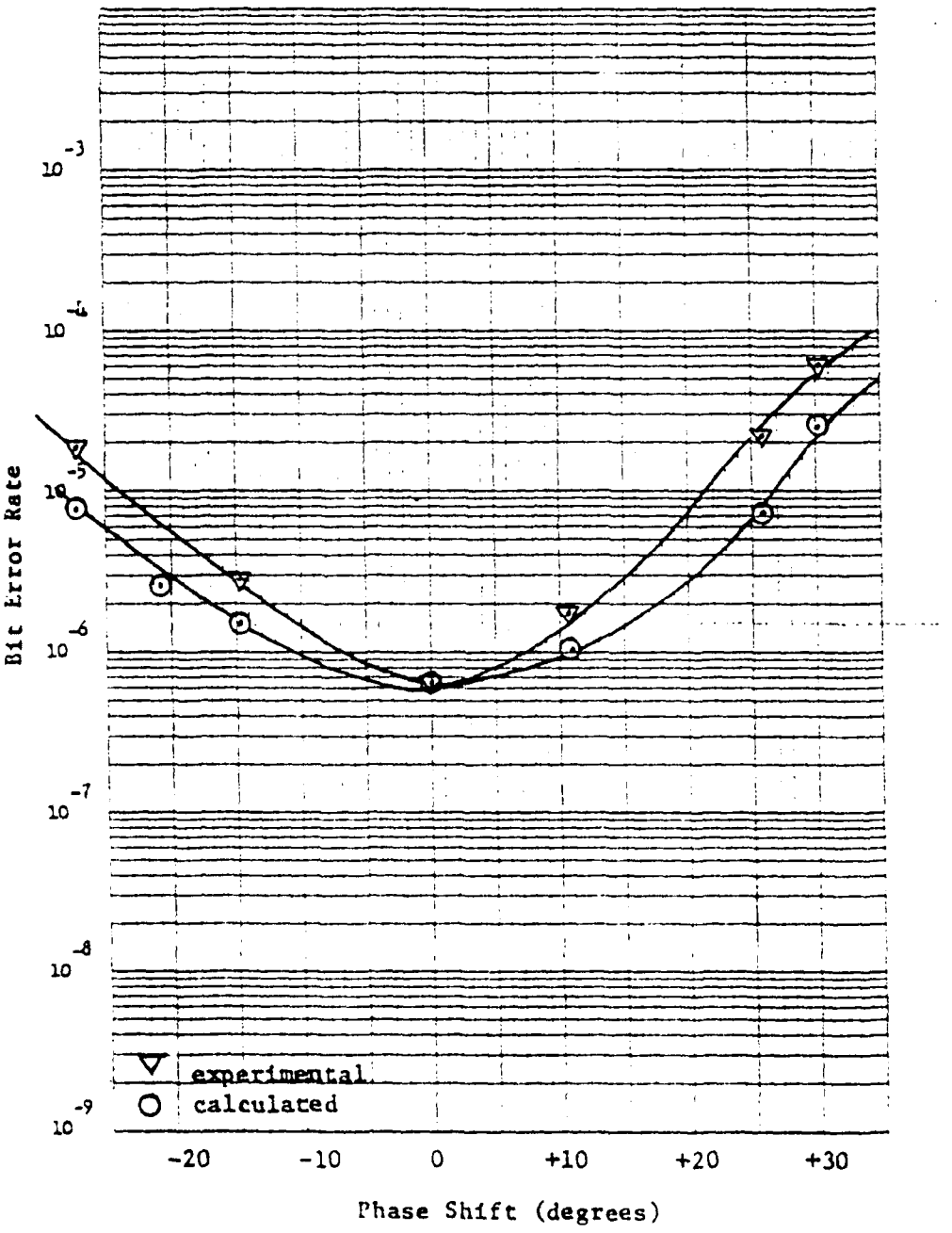

Fig. 5.10. BER vs. Carrier Phase Offset, RDS-80, RSL = -77 dbm.

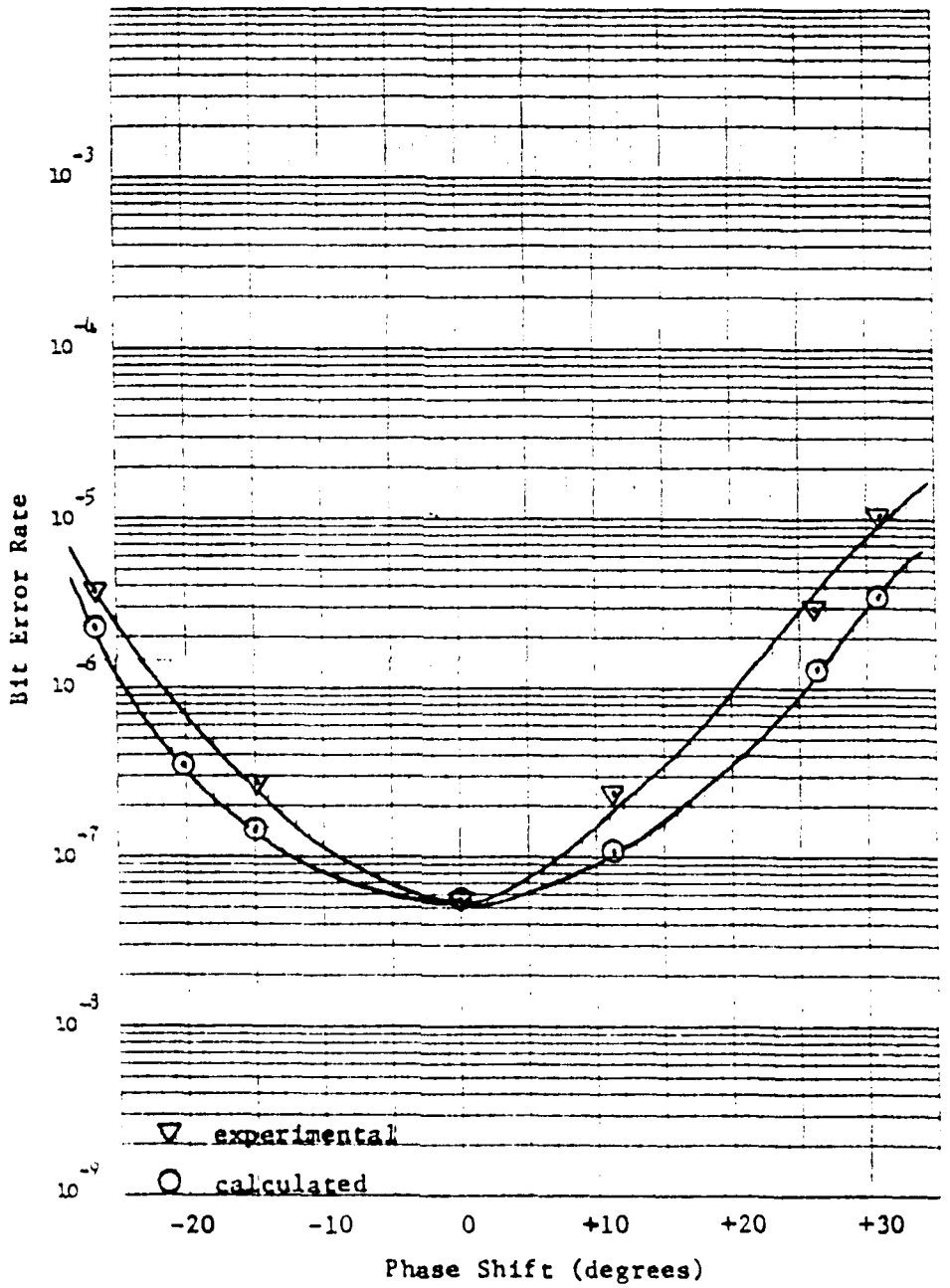

Fig. 5.11. BER vs. Carrier Phase Offset, RDS-80, RSL = -76 dbm.

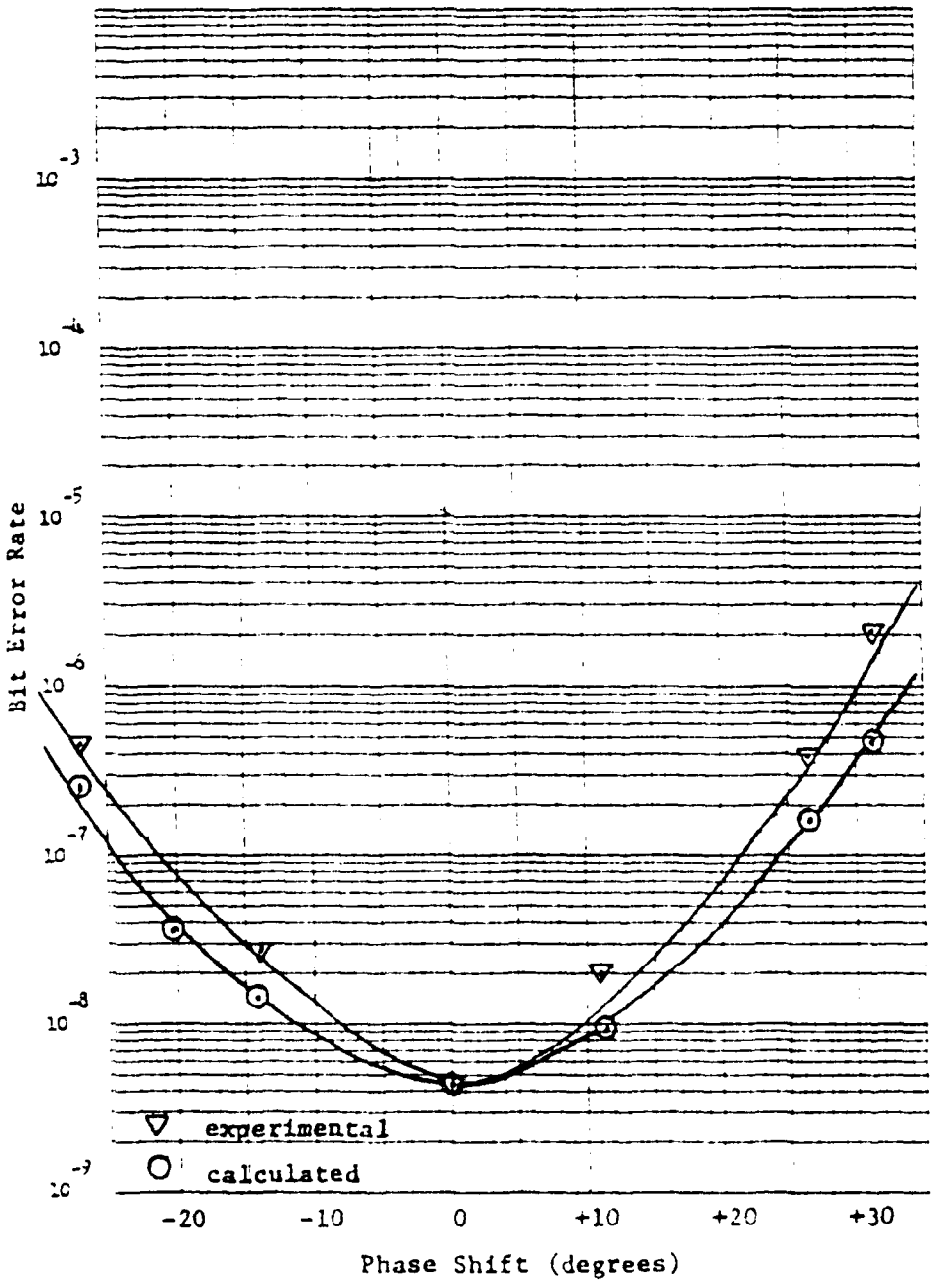

Fig. 5.12. BER vs. Carrier Phase Offset, RDS-80, RSL = -75 dbm.

the assumptions made in the calculations. In this regard, the assumption that the minimum error probability occurs at the center frequency of the timing circuit, is probably a very good one, and as was mentioned, small deviations would have little effect on the calculated results. On the other hand, the assumption that the extreme variation occurs at the 3 db point may or may not be valid. If the assumption were made that the extreme occurred at the 6 db point the phase variations would be greater and the calculated values would curve more sharply upward. The reverse would occur for smaller phase variations. In any case the relative effects are illustrated. It must also be pointed out that the phase offset will also contribute to the effects of other error causes such as intersymbol interference.

To further illustrate the comparison between theoretical calculations and experimental results, the experimental curves for 13.88°, and 26.57° phase offset corresponding to 1/2, and 2 turns counterclockwise were redrawn. These curves are shown in Figs. 5.13 and 5.14 in comparison to calculated curves determined using Eq.(5.8). The shapes of the curves are quite consistent and the differences in the magnitude of the shifts become less significant with the larger phase error.

Baud Timing Jitter

In a manner very similar to that described above, baud timing jitter was simulated in the RDS-80 by offsetting the 20 MHz timing signal in the data regeneration module of the receiver. This was accomplished by the adjustment of a trimming capacitor, C-69, in the

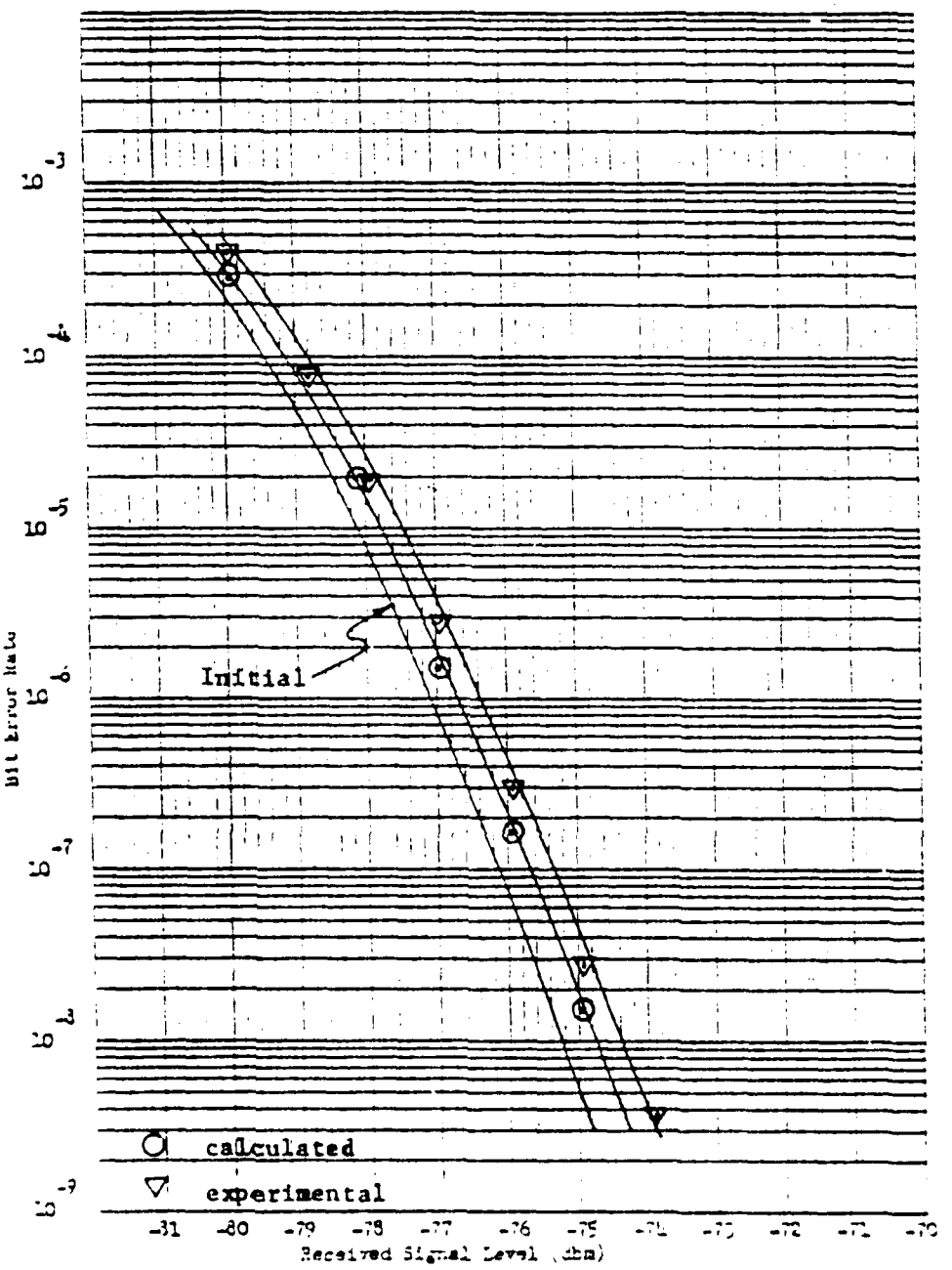

Fig. 5.13. BER vs. RSL, RDS-80, 13.88° Carrier Phase Offset.

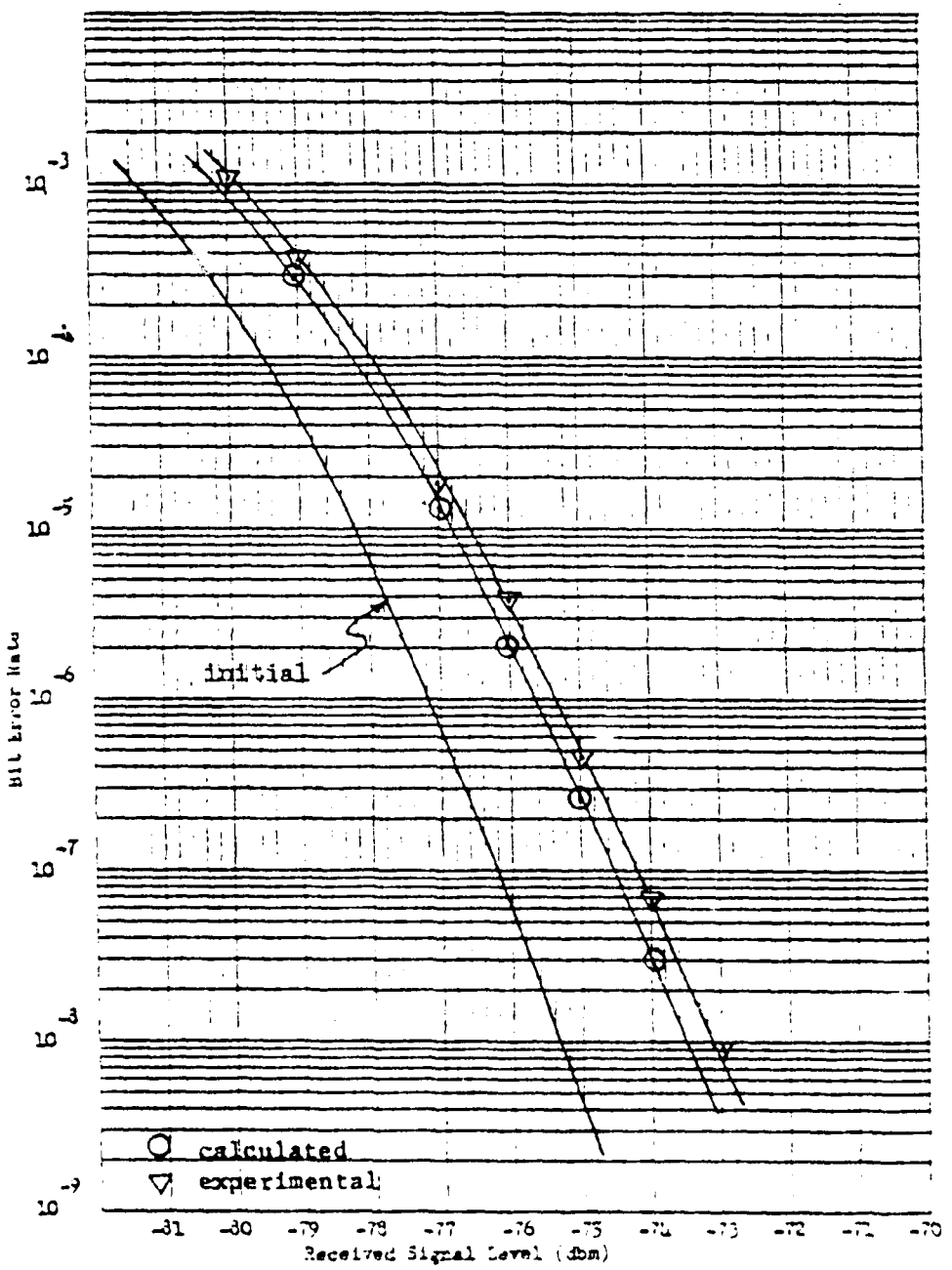

Fig. 5.14. BER vs. RSL, RDS-30, 26.57° Carrier Phase Offset.

output of the phase locked loop as shown in Fig. 5.15b. A detailed description of the operation of the timing circuit is contained in Schooley and Davis (1978).

Again it was not practicable to make measurements of the phase offset during the testing nor to make measurements of the module at 20 MHz. The same procedure as described above for carrier phase offset was followed. C-69 was removed from the circuit and the capacitance was measured directly with an impedance bridge for various settings of the trimmer adjustment. The circuit was then analyzed making assumptions similar to those described in the previous section.

If the phase adjustment part of the circuit is assumed to be working into a resistance R, and the total capacitive effect is C_T (predominantly C-51 and C-69 in parallel) the transfer function can be determined as:

$$T = \frac{L_{19}}{[(L_{18} + L_{19}) - \omega^2 L_{18}L_{19}C_T] + j\,\frac{\omega L_{18}L_{19}}{R}} \qquad (5.9)$$

and the resulting phase shift will be:

$$\theta = -\arctan \frac{\frac{\omega L_{18}L_{19}}{R}}{(L_{18} + L_{19} - \omega^2 L_{18}L_{19}C_T} \qquad (5.10)$$

Allowing 7 pf for wiring capacitance during measurements the value of C-69 that produced minimum error was 62.5 pf. Then with C-51 = 43 pf:

$$C_T = 62.5 - 9 + 43 = 98.5$$

the center frequency of the transfer function occurs at 20 MHz; i.e.:

$$(L_{18} + L_{19}) = \omega^2 L_{18} L_{19} C_T \quad . \tag{5.11}$$

It was observed during the experiments that the data errors became irreducible when the trimmer was adjusted 7/16 of a turn clockwise, corresponding to approximately 20 pf. This point was then assumed to be at the edge of the passband as was done previously and a constant value for $\frac{\omega L_{18} L_{19}}{R}$ was established. This value was then used to calculate the relative phase shifts for the various other settings of C-69. The complete results of these calculations are contained in Schooley and Davis (1979).

The results were then used to compare theoretical predictions with the experimental results. The experimental curves of BER versus capacitor position for constant values of RSL shown in Fig. 4.30 were redrawn using the calculated values of relative timing offset $\tau = \theta/360°$ as the abcissa. The zero phase values of BER for each curve were used to establish a reference value of $\left(\frac{E}{N_o}\right)^{1/2}$. The expression:

$$\text{BER} = \frac{1}{2} \operatorname{erfc}\left(\frac{E}{N_o}\right)^{1/2} + \frac{1}{2} \operatorname{erfc}\left[\left(\frac{E}{N_o}\right)^{1/2} \left(1 - \frac{2|\tau|}{T}\right)\right] \tag{5.12}$$

was then used to determine theoretical curves for comparison. Again since the phase was offset directly, the value of τ was a constant for each calculation rather than a random variable and the effects of the actual phase jitter are contained in the calculated value of $\left(\frac{E}{N_o}\right)^{1/2}$. Results are shown in Figs. 5.15, 5.16, and 5.17.

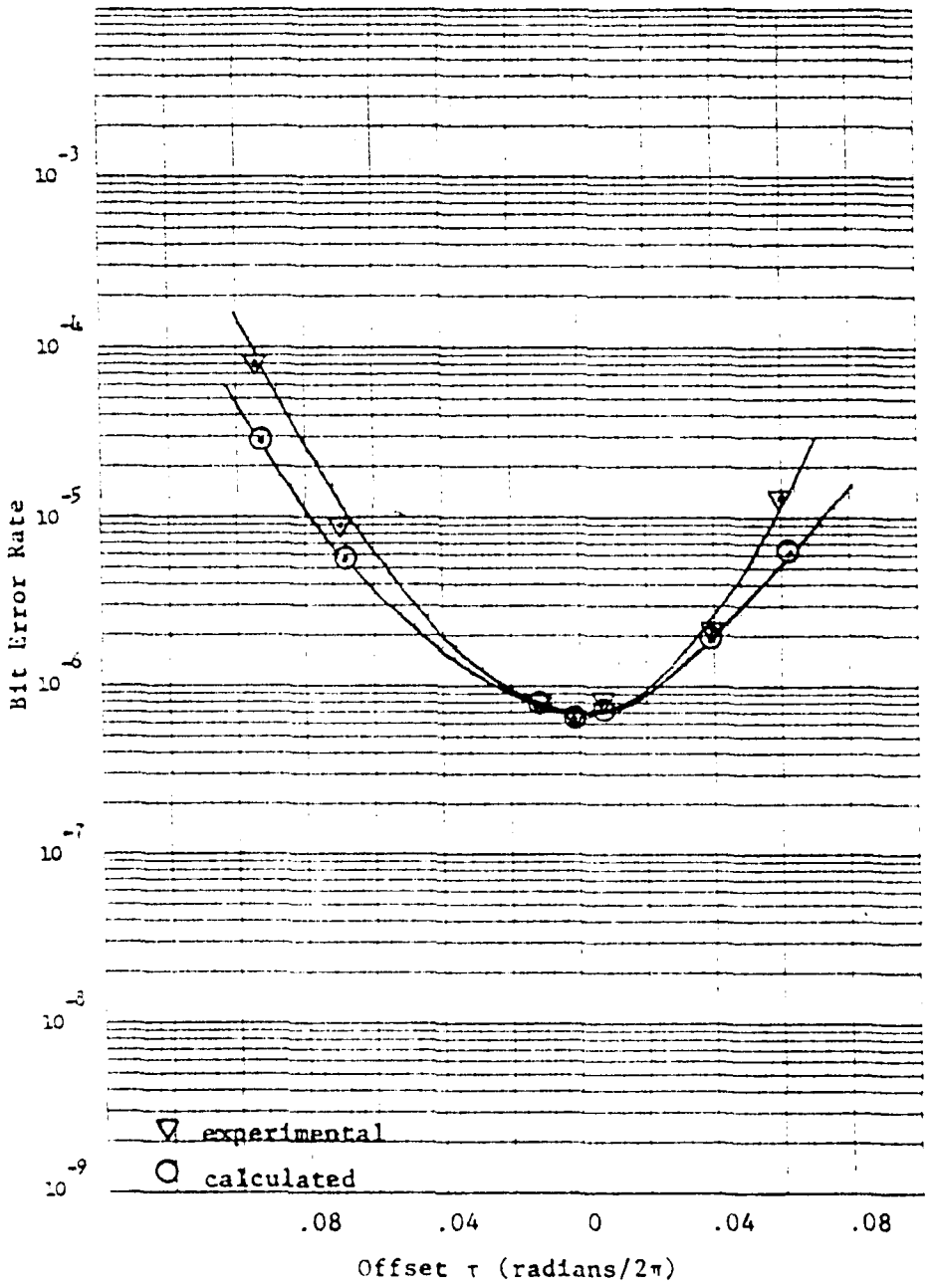

Fig. 5.15. BER vs. Baud Timing Offset, RSL = -77 dbm.

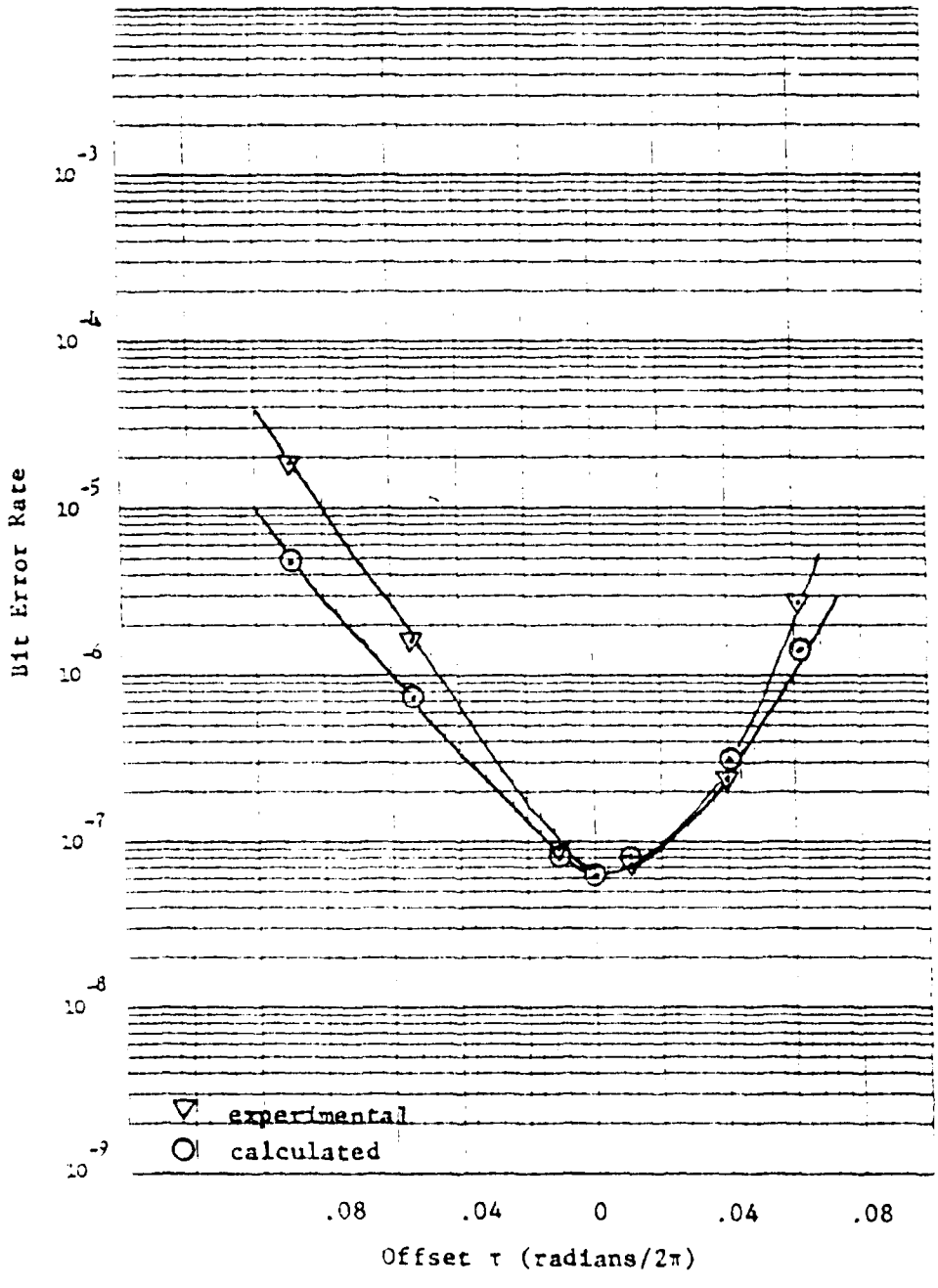

Fig. 5.16. BER vs. Baud Timing Offset, RSL = -76 dbm.

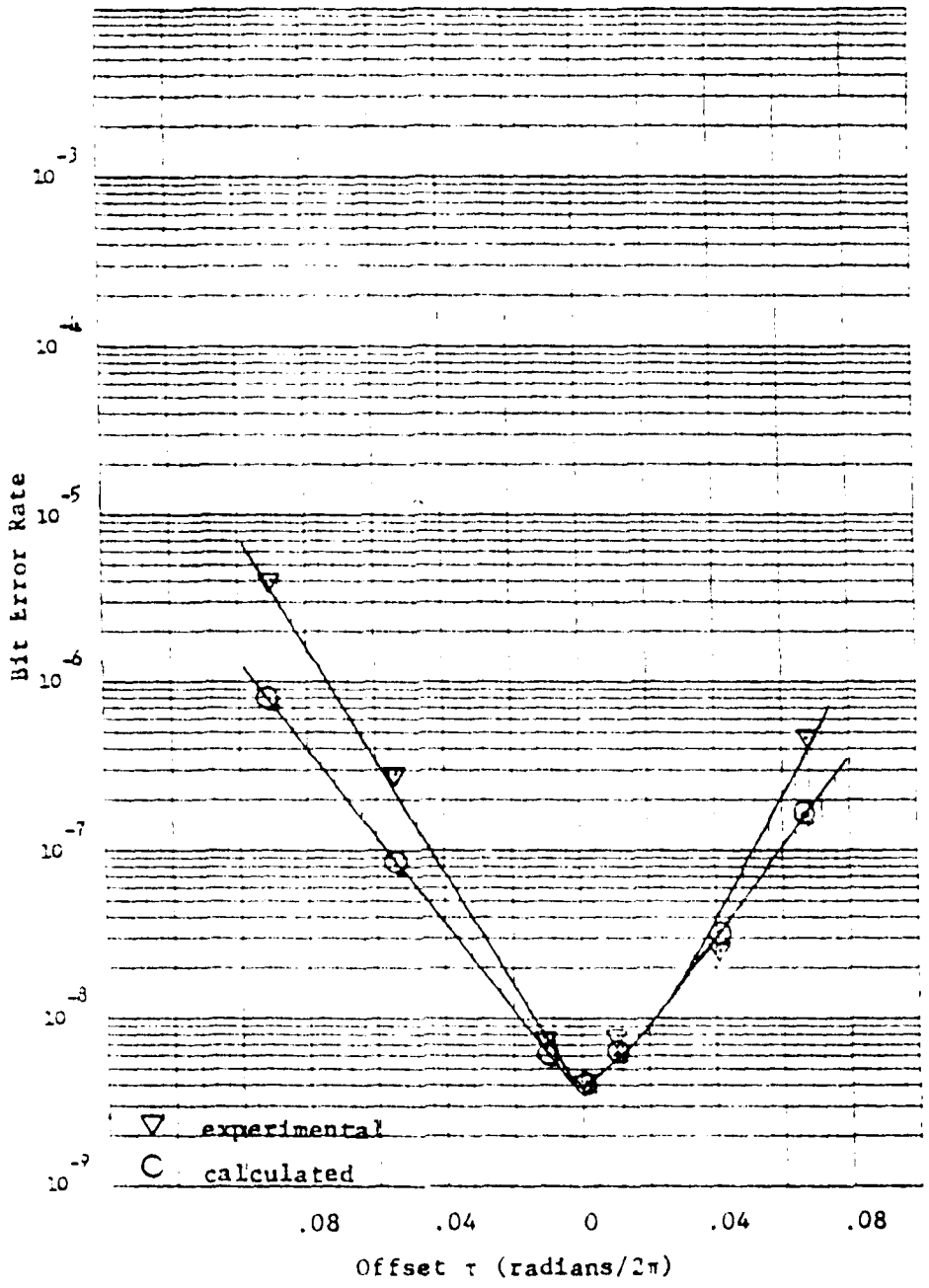

Fig. 5.17. BER vs. Baud Timing Offset, RSL = -75 dbm.

The results are reasonably consistent. The variations may be contributed to a variety of causes including the assumptions made during the calculations. The same comments apply to the assumptions as were made in the previous paragraph. At least the relative effects are illustrated.

As was done for carrier phase offset, BER versus RSL curves were calculated for baud timing offset and compared with the corresponding experimental results. These are contained in Figs. 5.18 and 5.19. The shapes of the curves are again comparable although there are slightly larger variations in the amount of offset. Because of the assumptions that were necessary and the fact that the phase offset does contribute to the effects of other error causes, it would be quite surprising if the results matched perfectly.

Summary of Comparisons

The seeming disparity between the calculated effects of jitter and experimental results was resolved. The flareout of the tails of the calculated curves was due to the assumption of constant jitter variance, whereas in reality it is composed of both a constant and a functional component. A reasonable proportionality between these components produces results consistent with the experimental.

It was found that, for small variations of internal receiver anomalies, the BER curves in general did not deviate more than 1 db from their theoretical shape. It was evident that deviations in excess of 1.5 db occurred only when the equipment was grossly misaligned.

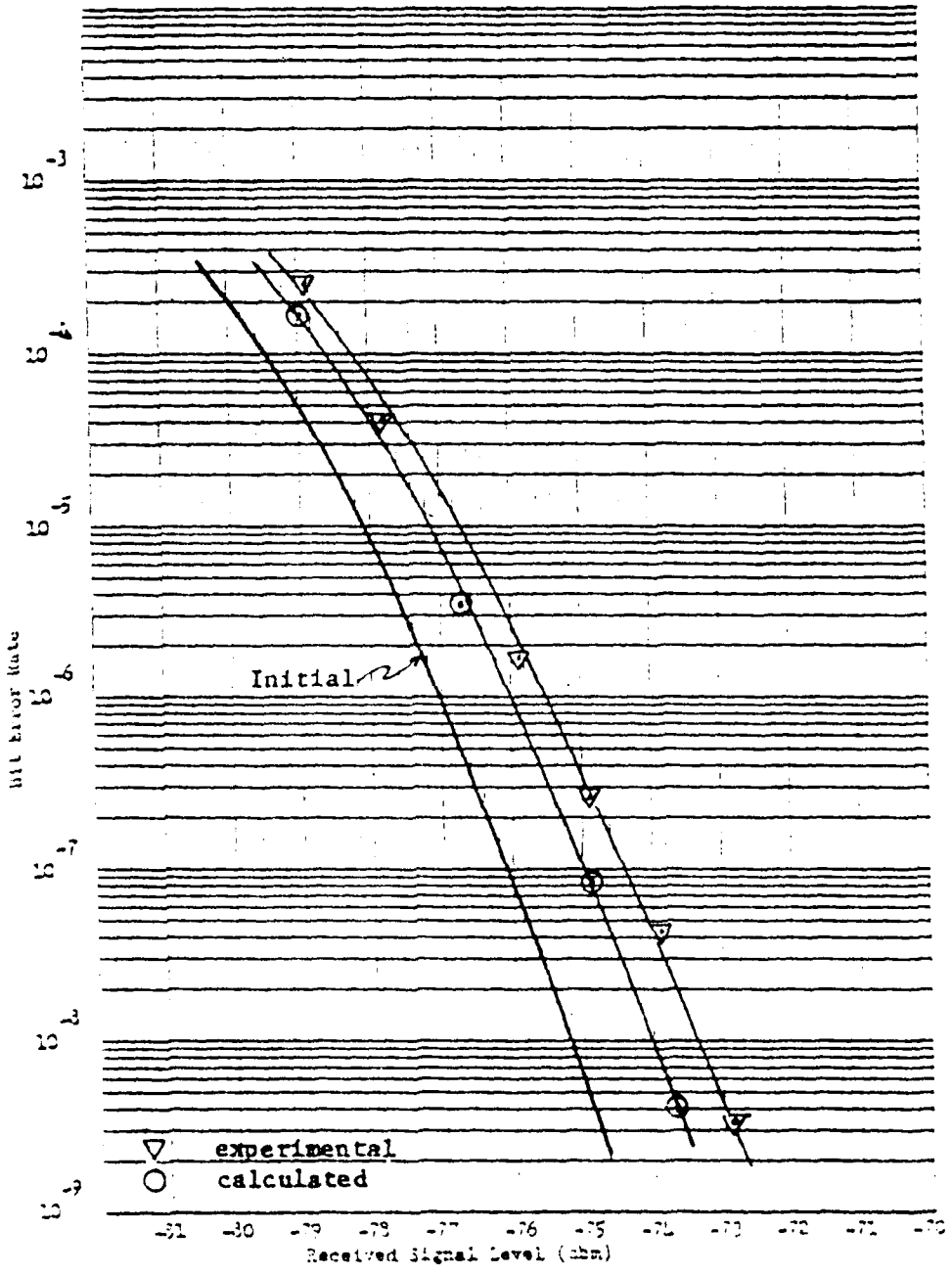

Fig. 5.18. BER vs. RSL, RDS-80, Baud Timing Offset, $\tau = 0.053$.

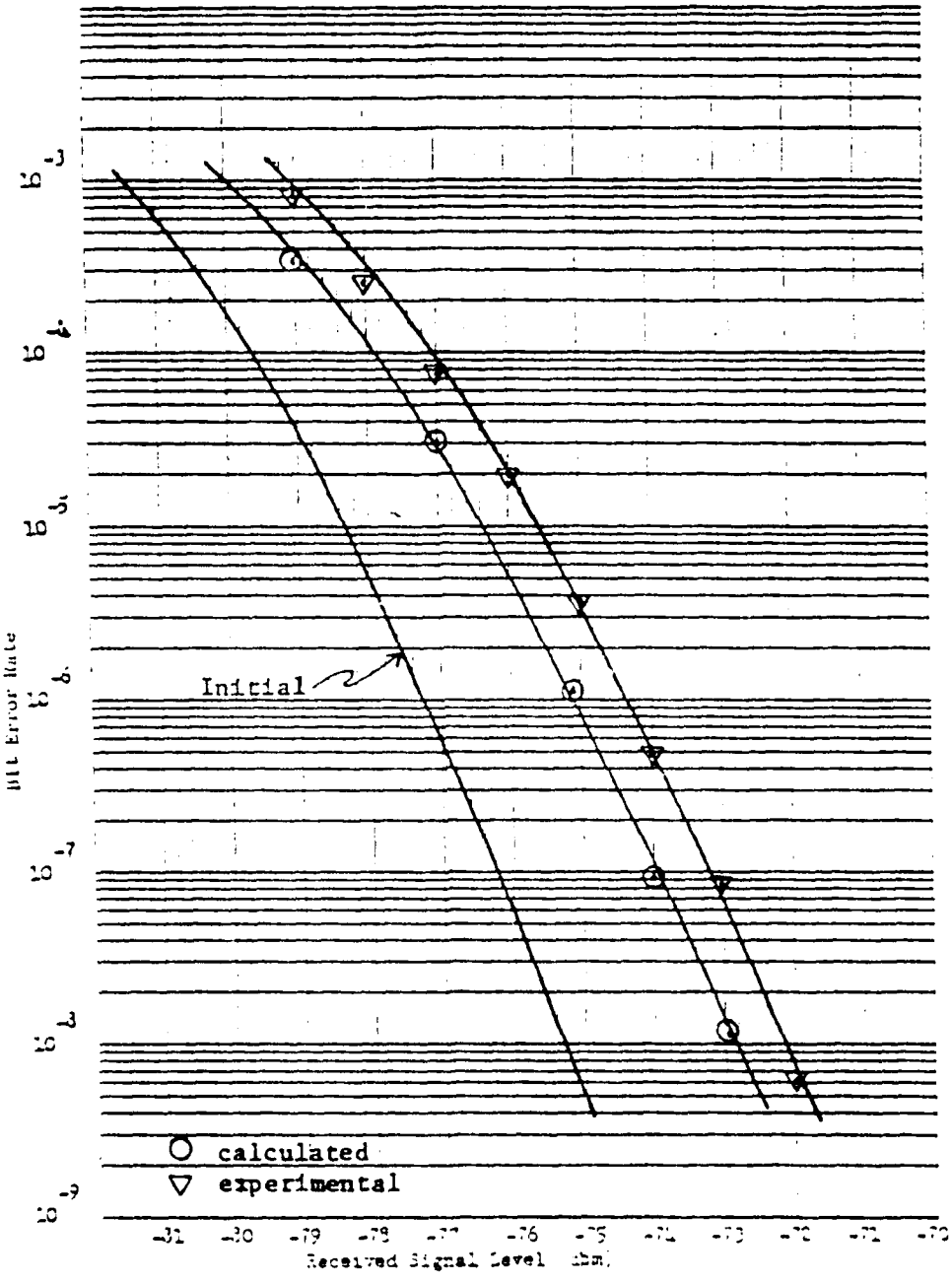

Fig. 5.19. BER vs. RSL, RDS-80, Baud Timing Offset, $\tau = 0.09$.

Calculations performed with measured values of jitter and phase offset resulted in shifts of the BER curves which were quite consistent with the experimentally determined curves. Although some assumptions were necessary in each calculation, the consistency of the results was sufficient to establish the validity of the experiments.

CHAPTER 6

SUMMARY AND CONCLUSIONS

In Chapter 2, theoretical expressions were derived for the probability of error of a number of modulation schemes and detection methods in the presence of white Gaussian noise. In general, these expressions were found to be complementary error functions if the detection methods were coherent or by sampling:

$$P_b = \operatorname{erfc}\left(\frac{KE}{N_o}\right)^{1/2} \tag{6.1}$$

or exponentials for non-coherent and differentially coherent detection:

$$P_b = \frac{1}{2}\exp\left(\frac{KE}{N_o}\right). \tag{6.2}$$

The argument in each case was the signal-to-Gaussian noise ratio multiplied by a constant K dependent upon the type of modulation. There were some exceptions to these general forms, but the resulting BER curves were later shown to be quite similar.

Each expression was then modified to show the effects of symbol synchronization error and carrier phase error where applicable. The method used in both cases was to derive the probability of error conditioned on a constant value of timing or phase error. The conditional expressions were found to have the form, for symbol synchronization error:

$$P_b = \frac{1}{2}\,\mathrm{erfc}\left(\frac{KE}{N_o}\right)^{1/2} + \frac{1}{2}\,\mathrm{erfc}\left[\left(\frac{KE}{N_o}\right)^{1/2}\left(1 - \frac{C|\tau|}{T}\right)\right] \qquad (6.3)$$

The sum of two functions occurred since baud timing errors generally have no effect when successive symbols are alike. The constant C multiplying the relative timing error $\frac{|\tau|}{T}$ was a function of the waveform. For carrier phase error the expressions invariably had the form:

$$P_b = \mathrm{erfc}\left[\left(\frac{KE}{N_o}\right)^{1/2}\cos\theta\right] \qquad (6.4)$$

where θ was the phase error. Again, there were a few exceptions to these forms which were shown to result in BER curves with similar shapes.

The major contribution of Chapter 2 is to consolidate comparable expressions in a common notation for the effects of jitter on different modulation schemes and methods of detection in the presence of white Gaussian noise. The point so far as proving the basic hypothesis was to establish the fact that the many and varied modulation and detection techniques result in a commonality of expressions for probability of error.

Chapter 3 was devoted primarily to an examination of the shapes and relative positions of BER curves calculated and plotted using the common forms of the derived expressions.

The chapter began with calculations of the effects of constant factors in expressions for probability of bit error upon the curves of BER versus signal-to-noise ratio. It was shown that constants multiplying the arguments of functions cause shifts but no change in the

shape of the curves. Constants multiplying the functions themselves and the summation of multiple functions cause only slight distortions of the curves which are completely insignificant at BERs below 10^{-4}, the area of general interest.

Before calculated curves of BER could be obtained for the effects of jitter, it was necessary to digress briefly to investigate the common source of symbol synchronization and carrier phase reference errors. Although the precise distribution of the phase error at the output of a second-order phase-locked-loop (PLL) is Tikhonov, it was shown that the Gaussian distribution was a very close approximation. It is generally accepted that the error variance due to additive white Gaussian noise is inversely proportional to the signal-to-noise ratio within the loop. Although second order loops are normally designed to minimize the steady state error to an input step function, there remains a constant component of error variance due to fluctuations in the transmitter oscillator and the VCO of the PLL. It was also shown that a shift in the mean of the phase error occurs if the quiescent frequency of the VCO is not precisely tuned to the received frequency but that in theory there is little effect upon the variance.

To determine the effects of jitter, BER curves were calculated by integrating the conditional expressions derived in Chapter 2 over the probability density functions of the phase and timing errors. It was found that for small values of mean and variance of the jitter the BER curves were shifted slightly but essentially retained the theoretical shape. However, when the jitter became substantial the curves were

seen to flare out dramatically at the tails. A discussion of this phenomenon was deferred until Chapter 5 where a comparison with experimental results could be made.

Sample calculations were made to verify that the Gaussian approximation produced results very similar to the Tikhonov distribution. Variations in the mean value of the phase and timing errors were found to produce the expected shifts of the BER curves. Additional calculations were made to show that irreducible bit errors, which result from the probability that the magnitude of the timing or phase error exceeds $\pi/2$, are generally negligible unless the mean or variance is exceptionally large.

The effects of jitter on non-coherent detection of FSK and on three-level partial response systems were examined separately since in the one case the expression for probability of error was considerably different from the common format and in the other no closed form expression could be obtained. In both cases the jitter was found to shift the BER curves without distortion of the shape.

The effects of intersymbol interference and frequency distortion were then discussed. Although closed form expressions for these effects were not found, it was shown that as long as the disturbances were not so severe as to cause errors by themselves, the effects were, in general, to reduce the signal-to-Gaussian noise ratio.

Chapter 4 described the results of experiments performed on four different types of digital communications systems. It was possible

to investigate the effects of baud timing jitter on three of these systems. Two provided data on the effects of carrier phase jitter, whereas frequency non-linearities could be introduced into only one of the systems.

Baud timing jitter was induced in the TI-4000, three-level partial response system by varying the quiescent frequency of the voltage controlled oscillator (VCO) of the phase-locked-loop (PLL) that provides recovered receiver timing. The results showed that small perturbations caused shifts of the BER curves with little deviation from the theoretical shape. With larger shifts, some tilting of the curves did occur, which was attributed to an increase in the jitter variance as well as the expected offset of the mean value.

Curves of BER versus settings of the VCO for constant values of received signal level illustrated the fact that optimum alignment can be obtained by monitoring the BER. The optimum settings were independent of received signal level which demonstrates that the alignment can be accomplished readily at a relatively high BER. Maintenance manuals for the TI-4000 contain no procedures for the tuning of the VCO even though modules recently received from the manufacturer were found to be not optimally aligned.

The effect of nonlinear frequency response was investigated in the TI-4000 by distorting the linearity of the discriminator in the FM receiver. As was expected from the theoretical analysis, the effect of the distortion was to reduce the signal-to-noise ratio at the input to the detector which caused the BER curves to shift with no additional

deviation from the theoretical shape. The effectiveness of the BER monitoring procedure for equipment alignment was rather dramatically demonstrated during this experiment.

The combined effects of two receiver anomalies were examined by simultaneously inducing baud timing jitter and distorting the frequency response of the discriminator. The effects were found to be additive, producing much larger shifts of the BER curves without distortion of the shapes. This Gaussian-like behavior was expected from consideration of the central limit theorem.

The experiment with the Lenkurt 261A and 26C equipments illustrated the fact that two supposedly electrically equivalent items can have a wide variation in their performances and yet still possess characteristic BER curves which adhere closely to the theoretical shape. Again, the multiple effects of internal anomalies can be expected to produce such phenomena.

An otherwise undetectable amount of baud timing jitter induced in the 261A resulted in a fairly large shift of the BER curve with no distortion of the shape. No other means were found for altering the performance of this equipment.

For a multitude of reasons described in Chapter 4, the experiment with the MW-518 was not very successful. Two separate curves of BER were obtained with the shift between them attributed to carrier phase jitter, but this was not firmly established nor was it possible to make meaningful measurements of the effects of other anomalies.

With the RDS-80 equipment it was possible to study the effects of both baud timing and carrier phase jitter. In each case, the recovered timing signal was offset at the output of the appropriate PLL. These experiments, again, demonstrated that small variations of the anomalies caused shifts of the BER curves without appreciable distortion of the characteristic shape. Curves of BER versus circuit component settings for fixed levels of received signal were used to further demonstrate the equipment alignment procedure by BER monitoring.

Chapter 4 ended with calculations of the variances and confidence limits of the experimental data. These were found to be very small and it was concluded that isolated irregularities in the data were probably due to experimental procedures, drifting signals, or other external influences.

Chapter 5 began with a resolution of the seeming disparity between the calculated effects of jitter on the BER curves and the experimental results. It was noted that the theoretical curves calculated in Chapter 3 which were in agreement with those widely accepted in the literature, predicted a dramatic flareout of the tails of the curves which was not found experimentally. A determination was made that this discrepancy was due to the assumption of constant variance in the calculations. Further investigation showed that curves plotted assuming only a variance that was inversely proportional to the signal-to-noise ratio also did not agree with experimental results. It was found that both constant and functional components of variance were

necessary to produce properly shaped curves. This is theoretically correct and seems a very logical conclusion, however, it was not discovered in the current literature.

A short discussion was then presented of the method used to obtain a quantitative estimate of the amount of deviation of the experimental curves from the theoretical shape. The experimental results for each item of equipment were then analyzed from this perspective. It was found in general that for small variations of the anomalies the curves deviated less than 1 db from the theoretical shape. It was very evident that deviations in excess of 1.5 db occurred only when the equipment was grossly misaligned.

Calculations were performed to obtain BER curves based on theoretical expressions and measured values of the mean and variance of the baud timing jitter induced in the T1-4000 system. The results were in remarkably close agreement with the experimental curves. It was very interesting to note that the measured increase in the jitter variance at the one extreme of the VCO offset was not predicted by PLL theory. However, PLLs are nonlinear devices whose performance can only be approximated by linear analysis. It was this increase in variance that caused the additional tilt of the calculated curves in agreement with the experimental results. This close correlation strongly reinforces the argument that, even in rather extreme cases of misalignment, the BER curves tend to tilt outward, but that flareout of the tails does not occur until irreducible errors become predominant.

The amounts of phase and timing offsets introduced into the RDS-80 equipment were estimated based upon component measurements and analyses of the circuitry. These estimates were used to calculate BER curves for comparison with the experimental data. Although the results did not agree exactly, they were sufficiently consistent to substantiate the validity of the experiments. The difficulty encountered in attempting to make meaningful analog measurements at the frequencies involved, when compared with the ease of monitoring BER, accentuates the potential value of the proposed alignment technique.

Conclusions

The conclusions contained herein were experimentally verified for a small but representative sampling of the types of modulation and detection techniques that are found in digital communications equipment. The experimental results were predictable from and closely correlated with calculations based on theoretical expressions. Adding this to the fact that similar expressions were derived for a wide variety of modulation and detection techniques leads naturally to a generalization of the conclusions to encompass these techniques.

It has been conclusively demonstrated that small variations in the internal receiver anomalies that contribute to detection errors cause a lateral displacement of the characteristic curves of bit error rate versus received signal-to-noise ratio, while the curves retain their theoretical shape at the higher levels of signal-to-noise ratio. As increased variations of the anomalies cause greater shifts, the

curves tend to tilt outward slightly causing deviations from the theoretical at very low bit error rates; however, no flareout of the tails will occur unless the receiver is severely misaligned.

This conclusion validates the use of the extrapolation technique for determination of curves of long-term bit error rate. The method is to obtain a single reliable data point at a BER of 10^{-4} or 10^{-5} and then to draw a theoretically shaped curve through this reference. An additional data point should be taken at a lower error rate (less than 10^{-6} if feasible). If this point lies within 1 to 1.5 db of the theoretical curve, the theoretical results can be accepted with a high degree of confidence. If desired, the theoretical curve can be tilted slightly to pass through the two data points and provide quite accurate results. It can be said without reservation that if the second data point is not within 1.5 db of the theoretical curve, there is definitely something wrong. If the test procedures are correct and the data is accurate, the equipment is most probably out of alignment.

The extrapolation technique as described will be particularly useful in those cases where many BER curves are required. The method will provide accurate results while reducing test time by 3 to 4 orders of magnitude. For example, at 32 Kbps, several days might be required to obtain data for a single complete curve, whereas with extrapolation an accurate curve could be generated in less than an hour and a half. The technique can also be used as a rapid means of checking equipment to insure proper operation.

Analog techniques for alignment of digital communications equipment are well established and necessary to obtain proper operation. However, these methods may not produce the best possible operational performance. Final alignment while monitoring the bit error rate can produce the desired optimum performance. This contention is strongly supported by the experimental results with both the T1-4000 and the RDS-80.

That optimum alignment can be obtained at low signal-to-noise ratios (high BER levels) is evidenced by the fact that, although the BER curves may tilt or even distort, they never cross. The curves that were drawn of BER versus alignment position for those components that were varied during the experiments show that the optimum alignment was the same for each received signal level.

That BER monitoring should be employed in equipment alignment appears to be an obvious conclusion. However, to the knowledge of the author, the procedure has not been previously employed by either equipment manufacturers or users. No mention of the technique has been found in the literature.

In final summary, the extrapolation procedure as described is valid and can be used for reducing test time where curves of long-term BER are required. The extrapolation principle can be extremely useful when employed in the new technique proposed for alignment of digital communications equipment.

LIST OF REFERENCES

Bennett, W. R., and J. R. Davey, Data Transmission, McGraw-Hill, New York, 1965.

Bennett, W. R., and J. Salz, "Binary Data Transmission by F.M. Over a Real Channel", Bell System Technical Journal, Sept., 1963, pp. 963-975.

Cahn, C. R., "Performance of Digital Phase Modulation Communication Systems," IRE Transactions on Communications Systems, Vol. CS-7, No. 1, May, 1959, pp. 3-6.

Chadwick, H. D., "Frequency Tracking in an MFSK Receiver," Jet Propulsion Laboratory, SPS 37-57, Vol. III, 1969.

Chadwick, H. D., and W. C. Springett, "The Design of a Low Data Rate MFSK Communication System," IEEE Transactions on Communication Technology, December, 1970, pp. 740-750.

Craig, J. W., "Eye Patterns and Timing Error Sensitivity in Partial Response Pulse Transmission Systems," Proceedings of IEEE International Conference on Communications, Vol. II, 1975, pp. 20-7.

De Buda, R., "Coherent Demodulation of Frequency-shift Keying with Low Deviation Ratio," IEEE Transactions on Communications, June, 1972, pp. 429-434.

Deffeback, H. L., and W. O. Frost, "A Survey of Digital Baseband Signalling Techniques," NASA Technical Memorandum TM X-64615, June, 1971.

Doob, J. L., Stochastic Processes, Wiley Interscience, New York, 1953.

Feller, W., An Introduction to Probability Theory and Its Applications, Wiley Interscience, New York, 1957, pp. 299-303.

Gregg, W. D., Analog and Digital Communication, Wiley Interscience, New York, 1977.

Gronemeyer, S. A., and A. L. McBride, "MSK and Offset QPSK Modulation," IEEE Transactions on Communications, August, 1976, pp. 809-819.

Haykin, S., Communication Systems, Wiley Interscience, New York, 1978.

Jones, J. J., "Filter Distortion and Intersymbol Interference Effects on PSK Signals," IEEE Transactions on Communications Technology, April, 1971, pp. 120-132.

Korn, G. A., and T. M. Korn, Mathematical Handbook for Scientists and Engineers, 2nd Edition, McGraw-Hill, New York, 1968.

Kretzmer, E. R., "Generalization of a Technique for Binary Data Communication," IEEE Transactions on Communication Technology, February, 1966, pp. 67-68.

Lender, A., "The Duobinary Technique for High-speed Data Transmission," AIEE Transactions on Communications and Electronics, May, 1963, pp. 214-218.

Lindsey, W. C., "Coded Non-coherent Communications," IEEE Trans., Space Electronics and Telemetry, March, 1965, pp. 6-13.

Lindsey, W. C., Synchronization Systems in Communication and Control, Prentice-Hall, New York, 1972.

Lindsey, W. C., and M. K. Simon, Telecommunications Systems Engineering, Prentice-Hall, New York, 1973.

Lucky, R. W., J. Salz, and E. J. Weldon, Jr., Principles of Data Communication, McGraw-Hill, New York, 1968.

Lugannani, R., "Intersymbol Interference and Probability of Error in Digital Systems," IEEE Transaction on Information Theory, Nov., 1969, pp. 473-477.

McLane, P. J., "Lower Bounds for Finite Intersymbol Interference Error Rates," IEEE Transactions on Communications, June, 1974, pp. 853-856.

Papoulis, A., Probability, Random Variables, and Stochastic Processes, McGraw-Hill, New York, 1965.

Reiger, S., "Error Probabilities of Binary Data Transmission Systems in the Presence of Random Noise," IRE Convention Record, Part 8, Information Theory, 1953.

Rhodes, S. A., "Effect of Noisy Phase Reference on Coherent Detection of Offset QPSK Signals," IEEE Transactions on Communications, Aug., 1974, pp. 1046-1054.

Rice, S. O., "Mathematical Analysis of Random Noise," Reprinted in Selected Papers on Noise and Stochastic Processes (N. Was, Ed.) Dover, 1954.

Schonhoff, T. A., "Symbol Error Probabilities for M-ary CPFSK: Coherent and Non-coherent detection", IEEE Transactions on Communication, June, 1976, pp. 644-652.

Schooley, L. C., and G. R. Davis, "Introduction to Testing and Evaluation of Digital Communications Systems and Equipment," Technical Report, Engineering Experiment Station, University of Arizona, Tucson, Arizona, April, 1977a.

Schooley, L. C., and G. R. Davis, "Instrumentation and Methodologies for Testing and Evaluation of Digital Communications Systems and Equipment," Technical Report, Engineering Experiment Station, University of Arizona, Tucson, Arizona, May, 1977b.

Schooley, L. C., and G. R. Davis, "Extrapolation of Bit Error Rate Measurements: Experimental Results (Interim Report)," Technical Report, Engineering Experiment Station, University of Arizona, Tucson, Arizona, November, 1978.

Schooley, L. C., and G. R. Davis, "Extrapolation of Bit Error Rate Measurements: Experimental Results," Technical Report, Engineering Experiment Station, University of Arizona, Tucson, Arizona, January 1979.

Schwartz, M., W. R. Bennet, and S. Stein, Communications Systems and Techniques, McGraw-Hill, New York, 1966.

Shimbo, O., M. I. Celebiler, and R. J. Fang, "Performance Analysis of DPSK Systems in Both Thermal Noise and Intersymbol Interference," IEEE Transactions on Communication Technology, Dec., 1971, pp. 1179-1188.

Shimbo, O., R. J. Fang, and M. I. Celebiler, "Performance of M-ary PSK Systems in Gaussian Noise and Intersymbol Interference," IEEE Transactions on Information Theory, Jan., 1973, pp. 44-58.

Smith, D. R., "A Performance Monitoring Technique for Partial Response Transmission Systems," Proceedings of IEEE International Conference on Communications, Vol. II, 1973, pp. 40-41.

Stein, S., and J. J. Jones, Modern Communication Principles, McGraw-Hill, New York, 1967.

Stiffler, J. J., "On the Allocation of Power in a Synchronous Binary PSK Communication System," Proceedings of National Telemetry Conference, 1964.

Stiffler, J. J., Theory of Synchronous Communications, Prentice-Hall, New York, 1971.

Sullivan, W. A., "High-capacity Microwave System for Digital Data Transmission," IEEE Transactions on Communications, June, 1972, pp. 466-470.

Tikhonov, V. I., "The Effects of Noise on Phase Locked Oscillator Operation," Automat. i Telemakh., Vol. 20, Sept., 1959.

Viterbi, A. J., "On Coded Phase-coherent Communication," IRE Trans., Space Electronics and Telemetry, March, 1961, pp. 3-14.

Viterbi, A. J., "Phase Locked Loop Dynamics in the Presence of Noise by Fokker-Planck Techniques," Proc. IEEE, Vol. 51, No. 12, December 1963, pp. 1737-1753.

Viterbi, A. J., Principles of Coherent Communication, McGraw-Hill, New York, 1966.

Whalen, A. D., Detection of Signals in Noise, Academic Press, New York, 1971.

Wozencraft, J. M., and I. M. Jacobs, Principals of Communication Engineering, Wiley Interscience, 1965.